On the relevance of spray drift from boom application for catchment-scale pesticide fate assessment

by

Mike Devin Fuchs

from Bad Dürkheim, Germany

Accepted Dissertation thesis for the partial fulfilment of the requirements for a

Doctor of Natural Sciences

Fachbereich: Natur- und Umweltwissenschaften

Rheinland-Pfälzische Technische Universität Kaiserslautern-Landau

Thesis examiners:

Prof. Dr. Andreas Lorke, Landau

Dr. Sebastian Gebler, Speyer

Date of disputation

07.08.2026

This dissertation thesis is based on the following three research articles submitted to peer-reviewed journals (ordered by publication date):

1. Fuchs, M.D., Gebler, S., Lorke, A., 2025. The droplet and atmospheric dispersion drift (DAD-drift) model – A modular approach for estimating spray drift at the landscape scale. Environ. Res. 271, 121104. https://doi.org/10.1016/j.envres.2025.121104

2. Fuchs, M.D., Gebler, S., Lorke, A., 2025. Landscape-level assessment of spray drift – A virtual experiment using the Droplet and Atmospheric Dispersion drift (DAD-drift) model. Environ. Model. Softw. 189, 106455. https://doi.org/10.1016/j.envsoft.2025.106455

3. Fuchs, M.D., Gebler, S., Lorke, A., 2026. Evaluating landscape-level pesticide exposure from spray drift: A modeling study in an agriculture-dominated watershed using SWAT+ and DAD-Drift. Environ. Pollut. 397, 128031. https://doi.org/10.1016/j.envpol.2026.128031

Table of Content

Abstract 1

1 Introduction 3

1.1 Pesticides in Agriculture: Use, Types, and Historical Development 3

1.2 Environmental Monitoring of Pesticides: Evidence and Limitations 4

1.3 Environmental Transport Pathways of Pesticides 6

1.4 Fate and Transport Modelling of Pesticides at the Catchment Scale 9

1.5 Research Gap and Thesis Aim: Integrating Spray Drift in Landscape Models 11

2 Research Objectives and Hypothesis 13

3 Outline 15

3.1 The droplet and atmospheric dispersion drift (DAD-drift) model – A modular approach for estimating spray drift at the landscape scale 16

3.2 Landscape-level assessment of spray drift – A virtual experiment using the Droplet and Atmospheric Dispersion drift (DAD-drift) model 16

3.3 Evaluating Landscape-Level Pesticide Exposure from Spray Drift - A Modeling Study in an Agriculture-Dominated Watershed Using SWAT+ and DAD-Drift 16

4 Discussion 19

4.1 Advancing Mechanistic Spray Drift Modeling at the Landscape Scale 19

4.2 How Spatial Simplifications Influence Spray Drift Modeling Outcomes 21

4.3 Identification of Key Spray Drift Drivers at the Landscape Scale 23

4.4 Incorporating Spray Drift into Catchment Scale Pesticide Fate Modeling 24

4.5 Hydrological Uncertainty and Its Influence on Landscape-Scale Pesticide Dynamics 27

4.6 Limitations of the Study 28

4.7 Directions for Future Research 30

5 Conclusion 33

References 35

Author Contributions 43

Declaration 45

Declaration of Use of Artificial Intelligence 47

Curriculum Vitae 49
Acknowledgements 51
Appendix I: 53
Appendix II: 65
Appendix III: 75
Appendix IV: 87
Appendix V: 107
Appendix VI: 135
Appendix VII: 161

Abstract

Pesticides are essential to modern agriculture, yet their movement through the environment poses risks to non-target ecosystems. Landscape-scale fate models are key tools for assessing environmental exposure, but they must adequately represent all relevant transport pathways to produce reliable predictions. Spray drift is a critical yet underrepresented pathway in landscape-scale pesticide fate models. This thesis addresses this knowledge gap by developing and applying a mechanistic modeling approach, the Droplet and Atmospheric Dispersion drift (DAD-drift) model, to simulate spray drift deposition from boom sprayers across complex and heterogeneous agricultural landscapes.

The DAD-drift model integrates a mechanistic droplet model, a micrometeorological module, and a three-dimensional Gaussian puff dispersion model to simulate the motion, evaporation, and atmospheric transport of spray droplets at high spatial resolution. Evaluation against two field-scale drift studies that cover a wide range of environmental conditions and nozzle types demonstrated very good agreement between predictions and observations, confirming accurate and robust model behavior across diverse application scenarios.

The role of spatial representations of application areas and non-target areas was evaluated by employing DAD-drift in virtual experiments, comparing its predictions with simplified algorithms previously applied in eco-hydrological modeling. The findings indicate that spatial simplifications can introduce errors of an order of magnitude in predicted pesticide deposition, with major consequences for subsequent exposure assessment. A complementary analysis identified the droplet size distribution and the distance to non-target areas as key drivers of spray drift deposition at the landscape scale. Crucially, the effects of wind speed, temperature, and humidity were found to be distance-dependent, reflecting the shift from near-field to far-field drift regimes and highlighting the necessity of scale-aware modeling strategies.

Finally, the DAD-drift model was integrated into a high-resolution Soil and Water Assessment Tool (SWAT+) eco-hydrological model of an agricultural catchment in Germany, extending the model with a previously absent drift component. The model setup was constructed entirely from publicly available datasets (e.g., terrain, soil, land use, hydrology, and meteorology), and included realistic multi-year crop rotations derived from field-level records. The catchment hydrology was calibrated and validated against observed discharge, achieving very good model performance. The coupled framework simulated both hydrological and atmospheric pesticide transport pathways across multiple years and active ingredients. Incorporating spray drift led to substantially higher predicted environmental concentrations in

adjacent surface waters, particularly for substances that are otherwise less mobile due to strong sorption to soil. Ensemble-based hydrological parameterization revealed considerable uncertainty in predicted concentrations, underscoring the importance of uncertainty assessment in landscape-scale fate evaluations.

Taken together, this work delivers the first mechanistic and transferable integration of spray-drift modelling into catchment-scale eco-hydrological modelling, providing a strong framework for linking landscape hydrology with atmospheric drift processes, thereby strengthening the scientific basis for environmental risk assessment, mitigation planning, regulatory evaluation, and ecological impact assessment.

1 Introduction

Pesticides are essential to modern agriculture, yet their movement through the environment is influenced by numerous interacting processes, creating complexity that must be understood to assess their environmental consequences. To provide the context for this thesis, this chapter introduces the role and development of pesticides in agriculture, summarizes evidence from environmental monitoring, outlines the major environmental transport pathways, reviews established catchment-scale modelling approaches, and concludes by identifying the research gap addressed in this work.

1.1 Pesticides in Agriculture: Use, Types, and Historical Development

Pesticides, referred to as plant protection products under EU regulation (EC No 1107/2009), are substances or preparations used to protect crops against harmful organisms, influence plant life processes, or control undesired plant growth. They play a pivotal role in contemporary agricultural systems by protecting crops against pests, diseases, and competing weeds, and since their widespread adoption in the 1950s they have become integral tools to sustain global agricultural production. Their fundamental objective is to guarantee food security by minimizing harvest losses, thereby ensuring the maintenance of high and stable yields in the face of continuously increasing global demand for food. This demand is driven by a growing global population and by evolving dietary preferences, especially in developing countries, where a shift towards high quality foods puts additional stress on agricultural production (Wang et al., 2019). Tudi et al. (2021) estimate that approximately one-third of the yield of agricultural products are contingent upon pesticide application, and without this intervention, global yield losses could reach up to 78% for fruits, 54% for vegetables, and 32% for cereals. However, despite the widespread use of pesticides, global agricultural output is still reduced by an estimated 40% due to pests, such as insects, fungi, and nematodes (Prechsl et al., 2022).

Pesticides are commonly classified by their target organisms, including herbicides, insecticides, fungicides, rodenticides, nematicides, and molluscicides. Beyond this categorization, pesticides can also be grouped by their chemical class. Examples of these classes include organophosphates, carbamates, chlorinated hydrocarbons, triazines, synthetic pyrethroids, and urea derivatives. These chemical classes reflect the pesticides' chemical structure and modes of action, which in turn are linked to differences in the persistence and toxicity of the pesticides (Tudi et al., 2021). The European Union (EU) reports

pesticide sales in broader categories, such as fungicides and bactericides, herbicides (including haulm destructors and moss killers), insecticides and acaricides, as well as molluscicides, plant growth regulators, and other plant protection products. In 2023, fungicides and bactericides accounted for 39% of total EU pesticide sales by mass of active substance, herbicides for 36%, and insecticides and acaricides for 17%. Molluscicides, plant growth regulators, and other products together represented less than 10% (Eurostat, 2025).

The historical evolution of pesticide technology has been characterized by a transition from early, broad-spectrum compounds that were highly toxic and lacked selectivity, to more targeted and efficient formulations. Beginning in the 1950s, synthetic pesticides such as dichlorodiphenyltrichloroethane (DDT) and benzene hexachloride (BHC) were introduced, providing far greater potency and broader efficacy than earlier inorganic compounds but exhibiting similar drawbacks, including environmental persistence and toxicity to non-target organisms (Tudi et al., 2021). After the 1970s, advances in synthetic chemistry and mode-of-action research led to the introduction of novel chemical families, thereby enabling greater specificity and reduced application rates. Coinciding with this technological advancement has been the drastic increase in global pesticide usage, reflecting the rising demand for agricultural production. The global usage rose from approximately 0.2 million metric tons in the 1950s to over 5 million metric tons by the early 2000s, with pesticide usage exceeding 3 million metric tons in the 2020s (Tudi et al., 2021).

1.2 Environmental Monitoring of Pesticides: Evidence and Limitations

Although pesticides are essential to modern agriculture, they frequently reach non-target areas and cause environmental exposure beyond their intended use. Monitoring programs have repeatedly demonstrated the presence of pesticides and their residues in non-target environmental compartments across agricultural landscapes especially in surface waters, such as small streams, ditches, and ponds (Ulrich et al., 2022; Vormeier et al., 2023). Furthermore, long-term surveys have demonstrated the presence of pesticides and their transformation products in groundwater systems (Wang et al., 2019). Such residues are also contained in soils and sediments, reflecting their accumulation resulting from repeated applications over time (van Capelle et al., 2012). Furthermore, the presence of pesticide residues has even been documented in non-target organisms, including fish, wildlife and terrestrial insects (Brühl et al., 2021). Collectively, these findings highlight the broad environmental dissemination of pesticides and their transformation products and establish monitoring as an indispensable tool for documenting their presence. Beyond their presence,

pesticide contamination has been associated with adverse effects on non-target organisms, including pollinators and aquatic communities, and poses risks to soil and water quality, biodiversity, and human health (Centanni et al., 2023; Prechsl et al., 2022). These ecological and societal consequences underscore the need for a thorough understanding of pesticide transport pathways, which constitutes the focus of this thesis.

Such monitoring programs serve a variety of purposes. They document the presence of pesticides in the environment and thereby provide essential evidence for evaluating environmental risk at relevant spatial and temporal scales (Bundschuh et al., 2014). Adequately designed programs have been shown to reveal the seasonal presence of pesticides and their transformation products across the landscape, with concentrations often peaking shortly after application (Warner et al., 2021). In addition, high-frequency sampling has shown that pesticide concentrations can increase rapidly during rainfall events, often reaching a peak within hours and subsequently decreasing (Vormeier et al., 2023). Event-driven approaches have been demonstrated to capture such exposure patterns that are frequently overlooked by conventional sampling methods, which rely on low-frequency, fixed-interval grab samples and therefore tend to underestimate the frequency and magnitude of concentration peaks (Vormeier et al., 2023).

Despite its critical role, pesticide monitoring faces considerable limitations that restrict its ability to fully characterize environmental exposure. Surveys conducted on small water bodies indicate that detections fluctuate significantly with precipitation patterns and pesticide application timing, emphasizing the interplay between the chemical diversity of pesticides and local hydrological conditions. Collectively they contribute to the emergence of highly heterogeneous contamination patterns (Ulrich et al., 2022). Although dense spatial and temporal sampling can improve detection, even intensive programs capture only snapshots of these dynamic processes, and monitoring designs are often constrained by financial and logistical barriers, resulting in incomplete coverage (Wang et al., 2019). Therefore, monitoring can hardly provide a comprehensive picture, since peak concentrations of highly dynamic substances are difficult to capture and it is impossible to analyze every compound everywhere (Ippolito and Fait, 2019). Long-term monitoring has further revealed that flow-triggered or event-based sampling detects concentration peaks that conventional approaches underestimate by several orders of magnitude or fail to capture entirely (Vormeier et al., 2023). Even when pesticide residues are detected, field data rarely permit the unambiguous attribution to transport processes, as a single detection on surface water may equally result from multiple diffuse pathways, whose relative importance varies across landscapes (Zhang et al., 2019).

1.3 Environmental Transport Pathways of Pesticides

Although the detection of pesticides in environmental monitoring programs confirms that active substances regularly escape treated fields, monitoring alone rarely identifies the exact mechanisms by which these compounds are transported across landscapes. That's why a mechanistic understanding of pesticide transport is required to address this gap. Pesticides applied in agricultural settings follow several distinct yet interconnected pathways, each of which is governed by a combination of physio-chemical properties, environmental conditions, and land management practices (Centanni et al., 2023; Reichenberger et al., 2007). The primary transport pathways are surface runoff, subsurface runoff, leaching, subsurface drainage, and spray drift. These pathways contribute to the movement of pesticides across different environmental compartments and time scales.

Surface runoff occurs when the amount of water from precipitation or irrigation exceeds the infiltration capacity of the soil (infiltration excess runoff) or when the soil is already saturated with water (saturation excess runoff). This excess water then generates overland flow, which can mobilize pesticides either dissolved in water or attached to eroded soil particles (Reichenberger et al., 2007). The extent of surface runoff is shaped by landscape and soil characteristics where; steep slopes and less permeable or crusted soils promote rapid overland flow and erosion (Fohrer et al., 2014; Holvoet et al., 2008a). The physio-chemical characteristics of pesticides further determine their transport behavior. Compounds with higher mobility are more likely to infiltrate into deeper soil layers, while strongly sorbing or less mobile compounds tend to be displaced via surface runoff and erosion (Lorenz et al., 2021; Zhang et al., 2019). Furthermore, the timing of precipitation relative to pesticide application is of particular importance, as rainfall occurring shortly after application significantly increases the likelihood of transport via surface runoff (Felsot et al., 2010; Warner et al., 2021).

Subsurface runoff, understood as the lateral downslope movement of water within the upper soil layers above less permeable horizons, serves as a significant transport pathway in structured soils. This process, also referred to as lateral flow or interflow in hydrological models, becomes dominant where macropores facilitate rapid water movement or where impeding soil layers promote lateral redistribution (Clothier et al., 2008; Reichenberger et al., 2007). The occurrence and magnitude of this phenomenon are significantly influenced by antecedent soil moisture, the intensity of rainfall, and the hydraulic properties of the soil profile (Clothier et al., 2008). Pesticides with moderate solubility and limited sorption affinity may be transported via moving water, while greater infiltration depth can promote sorption and microbial degradation, reducing mobility (Reichenberger et al., 2007).

Leaching refers to the vertical movement of pesticides through the soil profile and the unsaturated zone into the underlying groundwater (Reichenberger et al., 2007). This process is especially prevalent in coarse-textured soils with low organic matter and high permeability, where the capacity for retention is limited. Its significance increases under conditions of intense or prolonged rainfall and irrigation, which promote downward percolation (Reichenberger et al., 2007). The movement of pesticides through the soil can be further accelerated by preferential flow through macropores and soil cracks. During rainfall-runoff events, the rate of preferential flow may be so high that pesticide properties and soil characteristics lose much of their significance for leaching (Zajícek et al., 2018). Compounds with high solubility, low organic carbon partition coefficients (K_{oc}), and long degradation half-lives (DT_{50}) are especially prone to leaching because their mobility and persistence allow them to bypass retention and degradation processes during transport (Reichenberger et al., 2007; Tudi et al., 2021).

Subsurface drainage, which is most commonly accomplished through the use of tile or pipe drains, is a critical agricultural practice in soils with poor drainage capacities or high groundwater tables. The purpose of subsurface drainage is to prevent waterlogging, enhance field trafficability, and promote optimal crop growth. While these systems are essential for agriculture, they intercept percolating water and channel it directly to adjacent ditches and streams, thereby bypassing natural attenuation zones. Preferential flow through macropores or soil cracks further accelerate this process, allowing even strongly sorbing pesticides and their transformation products to reach surface waters (Beulke et al., 2001; Reichenberger et al., 2007). The risk is greatest when heavy rainfall follows shortly after application, producing sharp concentration peaks in drainage effluent (Zajícek et al., 2018). Similar to leaching, compounds with limited sorption are particularly susceptible to transport via subsurface drainage (Reichenberger et al., 2007; Zajícek et al., 2018). Recent monitoring confirms the significance of this pathway; however, its contribution depends on site-specific conditions and may be less relevant in landscapes with shallow groundwater or heavy-textured soils (Ulrich et al., 2022; Zhang et al., 2019).

Spray drift, defined as the movement of pesticide droplets through the air during or shortly after application, can result in deposition outside the intended treatment area (Felsot et al., 2010). The extent of drift is primarily determined by spray characteristics, such as droplet size distribution and release height, in conjunction with meteorological conditions, including wind speed, turbulence, temperature, and humidity (Felsot et al., 2010; Griesang et al., 2017). Smaller droplets are particularly susceptible to transport over greater downwind distances due to their low settling velocity. Evaporation further reduces their size and accelerates atmospheric dispersion (Felsot et al., 2010). Field and modeling studies have repeatedly

demonstrated that a proportion of the applied spray is deposited in adjacent areas (Miller, 2014). Consequently, spray drift represents a direct and immediate pathway of pesticide entry into neighboring habitats, including field margins and surface waters in close proximity to treated fields.

Pesticide transport pathways rarely act in isolation. Deposition from spray drift has been demonstrated to serve as an initial source on soil or vegetation, which is subsequently mobilized by surface or subsurface runoff (Beulke et al., 2001; Clothier et al., 2008). Preferential flow through macropores or soil cracks has been shown to accelerate both vertical and lateral movement, thereby allowing solutes to bypass matrix interactions that would otherwise slow their movement (Beulke et al., 2001; Clothier et al., 2008). Once in the soil, residues have been observed to sorb to particles and be retained for extended periods. However, these sorbed fractions have the capacity to be remobilized during rainfall events or erosion, leading to delayed pulses of contamination (Schulz, 2001; Warner et al., 2021). Concurrently, degradation processes generate transformation products that may exhibit distinct mobility and persistence characteristics, thereby expanding the spectrum of transport dynamics. In many instances, these compounds demonstrate increased mobility and persistence compared to their parent substances (Bundschuh et al., 2014; Reichenberger et al., 2007).

The outcome of overlapping pesticide transport pathways is determined by a multitude of factors. Whether pesticides are transported in dissolved or particle-bound form is influenced by compound-specific physio-chemical properties, including solubility, soil sorption coefficient (K_{oc}), degradation half-lives (DT_{50}), and, in some cases, volatility (Reichenberger et al., 2007). Landscape characteristics, such as soil type, organic matter content, slope, and hydrological connectivity, significantly impact transport potential (Clothier et al., 2008). Land use and vegetation cover further modulate exposure and retention, meanwhile meteorological drivers including rainfall intensity and timing, antecedent soil moisture, wind speed, and temperature determine the timing and magnitude of pesticide movement (Schulz, 2001). Finally, management decisions ranging from application methods and dosage to the presence of artificial drainage add another layer of variety (Beulke et al., 2001).

1.4 Fate and Transport Modelling of Pesticides at the Catchment Scale

Monitoring has demonstrated that pesticides regularly move from treated fields into surrounding ecosystems. However, field observations alone cannot disentangle the overlapping transport pathways responsible or explain their variability. Pesticide fate models

address this issue by providing a mechanistic framework that simulates the movement and transformation of applied pesticides under diverse environmental conditions. They are applied across a range of spatial scales, from field plots to entire catchments, and across temporal scales, from individual storm events to multi-year applications. By reproducing key fate processes, models enable the exploration of conditions that cannot be directly observed for logistical or economic reasons. This predictive capacity renders them indispensable for exposure assessment and risk management, including the elucidation of monitoring findings, the evaluation of mitigation strategies, the projection of climate change impacts, and the support of regulatory decision-making (Moriasi et al., 2007; Rouzies et al., 2023; Wang et al., 2019).

In Europe, pesticide exposure assessment for regulatory purposes primarily relies on the suite of models and scenarios developed under the Forum for the Co-ordination of Pesticide Fate Models and their Use (FOCUS), which operate at the field or waterbody scale under standardized conditions. Within this framework, the Pesticide Leaching Model (PELMO) is employed to simulate leaching and runoff processes in the root zone (Dubus et al., 2003). The MACRO model is utilized to represent water flow and solute transport in structured soils with macropores (Jarvis, 1994). The Pesticide Emission Assessment at Regional and Local scales model (PEARL) addresses leaching to groundwater under varying soil and climatic scenarios (Leistra et al., 2001). The TOXic substances in Surface WAters model (TOXSWA) describes pesticide fate in surface water bodies, including ditches, streams, and ponds (Beltman et al., 2006). Collectively, these models constitute the regulatory foundation of exposure assessment in the EU, as they provide conservative estimates of environmental concentrations under harmonized scenarios. These harmonized scenarios intentionally reflect worst-case conditions, addressing spatial variability through predefined conservative settings rather than spatially explicit representations. In the United States, comparable aquatic exposure assessments are conducted using the Pesticide in Water Calculator (PWC). PWC combines the Pesticide Root Zone Model (PRZM) (Carsel et al., 1985), which simulates leaching and runoff from agricultural fields, with the Variable Volume Water Model (VVWM) (Padilla et al., 2020), which represents pesticide fate in aquatic systems. These regulatory models are indispensable in their respective context; however, they are inherently constrained to local scales and standardized conditions. They were never designed to capture the spatial heterogeneity and hydrological connectivity that govern pesticide dynamics at catchment scale.

To address processes occurring beyond the field scale, catchment scale models have been developed to integrate hydrology, land use, and pesticide application across larger spatial domains. One of the most widely applied models is the Soil and Water Assessment

Tool (SWAT), which simulates runoff erosion, and the transport of nutrients and pesticides in agricultural landscapes using spatially distributed inputs for soil, land use, topography, and climate (Arnold et al., 1998). In SWAT the landscape is partitioned into hydrological response unit (HRUs), thereby representing key processes in a semi-distributed manner, enabling long-term simulations of pesticide transport under varying agricultural practices (Centanni et al., 2023; Mottes et al., 2014). The Hydrological Simulation Program–Fortran (HSPF) is another example of a model that has been extensively used in research contexts for the representation of watershed-scale hydrology and contaminant transport (Bicknell et al., 1997). The MIKE-SHE model provides a fully integrated hydrological framework capable of coupling surface and subsurface flows, thereby allowing detailed simulations of water and solute dynamics at the landscape scale (Refsgaard and Storm, 1995). In contrast to field-scale tools, these catchment-based approaches enable the assessment of cumulative effects from multiple fields, land use heterogeneity, and management practices, as well as complex hydrological connectivity between terrestrial and aquatic systems. Their capacity to integrate diverse datasets and simulate long-term scenarios renders them indispensable for exploring pesticide fate under realistic environmental conditions at the landscape scale.

Despite their strengths, catchment-scale models face important limitations that constrain their realism and reliability. Accurate simulations require high resolution, spatially explicit input data, yet detailed information on pesticide application and crop management is rarely available at the necessary resolution (Frey et al., 2011; Holvoet et al., 2005). Increasing availability of publicly accessible geospatial, soil, land-use, and climate datasets offers a potential pathway to alleviating some of these data limitations. Compound-specific properties, including degradation half-lives, solubility, and soil sorption coefficients, are typically documented in registration dossiers and serve as the foundation for model parameterization. However, the implementation of these models at the catchment scale introduces a degree of uncertainty due to the potential discrepancy between dossier-derived values and field behavior, particularly in the context of sorption and degradation processes (Luo and Zhang, 2009). Additionally, physio-chemical properties are typically determined only for major transformation products. Consequently, such data are often not available for many minor degradants and therefore cannot be used for modelling purposes (Gassmann, 2021). Furthermore, certain pesticide fate and transport processes remain simplified or entirely absent in most modeling frameworks, such as volatilization and aerial deposition processes (Mottes et al., 2014; Zhang et al., 2018). Calibration at the catchment outlet has the potential to further obscure internal process errors, as multiple often correlated parameter combinations may reproduce observed discharge while implying different underlying dynamics. This phenomenon is known as hydrological equifinality (Beven, 2006; Frey et al., 2011).

Consequently, model outputs can be sensitive to input assumptions and structural choices, which complicates their use for regulatory and management purposes (Wang et al., 2019). To address this, ensemble approaches that combine multiple parameter sets or even multiple models have been proposed as methodology to better quantify predictive uncertainty (Fohrer et al., 2014). However, application of ensemble approaches in pesticide exposure assessments remains limited, resulting in significant uncertainty in current practice.

1.5 Research Gap and Thesis Aim: Integrating Spray Drift in Landscape Models

Among the previously described pesticide transport pathways, spray drift is particularly noteworthy as it represents the most direct route through which pesticides can be transferred to non-target areas. However, despite its significance, catchment-scale models almost universally treat spray drift in an over simplified way (e.g., as a fixed loss fraction) or disregard it entirely. Popular tools such as SWAT, SWAT+, HSPF and MIKE-SHE do not natively support the explicit simulation of spray drift during application. Consequently, researchers have employed a range of strategies to approximate spray drift deposition at the catchment scale. These can be broadly categorized into two groups: mechanistic approaches that employ dedicated spray drift models, and empirical approaches that are based on spray drift databases or field trial data. The latter approach is more frequently used. The basic drift values published by Rautmann et al. (1999) are most commonly used in catchment scale approaches, with the pesticide fate modeling being performed via SWAT (Holvoet et al., 2008b; Zhang et al., 2018) and runoff connectivity modeling (Schönenberger et al., 2022). Padovani et al. (2004) combined spray drift curves derived from field trial data collected in the modeled catchment with surface water modeling using TOXSWA for individual stream segments. The SWAT model has also been coupled with mechanistic spray drift predictions from the AgDRIFT model (Teske et al., 2002; Winchell et al., 2018).

While these studies demonstrate the feasibility of incorporating spray drift into catchment-scale modeling, the implementations remain constrained in several important ways. The use of empirical spray drift curves is limited to conditions similar to those under which the data were collected, including wind speed, temperature, humidity, nozzle type, and field-edge distance (Teske et al., 2002). To accurately simulate spray drift under a wider range of conditions, a mechanistic representation of spray drift that considers droplet and atmospheric processes is needed. The adaptation of one-dimensional spray drift curves to a complex two-dimensional landscape was performed via a multitude of spatial representations

of the application and non-target areas (Holvoet et al., 2008b; Winchell et al., 2018; Zhang et al., 2018). However, none of these representations can capture the spatial heterogeneity of agricultural landscapes in a way that is adequate for landscape-scale spray drift assessment. Furthermore, some of the previously described approaches did not consider or oversimplified the wind direction during spray application (two or four wind directions). This increases the risk of inaccurately assigning spray drift deposition to areas that are not downwind of the application area, highlighting the need for an adequate representation of wind direction for landscape-scale spray drift prediction. Finally, in most catchment-scale modelling applications, spray drift deposition is restricted to stream surfaces, excluding other potentially sensitive non-target areas. A comprehensive landscape-scale pesticide assessment, however, necessitates the prediction of spray drift deposition across the entire spatial domain.

The aim of this thesis is to address the identified research gap by developing the Droplet and Atmospheric Dispersion drift (DAD-drift) model and coupling it with SWAT+ in a unified modelling framework. By combining a mechanistic droplet model with atmospheric dispersion based on a three-dimensional Gaussian puff model, which simulates the turbulent spread of an instantaneous point source as a time-evolving Gaussian distribution (Zannetti, 1990), DAD-drift accounts for inflight physics of spray droplets, wind direction, the spatial configuration of treated fields and non-target areas and predicts spray drift deposition over the complete spatial domain. Coupled with the eco-hydrological model SWAT+, this framework establishes the first integrated approach to jointly represent atmospheric and hydrological pesticide transport at the catchment scale, thereby providing a methodological advance for more realistic assessments of pesticide fate and environmental exposure.

2 Research Objectives and Hypothesis

Building on this aim, the following research questions and hypotheses were formulated to guide the development, application, and evaluation of the DAD-drift model and its integration into catchment-scale pesticide fate modeling.

Question 1:

How can existing atmospheric dispersion approaches for modeling spray drift deposition of pesticides be improved to enable accurate, spatially explicit, and computationally feasible predictions over extended downwind distances at the landscape scale?

Hypothesis 1.1: Integrating a mechanistic droplet model into an atmospheric dispersion approach will enhance accuracy over extended downwind distances.

Hypothesis 1.2: Employing a three-dimensional Gaussian puff model will improve parametrization and model performance under diverse wind and atmospheric conditions.

Question 2: How do simplified spatial representations of the arrangement of application and non-target areas influence spray drift predictions, and how do these differences propagate into higher-level modeling approaches such as eco-hydrological modelling?

Hypothesis 2.1: Different spatial representations of the arrangement of application and non-target areas will lead to significantly different deposition predictions under identical landscape organizations.

Hypothesis 2.2: Differences in spray drift predictions arising from simplified spatial representations will affect the modeled distribution of pesticides within the landscape, thereby altering the outcomes of subsequent hydrological or ecological models.

Question 3: What are the main drivers of spray drift deposition at the landscape scale, and how do they compare to those identified in field scale studies?

Hypothesis 3: Key drivers of spray drift deposition identified at the field scale do not fully explain spray drift deposition patterns at the landscape scale, as additional factors related to spatial heterogeneity and system complexity become relevant.

Question 4: Can a spatially detailed eco-hydrological model of an agriculturally dominated catchment be developed using publicly available data, while still achieving accurate prediction of catchment hydrology?

Hypothesis 4: Publicly available datasets in Germany provide sufficient spatial and temporal resolution to develop a high-resolution eco-hydrological model capable of accurately predicting catchment hydrology.

Question 5: How does the inclusion of spatially explicit spray drift deposition affect simulated pesticide dynamics in an eco-hydrological model?

Hypothesis 5.1: Implementing spray drift in the DAD-drift and SWAT+ modelling framework will result in predicted environmental concentration peaks at the catchment outflow shortly after pesticide application.

Hypothesis 5.2: Spray drift will modify the spatial distribution of pesticide mass across the landscape, thereby influencing the relative contributions and timing of other transport pathways such as surface runoff, subsurface runoff, drainage and leaching.

Question 6: To what extent does the parametrization of the eco-hydrological model contribute to uncertainty in predicted environmental concentrations?

Hypothesis 6: Predicted environmental concentrations are highly sensitive to the parametrization of the eco-hydrological model, with the magnitude of sensitivity varying across substances depending on their physio-chemical properties.

3 Outline

To address the previously outlined research questions, this thesis integrates method development, virtual experiments, and landscape scale model implementation. This thesis is organized around three research articles, each of which contributes to a different aspect of spray drift modeling and its implications for landscape scale environmental assessment. Each article is included in full in the appendices, with this section providing a summary of their scope and contribution to the overall research objectives (Figure 1).

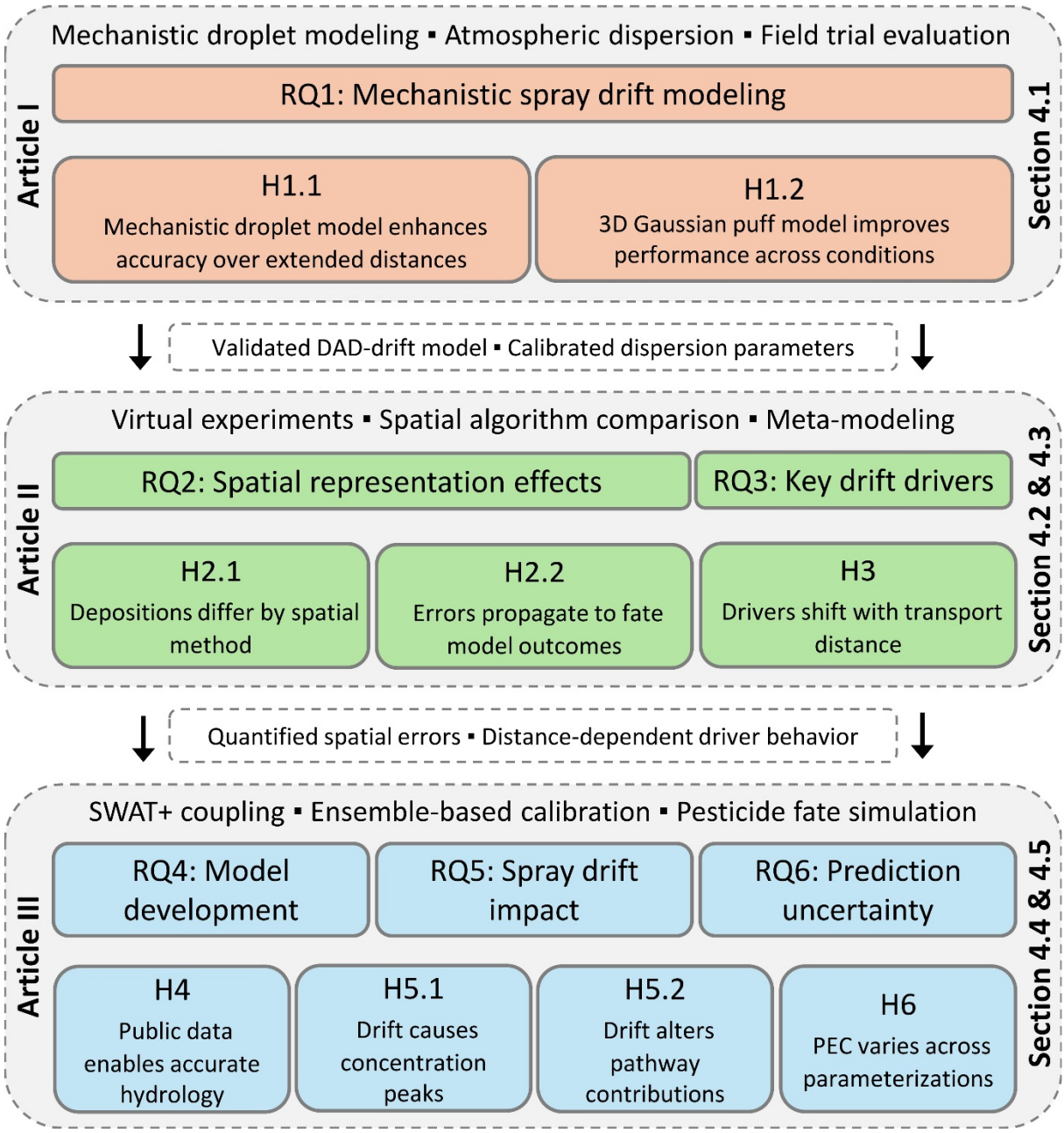


Figure 1: Schematic overview of the thesis structure, illustrating the progression from mechanistic spray drift model development (Article I) through virtual experiments on spatial representation and driver identification (Article II) to catchment-scale integration with SWAT+ and uncertainty analysis (Article III). Each article is linked to its research questions (RQ1–RQ6), associated hypotheses (H1.1–H6), and corresponding discussion sections (4.1–4.5). Arrows indicate how outputs from each stage serve as inputs to the next.

3.1 The droplet and atmospheric dispersion drift (DAD-drift) model – A modular approach for estimating spray drift at the landscape scale

The first research article introduces the novel Droplet and Atmospheric Dispersion drift (DAD-drift) model, a modular, mechanistic modeling approach designed to predict pesticide spray drift deposition from boom spray application at the landscape scale. The model sensitivity is assessed in a one-at-a-time sensitivity analysis, unknown model parameters are estimated and the model performance is evaluated against two field trial studies (Hypothesis 1.1 and 1.2).

Fuchs, M.D., Gebler, S., Lorke, A., 2025. The droplet and atmospheric dispersion drift (DAD-drift) model – A modular approach for estimating spray drift at the landscape scale. Environ. Res. 271, 121104. https://doi.org/10.1016/j.envres.2025.121104 (Appendix I)

3.2 Landscape-level assessment of spray drift – A virtual experiment using the Droplet and Atmospheric Dispersion drift (DAD-drift) model

The second research article compares spray drift deposition predictions from three previously published algorithms, each employing a different spatial representation of the arrangement of application and non-target areas, against results from the DAD-drift model. This comparison is performed across increasingly complex landscapes (Hypothesis 2.1 and 2.2). A meta-modeling analysis is conducted to identify key drivers of spray drift at the landscape scale using multiple linear regression on deposition data calculated by DAD-drift (Hypothesis 3).

Fuchs, M.D., Gebler, S., Lorke, A., 2025. Landscape-level assessment of spray drift – A virtual experiment using the Droplet and Atmospheric Dispersion drift (DAD-drift) model. Environ. Model. Softw. 189, 106455. https://doi.org/10.1016/j.envsoft.2025.106455 (Appendix II)

3.3 Evaluating Landscape-Level Pesticide Exposure from Spray Drift - A Modeling Study in an Agriculture-Dominated Watershed Using SWAT+ and DAD-Drift

The third research article implements the DAD-drift model within a high-resolution SWAT+ eco-hydrological model of the agriculturally dominated Funne catchment in Germany. This model is built entirely on publicly available geospatial and environmental data, including soil, land-use, topographic, and climate datasets. A global sensitivity analysis following the Sobol' approach was performed to identify the model parameters with the strongest influence on modelled hydrology. The model hydrology was calibrated based on observed discharge at the Selm-Ondrup measuring station (Hypothesis 4). A realistic pesticide application scheme was implemented in order to compare predicted environmental concentrations with and without spray drift deposition calculated by DAD-drift (Hypothesis 5.1 and 5.2). Uncertainties in predicted environmental concentrations were assessed across an ensemble of 20 hydrological parameter sets (Hypothesis 6)

Fuchs, M.D., Gebler, S., Lorke, A., 2026. Evaluating landscape-level pesticide exposure from spray drift: A modeling study in an agriculture-dominated watershed using SWAT+ and DAD-Drift. Environ. Pollut. 397, 128031. https://doi.org/10.1016/j.envpol.2026.128031 (Appendix III)

4 Discussion

This chapter presents an integrated discussion of the findings shown in the three research articles described in Chapter 3. The discussion progresses from model development to landscape-scale application and uncertainty analysis. Section 4.1 establishes the foundation by evaluating the development and performance of the DAD-drift model (Research Question 1). Section 4.2 then builds on this foundation by exploring how spatial simplifications influence spray drift predictions (Research Question 2). Section 4.3 examines the underlying drivers of spray drift at the landscape scale (Research Question 3). Subsequently, the focus shifts from isolated processes to system integration. Section 4.4 illustrates the impact of spray drift on the dynamics of pesticides when integrated into a catchment-scale eco-hydrological model (Research Questions 4 and 5). Section 4.5 extends this analysis by addressing the role of hydrological uncertainty in shaping predicted environmental concentrations (Research Question 6). Finally, Sections 4.6 and 4.7 reflect on methodological limitations and outline avenues for future research. Collectively, these sections progress from the development of methods to conducting applied fate assessments, thereby integrating the three studies into a unified framework for comprehending the fate of pesticides at the landscape scale.

4.1 Advancing Mechanistic Spray Drift Modeling at the Landscape Scale

Spray drift is a critical yet underrepresented transport pathway in landscape-scale pesticide fate assessment, while other relevant pathways, such as surface runoff, subsurface runoff, tile drainage flow, and leaching, are well established in existing modeling frameworks. As previously described, the frequently used eco-hydrological SWAT model as well as others do not account appropriately for pesticide transport via spray drift and available spray drift modeling tools are limited in their scope. As there was no mechanistic spray drift model for boom applications capable of predicting spray drift at the landscape scale, the DAD-drift model was developed specifically to address this gap, with the key goals of (i) computational efficiency, (ii) physical realism, (iii) accurate spatial representation, and (iv) landscape-scale spray drift prediction.

The atmospheric dispersion approach was chosen for DAD-drift as it allows spray drift predictions over large distances while being computationally efficient. Development was heavily inspired by the RTDrift model (Lebeau et al., 2011) and OML-SprayDrift (Løfstrøm et al., 2013), however some core innovations were included. A mechanistic droplet model was implemented to predict droplet trajectory based on aerodynamic drag and droplet evaporation.

A micrometeorological model was implemented to represent indirect droplet interactions via a feedback loop in local air temperature and humidity. Furthermore, the two-dimensional tilting plume approach was replaced by a three-dimensional Gaussian puff approach. The model requires droplet size distributions (DSD) as direct input and therefore allows for flexible application of different spraying technologies and techniques. A geodata interface was integrated into DAD-drift to allow for direct calculation of spray drift deposition at the landscape scale based on field raster data at 1m resolution. Finally, DAD-drift was programmed as a lightweight standalone model which allows for ease of integration with other modeling approaches.

The model was parameterized and evaluated against two field trial studies, both conducted on arable test plots under controlled field-trial conditions in the United States (Brain et al., 2019; Perine et al., 2021). These studies were selected based on the following criteria: (i) recent publication (after 2015), (ii) state-of-the-art experimental design (i.e., steel disk samplers), (iii) ground application with boom sprayers on bare soil or short vegetation, (iv) large edge-of-field distance, (v) use of different spray nozzle types, and (vi) detailed information on the application procedure and weather conditions (Section 2.8.2, Appendix I). To avoid overfitting each of the seven application scenarios with its own optimal set of dispersion parameters, a single parameter set for the two Gaussian puff dispersion parameters (horizontal and vertical standard deviations) was determined and applied to all trials (Section 2.8.2, Appendix I). Model evaluation resulted in an overall R^2 value of 0.931, with R^2 values of 0.930 and 0.926 for study 1 and study 2, respectively (Table 2, Appendix I).

The DAD-drift model demonstrated robust performance under various conditions, including environmental conditions (e.g., temperature, humidity, wind speed) and spray nozzle types ranging from fine to ultra-coarse DSD. Notably, the model evaluation revealed no systematic bias in simulated deposition rates at distances up to 122 m, the furthest distance included in the field trials (Figure 4, Appendix I). This is in contrast to earlier atmospheric dispersion models such as the RTDrift model which significantly underpredicted spray drift deposition beyond 20 meters from the field edge (Lebeau et al., 2011). This supports Hypothesis 1.1, which postulates that incorporating a mechanistic droplet model enhances the accuracy of atmospheric dispersion approaches over extended downwind distances.

Employing a three-dimensional Gaussian puff approach proved adaptable to a wide range of wind speeds and atmospheric conditions, demonstrating that the enhanced physical representation improves model parametrization and performance, thereby supporting Hypothesis 1.2. Taken together, the successful evaluation up to 122 meters confirms that DAD-drift is capable to extent the scope of spray drift predictions beyond the field scale. The

model's computational efficiency and its capacity to process raster-based inputs render it particularly well-suited for landscape-level assessments. These assessments include the entry of drift into surface waters and deposition on non-target habitats, such as neighboring fields, protected areas, and urban zones. The DAD-drift model is the first mechanistic spray drift model for boom application designed for landscape-scale use, and it fills a critical methodological gap in spatially explicit pesticide exposure modeling. Building on this, attention now turns to the role of spatial assumptions, specifically examining how simplified representations of the arrangement of application and non-target areas can shape spray-drift predictions and influence subsequent modeling outcomes.

4.2 How Spatial Simplifications Influence Spray Drift Modeling Outcomes

Due to the lack of suitable tools for predicting spray drift at the landscape scale and the need to represent this transport pathway in modeling approaches, authors have incorporated spray-drift curves into landscape-scale eco-hydrological models using simplified spatial representations of the relative position between application and non-target areas (i.e., surface waters) (Holvoet et al., 2008b; Padovani et al., 2004; Winchell et al., 2018; Zhang et al., 2018). A virtual experiment was conducted in order to assess the impact of such simplified spatial representations on predicted spray drift deposition at different levels of landscape complexity, by comparing spatially explicit DAD-drift predictions against three previously published spatial algorithms.

The three algorithms differ primarily in how they represent application areas and determine the receiving surface waterbody (Figure 2, Table 1, Appendix II). The first algorithm assumes a square application area. It predicts the surface area of the receiving surface waterbody based on stream width and the length of the square field. The deposition rate is integrated across the stream width based on the edge-of-field distance (Holvoet et al., 2008b). The second algorithm makes use of a circular field representation, which is projected in wind direction onto the surface water to determine the receiving surface area. The deposition rate is determined based on the shortest distance between the application area and surface waterbody (Zhang et al., 2018). The third algorithm also makes use of a circular field representation, which is buffered into multiple distance zones. For each of these zones the receiving surface area of the receiving surface waterbody as well as the deposition rate is determined individually (Winchell et al., 2018).

The results of the virtual experiment showed that predicted spray-drift deposition across the different spatial representations varied by approximately one order of magnitude,

referring here to total deposition mass on the surface waterbody (Figure 6, Appendix II). Differences between the methods increased with the level of landscape complexity and were largest for the most complex real-world scenarios (Figure 5, Appendix II). Because all four methods were evaluated under identical application and environmental conditions, these differences can be attributed directly to their underlying spatial representations. Therefore, the results strongly support Hypothesis 2.1, which states that different spatial representations of the arrangement of application areas and non-target areas lead to significantly different deposition predictions under identical landscape organizations.

While the DAD-drift model is spatially fully distributed and able to directly link the spray drift emissions from each unit of application area to each unit of non-target area, the simplified algorithms are unable to provide this level of detail. These algorithms are sensitive to factors such as the distance between the application area and the surface waterbody, the shape of the application area, and the flow path of the waterbody, with each algorithm reacting differently to these factors. Such differences not only influence the total amount of pesticide depositions but also the spatial distribution of spray drift depositions within the landscape. This potentially leads to differences in the assessment of the criticality of specific application areas depending on the spatial organization and algorithm used, which is of high relevance when spray drift predictions are used in subsequent modeling steps, such as pesticide fate modeling (Holvoet et al., 2008b; Padovani et al., 2004; Schönenberger et al., 2022; Winchell et al., 2018; Zhang et al., 2018) or ecotoxicological effect modeling (Schad and Schulz, 2011).

The authors of the first algorithm (Holvoet et al., 2008b) concluded that the contributions of spray drift losses to the total pesticide losses are of minor importance, while the authors of the second algorithm (Zhang et al., 2018) summarized that spray drift contributes significantly to the annual in-stream pesticide mass loadings. The authors of the third algorithm (Winchell et al., 2018) concluded that incorporation of spray drift predictions based on increasingly site-specific data combined with the SWAT model accurately predicted observed pesticide concentrations. These findings align with the results of this virtual experiment where the first algorithm resulted in the lowest spray drift deposition and the second algorithm resulted in the highest spray drift deposition (Figure 6, Appendix II).

The virtual experiment demonstrated that the different spatial representations produce substantially different levels of spray drift depositions. As outlined above, these differences are consistent with the divergent higher-level outcomes reported in the original studies (Holvoet et al., 2008b; Winchell et al., 2018; Zhang et al., 2018). It therefore remains unclear whether those studies would have reached the same conclusions had alternative spatial representations been used. Overall, the results support Hypothesis 2.2, demonstrating that

variations in spatial representation are propagated through subsequent hydrological or ecological models, thereby influencing their results. This thesis is among the first to systematically quantify the errors introduced by spatial simplifications in spray drift modeling. It demonstrates that such assumptions can substantially alter predicted depositions. This finding underscores that spatial representation, alongside the magnitude of drift, is a pivotal source of uncertainty in landscape-scale risk assessments. Against this background, the next step is to examine which drivers most strongly influence spray drift at landscape scale, and how their importance shifts compared to field-scale determinants.

4.3 Identification of Key Spray Drift Drivers at the Landscape Scale

The DAD-drift model demonstrated consistent and understandable model behavior when used to predict spray drift deposition at the field scale. The sensitivity analysis (Section 3.3, Figure 7, Appendix I) revealed that model outputs were most responsive to the variables identified as influential in literature. These are the droplet size distribution (DSD) (De Cock et al., 2017; Felsot et al., 2010; Lebeau et al., 2011; Thompson and Ley, 1983), boom height (Nuyttens et al., 2007a; Thompson and Ley, 1983), wind speed, atmospheric turbulence, and variables controlling the evaporation rate of droplets such as temperature and humidity (Thompson and Ley, 1983). These findings support the robustness of DAD-drift at the field scale and provide confidence in its applicability to the more complex landscape scale.

A second virtual experiment was conducted to explore the key drivers of spray drift deposition at the landscape scale using DAD-drift. The model was applied to five application areas for a wide range of environmental conditions (i.e., temperature, humidity, wind speed, wind direction) with a radius of 1 km around the application areas determining relevant non-target areas. Spray drift depositions determined for all areas were used in a multiple linear regression (MLR) analysis to identify dominant spray drift drivers (Section 2.3.3, Appendix I). Several of the known influential variables at the field scale were also found relevant at the landscape scale. The DSD as a result of the type of spray nozzle was the most influential variable at the landscape scale (Table 4, Appendix II). Notably, while DSD consistently emerged as the most influential driver, the DSD descriptor (i.e., DV01, DV05, V50, V100, V150, V200) selected as the strongest predictor differed depending on whether the model described deposition on the application area or on non-target areas. This is consistent with the literature which does not have a clear consensus on which parameter of the DSD best describes spray drift behavior (Felsot et al., 2010; Nuyttens et al., 2007a, 2007b). The distance between application and non-target areas was among the most relevant predictors of spray-

drift deposition at the landscape scale. At closer distances from the application area environmental factors such as wind speed, temperature and humidity retained their influence as expected from field scale experiments.

Substantial differences in spray drift behavior emerge with increasing transport distances. The performance of the model was enhanced when the deposition data were stratified into distance classes, thereby reflecting shifts in the influence of key environmental drivers (Table S5, Appendix IV). Near application areas, higher wind speeds enhance drift by transporting droplets horizontally and reducing evaporation time. This pattern is well-established at the field scale. At greater transport distances, however, this relationship reverses, as stronger winds disperse and dilute the plume, thereby reducing the deposition rate at any given non-target area. Temperature and humidity show a similar distance-dependent effect. High temperatures and low humidity accelerate evaporation, creating smaller droplets that travel greater distances. As a result, deposition that would occur close to the application area is shifted to greater distances, reversing the apparent influence of these variables when comparing near-field and far-field behavior.

These findings corroborate Hypothesis 3, which states that the variables responsible for spray drift at the field scale persist in exerting influence at the landscape scale, albeit with alterations to their effects caused by atmospheric dynamics and spatial structure. The identification of distance-dependent shift in driver importance offers a novel perspective on drift exposure beyond the field-versus-landscape comparison, and underscores the necessity for stratified, scale-aware modeling approaches. Such approaches also provide opportunities to refine exposure mitigation strategies by explicitly accounting for how key environmental and operational variables driving drift behave differently across distances. Building on these insights, the next step is to examine how spray drift contributes to overall pesticide dynamics at the landscape scale, using an integrated eco-hydrological model.

4.4 Incorporating Spray Drift into Catchment Scale Pesticide Fate Modeling

The coupling of DAD-drift with a high-resolution SWAT+ eco-hydrological model of the agriculturally dominated Funne catchment represents, to our knowledge, the first implementation of spatially explicit spray drift deposition into a fully coupled catchment-scale model. While SWAT+ simulates key pesticide transport pathways (i.e., surface and subsurface runoff, leaching, subsurface drainage), it lacks any representation of spray drift. Therefore, the DAD-drift model was integrated into the modeling framework to simulate spray drift deposition

across the catchment. Model development was entirely based on publicly available data (Section 2.2.3, Appendix III), and for a correct implementation, modifications of the SWAT+ source code (Version 61.0.1) were necessary to resolve issues related to compilation, pesticide simulation, pesticide mass input, and channel width representation (Appendix VII).

The model incorporates a realistic five-year crop rotation derived from field block data (Geobasis NRW, 2024), ensuring spatially and temporally explicit simulation of agricultural practices (Section 2.2.4, Appendix III). Plowing and field cultivation were integrated where agronomically appropriate, and red clover was added as a legume cover crop where fields would otherwise remain bare during winter. Two fungicides (F1, F2) and five herbicides (H1-H5) were selected as relevant active ingredients based on annual monitoring reports of the Stever catchment (Lammers, 2021, 2020, 2019), with physio-chemical properties taken from publicly available registration dossiers. Application windows were derived from label-specified crop growth stages and linked to realistic calendar dates, from which potential application dates were determined using a forward-oriented pesticide application timer similar to Bach et al. (2017).

The catchment hydrology was calibrated and validated against observed daily discharge at the Selm-Ondrup station, following a multi-step approach in which a one-at-a-time sensitivity analysis identified influential parameters and a subsequent global sensitivity analysis after Sobol' (1990) reduced the parameter space to the most relevant variables for sampling (Section 2.3, Appendix III). Discharge predictions were evaluated using Nash-Sutcliffe efficiency (NSE), the percent bias (PBIAS), and the Kling-Gupta efficiency (KGE) (Gupta et al., 2009; Moriasi et al., 2007). With NSE and KGE values of up to 0.79 and 0.86, respectively, and PBIAS below 8.7, the model performance was "very good" according to Moriasi et al. (2007) for the parameterization period, and overall "good" during validation. An ensemble of 20 high-performing parameter sets was selected to represent catchment hydrology. These results support Hypothesis 4, demonstrating that publicly available datasets provide sufficient resolution to develop a spatially detailed eco-hydrological model capable of accurately predicting catchment hydrology.

To assess the role of spray drift at the landscape scale, two model configurations were compared. The base model setup simulated pesticide transport via surface and subsurface runoff, leaching and subsurface drainage via the default SWAT+ routines. The drift model setup additionally incorporated spatially explicit spray drift depositions predicted with the DAD-drift model, using the previously calibrated TeeJet XR11003 nozzle scenario (Appendix I) with substance-specific inputs and date-specific weather conditions, assuming worst-case conditions with no buffer zones or drift reduction technology. The DAD-drift simulations

produced spatially explicit deposition maps for each application event. Drift deposition onto the channel network was transferred to SWAT+ via point sources for each channel segment, while terrestrial drift deposition was transferred using the input logic for application events. This setup enables a direct cross-comparison of atmospheric and hydrological transport pathways under realistic agricultural scenarios.

The implementation of the DAD-drift model into a high-resolution SWAT+ model of the Funne catchment, clearly indicates that spray drift deposition is of high relevance for pesticide exposure at the landscape scale. For all simulated substances additional concentration peaks at the outflow of the simulated catchment could be observed (Figure 3, Appendix III). Additionally, maximum and 90th percentile predicted environmental concentrations (PECmax & PEC90) were increased by 10% up to multiple orders of magnitude from the base setup to the drift setup (Figure 4, Appendix III). The impact of spray drift on exposure dynamics strongly depends on the physio-chemical properties, with less mobile substances (high soil adsorption coefficient) being more influenced than mobile substances, which are transported to the channel network via surface and subsurface runoff as well as subsurface drainage (Figure 3, Appendix III). Overall, these results strongly support Hypothesis 5.1, which posits that including spray drift leads to observable concentration peaks at the catchment outflow shortly after application.

The inclusion of spray drift deposition into the SWAT+ model has effects on the pesticide transport dynamics beyond the emergence of concentration peaks at the time of application due to immediate deposition onto the surface water. The analysis of the individual transport pathways (i.e., surface and subsurface runoff, leaching, subsurface drainage) showed altered behavior in surface and subsurface runoff as well as subsurface drainage when comparing the base setup to the drift setup (Figure S3, Appendix VI). These changes provide directional support for Hypothesis 5.2, which proposes that spray drift alters the distribution of pesticide mass across the landscape and thereby influences the relative importance of different transport pathways. However, the practical relevance of these altered dynamics appears limited, as the time series of predicted environmental concentrations were not substantially affected aside from the additional drift-induced peaks (Figure 3, Appendix III). These results highlight that, while spray drift alters transport dynamics, the robustness of exposure predictions ultimately depends on the representation of hydrological processes. The following section therefore addresses the influence of hydrological uncertainty on landscape-scale pesticide fate.

4.5 Hydrological Uncertainty and Its Influence on Landscape-Scale Pesticide Dynamics

Hydrological parameterization is a major source of uncertainty in landscape-scale pesticide fate assessment (Fohrer et al., 2014; Holvoet et al., 2005), as most pesticide transport processes are a direct function of hydrological flow processes. Yet the simulation of such hydrological processes is constrained by the limited availability of observational data for model calibration and structural simplifications in eco-hydrological models such as SWAT+. These include the discretization of the landscape into static hydrological response units (HRU), uniform soil profiles per HRU, and limited representation of hydrological connectivity between landscape elements. Hence, real-world flow pathways determined by soil heterogeneity, topography, land use, and artificial structures (e.g., tile drainage, pipes, ditches) are imperfectly captured by models.

Compounding these structural model limitations is the practice of model calibration based only on discharge at the catchment outlet. While this is mostly driven by data limitations and stream discharge is a necessary calibration target, integrative effects across the landscape do not allow for any insights into water distribution across different flow pathways. Consequently, equifinality arises not only from limited observational constraints but also from parameter correlation, where compensatory interactions among sensitive parameters allow very different parameter combinations to reproduce the observed hydrograph equally well while representing fundamentally different hydrological realities (Beven, 2006). Despite this, many SWAT-based pesticide assessments rely on a single “best” parameterization without explicit uncertainty analysis (Abbaspour et al., 2007). This is highlighted by the ensemble of 20 parameter sets selected to represent the hydrology of the Funne catchment in the SWAT+ model. The performance metrics Nash-Sutcliffe efficiency (NSE), Kling-Gupta efficiency (KGE), and percent bias (PBIAS), indicate that all 20 parameter sets are similarly capable of predicting the hydrological conditions within the simulated catchment (Table S8, Appendix VI). However, despite similar overall performance the spread amongst the 20 simulated hydrographs (Figure S2, Appendix VI) shows that these parameter sets produce notably different discharge dynamics. This indicates that water is distributed differently across surface runoff, subsurface runoff, leaching, and subsurface drainage, and that equally good discharge predictions can reflect different internal flow dynamics.

These hydrological uncertainties have a direct effect on the predicted environmental concentration (PEC) when simulating pesticide transport in the SWAT+ model. Uncertainties in modeled pesticide fate can be observed in the PEC_{90} values, the PEC_{max} values, the chemograph at the catchment outflow, and the pesticide masses transported via the different

pathways. The analysis of pesticide transport via different pathways clearly indicates large variances in the simulated transport via surface and subsurface runoff as well as subsurface drainage for the ensemble of 20 hydrological parametrizations (Figure S3, Appendix VI). These differences across the transport pathways are then reflected in the simulated concentration time series at the catchment outlet where significant uncertainty in PEC values can be observed (Figure 3, Appendix III). These uncertainties can be seen more clearly in the PEC_{90} boxplots where a very large spread can be observed for the substances H1, H2 and H5 and in the PECmax boxplots where a similar spread can be observed for the substances F2, H2, and H5 (Figure 4, Appendix III).

This thesis employs an ensemble-based approach of hydrological parameterization to demonstrate how equifinality in catchment hydrology translates directly into uncertainty in pesticide fate predictions. This addresses a significant shortcoming in pesticide modeling, where deterministic approaches tend to obscure the actual variability of exposure. The findings offer substantial evidence in support of Hypothesis 6, indicating that predicted environmental concentrations exhibit significant sensitivity to hydrological parameterization, with the magnitude of this sensitivity varying across substances. It is imperative to note that this sensitivity arises not only from differences in the magnitude and timing of total discharge but also from contrasting distributions of water across runoff, drainage, and leaching pathways. These pathways govern when and how pesticides are transported. Moreover, the findings highlight the inadequacy of relying on a single calibrated parameter set and emphasize the necessity of explicitly addressing hydrological uncertainty through ensemble-based approaches to capture the full uncertainty in pesticide fate predictions.

4.6 Limitations of the Study

While this thesis provides substantial contributions to the mechanistic modeling of spray drift and its integration into catchment-scale pesticide exposure assessments, several methodological and structural limitations must be acknowledged.

The limitations of the DAD-drift model have been described in great detail in Section 4.3 of Appendix I. However, most relevant is the inability of DAD-drift to simulate drifting droplets being intercepted by plant canopies. This is a technical limitation of the atmospheric dispersion approach at the core of the model. The missing interception by vegetation could potentially lead to overestimated predictions of spray drift deposition at the landscape scale as spray drift transport would be simulated downwind of the application area without considering mitigating processes. However, it is not clear whether this assumption represents

a true worst-case scenario, since plant canopies may induce vertical displacement of spray droplets, potentially increasing long-range spray drift. Findings by Isemer et al. (2024) show that drift capture is highest in the front rows and drops off considerably thereafter, even for porous canopy structures, which lends some support to this possibility. Nevertheless, the magnitude and practical relevance of such vertical displacement have not yet been conclusively demonstrated.

These limitations of DAD-drift are compounded by additional constraints when the model is integrated into the catchment-scale modeling framework. Due to the semi-distributed nature of SWAT+, the model is limited in its ability to represent actual hydrological connectivity. In order to achieve manageable model complexity many pesticide-related processes need to be simplified. The two most relevant processes concerning simplification are pesticide wash-off from the foliage and pesticide transport via the stream network. The latter was addressed by disabling uncertain and oversimplified processes within SWAT+, which ensured that the model operated under the worst-case assumption that the entire pesticide mass is transported downstream. The former remained unaddressed in this thesis, with triggering wash-off after 2.54 mm (0.1 inch) precipitation threshold being a substantial oversimplification of the process, as wash-off was found to follow first-order kinetics (Dang et al., 2016; Potter et al., 2011). This may reduce the accuracy of pesticide transport simulations, as wash-off after low-intensity precipitation might be underestimated, while wash-off after repeated high-intensity precipitation might be overestimated.

The modeling framework developed in this thesis including spray drift, is in principle transferable to any catchment. However, the application in this study was limited to the Funne catchment. Specific findings, such as parameter sensitivities and calibrated parameter sets, may be shaped by the catchment's particular characteristics (i.e., flat topography, intensive agriculture, and artificial drainage). These features exert a significant influence on hydraulic connectivity and the partitioning of flow pathways, which in turn govern the dynamics of pesticide transport. Applying the framework to other landscapes could alter the relative importance of transport processes, particularly in regions with steeper topography, different drainage infrastructure, or more heterogeneous land use. Thus, while the Funne case study demonstrates the framework's utility, extending it to other catchments is required for testing of its robustness and broadening its applicability.

4.7 Directions for Future Research

Building upon the insight gained in this thesis, several promising avenues for future research emerge, particularly in relation to the DAD-drift model and the modeling framework complementing the eco-hydrological SWAT+ model with spray drift predictions of DAD-drift. These research directions aim to improve model performance, advancing the understanding of pesticide fate, improving environmental risk assessment and furthering the regulatory framework for pesticide registration.

The DAD-drift model itself offers a rich set of opportunities to further improve the representation of spray drift. On a basic level the model could be improved (i) by increasing the precision of the predicted droplet trajectories, (ii) by incorporating droplet speed distribution, (iii) by extending the representation of the mixture from the current two-phasic (water-a.i.) approach to a multi-phasic approach considering spray adjuvants, and (iv) by implementing an air entrainment model representing interaction between the air and the spray jet.

In addition to targeted model improvements, future work should broaden the empirical basis of DAD-drift by validating its performance across more diverse field conditions. Such expanded datasets would not only strengthen confidence in model robustness but also provide the foundation needed to develop regionally parameterized versions of DAD-drift, particularly since it meets the criteria proposed by Holterman et al. (2025) for a unified European spray drift model. This could extend the model's applicability beyond case studies and establish it as a reference tool for regulatory and scientific assessments.

At the landscape scale, the potential benefits of testing the integrated modeling framework in catchments with dense, high-resolution monitoring networks are significant. These settings would not only enable more rigorous calibration and evaluation but also provide empirical data to benchmark scenario simulations and retrospective exposure assessments. Consequently, the framework has the potential to evolve from a proof-of-concept demonstrated in the Funne catchment to a widely applicable tool for pesticide fate analysis under diverse environmental conditions.

In its current form, the integrated Funne catchment model provides a ready-to-use platform for a wide range of future research applications, as it enables further analyses without additional hydrological parameterization or geodata preparation. Firstly, the model could be coupled with ecotoxicological effect modeling approaches in order to evaluate the effect of spray drift on different non-target species. Secondly, this modeling framework could be employed in order to evaluate the effectiveness of spray drift mitigation measures such as

buffer zones and spray reduction nozzles in a systematic manner. Thirdly, a critical source area (CSA) analysis could be conducted to identify which application areas within the catchment contribute most to pesticide mass outflow. Using an ensemble-based approach for the CSA analysis would additionally allow assessing how hydrological parametrization influences the criticality of individual application areas. Finally, a detailed sensitivity analysis of application timing could be performed using the Funne catchment model. By comparing fixed application dates, random dates within the allowed application window, and different pesticide application timer (PAT) algorithms (e.g., with or without wind constraints), valuable insights into how application timing influences pesticide fate could be gained.

5 Conclusion

This thesis addressed several long-standing methodological and conceptual limitations in pesticide fate modeling, particularly in the treatment of spray drift at the landscape-scale where spray drift was often represented in overly simplified ways or completely ignored. This led to a systematic misrepresentation of exposure levels in environmental risk assessment. Conversely, spatial variability was frequently reduced to abstract geometric representations, and hydrological uncertainties were rarely quantified. These limitations introduced notable uncertainty in our understanding of the movement of pesticides through agricultural landscapes and reduced the reliability of predictions that inform management and regulation.

In light of these challenges, this thesis developed and implemented a series of mechanistic, spatially explicit, and uncertainty-aware approaches. These approaches aimed to improve landscape-scale pesticide assessment. Among these contributions, the Droplet and Atmospheric Dispersion drift (DAD-drift) model is of particular significance. This model is the first mechanistic spray drift model for boom application that was specifically designed to operate efficiently at the landscape-scale. The integration of droplet-scale physics with atmospheric dispersion and micrometeorological feedback enables DAD-drift to make spatially explicit, high-resolution spray drift predictions, thus addressing the limitations of empirical or curve-based approaches. Evaluation against recent field experiments confirmed its robustness and reliability across different spray nozzles, meteorological conditions, and downwind distances, demonstrating its applicability to a wide range of agricultural contexts.

Building on this development, the thesis explored the consequences of how spray drift is represented in different modeling approaches. A virtual experiment demonstrated that simplified spatial assumptions can alter the predicted deposition by an order of magnitude, especially in complex landscapes. This finding shifts the perspective from considering only drift magnitude to recognizing that the spatial representation itself is a key source of uncertainty. Complementary meta-modeling analysis revealed that environmental drivers, such as wind speed, humidity, and temperature, have distance-dependent effects on deposition. These insights underscore the necessity for scale-aware modeling strategies that extend beyond field-scale heuristics and explicitly consider landscape heterogeneity.

The incorporation of DAD-drift into a high-resolution SWAT+ eco-hydrological model represented a substantial advancement in the representation of spray drift at the catchment scale. This coupled framework enables the simultaneous simulation of atmospheric and hydrological transport pathways within a catchment model and was completely parameterized with publicly available data. The application of this model to the agriculturally dominated Funne

catchment demonstrated that spray drift can substantially alter predicted environmental concentrations, often increasing peaks and percentiles by multiple orders of magnitude. Spray drift emerged as a predominant factor influencing the exposure of less mobile substances, which otherwise exhibited minimal transport. This finding underscores the broader significance of incorporating atmospheric pathways into pesticide fate assessment.

In general, the thesis explicitly addressed the role of hydrological uncertainty in the prediction of pesticide fate. The use of an ensemble-based calibration approach of the catchment hydrology has demonstrated how equifinality in discharge modeling propagates into pesticide fate outcomes. Specifically, predicted environmental concentrations varied by orders of magnitude across hydrological parameterizations that performed equally well. This variability arises because equally well-performing calibrations can reflect different underlying hydrological behaviors that affect pesticide transport. The ensemble-based approach captures this variability and therefore offers a more transparent basis for risk assessment.

Overall, this work established a novel and transferable framework for assessing spray drift and pesticide fate at the landscape scale. The findings indicate that spray drift is not a marginal process but can be a central determinant of exposure. In addition, the framework supports the evaluation of mitigation measures such as buffer strips or drift-reducing technologies. Moreover, the results underscore the profound impact of spatial assumptions on model outcomes. The study emphasizes the necessity of accounting for hydrological uncertainty to ensure realistic pesticide fate assessments, highlighting the need to move beyond the conventional reliance on single calibrated parameter sets. Although the empirical focus was on a single case study watershed, the methods and insights are applicable to agricultural systems and regulatory contexts more broadly. Furthermore, this thesis demonstrates how mechanistic modeling, coupled with the use of publicly available data and the explicit treatment of uncertainty, can meaningfully improve the scientific basis for evaluating the ecological risks of pesticide use.

By addressing these gaps, the work not only filled important methodological voids but also provided the basis for novel research, policy, and practical applications. By providing a framework that unites atmospheric and hydrological processes, it offers a foundation for next-generation risk assessments that more accurately reflect the complexity of agricultural landscapes and better inform strategies to mitigate pesticide impacts on the environment.

References

Abbaspour, K.C., Yang, J., Maximov, I., Siber, R., Bogner, K., Mieleitner, J., Zobrist, J., Srinivasan, R., 2007. Modelling hydrology and water quality in the pre-alpine/alpine Thur watershed using SWAT. J. Hydrol. 333, 413–430. https://doi.org/10.1016/j.jhydrol.2006.09.014

Arnold, J.G., Srinivasan, R., Muttiah, R.S., Williams, J.R., 1998. Large Area Hydrologic Modeling and Assessment Part I: Model Development. JAWRA J. Am. Water Resour. Assoc. 34, 73–89. https://doi.org/10.1111/j.1752-1688.1998.tb05961.x

Bach, M., Guerniche, D., Thomas, K., Trapp, M.M., Kubiak, R., Hommen, U., Klein, M., Reichenberger, S., Pires, J., Preuß, T., 2017. Bewertung des Eintrags von Pflanzenschutzmitteln in Oberflächengewässer – Runoff, Erosion und Drainage (GERDA – GEobased Runoff, Erosion and Drainage risk Assessment for Germany): Abschlussbericht, German Federal Environment Agency, Dessau. Dessau-Roßlau, Germany.

Beltman, W.H.J., Horst, M.M.S. Ter, Adriaanse, P.I., Jong, A. De, 2006. Manual of FOCUS_TOXSWA version 2.2.1. Alterra, Wageningen UR, Wageningen, Netherlands.

Beulke, S., Brown, C.D., Jarvis, N.J., 2001. Macro: A Preferential Flow Model to Simulate Pesticide Leaching and Movement to Drains, in: Modelling of Environmental Chemical Exposure and Risk. pp. 117–132.

Beven, K., 2006. A manifesto for the equifinality thesis. J. Hydrol. 320, 18–36. https://doi.org/10.1016/j.jhydrol.2005.07.007

Bicknell, B.R., Imhoff, J.C., Kittle, J.L., Donigian, A.S., Johanson, R.C., 1997. Project Summary Hydrological Simulation Program — FORTRAN User ' s Manual for Version 11. U.S. Environmental Protection Agency, Athens, GA, USA.

Brain, R., Goodwin, G., Abi-Akar, F., Lee, B., Rodgers, C., Flatt, B., Lynn, A., Kruger, G., Perkins, D., 2019. Winds of change, developing a non-target plant bioassay employing field-based pesticide drift exposure: A case study with atrazine. Sci. Total Environ. 678, 239–252. https://doi.org/10.1016/j.scitotenv.2019.04.411

Brühl, C.A., Bakanov, N., Köthe, S., Eichler, L., Sorg, M., Hörren, T., Mühlethaler, R., Meinel, G., Lehmann, G.U.C., 2021. Direct pesticide exposure of insects in nature conservation areas in Germany. Sci. Rep. 11, 1–10. https://doi.org/10.1038/s41598-021-03366-w

Bundschuh, M., Goedkoop, W., Kreuger, J., 2014. Evaluation of pesticide monitoring strategies in agricultural streams based on the toxic-unit concept - Experiences from long-term measurements. Sci. Total Environ. 484, 84–91. https://doi.org/10.1016/j.scitotenv.2014.03.015

Capelle, C. van, Schrader, S., Brunotte, J., 2012. Tillage-induced changes in the functional diversity of soil biota - A review with a focus on German data. Eur. J. Soil Biol. 50, 165–181. https://doi.org/10.1016/j.ejsobi.2012.02.005

Carsel, R.F., Mulkey, L.A., Lorber, M.N., Baskin, L.B., 1985. The Pesticide Root Zone Model (PRZM): A procedure for evaluating pesticide leaching threats to groundwater. Ecol. Modell. 30, 49–69. https://doi.org/10.1016/0304-3800(85)90036-5

Centanni, M., Ricci, G.F., Girolamo, A.M. De, Romano, G., Gentile, F., 2023. A review of modeling pesticides in freshwaters: Current status, progress achieved and desirable improvements. Environ. Pollut. 316, 120553. https://doi.org/10.1016/j.envpol.2022.120553

Clothier, B.E., Green, S.R., Deurer, M., 2008. Preferential flow and transport in soil: Progress and prognosis. Eur. J. Soil Sci. 59, 2–13. https://doi.org/10.1111/j.1365-2389.2007.00991.x

Cock, N. De, Massinon, M., Salah, S.O.T., Lebeau, F., 2017. Investigation on optimal spray properties for ground based agricultural applications using deposition and retention models. Biosyst. Eng. 162, 99–111. https://doi.org/10.1016/j.biosystemseng.2017.08.001

Dang, A., Silburn, M., Craig, I., Shaw, M., Foley, J., 2016. Washoff of Residual Photosystem II Herbicides from Sugar Cane Trash under a Rainfall Simulator. J. Agric. Food Chem. 64, 3967–3974. https://doi.org/10.1021/acs.jafc.5b04717

Dubus, I.G., Brown, C.D., Beulke, S., 2003. Sensitivity analyses for four pesticide leaching models. Pest Manag. Sci. 59, 962–982. https://doi.org/10.1002/ps.723

Eurostat, 2025. Agri-environmental indicator - consumption of pesticides [WWW Document]. Eurostat. URL https://ec.europa.eu/eurostat/statistics-explained/index.php?title=Agri-environmental_indicator_-_consumption_of_pesticides&stable=1 (accessed 9.3.25).

Felsot, A.S., Unsworth, J.B., Linders, J.B.H.J., Roberts, G., Rautman, D., Harris, C., Carazo, E., 2010. Agrochemical spray drift; assessment and mitigation—A review*. J. Environ. Sci. Heal. Part B 46, 1–23. https://doi.org/10.1080/03601234.2010.515161

Fohrer, N., Dietrich, A., Kolychalow, O., Ulrich, U., 2014. Assessment of the Environmental Fate of the Herbicides Flufenacet and Metazachlor with the SWAT Model. J. Environ. Qual. 43, 75–85. https://doi.org/10.2134/jeq2011.0382

Frey, M.P., Stamm, C., Schneider, M.K., Reichert, P., 2011. Using discharge data to reduce structural deficits in a hydrological model with a Bayesian inference approach and the implications for the prediction of critical source areas. Water Resour. Res. 47, 1–18. https://doi.org/10.1029/2010WR009993

Gassmann, M., 2021. Modelling the Fate of Pesticide Transformation Products From Plot to Catchment Scale—State of Knowledge and Future Challenges. Front. Environ. Sci. 9, 1–12. https://doi.org/10.3389/fenvs.2021.717738

Geobasis NRW, 2024. Beantragte und als förderfähig festgestellte Teilschläge in NRW als Shape [WWW Document]. URL https://www.opengeodata.nrw.de/produkte/umwelt_klima/bodennutzung/landwirtschaft/LWK-TSCHLAG_EPSG25832_Shape.zip (accessed 7.1.24).

Griesang, F., Decaro, R.A., Santos, C.A.M. dos, Santos, E.S., Lima Roque, N.H. de, Costa Ferreira, M. da, 2017. How Much Do Adjuvant and Nozzles Models Reduce the Spraying Drift? Drift in Agricultural Spraying. Am. J. Plant Sci. 08, 2785–2794. https://doi.org/10.4236/ajps.2017.811188

Gupta, H. V., Kling, H., Yilmaz, K.K., Martinez, G.F., 2009. Decomposition of the mean squared error and NSE performance criteria: Implications for improving hydrological modelling. J. Hydrol. 377, 80–91. https://doi.org/10.1016/j.jhydrol.2009.08.003

Holterman, H.J., Horst, M. ter, Adriaanse, P., 2025. Improving environmental risk assessment of pesticides: the need for advanced spray drift models in EU regulatory framework Exploring modelling approaches for spray drift deposition for downward spraying for use in off-crop exposure assessment. EFSA Support. Publ. 22. https://doi.org/10.2903/sp.efsa.2025.en-9506

Holvoet, K., Gevaert, V., Griensven, A. Van, Seuntjens, P., Vanrolleghem, P.A., 2008a. SWAT developments and recommendations for modelling agricultural pesticide mitigation measures in river basins. Hydrol. Sci. J. 53, 1075–1089. https://doi.org/10.1623/hysj.53.5.1075

Holvoet, K., Griensven, A. van, Gevaert, V., Seuntjens, P., Vanrolleghem, P.A., 2008b. Modifications to the SWAT code for modelling direct pesticide losses. Environ. Model. Softw. 23, 72–81. https://doi.org/10.1016/j.envsoft.2007.05.002

Holvoet, K., Griensven, A. van, Seuntjens, P., Vanrolleghem, P.A., 2005. Sensitivity analysis for hydrology and pesticide supply towards the river in SWAT. Phys. Chem. Earth 30, 518–526. https://doi.org/10.1016/j.pce.2005.07.006

Ippolito, A., Fait, G., 2019. Pesticides in surface waters: from edge-of-field to global modelling. Curr. Opin. Environ. Sustain. 36, 78–84. https://doi.org/10.1016/j.cosust.2018.10.023

Isemer, R., Chapple, A.C., Butler Ellis, M.C., Lane, A.G., O'Sullivan, C.M., 2024. Preliminary investigations into drift capture efficiency of off-field plant canopies, in: Aspects of Applied Biology 148, International Advances in Pesticide Application. Association of Applied Biologists, pp. 263–270.

Jarvis, N.J., 1994. The MACRO model (version 3.1), Technical description and sample simulations. Reports and Dissertations. Department of Soil Science, Swedish University of Agricultural Sciences, Uppsala, Sweden.

Lammers, M., 2021. Kooperation Landwirtschaft und Wasserwirtschaft im Einzugsgebiet der Stevertalsperre. Ein Bericht über die Ergebnisse der Beratung in 2021. Landwirtschaftskammer Nordrhein-Westfalen, Coesfeld, Germany.

Lammers, M., 2020. Kooperation Landwirtschaft und Wasserwirtschaft im Einzugsgebiet der Stevertalsperre. Ein Bericht über die Ergebnisse der Beratung in 2020. Landwirtschaftskammer Nordrhein-Westfalen, Coesfeld, Germany.

Lammers, M., 2019. Kooperation Landwirtschaft und Wasserwirtschaft im Einzugsgebiet der Stevertalsperre: Ein Bericht über die Ergebnisse der Beratung in 2019. Landwirtschaftskammer Nordrhein-Westfalen, Coesfeld, Germany.

Lebeau, F., Verstraete, A., Stainier, C., Destain, M.-F., 2011. RTDrift: A real time model for estimating spray drift from ground applications. Comput. Electron. Agric. 77, 161–174. https://doi.org/10.1016/j.compag.2011.04.009

Leistra, M., Linden, A.M.A. der, Boesten, J., Tiktak, A., Berg, F. den, 2001. PEARL model for pesticide behaviour and emissions in soil-plant systems: description of the processes in FOCUS PEARL v 1.1. 1. Alterra, Wageningen UR, Wageningen, Netherlands.

Løfstrøm, P., Bruus, M., Andersen, H.V., Kjær, C., Nuyttens, D., Astrup, P., 2013. The OML-SprayDrift model for predicting pesticide drift and deposition from ground boom sprayers. J. Pestic. Sci. 38, 129–138. https://doi.org/10.1584/jpestics.D12-064

Lorenz, S., Raja Dominic, A., Heinz, M., Süß, A., Stähler, M., Strassemeyer, J., 2021. Effect of buffer strips on pesticide risks in freshwaters. Crop Prot. 154, 105891.

https://doi.org/10.1016/j.cropro.2021.105891

Luo, Y., Zhang, M., 2009. Managementoriented sensitivity analysis for pesticide transport in watershedscale water quality modeling using SWAT. Environ. Pollut. 157, 3370–3378. https://doi.org/10.1016/j.envpol.2009.06.024

Miller, P., 2014. Spray drift, in: Pesticide Application Methods. Wiley, pp. 337–361. https://doi.org/10.1002/9781118351284.ch12

Moriasi, D.N., Arnold, J.G., Liew, M.W. Van, Bingner, R.L., v, R.D., Veith, T.L., 2007. Model Evaluation Guidelines for Systematic Quantification of Accuracy in Watershed Simulations. Trans. ASABE 50, 885–900. https://doi.org/10.13031/2013.23153

Mottes, C., Lesueur-Jannoyer, M., Bail, M. Le, Malézieux, E., 2014. Pesticide transfer models in crop and watershed systems: A review. Agron. Sustain. Dev. 34, 229–250. https://doi.org/10.1007/s13593-013-0176-3

Nuyttens, D., Schampheleire, M. De, Baetens, K., Sonck, B., 2007a. The influence of operator-controlled variables on spray drift from field crop sprayers. Trans. ASABE 50, 1129–1140. https://doi.org/10.13031/2013.23622

Nuyttens, D., Baetens, K., Schampheleire, M. De, Sonck, B., 2007b. Effect of nozzle type, size and pressure on spray droplet characteristics. Biosyst. Eng. 97, 333–345. https://doi.org/10.1016/j.biosystemseng.2007.03.001

Padilla, L.E., Peranginangin, N., Dunne, J.B., Winchell, M., 2020. Comparison of pesticide concentrations observed in community water systems to predictions from U.S. regulatory aquatic exposure models. J. Environ. Qual. 49, 128–139. https://doi.org/10.1002/jeq2.20035

Padovani, L., Capri, E., Trevisan, M., 2004. Landscape-Level Approach To Assess Aquatic Exposure via Spray Drift for Pesticides: A Case Study in a Mediterranean Area. Environ. Sci. Technol. 38, 3239–3246. https://doi.org/10.1021/es049699p

Perine, J., Anderson, J.C., Kruger, G.R., Abi-Akar, F., Overmyer, J., 2021. Effect of nozzle selection on deposition of thiamethoxam in Actara® spray drift and implications for off-field risk assessment. Sci. Total Environ. 772, 144808. https://doi.org/10.1016/j.scitotenv.2020.144808

Potter, T.L., Truman, C.C., Webster, T.M., Bosch, D.D., Strickland, T.C., 2011. Tillage, Cover-Crop Residue Management, and Irrigation Incorporation Impact on Fomesafen Runoff. J. Agric. Food Chem. 59, 7910–7915. https://doi.org/10.1021/jf201731u

Prechsl, U.E., Bonadio, M., Wegher, L., Oberhuber, M., 2022. Long-term monitoring of pesticide residues on public sites: A regional approach to survey and reduce spray drift. Front. Environ. Sci. 10, 1–13. https://doi.org/10.3389/fenvs.2022.1062333

Rautmann, D., Streloke, M., Winkler, R., 1999. New basic drift values in the Authorization procedure for plant protection products, in: Workshop on Risk Management and Risk Mitigation Measures in the Context of Authorization of Plant Protection Products. Biologische Bundesanstalt fur Land- und Forstwirtschaft, Berlin-Dahlem, Germany, pp. 133–141.

Refsgaard, J.C., Storm, B., 1995. MIKE SHE, in: Singh, V.P. (Ed.), Computer Models of Watershed Hydrology. Water Resources Publications, Highlands Ranch, Colorado, USA, pp. 809–846.

Reichenberger, S., Bach, M., Skitschak, A., Frede, H.G., 2007. Mitigation strategies to reduce pesticide inputs into ground- and surface water and their effectiveness; A review. Sci. Total Environ. 384, 1–35. https://doi.org/10.1016/j.scitotenv.2007.04.046

Rouzies, E., Lauvernet, C., Sudret, B., Vidard, A., 2023. How is a global sensitivity analysis of a catchment-scale, distributed pesticide transfer model performed? Application to the PESHMELBA model. Geosci. Model Dev. 16, 3137–3163. https://doi.org/10.5194/gmd-16-3137-2023

Schad, T., Schulz, R., 2011. Xplicit, a novel approach in probabilistic spatiotemporally explicit exposure and risk assessment for plant protection products. Integr. Environ. Assess. Manag. 7, 612–623. https://doi.org/10.1002/ieam.205

Schönenberger, U.T., Simon, J., Stamm, C., 2022. Are spray drift losses to agricultural roads more important for surface water contamination than direct drift to surface waters? Sci. Total Environ. 809. https://doi.org/10.1016/j.scitotenv.2021.151102

Schulz, R., 2001. Rainfall-induced sediment and pesticide input from orchards into the Lourens River, Western Cape, South Africa: Importance of a single event. Water Res. 35, 1869–1876. https://doi.org/10.1016/S0043-1354(00)00458-9

Sobol', I.M., 1990. On sensitivity estimation for nonlinear mathematical models, Matematicheskoe modelirovanie. Russian Academy of Sciences, Branch of Mathematical Sciences.

Teske, M.E., Bird, S.L., Esterly, D.M., Curbishley, T.B., Ray, S.L., Perry, S.G., 2002. AgDRIFT®: A model for estimating near-field spray drift from aerial applications. Environ. Toxicol. Chem. 21, 659–671. https://doi.org/10.1002/etc.5620210327

Thompson, N., Ley, A.J., 1983. Estimating spray drift using a random-walk model of evaporating drops. J. Agric. Eng. Res. 28, 419–435. https://doi.org/10.1016/0021-8634(83)90134-8

Tudi, M., Daniel Ruan, H., Wang, L., Lyu, J., Sadler, R., Connell, D., Chu, C., Phung, D.T., 2021. Agriculture Development, Pesticide Application and Its Impact on the Environment. Int. J. Environ. Res. Public Health 18, 1112. https://doi.org/10.3390/ijerph18031112

Ulrich, U., Lorenz, S., Hörmann, G., Stähler, M., Neubauer, L., Fohrer, N., 2022. Multiple pesticides in lentic small water bodies: Exposure, ecotoxicological risk, and contamination origin. Sci. Total Environ. 816, 151504. https://doi.org/10.1016/j.scitotenv.2021.151504

Vormeier, P., Schreiner, V.C., Liebmann, L., Link, M., Schäfer, R.B., Schneeweiss, A., Weisner, O., Liess, M., 2023. Temporal scales of pesticide exposure and risks in German small streams. Sci. Total Environ. 871, 162105. https://doi.org/10.1016/j.scitotenv.2023.162105

Wang, R., Yuan, Y., Yen, H., Grieneisen, M., Arnold, J.G., Wang, D., Wang, C., Zhang, M., 2019. A review of pesticide fate and transport simulation at watershed level using SWAT: Current status and research concerns. Sci. Total Environ. 669, 512–526. https://doi.org/10.1016/j.scitotenv.2019.03.141

Warner, W., Zeman-Kuhnert, S., Heim, C., Nachtigall, S., Licha, T., 2021. Seasonal and spatial dynamics of selected pesticides and nutrients in a small lake catchment – Implications for agile monitoring strategies. Chemosphere 281, 130736. https://doi.org/10.1016/j.chemosphere.2021.130736

Winchell, M.F., Pai, N., Brayden, B.H., Stone, C., Whatling, P., Hanzas, J.P., Stryker, J.J., 2018. Evaluation of Watershed-Scale Simulations of In-Stream Pesticide Concentrations from Off-Target Spray Drift. J. Environ. Qual. 47, 79–87. https://doi.org/10.2134/jeq2017.06.0238

Zajícek, A., Fucík, P., Kaplická, M., Liška, M., Maxová, J., Dobiáš, J., 2018. Pesticide leaching by agricultural drainage in sloping, mid-textured soil conditions - The role of runoff components. Water Sci. Technol. 77, 1879–1890. https://doi.org/10.2166/wst.2018.068

Zannetti, P., 1990. Gaussian Models, in: Air Pollution Modeling. Springer US, Boston, MA, pp. 141–183. https://doi.org/10.1007/978-1-4757-4465-1_7

Zhang, X., Luo, Y., Zhang, M., Goh, K.S., 2019. Modeling the Effectiveness of Management Practices for Reducing Pesticide Residues in Surface Water. ACS Symp. Ser. 1308,

233–258. https://doi.org/10.1021/bk-2019-1308.ch012

Zhang, X., Luo, Y., Goh, K.S., 2018. Modeling spray drift and runoff-related inputs of pesticides to receiving water. Environ. Pollut. 234, 48–58. https://doi.org/10.1016/j.envpol.2017.11.032

Author Contributions

This dissertation thesis is based on three research articles submitted to peer-reviewed journals provided in Appendix I, II, and III. I am the lead author of all research articles. The contributions of all authors are explained in the following:

Appendix I

Fuchs, M.D., Gebler, S., Lorke, A., 2025. The droplet and atmospheric dispersion drift (DAD-drift) model – A modular approach for estimating spray drift at the landscape scale. Environ. Res. 271, 121104. https://doi.org/10.1016/j.envres.2025.121104

Conceptualization:	Mike Fuchs, Sebastian Gebler
Methodology:	Mike Fuchs, Sebastian Gebler
Software:	Mike Fuchs
Validation:	Mike Fuchs
Formal Analysis:	Mike Fuchs
Investigation:	Mike Fuchs
Data Curation:	Mike Fuchs
Writing – Original Draft:	Mike Fuchs, Sebastian Gebler
Writing – Review & Editing:	Sebastian Gebler, Andreas Lorke
Visualization:	Mike Fuchs
Supervision:	Sebastian Gebler, Andreas Lorke

Appendix II

Fuchs, M.D., Gebler, S., Lorke, A., 2025. Landscape-level assessment of spray drift – A virtual experiment using the Droplet and Atmospheric Dispersion drift (DAD-drift) model. Environ. Model. Softw. 189, 106455. https://doi.org/10.1016/j.envsoft.2025.106455

Conceptualization:	Mike Fuchs, Sebastian Gebler
Methodology:	Mike Fuchs, Sebastian Gebler
Software:	Mike Fuchs

Validation:	Mike Fuchs
Formal Analysis:	Mike Fuchs
Investigation:	Mike Fuchs
Data Curation:	Mike Fuchs
Writing – Original Draft:	Mike Fuchs
Writing – Review & Editing:	Sebastian Gebler, Andreas Lorke
Visualization:	Mike Fuchs
Supervision:	Sebastian Gebler, Andreas Lorke

Appendix III

Fuchs, M.D., Gebler, S., Lorke, A., 2026. Evaluating landscape-level pesticide exposure from spray drift: A modeling study in an agriculture-dominated watershed using SWAT+ and DAD-Drift. Environ. Pollut. 397, 128031. https://doi.org/10.1016/j.envpol.2026.128031

Conceptualization:	Mike Fuchs, Sebastian Gebler
Methodology:	Mike Fuchs, Sebastian Gebler
Software:	Mike Fuchs
Validation:	Mike Fuchs
Formal Analysis:	Mike Fuchs
Investigation:	Mike Fuchs
Data Curation:	Mike Fuchs
Writing – Original Draft:	Mike Fuchs
Writing – Review & Editing:	Sebastian Gebler, Andreas Lorke
Visualization:	Mike Fuchs
Supervision:	Sebastian Gebler, Andreas Lorke

Declaration

I hereby declare that the thesis entitled “On the relevance of spray drift from boom application for catchment-scale pesticide fate assessment” is the result of my own work except where otherwise indicated.

The thesis has not been submitted for any other degree at another university or scientific institution.

Freinsheim, 18.08.2026 ……..……

Mike Devin Fuchs

Declaration of Use of Artificial Intelligence

In the preparation of this dissertation, I used several generative AI tools in a clearly limited and transparent manner. DeepL was employed for language refinement, including improvements in clarity, grammar, and overall readability. ScholarGPT supported the verification of citation attributions and assisted in locating relevant literature when needed. ChatGPT and Claude were used for language refinement, for checking the clarity and logical flow of arguments, for exploring alternative ways to structure or present sections of the text, for occasionally generating initial phrasing when starting new paragraphs, and for identifying repetitive or stylistically weak formulations.

All AI-assisted outputs were carefully reviewed, edited, and integrated by me. The research design, scientific reasoning, argumentation, and final formulations are entirely my own, and I take full responsibility for the academic integrity and originality of this work.

Freinsheim, 18.08.2026 ……..……

Mike Devin Fuchs

Curriculum Vitae



MIKE DEVIN FUCHS

Date of Birth	14.03.1994
Place of Birth	Bad Dürkheim
Nationality	German
E-Mail	m.d.fuchs@protonmail.com

EDUCATION

December 2020 - Present	**RPTU University Kaiserslautern-Landau, Landau in der Pfalz**
Degree	Ph.D. Candidate in Natural and Environmental Sciences
Thesis	"On the relevance of spray drift from boom application for catchment-scale pesticide fate assessment "
October 2017 – December 2020	**University Koblenz-Landau, Landau in der Pfalz**
Degree	Master of Science in Environmental Science
Thesis	"Modelling landscape level pesticide concentrations with SWAT+ - an uncertainty assessment of application timing"
October 2013 – March 2018	**University Koblenz-Landau, Landau in der Pfalz**
Degree	Bachelor of Science in Environmental Science
Thesis	"Relationship between methane production and methane emission of aquatic sediments"

PROFESSIONAL EXPERIENCE

April 2025 – Present — **RPTU University Kaiserslautern-Landau, Landau in der Pfalz – Environmental Physics Working Group**

Position: Research Associate

Key Responsibilities:

- Project: "High-resolution modeling of exposure in small water bodies following precision pesticide application (drift)"
- Development of a Patch Generator tool to predict application patterns in precision spraying
- Implementation of DAD-drift into the XAquatic framework
- Environmental fate modeling of pesticide exposure after precision application at landscape scale
- Interpretation and synthesis of environmental fate and effect modeling results for project reporting and scientific evaluation

December 2020 – November 2024 — **BASF SE, Limburgerhof – APD/EFM**

Position: Doctoral Researcher

Key Responsibilities:

- Processing and preparation of geospatial data in QGIS
- Hydrological modeling of the Funne catchment using SWAT+
- Modeling active ingredients at the landscape scale with SWAT+
- Development of the DAD-Drift model for predicting spray drift after broadband and precision application at the landscape level
- Writing scientific articles for publication in international peer-reviewed journals
- Analysis of environmental monitoring data from the Funne watershed

Acknowledgements

I would like to express my sincere gratitude to all those who supported and accompanied me throughout my doctoral studies in Environmental and Natural Sciences.

First and foremost, I am deeply grateful to Prof. Andreas Lorke for his long-standing mentorship and trust. Having worked with him since my early academic years, he continuously supported my scientific development and provided valuable guidance throughout my Bachelor's, Master's, and doctoral studies. During my PhD, he encouraged intellectual independence, offered thoughtful feedback when needed, and served as a reliable sounding board for ideas and plans. I am thankful for the academic freedom he granted me and for the many opportunities he enabled over the years.

I would also like to thank Sebastian Gebler for his close and dedicated supervision, particularly during the early stages of my doctoral research. Despite his demanding role as a regulatory scientist, he consistently made time for regular discussions, provided practical guidance, and was always available for questions. His support laid an essential foundation for my work and significantly shaped my scientific approach.

My sincere thanks go to Bernhard Gottesbüren, who as team lead created the framework for this dissertation by offering me the opportunity to pursue my PhD following my Master's internship. I am grateful for his inspiring leadership, his trust, and his down-to-earth attitude, which contributed greatly to a motivating working environment. I also would like to thank Carola Schriever for her continued support and commitment. Despite the challenging structural circumstances she faced after taking over the team, she made every effort to support my work and enabled an additional year with the team, which was crucial for completing this dissertation. Together, they enabled the full financing of my doctoral research through my employment at BASF SE. I thank both for their role as reviewers of this thesis and their constructive feedback.

I would further like to acknowledge Bernhard Jene, who first enabled my entry into the industrial research environment by being open to my interest in an internship. His early encouragement proved pivotal for my academic and professional path. I am grateful that he took the time to read and comment on this dissertation, providing valuable insights.

My thanks also extend to Prof. Hermann Jungkunst, who kindly agreed to serve as chair of the examination committee. I appreciate his willingness to take on this responsibility and contribute to the successful completion of this doctoral process.

I gratefully acknowledge the entire exposure modelling working group at BASF, whose members supported me at various stages of my doctoral research and contributed to a collaborative and supportive working environment. Special thanks go to Christopher Hassinger and Eric Henry for carefully reviewing my manuscripts and providing valuable feedback on language and clarity.

Finally, I would like to thank my parents for their continuous support and for enabling me in pursuing an academic education and career in the first place. Although they do not come from an academic background, they were always curious, willing to learn alongside me, and continuously showed genuine interest in my scientific work. I am also deeply grateful to my close friend Lukas Hey for his companionship throughout this doctoral journey. Our shared experiences, discussions, and mutual support were invaluable, and without them, completing this dissertation would not have been possible.

Appendix I:

Environmental Research 271 (2025) 121104

Contents lists available at ScienceDirect

Environmental Research

journal homepage: www.elsevier.com/locate/envres

The droplet and atmospheric dispersion drift (DAD-drift) model – A modular approach for estimating spray drift at the landscape scale

Mike Devin Fuchs [a,b,*], Sebastian Gebler [a], Andreas Lorke [b]

[a] BASF SE, Exposure Modelling, Speyerer Straße 2, 67117, Limburgerhof, Germany
[b] Institute for Environmental Sciences, University of Kaiserslautern-Landau, Forststraße 7, 76829, Landau, in der Pfalz, Germany

ARTICLE INFO

Keywords:
Spray-drift
Atmospheric dispersion
Droplet evaporation
Landscape scale
Pesticide deposition
Boom application

ABSTRACT

Spray drift describes the off-target movement of pesticides by wind during or immediately after application, and its mechanism is highly complex and influenced by many factors. Spray drift modeling has become an increasingly important tool as spray drift field experiments are very expensive to conduct. Many modeling approaches are available to describe spray drift deposition after aerial and ground application at the field scale. We have developed a novel modeling approach to predict spray drift deposition after ground application at the landscape scale. The Droplet and Atmospheric Dispersion drift (DAD-drift) model combines a mechanistic droplet model, a micrometeorological model, and a three-dimensional Gaussian diffusion model. It is an iteration of the two-dimensional tilting plume approach and allows for the prediction of spray drift deposition from ground spray applications while accounting for environmental conditions, spray nozzle characteristics, and spray application characteristics. The DAD-drift model was evaluated against two field trial studies for a wide range of environmental conditions (i.e., temperature, humidity, wind speed) and four spray nozzles (fine to ultra-coarse). Model predictions were in very good agreement ($R^2 = 0.931$, RSR = 0.260) with spray drift observations from these studies, demonstrating the applicability of the model over a wide range of conditions. During a one-at-a-time sensitivity analysis, the model showed clear and understandable behavior when input parameters were varied. Droplet size distribution, boom height, temperature, wind speed, and atmospheric turbulence were identified as the most important factors.

1. Introduction

Spray drift describes the phenomenon of airborne spray droplets originating from aerial or ground-based spray operations being transported downwind beyond the intended area of application (Felsot et al., 2010). During spray application, a mixture of water and a plant protection product (liquid or solid) is pressurized and forced through small orifices in spray nozzles, creating a liquid sheet that further breaks up into a cloud of droplets of various size (Cock et al., 2017). The fate of these droplets is determined by their size, gravitational force, air viscosity, and weather conditions, with temperature, humidity, and wind speed being the most important (Nuyttens et al., 2007a). Larger droplets travel the distance to the receiving surfaces in a relatively short time (Thompson and Ley, 1983), while smaller droplets take significantly longer, due to lower settling velocity. As droplets travel through the air, they are subject to evaporation, which reduces their volume, diameter, and settling velocity (Holterman et al., 2017), thereby increasing their travel time to receiving surfaces. Increased droplet residence time in the air and higher wind speed each contribute to droplet transport over greater distances, making smaller droplets more susceptible to off-target spray drift (Cock et al., 2017; Felsot et al., 2010). The variability of conditions during spray application does not allow for an exact determination of the droplet size range associated with spray drift, droplet diameters of 100 μm (Felsot et al., 2010; Nuyttens et al., 2007a) or 200 μm (Nuyttens et al., 2007a, 2008) are reported as droplet size thresholds.

Based on these findings, an effective mitigation strategy to reduce off-target spray drift is to adopt measures that reduce the occurrence of small droplets. Cone type nozzles were found to produce the finest droplet size distribution (DSD), followed by standard flat fan nozzles, low-drift flat fan nozzles, and finally air injection nozzles for the same nozzle size and spray pressure (Nuyttens et al., 2007b). Larger nozzle sizes or lower application pressures will generally result in a coarser DSD (Miller, 2014; Nuyttens et al., 2007b). However, lower application

* Corresponding author. BASF SE, Exposure Modelling, Speyerer Straße 2, 67117, Limburgerhof, Germany.
E-mail address: m.d.fuchs@protonmail.com (M.D. Fuchs).

https://doi.org/10.1016/j.envres.2025.121104
Received 4 November 2024; Received in revised form 17 January 2025; Accepted 10 February 2025
Available online 11 February 2025
0013-9351/© 2025 The Authors. Published by Elsevier Inc. This is an open access article under the CC BY-NC-ND license (http://creativecommons.org/licenses/by-nc-nd/4.0/).

pressure also results in lower droplet velocities, which tend to increase drift potential. Thus, the positive and negative effects of lower application pressures may off-set each other (Miller, 2014). Physical properties of the spray formulation, such as extensional and shear viscosity, the presence of inhomogeneities (e.g., emulsion droplets or solid particles), and surface tension, have the potential to alter the DSD (Hilz and Vermeer, 2013). However, the adoption of large droplets can result in reduced coverage and efficacy due to bounce and runoff at the leaf surface, creating a conflict between spray drift mitigation and application efficiency (Griesang et al., 2017; Hewitt, 2000; Nuyttens et al., 2007b).

Additional measures can be taken to mitigate the negative effects of off-target spray drift. Spray drift decreases exponentially with increasing distance from the field edge, therefore "no-spray" buffer zones have been shown to be an effective measure for reducing spray drift (Miller, 2014). Research has shown that covering spray booms with various types of mechanical shields (i.e., hooded sprayers) that restrict airflow around the spray nozzles can reduce spray drift (Felsot et al., 2010). Reducing spray boom height, without sacrificing spray uniformity, decreases the distance spray droplet travel to receiving surfaces, thereby reducing off-target spray drift (Nuyttens et al., 2007a). Windbreaks such as hedgerows, trees, shelterbelts, or other vegetative barriers can also be effective measures to reduce off-target spray drift, by reducing the wind force on airborne droplets. Height, length, vegetation density, number of rows, continuity, orientation, and species composition are important factors in windbreaks efficiency (Felsot et al., 2010). Finally, agrochemical applicators are responsible for implementing best management practices (e.g., spraying only when wind speed is below a certain threshold) to further minimize off-target spray drift (Felsot et al., 2010).

Computer models and mathematical simulations have become increasingly important tools in the study of spray drift behavior (Delele et al., 2007; Gil and Sinfort, 2005), as it is not feasible to rely solely on field experiments to evaluate spray drift. This is because field spray drift experiments are expensive to conduct and observed spray drift is highly influenced by environmental conditions (e.g., wind speed, wind direction, temperature, humidity), operational parameters (e.g., application method, nozzle type, mixture formulation), crop type, unique local conditions and other considerations (Bub et al., 2020). Spray drift models distinguish between aerial application (i.e., airplanes, helicopters, drones) and ground application and can be differentiated into empirical models (Bub et al., 2020; Hewitt et al., 2002; Holterman et al., 2017; Rautmann et al., 2001; Wang and Rautmann, 2008), random walk trajectory models (Butler Ellis and Miller, 2010; Holterman et al., 1998; Teske et al., 2002; Thompson and Ley, 1983), computational fluid dynamics (CFD) models (Baetens et al., 2007; Delele et al., 2007; Duga et al., 2017; Hong et al., 2018a, 2018b), and atmospheric dispersion models (Baetens et al., 2009; Craig, 2004; Lebeau et al., 2011; Løfstrøm et al., 2013; Raupach et al., 2001).

Empirical spray drift models predict spray drift exposure by utilizing statistical analysis (e.g., multiple regression analysis) and rely on large data sets of spray drift field observations to represent a wide variety of conditions (Butler Ellis and Miller, 2010). These models are easy to apply with short computational times (Baetens et al., 2009), however they do not account for the physical basis of spray drift and therefore their application is limited to conditions very similar to those for which they were developed (Teske et al., 2002).

Random walk trajectory models are based on the Lagrangian approach where individual particles are tracked in a complex force field, with a random walk component representing particle motion caused by atmospheric turbulence (Djouhri et al., 2023; Gil and Sinfort, 2005; Teske et al., 2002). This approach allows the effect of application equipment to be modelled (Teske et al., 2002) and accounts for the complex flow structures near the nozzle (Butler Ellis and Miller, 2010). However, to predict spray drift farther from the source, an increasing number of particles must be tracked, resulting in large computational effort (Butler Ellis and Miller, 2010).

Computational fluid dynamics (CFD) models allow spray drift to be represented as a two-phased (spray droplet and air) flow (Butler Ellis and Miller, 2010). Most commonly the Navier-Stokes equation is solved for the continuous air phase and the Lagrangian particle tracking equation is solved for the discrete spray droplet phase (Hong et al., 2018a). The approach allows for the direct implementation of complex systems (Butler Ellis and Miller, 2010) and accurate prediction of airflow and droplet trajectories in complex geometric arrangements (Miller, 2014). However, running CFD models over reasonable downwind distances requires significant computing power and time (Butler Ellis and Miller, 2010).

Atmospheric dispersion models are based on Gaussian concentration distributions in the atmospheric boundary layer (Butler Ellis and Miller, 2010). Pollutants are assumed to be emitted continuously or instantaneously from point or line sources. These models are computationally efficient and are particularly well suited for spray drift predictions over larger distances (Butler Ellis and Miller, 2010) because the three-dimensional droplet mass distribution becomes more Gaussian in the far-field of the spreading plume (Felsot et al., 2010). However, this approach is relatively inaccurate for the representation of complex droplet behavior near the source (Butler Ellis and Miller, 2010; Teske et al., 2002) due to the low-resolution depiction of application equipment (i.e., nozzles, boom, tractor) and the flow field near the source.

In this paper, we present the Droplet and Atmospheric Dispersion drift (DAD-drift) model, which was developed to allow for computationally efficient and accurate modeling of off-target spray drift after boom application at the landscape scale. Therefore, DAD-drift combines a three-dimensional Gaussian diffusion model, a mechanistic droplet model, and a micrometeorological model and was inspired by pre-existing tilting plume atmospheric dispersion models. By neglecting droplet evaporation and the subsequent decrease in droplet size and velocity (Baetens et al., 2009; Lebeau et al., 2011; Raupach et al., 2001), Gaussian diffusion models alone can underestimate spray drift with increasing distance. For example, the RTDrift model (Lebeau et al., 2011) significantly underestimated spray drift at distances greater than 20 m. This was overcome by combining a mechanistic droplet model similar to OML-SprayDrift (Løfstrøm et al., 2013), which is not openly available, with a micrometeorological model to accurately predict droplet trajectories. In addition, the three-dimensional Gaussian puff model (instantaneous point source) implemented in DAD-drift avoids the problems observed previously at low to zero wind conditions (Lebeau et al., 2011), by better distinguishing between vertical and horizontal dispersion processes.

The aims of this paper are to (1) describe the theoretical basis and the technical implementation of our modeling approach; (2) assess the sensitivity of the input parameters, providing an insight into how spray drift estimates are impacted; (3) evaluate model performance against field studies with different environmental conditions and technical equipment (i.e., nozzle types), demonstrating the applicability of the model at the landscape scale under a wide range of conditions.

2. Material and methods

2.1. General model description

The DAD-drift model consists of multiple sub-models (Fig. 1). First, the droplet model and the micrometeorological model are run in parallel for all defined droplet classes, with a droplet class representing droplets in a specific size range characterized by the mean droplet diameter. The droplet model predicts the motion and mass balance of droplets representative of their droplet class based on weather conditions (e.g., wind speed, wind direction, ambient pressure), droplet parameters (e.g., velocity, size, density), release height, and the micrometeorological model (i.e., humidity, temperature). The micrometeorological model accounts for indirect interactions between individual droplets within the spray cloud by estimating the change in humidity and temperature caused by

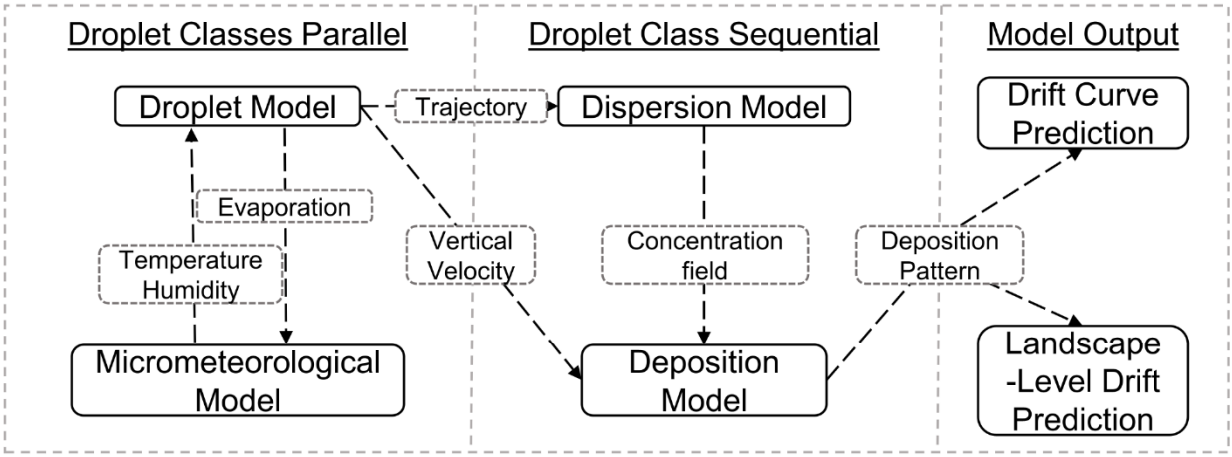


Fig. 1. Schematic representation of the DAD-drift model. With solid boxes representing sub-models, and dashed boxes and arrows representing intermediate results being forwarded between sub-models. The sub-models in the left column are executed first and in parallel for all droplet classes, the sub-models in the middle column are executed second and sequentially for all droplet classes, finally the model outputs are calculated in the right column.

droplet evaporation in the droplet model. Second, the dispersion model describes the atmospheric dispersion of a cloud of airborne droplets. The droplet trajectories provided by the droplet model are used to estimate the mean position of the three-dimensional puff and to predict the three-dimensional concentration field. Third, the deposition model combines the vertical droplet velocity and the concentration field to predict the deposition mass flux a given height, resulting in a two-dimensional deposition pattern. The dispersion model and the deposition model are executed sequentially for all droplet classes. Finally, the two-dimensional deposition pattern is used to predict either a drift deposition curve or a two-dimensional landscape-level drift deposition flux as model output. The individual sub-models are described in the following sections, for additional details please refer to the theoretical model documentation available on GitHub and archived in Zenodo (Fuchs, 2024).

2.2. Droplet model

The droplet model was developed to predict the trajectory of a representative droplet after ejection from the spray nozzle to the ground, which is unrestricted by plant canopies (i.e., no interception). The initial vertical position of the droplet is given by the nozzle height above the ground during the spray application and is a user-defined input to the model. The initial droplet velocity is assumed to be equal to the nozzle liquid discharge velocity (U_L, m s^{-1}), which can be described as:

$$U_L = \left(\frac{2P_n}{\rho_L}\right)^{\frac{1}{2}} \quad (1)$$

where, P_n (Pa) is the spray pressure and ρ_L (kg m^{-3}) is the density of the spray liquid, (Dorr et al., 2013). The initial vertical droplet velocity is then determined by the initial droplet velocity and the nozzle angle, with 0° and 90° representing vertical and horizontal nozzle orientations, respectively.

After ejection from the nozzle, the droplet is subject to atmospheric drag and gravity. The momentum equation describing the change rate of the vertical droplet velocity (m s^{-1}) is defined as follows:

$$\frac{\delta v_d}{\delta t} = g - \frac{v_d 18 \mu_{air} f}{\rho_d (D_d)^2} \quad (2)$$

where, g (m s^{-2}) is the gravitational acceleration, V_d (m s^{-1}) is the vertical droplet velocity, ρ_d (kg m^{-3}) is the droplet density, D_d (m) is the droplet diameter, μ_{air} (kg m^{-1} s^{-1}) is the dynamic viscosity of air, and f (−) is a factor describing the deviation from the Stokes flow (Løfstrøm et al., 2013).

During an initial period after droplet ejection, the evaporation rate is mainly driven by the cooling of the droplet until it reaches an equilibrium (wet-bulb) temperature. After this transient process, the mass loss of the droplet can be approximated by steady-state evaporation. This cooling period has been shown to be much shorter than the lifetime of the droplet and is therefore neglected (Holterman, 2003).

The rate of change of droplet mass (kg s^{-1}) is described as the mass flux across the droplet surface area:

$$\frac{\delta m_*}{\delta t} = \pi (D_d)^2 F_* \quad (3)$$

where D_d (m) is the droplet diameter, F (kg $m^{-2}s^{-1}$) is the mass flux, and * refers to either water or active ingredient (AI).

The mass flux of water (kg $m^{-2}s^{-1}$) can be described as a function of diffusion and the vapor pressure difference between the atmosphere and the droplet surface:

$$F_{water} = \frac{Sh_{H2O} D_{V_{H2O}} M_{H2O}}{D_d T_f R} \left[(p_{sat} Rh) - \left(p_{sat_f} x_{mol_{H2O}} \right) \right] \quad (4)$$

where $D_{V,H2O}$ (m^2 s^{-1}) is the diffusion coefficient of water vapor in the saturated film around the droplet, T_f (K) is the absolute temperature in this film, M_{H2O} (kg mol^{-1}) is the molar mass of water, D_d (m) is the droplet diameter, R (J $mol^{-1}K^{-1}$) is the universal gas constant, p_{sat} (Pa) is the saturated vapor pressure of water at ambient temperature, Rh (−) is the relative humidity, $p_{sat,f}$ (Pa) is the saturated vapor pressure of water at the film temperature, $x_{mol,H2O}$ (−) is the molar fraction of water in the droplet, and Sh_{H2O} (−) is the Sherwood number for water (Løfstrøm et al., 2013). The temperature of the saturated film at the droplet surface is assumed to be the average value of the ambient temperature and the wet-bulb temperature.

Most likely, not all the necessary physio-chemical parameters needed for equation (4) are available for AIs. Therefore, the mass flux (kg $m^{-2}s^{-1}$) of the AI was estimated based on an empirical relationship with vapor pressure:

$$F_{AI} = 4.07 * 10^{-7} p_{AI} M_{AI} \quad (5)$$

where p_{AI} (Pa) is the vapor pressure of the AI and M_{AI} (kg mol^{-1}) is the molar mass of the AI (Mackay and Wesenbeeck, 2014). The droplet

model forwards evaporated water masses to the micrometeorological model and droplet trajectories to the dispersion model (Fig. 1).

2.3. Micrometeorological model

At the time of spraying, droplets are emitted into the same volume of air, thus interactions between individual droplets are expected. In this approach, direct interactions such as droplet collision and merging are not represented as this would require the tracking of all individual droplets. In the micrometeorological model, indirect interactions of individual droplets within the spray cloud are represented. During the process of in-flight evaporation of airborne droplets, energy is withdrawn from the surrounding air in exchange for water, decreasing air temperature and increasing humidity.

In the micrometeorological model, the control volume relevant to indirect droplet interactions is estimated as the volume above one unit of application area. Which is defined as one square meter with the nozzle positioned at the center. The ground level at the center of one unit of application area is defined as the origin (0,0,0) of the coordinate system which is consistent for all sub-models. The control volume represents the volume below the spray boom into which droplets are emitted and are transported over time by wind. The lower boundary condition of the control volume is the ground. The upper boundary condition is initially limited by nozzle height (no droplets above nozzles) and increases with time and distance based on the vertical dispersion parameter. Conditions within the application area are assumed to be uniform, thus horizontal mass transport between adjacent units of application area has been neglected (i.e., mass flux between adjacent control volumes are assumed to be equal).

The mass of water vapor (kg) within the control volume is defined as follows:

$$m_{H2O} = AhV + m_{H2O.evap} \tag{6}$$

where, Ah (kg m^{-3}) is the absolute humidity, V (m^3) is the volume of the control volume, and $m_{H2O,evap}$ (kg) is the mass of evaporated water.

The internal energy (J) of the control volume is calculated as follows:

$$E = m_{H2O}c_{p_{H2O}} + m_{air}c_{p_{air}} - E_{evap} \tag{7}$$

where, m_{H2O} (kg) is the mass of water vapor, $c_{p,\ H2O}$ (J kg^{-1}) is the specific heat capacity of water, m_{air} (kg) is the mass of air, $c_{p,air}$ (J kg^{-1}) is the specific heat capacity of air, and E_{evap} (J) is the energy withdrawn by evaporation.

The temperature (K) of the control volume is estimated as a function of the internal energy and the masses of water vapor and air:

$$T = \frac{E}{m_{H2O}c_{p_{H2O}} + m_{air}c_{p_{air}}} \tag{8}$$

where, E (J) is the internal energy of the control volume, m_{H2O} (kg) is the mass of water vapor, m_{air} (kg) is the mass of air, $c_{p,\ H2O}$ (J kg^{-1}) is the specific heat capacity of water, and $c_{p,air}$ (J kg^{-1}) is the specific heat capacity of air.

The relative humidity (−) of the control volume is estimated as follows:

$$Rh = \frac{m_{H2O}R_{H2O}T}{Vp_{sat}(T)} \tag{9}$$

where, m_{H2O} (kg) is the mass of water vapor, R_{H2O} (J kg^{-1}K^{-1}) is the specific gas constant of water, T (K) is the temperature, V (m^3) is the volume, and $p_{sat}(T)$ (Pa) is the saturated vapor pressure estimated by an empirical relation to temperature. The micrometeorological model forwards temperatures and humidity to the droplet model (Fig. 1).

2.4. Dispersion model

In the dispersion model, the landscape is represented by a flat plane without canopy interception and the atmospheric conditions are described by a single vertical wind profile. Mass is released from a single nozzle in the center of one unit of application area at the defined boom height represented as an instantaneous point source, with mass deposition at the deposition plane being assumed to be complete (i.e., all released AI mass is deposited). Therefore, a three-dimensional Gaussian puff model without a reflection term is used to describe the dispersion in three-dimensional space, which is mainly driven by wind advection and atmospheric turbulence. The Gaussian puff predicts the droplet concentration (kg m^{-3}) at a given position (x,y,z) and as function of time as follows:

$$C(x,y,z,t) = \frac{M}{(2\pi)^{\frac{3}{2}}\sigma_h^2\sigma_v}\exp\left[-\frac{1}{2}\left(\frac{x-Ut}{\sigma_h}\right)^2\right]\exp\left[-\frac{1}{2}\left(\frac{y}{\sigma_h}\right)^2\right]\exp\left[-\frac{1}{2}\left(\frac{z-z_c(t)}{\sigma_v}\right)^2\right] \tag{9}$$

where, x, y and z (m) are the coordinates in x, y and z direction, respectively, t (s) is the time, M (kg) is the mass release from the nozzle, σ_h and σ_v (m) are the dispersion coefficients in the horizontal and vertical directions, respectively, U (m s-1) is the wind speed, and z_c (m) is the mean puff position in z direction as a function of time as predicted in the droplet model (Zannetti, 1990).

The vertical (σ_v) and horizontal (σ_h) dispersion coefficients are described by the following empirical relations to time, distance, and wind speed:

$$\sigma_v = \alpha\frac{\sigma_w{}^*x}{u^*\left(1+0.9\left(0.02{}^*\frac{x}{U}\right)^{\frac{1}{2}}\right)}\quad \sigma_h = \beta\frac{\sigma_\theta{}^*x}{1+0.9\left(0.001{}^*\frac{x}{U}\right)^{\frac{1}{2}}} \tag{10}$$

where, x (m) is the distance, U (m s^{-1}) is the wind speed, σ_w and σ_θ (−) are the unitless vertical and horizontal wind velocity standard deviation used as empirical calibration parameters, α (m s$^{-1/2}$) is the empirical unit-correction factor for the vertical dispersion coefficient, and β (s$^{1/2}$) is the empirical unit-correction factor for the horizontal dispersion coefficient (Draxler, 1976; Souto et al., 2001). The dispersion model forwards a time series of the three-dimensional concentration field to the deposition model (Fig. 1).

2.5. Deposition model

The deposition model predicts the deposition pattern emitted by one unit of application area. The droplet deposition rate (F_{dep}, kg m^{-2}s^{-1}) at a given position (x,y,z) and as function of time is estimated as follows:

$$F_{dep}(x,y,z,t) = v_d(t)^*C(x,y,z,t) \tag{11}$$

where, v_d (m s^{-1}) is the vertical droplet velocity as a function of time as predicted by the droplet model and C (kg m^{-3}) is the concentration as a function of the position in three-dimensional space and time as predicted by the dispersion model (Lebeau et al., 2011; Løfstrøm et al., 2013).

2.6. Vertical wind profile

The wind speed (m s^{-1}) in the atmospheric surface layer is not constant and varies with the height above the ground. While canopy interception is not represented in DAD-drift, the drag forces inside the canopy have a mayor influence on the vertical wind profile. Above the canopy the vertical wind profile is described by the logarithmic law. Within the canopy the vertical wind profile is described as an exponential function of the leaf area index.

$$U(z) = \frac{U_*}{\kappa} * \ln\left(\frac{z-d}{z_0}\right) \quad if\ z \geq Hc \tag{12}$$

$$U(z) = U_H * \exp\left[\frac{LAI}{2} * \left(\frac{z}{H_c} - 1\right)\right] \quad if\ z < Hc \tag{13}$$

where, U^* (m s^{-1}) is the friction velocity, κ (−) is the von Karman constant (0.4), z (m) is the height above ground, d (m) is the zero plane displacement, z_0 (m) is the roughness length, H_c (m) is the canopy height, U_H (m) is the wind speed at the top of the canopy as calculated by equation (12), and LAI (m^2 m^{-2}) is the leaf area index (Sypka and Starzak, 2013). The roughness length is the height at which the wind speed becomes zero and can be approximated as one-tenth of the height of the surface roughness elements. The zero plane displacement can be assumed to be 0.63 times the canopy height (Butler Ellis and Miller, 2010).

2.7. Model implementation

The DAD-drift model was written in the Fortran90 programming language because of its performance in scientific computing scenarios. The model reads inputs from text files (.txt) and raster data in ASCII grid format (.asc). Drift curves are returned in text file format (.txt) and are given as drift fractions in relation to distance from the edge-of-field with drift fractions (−) defined as the spray drift depositions (kg ha^{-1}) relative to the application rate (kg ha^{-1}). Landscape-level spray drift predictions are returned as raster of the deposition rate in ASCII grid format (.asc). The base model resolution is one square meter, and the drift curve model output is returned at a distance resolution of 1 m. The landscape-level drift prediction raster uses the input raster resolution, with a minimum resolution of 1 × 1 m. The DAD-drift executable, the source code, extensive model documentation, and example setups are available on GitHub and archived in Zenodo (Fuchs, 2024).

2.8. Model setup and evaluation

2.8.1. Setup

For the model evaluation, a literature search was conducted using the following criteria in order to obtain suitable evaluation data. The studies shall be recently published (after 2015) and use state-of-the-art experimental design (i.e., steel disk samplers). Ground application with boom sprayers on bare soil or very short vegetation shall be the mode of application. Detailed information on application procedures and weather conditions shall be reported. The experimental design shall cover large distances from the edge-of-field. Different types of spray nozzles shall be used in the field trials.

The first study selected is a spray drift study of atrazine by Brain et al. (2019), hereafter referred to as Study 1. Atrazine (AAtrex® 4L) was applied using the TeeJet TTI11004 spray nozzle on four field plots with one replicate per field plot. Based on Study 1, four application scenarios (i.e., "TTI11004 trial 1", "TTI11004 trial 2", "TTI11004 trial 3", "TTI11004 trial 4") were defined, one per field plot.

The second study selected is a spray drift case study of thiamethoxam by Perine et al. (2021), hereafter referred to as Study 2. Thiamethoxam (Actara® 25WG) was applied using three different spray nozzles (TeeJet XR11003, TeeJet DG11004, TeeJet AIXR11002) on a field plot with four replicates per nozzle. Based on Study 2, three application scenarios (i.e., "XR11003", "DG11004", "AIXR11002") were defined, one per nozzle.

Most input parameters required to run the DAD-drift model were adapted from the real-world conditions during the field trials of studies 1 and 2 (Table 1). Density, molar mass, and vapor pressure of the applied active ingredients were obtained from the PubChem database (Kim

Table 1
Parameter values used during model evaluation for the seven application scenarios, see Table S4 for parameter description.

Parameter Name	XR11003	DG11004	AIXR11002	TTI11004 trial 1	TTI11004 trial 2	TTI11004 trial 3	TTI11004 trial 4
Application Parameters							
tractor_speed (m s-1)	2.6 [a]	3.1 [a]	4.6 [a]	3.6 [b]	3.6 [b]	3.6 [b]	3.6 [b]
boom_width (m)	30.5 [a]	30.5 [a]	30.5 [a]	28.0 [b]	28.0 [b]	28.0 [b]	28.0 [b]
boom_height (m)	0.600 [a]	0.600 [a]	0.600 [a]	0.635 [b]	0.635 [b]	0.635 [b]	0.635 [b]
nozzle_angle (°)	0 [a]	0 [a]	0 [a]	0 [b]	0 [b]	0 [b]	0 [b]
application_pres (kPa)	275.8 [a]	165.5 [a]	206.8 [a]	275.8 [b]	275.8 [b]	275.8 [b]	275.8 [b]
app_rate_mha (m^3 ha^{-1})	0.0935 [a]	0.0935 [a]	0.0935 [a]	0.0935 [b]	0.0935 [b]	0.0935 [b]	0.0935 [b]
app_rate_kgha (kg ha^{-1})	0.096 [a]	0.096 [a]	0.096 [a]	2.240 [b]	2.240 [b]	2.240 [b]	2.240 [b]
swath_number (−)	2 [a]	2 [a]	2 [a]	2 [b]	2 [b]	2 [b]	2 [b]
field_length (m)	183 [a]	183 [a]	183 [a]	182 [b]	182 [b]	182 [b]	182 [b]
Formulation Parameters							
AI_density (kg m^{-3})	1570 [c]	1570 [c]	1570 [c]	1230 [c]	1230 [c]	1230 [c]	1230 [c]
AI_molar_mass (kg mol^{-1})	0.292 [c]	0.292 [c]	0.292 [c]	0.216 [c]	0.216 [c]	0.216 [c]	0.216 [c]
AI_vapor_pressure (Pa)	6.6E-9 [c]	6.6E-9 [c]	6.6E-9 [c]	3.9E-5 [c]	3.9E-5 [c]	3.9E-5 [c]	3.9E-5 [c]
sol_concentration (kg m^{-3})	1.03 [a]	1.03 [a]	1.03 [a]	25.54 [b]	25.54 [b]	25.54 [b]	25.54 [b]
Environmental Conditions							
temperature (C°)	23.4 [a]	23.6 [a]	23.7 [a]	30.6 [b]	30.6 [b]	30.0 [b]	29.3 [b]
humidity (−)	0.61 [a]	0.62 [a]	0.59 [a]	0.50 [b]	0.48 [b]	0.44 [b]	0.44 [b]
wind_speed (m s^{-1})	3.9 [a]	4.3 [a]	4.0 [a]	4.4 [b]	7.8 [b]	4.5 [b]	9.0 [b]
wind_height (m)	2 [e]	2 [e]	2 [e]	2 [b]	2 [b]	2 [b]	2 [b]
wind_direction (°)	71.5 [a]	65.3 [a]	75.3 [a]	88.1 [b]	50.5 [b]	101.3 [b]	55.4 [b]
ambient_pressure (kPa)	100.0 [e]	100.0 [e]	100.0 [e]	97.8 [b]	97.7 [b]	97.7 [b]	97.6 [b]
Calibration Parameters							
sigma_horizontal (m s^{-1})	1.05 [f]	1.05 [f]	1.05 [f]	1.05 [f]	1.05 [f]	1.05 [f]	1.05 [f]
sigma_vertical (m s^{-1})	0.22 [f]	0.22 [f]	0.22 [f]	0.22 [f]	0.22 [f]	0.22 [f]	0.22 [f]
roughness_height (m)	0.05 [d]	0.05 [d]	0.05 [d]	0.05 [d]	0.05 [d]	0.05 [d]	0.05 [d]
canopy_height (m)	0.025 [e]	0.025 [e]	0.025 [e]	0.025 [e]	0.025 [e]	0.025 [e]	0.025 [e]
LAI (m^2 m^{-2})	0.5 [e]	0.5 [e]	0.5 [e]	0.5 [e]	0.5 [e]	0.5 [e]	0.5 [e]
deposition_height (m)	0.145 [a]	0.145 [a]	0.145 [a]	0.146 [b]	0.146 [b]	0.146 [b]	0.146 [b]

[a] Perine et al. (2021).
[b] Brain et al. (2019).
[c] Kim et al., 2023
[d] L. Zhang et al., 2001
[e] Section 2.8.1.
[f] Section 3.1.

et al., 2023). Surface roughness height was set to 0.05 m based on the reported parameter values for grass, crops, and mixed farming by Zhang et al. (2001). The downwind sampling area of Study 1 was described as tilled, and the images in the supplementary materials depicted a rough surface (Brain et al., 2019). For Study 2, the downwind sampling area was described as short stubble below the sampling height of 0.145 m (Perine et al., 2021). Based on this information, the canopy height was set to 0.025 m, representing the influence of the surface conditions on the vertical wind profile (Section 2.6). Since the canopy height was set below the sampling height, the leaf area index has no influence on the drift predictions and was set to 0.5. Standard deviation of the vertical and horizontal wind velocities was determined during model parameterization.

Both studies reported the spray pressures and spray nozzles (i.e., nozzle type, spray cone angle, and nozzle size) used during application. However, a DSD is required to run the DAD-drift model. Therefore, a literature search was conducted based on the information reported in the two studies to obtain information on DSD characteristics (Alves et al., 2020; Ferguson et al., 2016, 2023; Gil et al., 2014; Zande et al., 2012, 2014; Porskamp et al., 2002), such as 10% volume diameter (DV0.1), volume median diameter (DV0.5), 90% volume diameter (DV0.9), and volume fraction less than 100 μm (V100). Nozzle type, spray cone angle, and nozzle size were exactly matched, while application pressure was approximately matched. Drop size distributions were then generated based on the obtained values for DV0.1, DV0.5, DV0.9, and V100 (Table S1).

2.8.2. Parametrization

Final model parameterization was performed manually for the standard deviations of the vertical and horizontal wind velocities for all application scenarios (except for the "XR11003" scenario). The "XR11003" scenario showed large discrepancies between simulated and observed drift data, which was likely caused by an underreporting of spray drift in Study 2, see Section 4.1 for more information. The "XR11003" scenario was therefore excluded to avoid biasing the parameterization. A single parameter set was determined for all application scenarios to avoid overparameterization. Initially, the standard deviations of the vertical and horizontal wind velocities were set to a value of 1 m, with a parameter range from 0.01 m to 10 m (Table S2). The standard deviation of the vertical wind velocity was optimized first, followed by the standard deviation of the horizontal wind velocity. The parameter space around the optimized values was checked for the local minimum, by varying both parameters by −10%, −5%, 0%, 5%, and 10% for a total of 25 parameter combinations (Table S3).

The performance of each parameter set was determined by comparing model predictions with observational data from studies 1 and 2, using visual and statistical analyses described below. For all analytical methods, the drift fraction was scaled by the decimal logarithm, to avoid overweighting high drift fractions near the edge-of-field. Visual analysis was performed using line plots showing the drift fraction as a function of distance, or scatter plots directly comparing model predictions and observations. Statistical analysis was performed using the coefficient of determination (R^2) and the root mean square error - observations standard deviation ratio (RSR).

R^2 describes the proportion of the variance in the measured data that is explained by the model. The ideal model has an R^2 value of 1, a model that always predicts the mean observation value would have an R^2 score of 0, whereas negative scores are possible (Tercan et al., 2018). R^2 is defined as:

$$R^2 = 1 - \frac{\sum_{i=0}^{n} \left(y_i^{obs} - y_i^{sim}\right)^2}{\sum_{i=0}^{n} \left(y_i^{obs} - y^{mean}\right)^2} \tag{14}$$

The RSR normalizes the root mean square error by the observation standard deviation. Thus, the RSR integrates the benefits of an error index statistic while incorporating a normalization factor, so that the resulting statistic can be applied to various constituents (Moriasi et al., 2007). RSR ranges from 0 to infinity, and the ideal model has an RSR value of 0. Model performance can be classified as very good, good, satisfactory, and unsatisfactory with RSR $\leq$0.5, 0.5 < RSR $\leq$0.6, 0.6 < RSR $\leq$0.7, and RSR >0.7, respectively (Küçüktopcu and Cemek, 2021). RSR is defined as:

$$RSR = \frac{\sqrt{\sum_{i=0}^{n} \left(y_i^{obs} - y_i^{sim}\right)^2}}{\sqrt{\sum_{i=0}^{n} \left(y_i^{obs} - y^{mean}\right)^2}} \tag{15}$$

Statistical analysis was performed to summarize multiple application scenarios. First the observation and simulation data of all scenarios were combined and second the performance metric was calculated for the unified dataset.

2.8.3. Model evaluation

The DAD-drift model was evaluated using the parameterized values for the standard deviation of the vertical and horizontal wind velocities, see Table 1 for the full parameter set and Table S4 for parameter description. Model performance was determined using the visual and statistical analyses described in Section 2.8.2.

2.8.4. Sensitivity analysis

For a better understanding of model behavior with changes in input parameters, a sensitivity analysis was performed for all application scenarios varying one input parameter at a time. The values of 22 input parameters were changed by −25%, 0%, and +25%, the values of the nozzle angle were set to 0°, 22.5°, and 45°, and the values of the number of application swaths were set to 1, 2, and 3 (Table S5). The sensitivity of each parameter was assessed using the RSR statistic (Section 2.7.2), with the no change run representative of the parameterized value regarded as the reference. The two RSR values of the positive and negative parameter change were then averaged to describe parameter sensitivity by a single value. The analysis was performed separately for each application scenario to gain insight into how model sensitivity might vary with the respective parameter spaces of the application scenarios (inter-scenario variation).

In order to gain a better understanding of the effect of the DSD on model prediction, the "XR11003" scenario was run with 10 different DSDs (Fig. 2), based on DV0.1, DV0.5, DV0.9, V100, and volume fraction less than 150 μm (V150) as in a literature search (Table S1). Drift fractions at 50 m from the edge-of-field were selected to represent the drift curves to allow numerical spray drift comparisons of individual DSDs.

2.8.5. Drift reduction potential

The drift reduction potential (DRP) of a spray nozzle describes its ability to reduce spray drift emissions (%) when compared to the XR11003 reference nozzle (Bueno et al., 2017; Gil et al., 2014) and can be calculated as follows:

$$DRP = \frac{1}{n} \sum_{i=1}^{n} \frac{f_{ref,i} - f_{com,i}}{f_{ref,i}} * 100 \tag{17}$$

where, n is the number of distances at which drift fractions have been sampled, $f_{ref,i}$ (−) is the drift fraction of the reference nozzle at distance i, and $f_{com,i}$ (−) is the drift fraction of the compared nozzle at distance i (Nuyttens et al., 2007a).

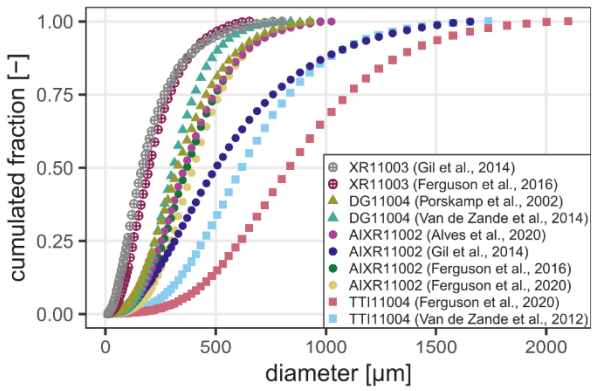


Fig. 2. Drop size distributions representing the XR11003 nozzle (circle with cross), the DG11004 nozzle (triangle), the AIXR11002 nozzle (circle), and TTI11004 nozzle (square). Each drop size distribution was generated based on reported values of 10% volume diameter (DV0.1), volume median diameter (DV0.5), 90% volume diameter (DV0.9), volume fraction less than 100 µm (V100), or volume fraction less than 150 µm (V150).
(For interpretation of the references to color in this figure legend, the reader is referred to the Web version of this article.)

3. Results

3.1. Model parametrization

In the first parameterization step, by independently varying the horizontal and vertical wind standard deviation (σ_θ and σ_w), values of 0.2 m for σ_w and 1 m for σ_θ were determined with respective R^2 and RSR values of 0.929 and 0.264, respectively (Fig. 3). In the second parameterization step, the parameter space around these values was screened for the local minimum. Values of 0.22 m for σ_w and 1.05 m for σ_θ, with a performance of 0.931 (R^2) and 0.621 (RSR), respectively, were found to be optimal solutions (Table S2) and were subsequently used for the model evaluation (Table 1).

3.2. Model evaluation

Model evaluation for the seven application scenarios of the two studies was successful. The visual analysis comparing model simulations

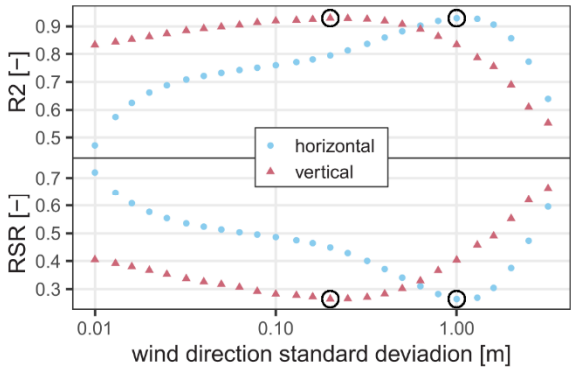


Fig. 3. Model performance of all application scenarios (except "XR11003") compared to the observations, for the variation of the horizontal and vertical wind direction standard deviation, with the coefficient of determination (R^2) in the top, the RSR in the bottom, and the black circles indicating best performing parameters.
(For interpretation of the references to color in this figure legend, the reader is referred to the Web version of this article.)

with observed drift fractions showed a high predictive power of the DAD-drift model (Fig. 4). In the scatterplot, data points are close to the 1:1-line indicating good agreement of simulated and observed values, with less than 35% deviation over two orders of magnitude in drift fractions. Besides the "XR11003" application scenario no systematic bias can be observed for the remaining application scenarios. This was confirmed in the statistical analysis, model performance could be classified as very good with $R^2 = 0.878$ and RSR = 0.346.

For Study 1, visual analysis showed good agreement between simulated and observed spray drift fractions (Fig. 4). In addition, the R^2 (0.930) and RSR (0.262) indicate very good model performance (Table 2). Comparison of the four application scenarios of Study 1 showed very consistent model performance for the four individual field plots. With metrics ranging from an R^2 value of 0.918 and an RSR value of 0.271 for "TTI11004 trial 1", to an R^2 value of 0.946 and an RSR value of 0.220 for "TTI11004 trial 2", which is the best performing individual application scenario of both studies (Fig. 5).

For Study 2, the model performance can be classified as very good with an R^2 value of 0.794 and an RSR value of 0.446. Visual analysis showed very good agreement between model simulated and observed data for the "DG11004" and "AIXR11002" scenarios, with a slight overprediction of simulated drift values in the first 15 m (Fig. 4). However, the simulation of the "XR11003" scenario systemically overestimates drift values, which is the worst performing individual application scenario of the two studies (Fig. 6). These differences in performance are confirmed by the statistical analysis, where the model performance for the "DG11004" and "AIXR11002" scenarios is classified as very good, while for the "XR11003" scenario it is only satisfactory to good (Table 2). Comparing the simulated drift fractions of the DG11004 and AIXR11002 nozzles with the simulated drift fractions of the XR11003 reference nozzle (Bueno et al., 2017; Gil et al., 2014), shows a drift reduction potential of 73.7% and 85.0% for the DG11004 and AIXR11002 nozzle, respectively (Table S6).

Excluding the "XR11003" application scenario from the statistical analysis of Study 2 results in an improved model performance with an R^2 value of 0.926 and an RSR value of 0.265. This is very similar to the performance of Study 1. In addition, the overall model performance is improved to an R^2 value of 0.931 and an RSR value of 0.260 (Table 2).

3.3. Sensitivity analysis

Mean droplet diameter (*mean_size*), the spray boom height (*boom_height*), the number of application swaths (*swath_number*), the ambient air temperature (*temperature*), and the wind speed (*wind_speed*) were the five most sensitive input parameters (Fig. 7, Table S7). Changes in leaf area index (*LAI*) and active ingredient vapor pressure (*AI_vapor_pressure*) were found to have no significant effect on the model results for the seven application scenarios. The sensitivity of the relative humidity (*humidity*), the wind speed (*wind_speed*), the horizontal wind standard deviation (*sigma_horizontal*), and the wind direction relative to the spray path (*wind_direction*) showed the largest inter-scenario variation, indicating the sensitivity of these parameters is highly dependent on the respective parameter space.

In order to evaluate model behavior in response to changes in input parameters, mechanistic parameter impact on the model results was characterized using four distinct operating principles for the DAD-drift model: an effect on the droplet evaporation (principle 1), an effect on the atmospheric dispersion and concentration field (principle 2), an effect on the droplet travel time to receiving surfaces (principle 3), and an effect on the horizontal distance traveled while airborne (principle 4).

Principle 1 describes the impact of a parameter on the evaporation rate of a droplet. A change in the evaporation rate has a direct effect on the droplet diameter, which in turn affects the drag coefficient and the velocity of such a droplet, which affects the vertical position of the Gaussian puff and the deposition velocity of that droplet. Ambient

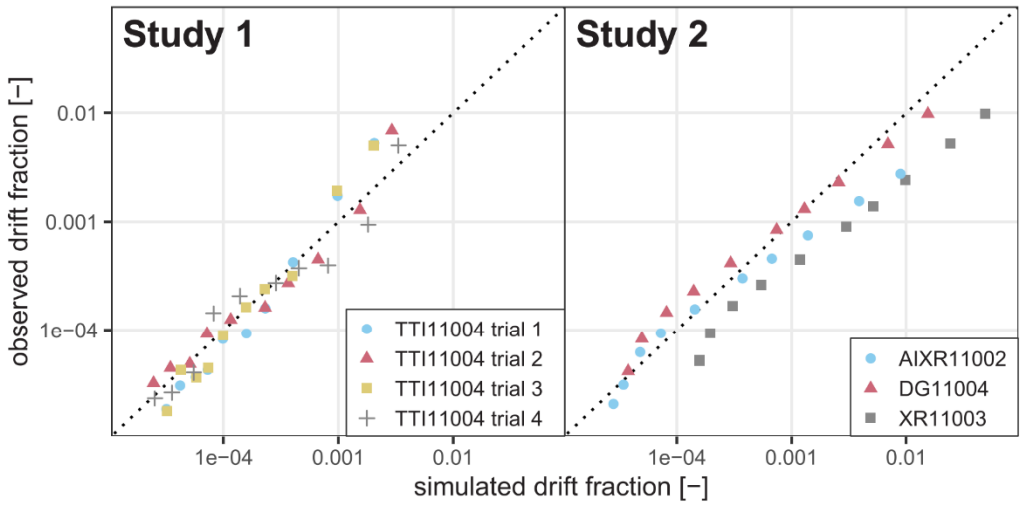


Fig. 4. Observed drift fraction (y-axis) versus simulated drift fractions (x-axis) for the four application scenarios of study 1 on the left and the three application scenarios of study 2 on the right. With data points above the one-to-one line indicating model underprediction, data points below the one-to-one line indicating model overprediction. For the four application scenarios of study 1 as well as the "DG11004" and "AIXR11002" scenario of study 2 the plot shows good agreement between simulated and observed drift fractions. For "XR11003" scenario of study 2 the plot shows systematic overprediction of drift fractions by the model.
(For interpretation of the references to color in this figure legend, the reader is referred to the Web version of this article.)

Table 2
Evaluation performance, for each application scenario, summarized for each study and summarized for all scenarios.

Scenarios	R^2 [-]	RSR [-]
XR11003	0.492	0.676
DG11004	0.956	0.200
AIXR11002	0.874	0.336
TTI11004 trial 1	0.918	0.271
TTI11004 trial 2	0.946	0.220
TTI11004 trial 3	0.927	0.257
TTI11004 trial 4	0.927	0.256
Study 1	0.930	0.262
Study 2	0.794	0.446
Study 2 without XR11003	0.926	0.265
All scenarios	0.878	0.346
All scenarios without XR11003	0.931	0.260

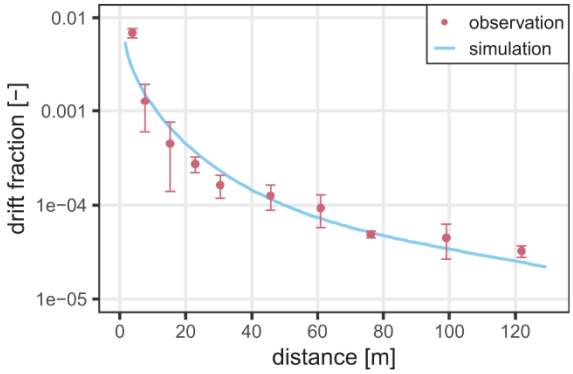


Fig. 5. Model evaluation for the "TTI11004 trial 2" scenario, with simulated drift fractions in blue, observed drift fractions in red, error bars indicate the standard deviation of measured drift fractions, and points indicate mean drift fractions. The plot indicates very good agreement between simulated and observed drift fractions, further substantiated by the statistical performance ($R^2 = 0.946$, RSR = 0.220).
(For interpretation of the references to color in this figure legend, the reader is referred to the Web version of this article.)

temperature (*temperature*) and relative humidity (*humidity*), with decreasing sensitivity, have a direct effect on the evaporation rate. The spray solution concentration (*sol_concentration*) and the application rate (*app_rate_kgha*), with decreasing sensitivity, have an indirect impact on the evaporation rate through the micrometeorological model.

Principle 2 characterizes the impact of a parameter on the atmospheric dispersion and the concentration field of the Gaussian puff, which subsequently affects the calculated deposition flux. With decreasing sensitivity wind speed (*wind_speed*), horizontal wind standard deviation (*sigma_horizontal*), and vertical wind standard deviation (*sigma_vertical*), directly affect the Gaussian puff, by influencing the horizontal distance traveled and the atmospheric dispersion of the puff, respectively. Number of application swaths (*swath_number*), field/swath length (*field_length*), and boom width (*boom_width*), with decreasing sensitivity, affect the total application area, which in turn affects the total amount of pesticide being transported by the Gaussian puff model to the virtual sampling line.

Principle 3 describes the influence of a parameter on the time a droplet travels to receiving surfaces, where a longer travel time allows a droplet to be transported horizontally by the wind. The mean droplet diameter (*mean_size*), boom height (*boom_height*), angle of the application nozzle (*nozzle_angle*), ambient pressure (*ambient_pressure*), deposition height (*deposition_height*), and application pressure (*application_pres*), with decreasing sensitivity, directly influence the travel time of a droplet.

Principle 4 characterizes the influence of a parameter on the horizontal distance traveled per unit of time. By changing the vertical wind profile through which a droplet travels to receiving surfaces, wind speed (*wind_speed*), surface roughness height (*roughness_height*), height at which the wind speed was measured (*wind_height*), canopy height (*canopy_height*), and leaf area index (*LAI*), with decreasing sensitivity, affect the horizontal distance traveled. The wind direction relative to the spray swath (*wind_direction*) affects the distance required to detect a droplet on

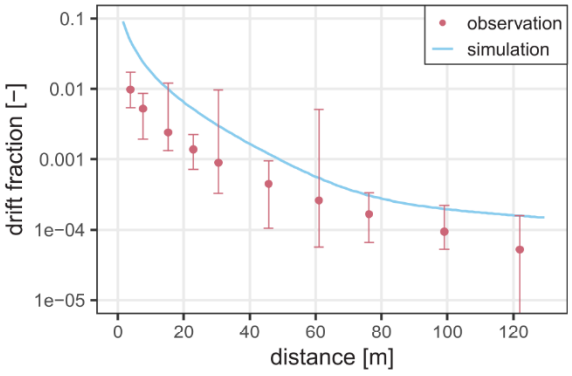


Fig. 6. Model evaluation for the "XR11003" scenario, with simulated drift fractions in blue, observed drift fractions in red, error bars indicate lowest and highest drift fractions measured, and points indicate mean drift fractions. The plot indicates a systematic overprediction of spray drift fractions by the model, resulting in poor statistical performance (R^2 = 0.492, RSR = 0.676).
(For interpretation of the references to color in this figure legend, the reader is referred to the Web version of this article.)

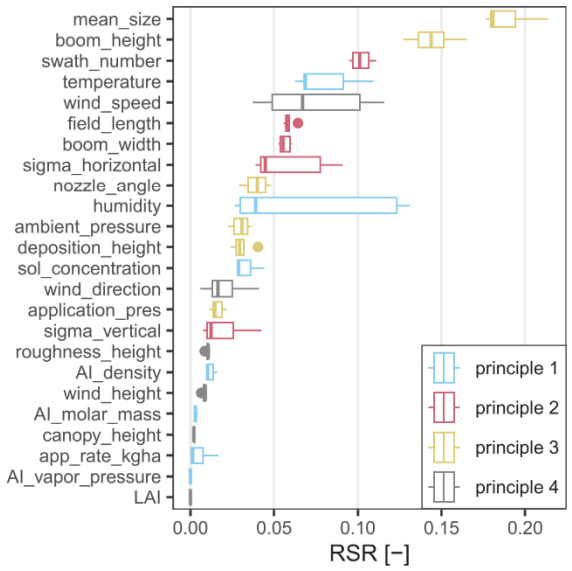


Fig. 7. Boxplots of DAD-drift input parameter sensitivity ranked from most to least sensitive based on RSR. Boxplots show median, 25th percentile, 75th percentile, with whisker indicating minimum and maximum values and points indicating potential outliers. With operating principle 1 (effect on evaporation) in blue, operating principle 2 (effect on atmospheric dispersion) in red, operating principle 3 (effect on droplet travel time) in yellow, and operating principle 4 (effect on horizontal droplet transport) in grey. Mean droplet diameter (*mean_size*), the spray boom height (*boom_height*), the number of application swaths (*swath_number*), the ambient air temperature (*temperature*), and the wind speed (*wind_speed*) show the highest sensitivity.
(For interpretation of the references to color in this figure legend, the reader is referred to the Web version of this article.)

the centerline.

Analysis of 10 DSDs used for the "XR11003" application scenario showed large differences between spray nozzle types (Fig. 8). The XR11003 nozzle is the most drift-prone with drift fractions ranging from 9.4×10^{-4} to 2.0×10^{-3} at 50 m from the edge-of-field and the TTI11004 nozzle is the least drift-prone with drift fractions ranging from 1.2×10^{-5} to 2.5×10^{-5} at 50 m from the edge-of-field. The drift fractions for the DG11004 and AIXR11002 nozzles are similar. Drift fractions range from 1.0×10^{-4} to 1.7×10^{-4} at 50 m from the edge-of-field for the DG11004 nozzle and from 4.7×10^{-5} to 1.3×10^{-4} at 50 m from the edge-of-field for the AIXR11002 nozzle (i.e., DG11004 is generally more drift-prone than AIXR11002). Comparing drift curves for the same nozzle type shows that small differences in DSD characteristics (i.e., DV0.1, DV0.5, DV0.9, V100, V150) have a large effect on the resulting drift curves. With maximum drift fractions at 50 m from the edge-of-field being larger than minimum drift fractions by a factor of 2.1, 1.7, 2.7 and 2.1, for the XR11003 nozzle, DG11004 nozzle, AIXR11002 nozzle and TTI11004 nozzle, respectively.

4. Discussion

4.1. Model evaluation

The parameterized DAD-drift model could successfully reproduce the spray drift observations of two field trial studies (Brain et al., 2019; Perine et al., 2021) and was therefore able to correctly represent spray drift behavior under a wide range of environmental conditions (i.e., temperature, humidity, wind speed), for four spray nozzles (fine to ultra-coarse DSD), and for distances up to 122 m. Since the vertical and horizontal wind direction standard deviation were used as empirical calibration parameters, a single parameter set was determined for all application scenarios to avoid overfitting to the respective application scenarios and to show general applicability of those parameter vales for modelling approaches where parameterization is not possible due to data constraints.

The model evaluation was performed up to 122 m from the edge-of-field, with no systematic bias in spray drift deposition far from the field. This is in contrasts to the RTDrift model, where spray drift deposition was underpredicted for distances greater than 20 m from the edge-of-field (Lebeau et al., 2011). This suggests that the implementation of a mechanistic droplet model in combination with a micrometeorological model, as well as the use of a three-dimensional Gaussian puff model, enabled significant improvements in long-range drift prediction. In addition, there was a slight overprediction of simulated drift values in the first 15 m for the "DG11004" and "AIXR11002" scenarios. Since an atmospheric dispersion model is at the core of DAD-drift, inaccuracies near the edge-of-field are to be expected, and since this modeling approach was developed to predict spray drift at the landscape scale, small discrepancies near the edge-of-field are acceptable.

The DAD-drift model was found to overpredict the spray drift for the "XR11003" application scenario. However, Study 2 found no significant difference between the deposition curves of the XR11003 and DG11004 nozzles (Perine et al., 2021), which is unexpected. The nozzle manufacturer classifies the XR11003 nozzle spray as "fine" and the DG11004 nozzle spray as "coarse" (TeeJet, 2023), which is supported by reported DSD characteristics (Gil et al., 2014; Porskamp et al., 2002). In addition, a drift reduction potential of 75% has been reported when comparing the DG nozzle to the XR nozzle (Perine et al., 2021), which is in good agreement with the drift reduction potential predicted by the DAD-drift model. Therefore, an underreporting of spray drift from the XR11003 nozzle in Study 2 is most likely causing the discrepancy between simulated and observed drift fractions for this nozzle. The subsequent exclusion of the "XR11003" scenario from the model parameterization reducing the available data points by ca. 15% lowering statistical power. Furthermore, no fine DSD is present in the parameterization dataset, however, the agreement between simulated and observed drift reduction potentials (DG11004 vs XR11003) indicates predictions for the "XR11003" scenario being accurate relative to the "DG11004" scenario.

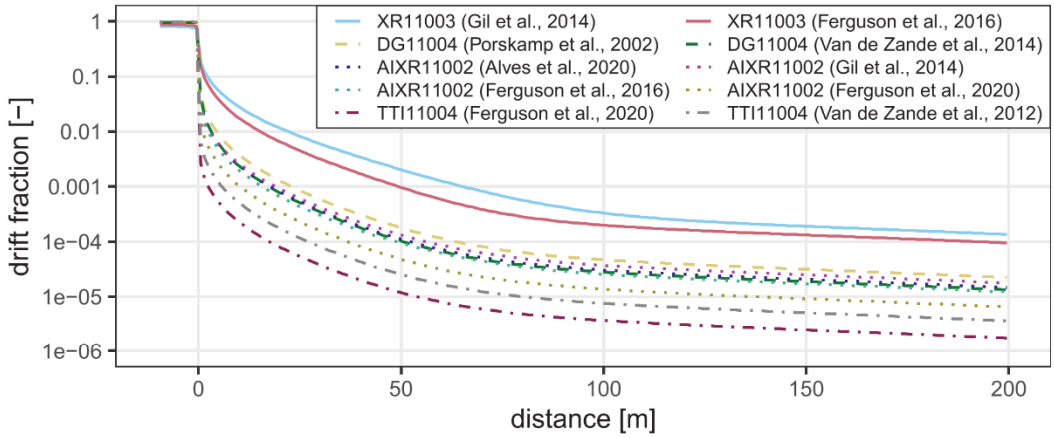


Fig. 8. Simulated drift curves for 10 drop size distributions generated based on reported values of 10% volume diameter (DV0.1), volume median diameter (DV0.5), 90% volume diameter (DV0.9), volume fraction less than 100 μm (V100), or volume fraction less than 150 μm (V150), all drop size distributions were combined with the application conditions of the "XR11003" application scenario.
(For interpretation of the references to color in this figure legend, the reader is referred to the Web version of this article.)

4.2. Sensitivity analysis

The sensitivity analysis showed clear and understandable model behavior when input parameters are varied. The DAD-drift model is in good agreement with the literature regarding the important factors that affect spray drift. The importance of the DSD has been frequently reported (De Cock et al., 2017; Felsot et al., 2010; Lebeau et al., 2011; Thompson and Ley, 1983). The importance of the boom height has also been reported previously (Nuyttens et al., 2007a; Thompson and Ley, 1983). Furthermore, wind speed and atmospheric turbulence as well as the evaporation rate of a droplet have been reported as relevant factors for spray drift (Thompson and Ley, 1983).

For some of the input parameters of the DAD-drift model, a large inter-scenario variation in parameter sensitivity was observed. For temperature, wind speed, humidity, and wind direction, these inter-scenario differences can be explained by the large range of absolute parameter values. Applying the same percentage change to a small parameter value will result in a smaller range when compared to a larger parameter value. The inter-scenario variation for the horizontal and vertical wind direction standard deviations can be explained by the different nozzle types used in the application scenarios. Smaller droplets stay airborne longer and are therefore more strongly affected by horizontal and vertical dispersion. Therefore, the "XR11003" with the largest fraction of small droplets also showed the highest sensitivity to these parameters (Table S6). The negligibly small effect sizes for canopy height and LAI are caused by their small absolute value and the deposition height being larger than the canopy height, hence the droplets never enter the part of the wind profile determined by canopy height and LAI (Section 2.6). The evaporation rate of the water within the droplet is multiple magnitudes larger than the evaporation rate of the AI, hence the AI vapor pressure shows no effect on the model outcome.

The analysis of 10 droplet size distributions using the "XR11003" application scenario clearly demonstrated the previously reported importance of the spray nozzle type (Nuyttens et al., 2007b). Additionally, when comparing multiple DSDs for the same nozzle type, it is clear, that small variations in DV0.1, DV0.5, DV0.9, V100, and V150 result in significantly different spray drift predictions. This indicates that high quality nozzle information is essential for accurate spray drift prediction. However, it remains unclear how to determine "correct" nozzle information, due to the considerable variation in reported values caused by differences in measuring protocol and settings as well as the type of measuring equipment (Nuyttens et al., 2007b).

4.3. Model limitations and potential improvements

In its current form DAD-drift has no representation of the spatial arrangement of the nozzles on the spray boom, this allows for the prediction of a universal deposition pattern as emitted by one unit of application area, substantially improving computation time and model versatility. Further, droplet ejection from the nozzle is represented by an instantaneous point source, with no representation of the spray cone, which mainly affects the prediction of spray drift near the edge-of-field. By splitting the spray cone into multiple segments and running the droplet model and the dispersion model for each segment, an improvement of near field predictions and nozzle representation could be achieved.

The process of plant canopy interception is not represented in the DAD-drift model, furthermore the landscape is represented as a flat plane. These are assumed to be the worst-case representation of spray drift at the landscape scale, since droplet trajectories are unrestricted over large distances.

Currently, the droplet model within DAD-drift represents a droplet as a two-component mixture of water and the active ingredient. However, spray mixtures often contain additional adjuvants, designed to reduce spray drift and to increase droplet retention (Felsot et al., 2010; Griesang et al., 2017). Therefore, it may be useful to introduce additional adjuvant components to the spray mixture. This change would most likely affect small droplets the most, as the additional adjuvant mass would increase the minimum droplet size once the water has evaporated.

The downward motion of spray droplets is known to transfer its momentum to the surrounding air, causing air to be entrained in the spray. This entrained air reduces the drag forces on the droplets and increases the distance droplets travels until they decelerate from their initial velocity to their settling velocity (stopping distance) (Butler Ellis and Miller, 2010; Thompson and Ley, 1983), resulting in lower vertical droplet positions. For a more accurate representation of droplet trajectories, it may be beneficial to implement an air entrainment model similar to the Silsoe spray drift model (Butler Ellis and Miller, 2010) into DAD-drift.

5. Summary & conclusion

The Droplet and Atmospheric Dispersion drift (DAD-drift) model is a novel modeling approach that combines a mechanistic droplet model, a micrometeorological model, and a three-dimensional Gaussian diffusion

model. It is an iteration of the previously published two-dimensional tilting plume approach and allows for the prediction of spray drift deposition from ground spray applications while accounting for environmental conditions, spray nozzle characteristics, and spray application characteristics.

Model evaluation was performed against two field trial studies for a wide range of environmental conditions (i.e., temperature, humidity, wind speed) for four spray nozzles (fine to ultra-coarse). The DAD-drift model was able to predict the spray drift observations from these studies with very good agreement ($R^2 = 0.931$, RSR = 0.260), demonstrating its applicability over a wide range of conditions.

The DAD-drift model showed clear and understandable behavior when input parameters were varied during a one-at-a-time sensitivity analysis. It was also in good agreement with the literature regarding the important factors that determine spray drift, including the droplet size distribution, the boom height, the temperature, the wind speed, and the atmospheric turbulence. The sensitivity analysis substantiates best management practices such as applying pesticides using drift reduction nozzles and low boom heights during low wind and low temperature conditions.

We are confident that the mechanistic nature of the DAD-drift model, combined with the evaluation up to 122 m, allows for the prediction of spray drift over distances significantly larger than the field scale. It is therefore, a computationally efficient modeling approach that allows landscape-level spray drift assessment, including spray drift entries into surface waterbodies and deposition onto other non-target areas (e.g., fields, protected areas, urban areas). In combination with other modeling approaches, such as ecotoxicological modeling or eco-hydrological modeling (e.g., SWAT+), DAD-drift is a useful tool to further the understanding of pesticide transport at the landscape scale.

CRediT authorship contribution statement

Mike Devin Fuchs: Writing – original draft, Visualization, Validation, Software, Methodology, Investigation, Formal analysis, Data curation, Conceptualization. **Sebastian Gebler:** Writing – review & editing, Writing – original draft, Supervision, Methodology, Conceptualization. **Andreas Lorke:** Writing – review & editing, Supervision.

Declaration of competing interest

The authors declare the following financial interests/personal relationships which may be considered as potential competing interests: Mike Devin Fuchs reports financial support was provided by BASF SE, Carl-Bosch-Str. 38, 67056 Ludwigshafen, Germany. Sebastian Gebler reports financial support was provided by BASF SE, Carl-Bosch-Str. 38, 67056 Ludwigshafen, Germany. If there are other authors, they declare that they have no known competing financial interests or personal relationships that could have appeared to influence the work reported in this paper.

Acknowledgements

The authors thank Christopher Hassinger (BASF Corporation, United States) for the valuable language editing.

Appendix A. Supplementary data

Supplementary data to this article can be found online at https://doi.org/10.1016/j.envres.2025.121104.

Data availability

Data will be made available on request.

References

Alves, G.S., Vieira, B.C., Butts, T.R., Silva, S.M., Cunha, J.P.A.R. Da, Kruger, G.R., 2020. Drift potential from glyphosate and 2,4-d applications as influenced by nozzle type, adjuvant, and airspeed. Appl. Eng. Agric. 36, 687–696. https://doi.org/10.13031/AEA.13604.

Baetens, K., Ho, Q.T., Nuyttens, D., Schampheleire, M. De, Melese Endalew, A., Hertog, M.L.A.T.M., Nicolaï, B., Ramon, H., Verboven, P., 2009. A validated 2-D diffusion–advection model for prediction of drift from ground boom sprayers. Atmos. Environ. 43, 1674–1682. https://doi.org/10.1016/j.atmosenv.2008.12.047.

Baetens, K., Nuyttens, D., Verboven, P., Schampheleire, M. De, Nicolaï, B., Ramon, H., 2007. Predicting drift from field spraying by means of a 3D computational fluid dynamics model. Comput. Electron. Agric. 56, 161–173. https://doi.org/10.1016/j.compag.2007.01.009.

Brain, R., Goodwin, G., Abi-Akar, F., Lee, B., Rodgers, C., Flatt, B., Lynn, A., Kruger, G., Perkins, D., 2019. Winds of change, developing a non-target plant bioassay employing field-based pesticide drift exposure: a case study with atrazine. Sci. Total Environ. 678, 239–252. https://doi.org/10.1016/j.scitotenv.2019.04.411.

Bub, S., Schad, T., Gao, Z., 2020. XDrift—an R package to simulate spatially explicit pesticide spray-drift exposure of non-target-species habitats at landscape scales. SoftwareX 12, 100610. https://doi.org/10.1016/j.softx.2020.100610.

Bueno, M.R., Cunha, J.P.A.R. da, Santana, D.G. de, 2017. Assessment of spray drift from pesticide applications in soybean crops. Biosyst. Eng. 154, 35–45. https://doi.org/10.1016/j.biosystemseng.2016.10.017.

Butler Ellis, M.C., Miller, P.C.H., 2010. The Silsoe Spray Drift Model: a model of spray drift for the assessment of non-target exposures to pesticides. Biosyst. Eng. 107, 169–177. https://doi.org/10.1016/j.biosystemseng.2010.09.003.

Cock, N. De, Massinon, M., Salah, S.O.T., Lebeau, F., 2017. Investigation on optimal spray properties for ground based agricultural applications using deposition and retention models. Biosyst. Eng. 162, 99–111. https://doi.org/10.1016/j.biosystemseng.2017.08.001.

Craig, I., 2004. The GDS model—a rapid computational technique for the calculation of aircraft spray drift buffer distances. Comput. Electron. Agric. 43, 235–250. https://doi.org/10.1016/j.compag.2004.02.001.

Delele, M.A., Jaeken, P., Debaer, C., Baetens, K., Endalew, A.M., Ramon, H., Nicolaï, B., Verboven, P., 2007. CFD prototyping of an air-assisted orchard sprayer aimed at drift reduction. Comput. Electron. Agric. 55, 16–27. https://doi.org/10.1016/j.compag.2006.11.002.

Djouhri, M., Loubet, B., Bedos, C., Dages, C., Douzals, J.-P., Voltz, M., 2023. ADDI-Spraydrift: a comprehensive model of pesticide spray drift with an assessment in vineyards. Biosyst. Eng. 231, 57–77. https://doi.org/10.1016/j.biosystemseng.2023.05.008.

Dorr, G.J., Hewitt, A.J., Adkins, S.W., Hanan, J., Zhang, H., Noller, B., 2013. A comparison of initial spray characteristics produced by agricultural nozzles. Crop Prot. 53, 109–117. https://doi.org/10.1016/j.cropro.2013.06.017.

Draxler, R.R., 1976. Determination of atmospheric diffusion parameters. Atmos. Environ. 10, 99–105. https://doi.org/10.1016/0004-6981(76)90226-2.

Duga, A.T., Delele, M.A., Ruysen, K., Dekeyser, D., Nuyttens, D., Bylemans, D., Nicolai, B. M., Verboven, P., 2017. Development and validation of a 3D CFD model of drift and its application to air-assisted orchard sprayers. Biosyst. Eng. 154, 62–75. https://doi.org/10.1016/j.biosystemseng.2016.10.010.

Felsot, A.S., Unsworth, J.B., Linders, J.B.H.J., Roberts, G., Rautman, D., Harris, C., Carazo, E., 2010. Agrochemical spray drift; assessment and mitigation—a review. J. Environ. Sci. Heal. Part B 46, 1–23. https://doi.org/10.1080/03601234.2010.515161.

Ferguson, J.C., Hewitt, A.J., O'Donnell, C.C., Kruger, G.R., 2023. Comparison of water-sensitive paper, Kromekote and Mylar collectors for droplet deposition with a visible fluorescent dye solution. J. Plant Prot. Res. 60, 98–105. https://doi.org/10.24425/jppr.2020.132210.

Ferguson, J.C., Chechetto, R.G., O'Donnell, C.C., Dorr, G.J., Moore, J.H., Baker, G.J., Powis, K.J., Hewitt, A.J., 2016. Determining the drift potential of Venturi nozzles compared with standard nozzles across three insecticide spray solutions in a wind tunnel. Pest Manag. Sci. 72, 1460–1466. https://doi.org/10.1002/ps.4214.

Fuchs, M.D., 2024. DAD-drift. https://doi.org/10.5281/zenodo.11486371.

Gil, E., Balsari, P., Gallart, M., Llorens, J., Marucco, P., Andersen, P.G., Fàbregas, X., Llop, J., 2014. Determination of drift potential of different flat fan nozzles on a boom sprayer using a test bench. Crop Prot. 56, 58–68. https://doi.org/10.1016/j.cropro.2013.10.018.

Gil, Y., Sinfort, C., 2005. Emission of pesticides to the air during sprayer application: a bibliographic review. Atmos. Environ. 39, 5183–5193. https://doi.org/10.1016/j.atmosenv.2005.05.019.

Griesang, F., Decaro, R.A., Santos, C.A.M. dos, Santos, E.S., Lima, Roque, de, N.H., Ferreira, Costa, da, M., 2017. How much do adjuvant and nozzles models reduce the spraying drift? Drift in agricultural spraying. Am. J. Plant Sci. 8, 2785–2794. https://doi.org/10.4236/ajps.2017.811188.

Hewitt, A., 2000. Spray drift: impact of requirements to protect the environment. Crop Prot. 19, 623–627. https://doi.org/10.1016/S0261-2194(00)00082-X.

Hewitt, A.J., Johnson, D.R., Fish, J.D., Hermansky, C.G., Valcore, D.L., 2002. Development of the Spray Drift Task force database for aerial applications. Environ. Toxicol. Chem. 21, 648–658. https://doi.org/10.1002/etc.5620210326.

Hilz, E., Vermeer, A.W.P., 2013. Spray drift review: the extent to which a formulation can contribute to spray drift reduction. Crop Prot. 44, 75–83. https://doi.org/10.1016/j.cropro.2012.10.020.

Holterman, H.J., Zande, J.C. van de, Huijsmans, J.F.M., Wenneker, M., 2017. An empirical model based on phenological growth stage for predicting pesticide spray

Appendix I:

drift in pome fruit orchards. Biosyst. Eng. 154, 46–61. https://doi.org/10.1016/j.biosystemseng.2016.08.016.
Holterman, H.J., 2003. Kinetics and evaporation of water drops in air. IMAG rapport 2003–12. https://doi.org/10.18174/562300.
Holterman, H.J., Zande, J.C. Van De, Porskamp, H.A.J., Michielsen, J., 1998. IDEFICS : a Physical Model of Spray drift from Boom Sprayers in Agriculture. ILASS-Europe, Manchester.
Hong, S.-W., Zhao, L., Zhu, H., 2018a. CFD simulation of pesticide spray from air-assisted sprayers in an apple orchard: tree deposition and off-target losses. Atmos. Environ. 175, 109–119. https://doi.org/10.1016/j.atmosenv.2017.12.001.
Hong, S.-W., Zhao, L., Zhu, H., 2018b. CFD simulation of airflow inside tree canopies discharged from air-assisted sprayers. Comput. Electron. Agric. 149, 121–132. https://doi.org/10.1016/j.compag.2017.07.011.
Kim, S., Chen, J., Cheng, T., Gindulyte, A., He, J., He, S., Li, Q., Shoemaker, B.A., Thiessen, P.A., Yu, B., Zaslavsky, L., Zhang, J., Bolton, E.E., 2023. PubChem 2023 update. Nucleic Acids Res. 51, D1373–D1380. https://doi.org/10.1093/nar/gkac956.
Küçüktopcu, E., Cemek, B., 2021. The use of artificial neural networks to estimate optimum insulation thickness, energy savings, and carbon dioxide emissions. Environ. Prog. Sustain. Energy 40, 1–13. https://doi.org/10.1002/ep.13478.
Lebeau, F., Verstraete, A., Stainier, C., Destain, M.-F., 2011. RTDrift: a real time model for estimating spray drift from ground applications. Comput. Electron. Agric. 77, 161–174. https://doi.org/10.1016/j.compag.2011.04.009.
Løfstrøm, P., Bruus, M., Andersen, H.V., Kjær, C., Nuyttens, D., Astrup, P., 2013. The OML-SprayDrift model for predicting pesticide drift and deposition from ground boom sprayers. J. Pestic. Sci. 38, 129–138. https://doi.org/10.1584/jpestics.D12-064.
Mackay, D., Wesenbeeck, I. van, 2014. Correlation of chemical evaporation rate with vapor pressure. Environ. Sci. Technol. 48, 10259–10263. https://doi.org/10.1021/es5029074.
Miller, P., 2014. Spray drift. In: Pesticide Application Methods. Wiley, pp. 337–361. https://doi.org/10.1002/9781118351284.ch12.
Moriasi, D.N., Arnold, J.G., Liew, M.W. Van, Bingner, R.L., v, R.D., Veith, T.L., 2007. Model evaluation guidelines for systematic quantification of accuracy in watershed simulations. Trans. ASABE (Am. Soc. Agric. Biol. Eng.) 50, 885–900. https://doi.org/10.13031/2013.23153.
Nuyttens, D., Schampheleire, M. De, Baetens, K., Sonck, B., 2008. Comparison of different drift risk assessment means. In: International Advances in Pesticide Application (2008). AAB, pp. 35–42, 1999.
Nuyttens, D., Schampheleire, M. De, Baetens, K., Sonck, B., 2007a. The influence of operator-controlled variables on spray drift from field crop sprayers. Trans. ASABE (Am. Soc. Agric. Biol. Eng.) 50, 1129–1140. https://doi.org/10.13031/2013.23622.
Nuyttens, D., Baetens, K., Schampheleire, M. De, Sonck, B., 2007b. Effect of nozzle type, size and pressure on spray droplet characteristics. Biosyst. Eng. 97, 333–345. https://doi.org/10.1016/j.biosystemseng.2007.03.001.
Perine, J., Anderson, J.C., Kruger, G.R., Abi-Akar, F., Overmyer, J., 2021. Effect of nozzle selection on deposition of thiamethoxam in Actara® spray drift and implications for off-field risk assessment. Sci. Total Environ. 772, 144808. https://doi.org/10.1016/j.scitotenv.2020.144808.
Porskamp, H.A.J., Zande, J.C. Van de, Porskamp, J., 2002. Druppelgroottemetingen Teejet, Hardi en Lechler spuitdoppen ter verkrijging van de status driftarm volgens het Lozingenbesluit. IMAG Vol. 2002, No 60.
Raupach, M.R., Briggs, P.R., Ahmad, N., Edge, V.E., 2001. Endosulfan transport: II. Modeling airborne dispersal and deposition by spray and vapor. J. Environ. Qual. 30, 729–740. https://doi.org/10.2134/jeq2001.303729x.
Rautmann, D., Streloke, M., Winkler, R., 2001. New basic drift values in the Authorization procedure for plant protection products. Mitteilungen aus der Biol. Bundesanstalt für L. 388, 133–141.
Souto, M.J., Souto, J.A., Pérez-Muñuzuri, V., Casares, J.J., Bermúdez, J.L., 2001. A comparison of operational Lagrangian particle and adaptive puff models for plume dispersion forecasting. Atmos. Environ. 35, 2349–2360. https://doi.org/10.1016/S1352-2310(00)00537-9.
Sypka, P., Starzak, R., 2013. Simplified, empirical model of wind speed profile under canopy of Istebna spruce stand in mountain valley. Agric. For. Meteorol. 171–172, 220–233. https://doi.org/10.1016/j.agrformet.2012.11.003.
TeeJet, 2023. TeeJet: broadcast nozzles [WWW Document]. URL. https://www.teejet.com/-/media/dam/agricultural/usa/sales-material/catalog/broadcast_nozzles.pdf.
Tercan, H., Guajardo, A., Heinisch, J., Thiele, T., Hopmann, C., Meisen, T., 2018. Transfer-learning: bridging the gap between real and simulation data for machine learning in injection molding. Procedia CIRP 72, 185–190. https://doi.org/10.1016/j.procir.2018.03.087.
Teske, M.E., Bird, S.L., Esterly, D.M., Curbishley, T.B., Ray, S.L., Perry, S.G., 2002. AgDRIFT®: a model for estimating near-field spray drift from aerial applications. Environ. Toxicol. Chem. 21, 659. https://doi.org/10.1897/1551-5028(2002)021<0659:aamfen>2.0.co, 2.
Thompson, N., Ley, A.J., 1983. Estimating spray drift using a random-walk model of evaporating drops. J. Agric. Eng. Res. 28, 419–435. https://doi.org/10.1016/0021-8634(83)90134-8.
Wang, M., Rautmann, D., 2008. A simple probabilistic estimation of spray drift—factors determining spray drift and development of a model. Environ. Toxicol. Chem. 27 (1), 2617–2626. https://doi.org/10.1897/08-109.
Zande, J.C. van de, Groot, T.T., Holterman, H.J., 2012. Drift bij hoge rijsnelheid: modelberekeningen naar effect van rijsnelheid, doptype, spuitboomhoogte en dopafstand op de spuitboom.
Zande, J.C. Van de, Michielsen, J.G.P., Stallinga, H., Velde, P. van, 2014. Spray drift of reducing nozzle types spraying a bare soil surface with a boom sprayer. Int. Adv. Pestic. Appl. Oxford, UK 122, 245–254.
Zannetti, P., 1990. Gaussian models. In: Air Pollution Modeling. Springer US, Boston, MA, pp. 141–183. https://doi.org/10.1007/978-1-4757-4465-1_7.
Zhang, L., 2001. A size-segregated particle dry deposition scheme for an atmospheric aerosol module. Atmos. Environ. 35, 549–560. https://doi.org/10.1016/S1352-2310(00)00326-5.

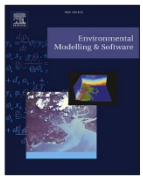
Appendix II:

Environmental Modelling and Software 189 (2025) 106455

Contents lists available at ScienceDirect

Environmental Modelling and Software

journal homepage: www.elsevier.com/locate/envsoft



Landscape-level assessment of spray drift – A virtual experiment using the Droplet and Atmospheric Dispersion drift (DAD-drift) model

Mike Devin Fuchs [a,b,*], Sebastian Gebler [a], Andreas Lorke [b]

[a] BASF SE, Exposure Modelling, Speyerer Straße 2, 67117, Limburgerhof, Germany
[b] Institute for Environmental Sciences, University of Kaiserslautern-Landau, Forststraße 7, Landau in der Pfalz, 76829, Germany

ARTICLE INFO

Handling Editor: Daniel P Ames

Keywords:
Spray-drift
Landscape scale
Pesticide deposition
Boom application
Meta-modeling

ABSTRACT

Spray drift significantly contributes to the off-target movement of pesticides. While factors influencing spray drift at the field scale, such as environmental conditions, equipment, and buffer zones, are well understood, deposition at landscape scale, is influenced by additional factors including landscape characteristics and the proximity of non-target areas. The DAD-drift model accounts for the physical basis of spray drift, application location, wind direction, and deposition at the landscape scale. In a virtual experiment we compared DAD-drift with simplified spatial representations of application areas, commonly used in other modelling approaches, the results showed large differences in spray drift predictions. In a second virtual experiment, results from DAD-drift were analyzed using multiple linear regressions to identify spray drift drivers at the landscape scale. Results showed that the droplet size distribution, determined by nozzle type, closely followed by proximity to non-target area, are the two most influential factors determining deposition in non-target areas.

1. Introduction

The determination of the fate and transport of pesticides after application on agricultural crops is of high relevance for pesticide registration, product stewardship, authorities, and other stakeholders. Pesticides are transported from treated fields to non-target areas via surface and subsurface runoff, leaching, surface drainage and spray drift (Vallée et al., 2014; Zhang et al., 2018). While surface runoff is recognized as the most prevalent pesticide transport pathway, spray drift was found to potentially contribute significantly to the off-target movement of pesticides. With, Zhang et al. (2018) concluding that spray drift contributed 24 % of the total annual off-target? mass load and more than half of the pesticide mass load during the summer months in the surface waters in their study area.

Research on spray drift is mostly limited to the field scale, i.e., up to 50–100 m from the edge-of-field. These studies analyzed the influence of various processes and factors on spray drift, including weather conditions during spray application, such as wind speed, temperature, and humidity (Nuyttens et al., 2007a); in-flight movements of spray droplets (Cock et al., 2017; Holterman et al., 2017; Thompson and Ley, 1983); spray equipment mainly through the drop size distribution emitted by spray nozzles (Miller, 2014; Nuyttens et al., 2007b); spray formulation (Hilz and Vermeer, 2013); and unsprayed buffers zones, hooded sprayers, and windbreaks as mitigation measures (Felsot et al., 2010; Miller, 2014). Unlike individual spray applications that are performed at the field scale, spray drift deposition occurs at the landscape scale and is dependent on a wide range of factors. Environmental conditions (e.g., wind speed, wind direction, temperature, humidity), operational parameters (e.g., application method, nozzle type, mixture formulation), crop type, and application date are highly relevant for spray applications on individual fields in a catchment, and can vary greatly in space and time (Reeg et al., 2017). Furthermore, the relative location of application areas to non-target areas is important to accurately account for the spatial organization and characteristics of the landscape in spray drift assessments (Mottes et al., 2014). In light of this complexity and the prohibitive costs of monitoring, modeling is best suited to understand spray drift at the landscape scale. In the following section, a brief overview of different modeling approaches is provided.

Existing landscape-level modeling approaches can be categorized into spray drift deposition modeling (Bub et al., 2020; Holterman and Zande, 2008), spray drift exposure and effect modeling (Schad and Schulz, 2011), and spray drift deposition and pesticide fate modeling. For the latter approach, either the soil and water assessment tool (SWAT) (Arnold et al., 1998; Holvoet et al., 2008; Winchell et al., 2018;

* Corresponding author. BASF SE, Exposure Modelling, Speyerer Straße 2, 67117, Limburgerhof, Germany.
E-mail address: m.d.fuchs@protonmail.com (M.D. Fuchs).

https://doi.org/10.1016/j.envsoft.2025.106455
Received 17 December 2024; Received in revised form 3 March 2025; Accepted 1 April 2025
Available online 2 April 2025
1364-8152/© 2025 The Authors. Published by Elsevier Ltd. This is an open access article under the CC BY-NC-ND license (http://creativecommons.org/licenses/by-nc-nd/4.0/).

Zhang et al., 2018), the toxic substances in surface waters (TOXSWA) model (Adriaanse, 1996; Padovani et al., 2004), or a surface runoff connectivity model (Schönenberger et al., 2022) have been used.

Spray drift prediction was performed using either the deterministic AgDRIFT model (Teske et al., 2002; Winchell et al., 2018), or empirical models based on field trials conducted in the modeled landscape (Padovani et al., 2004), multiple linear regression of the deterministic IDEFICS model (Holterman and Zande, 2008; Holterman et al., 1998), unspecified field trials (Schad and Schulz, 2011), or the basic drift values (Bub et al., 2020; Ganzelmeier et al., 1995; Holvoet et al., 2008; Rautmann et al., 2001; Schönenberger et al., 2022; Zhang et al., 2018). These empirical models do not account for the physical basis of spray drift; therefore, their application is limited to environmental conditions (e.g., wind speed, temperature, humidity, nozzle type) and distances from the edge-of-field that closely match the observational data from which they were developed (Teske et al., 2002). The relative location of application areas to non-target areas was described by a simplified spatial representation in some approaches (Holvoet et al., 2008; Padovani et al., 2004; Winchell et al., 2018; Zhang et al., 2018) and by a detailed spatial representation in others (Bub et al., 2020; Holterman and Zande, 2008; Schad and Schulz, 2011; Schönenberger et al., 2022). The wind direction was either considered (Bub et al., 2020; Holterman and Zande, 2008; Schönenberger et al., 2022; Zhang et al., 2018), not considered (Padovani et al., 2004), simplified to four cardinal wind directions (Schad and Schulz, 2011), simplified to two wind direction (northwest/southeast) (Winchell et al., 2018), or not further specified (Holvoet et al., 2008). Spray drift deposition was predicted for surface waters for most approaches (Holterman and Zande, 2008; Holvoet et al., 2008; Padovani et al., 2004; Winchell et al., 2018; Zhang et al., 2018), for surface waters and drained roads for one (Schönenberger et al., 2022), and over the entire spatial domain for two (Bub et al., 2020; Schad and Schulz, 2011).

With the droplet and atmospheric dispersion drift (DAD-drift) model, a spray drift modeling approach simultaneously accounting for the physical basis of spray drift, the relative location of application areas to non-target areas, the wind direction, and spray drift deposition over the complete domain at the landscape scale was presented. The theoretical basis of the model, a one-at-a-time sensitivity analysis, and a model evaluation using two field studies with different environmental conditions and technical equipment (i.e., nozzle types) have been described previously (Fuchs et al., 2025).

The aim of this paper is (1) to assess the influence of simplified spatial representations of the relative location of application areas to non-target areas on the predicted spray drift deposition and how these predictions might influence higher level modelling; (2) to identify important spray drift drivers at the landscape scale.

2. Material and methods

2.1. DAD-drift introduction

The DAD-drift model combines a mechanistic droplet model, a micrometeorological model, and a three-dimensional Gaussian diffusion model, see Fig. S1 in the supplementary materials. The Motion and mass balance of representative droplets for each size class are predicted by the droplet model based on droplet parameters (e.g., density, size, velocity), release height, environmental conditions (e.g., ambient pressure, wind direction, wind speed), and output from the micrometeorological model (i.e., temperature, humidity). The micrometeorological model estimates the change in humidity and temperature caused by droplet evaporation, thus accounting for indirect droplet interaction within the spray cloud. Both models are calculated simultaneously and for all size classes defined in the droplet size distribution (DSD). In the dispersion model the atmospheric dispersion of the droplet cloud is predicted by estimating the mean position of a three-dimensional puff based on the droplet trajectories derived by the droplet model and subsequently predicting the three-dimensional concentration field. The deposition mass flux at a user-defined deposition height is predicted by the deposition model by combining the concentration field (dispersion model) and the vertical droplet velocity (droplet model), resulting in a two-dimensional deposition pattern representative of a unit of application area (1 × 1 m). For the landscape-level mode of DAD-drift, the application area is provided by the user as a raster file and the resulting deposition flux is returned as model output (Fig. 1a). For the drift curve mode, the application area is defined by the model inputs boom width, number of spray swaths, and field length and is intended to represent field trials, where spraying is performed perpendicular to the wind direction and collectors are positioned downwind of the spray swath. The drift fraction as a function of downwind distance is returned as model output (Fig. 1b). More details on the theoretical background of the model can be found in Fuchs et al. (2025) and in the model documentation (Fuchs, 2024).

DAD-drift requires model inputs for application parameters, formulation parameters, environmental conditions, and calibration parameters (Table S1). An important factor in the determination of spray drift distributions is the droplet size distribution (DSD) emitted by the spray nozzle during application. The user needs to define the DSD in a separate input file in the form of a cumulated distribution with mean droplet diameter and fraction. In the previously presented model evaluation (Fuchs et al., 2025) and in this work the DSDs are modeled based on 10 % volume diameter (DV0.1), volume median diameter (DV0.5), 90 % volume diameter (DV0.9), and volume fraction less than 100 μm (V100) reported in the literature. To ensure a correct and adequate spatial representation of the application area in the landscape mode and to avoid application outside the intended area of application (overspray), the shapefile was buffered (−0.75 m) before rasterization, see the grey raster and black outline of the shapefile in Fig. 1a.

2.2. Spatial spray drift representation

Due to the complex spatial organization at the landscape, some modelling approaches used simplified spatial representations of the relative location of application areas to non-target areas (Holvoet et al., 2008; Padovani et al., 2004; Winchell et al., 2018; Zhang et al., 2018). The impact of these simplified spatial representations on predicted spray drift deposition is evaluated by comparing DAD-drift in landscape mode against three simplified spatial algorithms used in the past, varying in their representation of source areas, drift fractions, and receiving areas.

2.2.1. Model inputs

Model inputs were adapted from the “DG11004” application scenario, previously parameterized using field observation data (Fuchs et al., 2025), see Table S1. The deposition height parameter was changed from the collector height in the field trial to a value of 0 m since deposition at the ground level was of interest in this approach. Model inputs were combined with four TeeJet spray nozzles (XR11003, DG11004, AIXR11002, and TTI11004) at their respective application pressures (276 kPa, 165 kPa, 207 kPa, 276 kPa), classified as having a “fine”, “coarse”, “very-coarse”, and “ultra-coarse” DSD (TeeJet, 2023), respectively and hereafter referred to as to as XR, DG, AIXR, and TTI, respectively. Drift curve prediction was performed with a wind direction of 90° to adhere to the ideal scenario of the wind speed blowing orthogonal to the spray swath orientation (Table S1).

2.2.2. Spray drift prediction methods

Four methods were considered. For method A the DAD-drift model was executed in landscape mode. For methods B, C, and D the required drift curves were generated with DAD-drift in drift curve mode, to allow for better comparability between the methods. See Table 1 for a summary of the spray drift prediction methods and Fig. 2 for a schematic representation of methods B, C, and D. All spray drift prediction methods were applied to various combinations of application areas and receiving

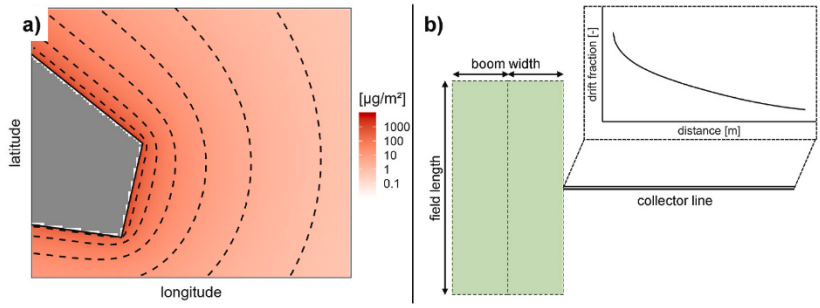


Fig. 1. Schematic representation of the DAD-drift model modes. A) The landscape-level mode, with the outline of the shapefile in black, the raster in grey, the predicted spray deposition in red, and concentration field lines in dashed black indicating steps of $10^{\circ \cdot 5}$ µg/m^2. B) The drift curve mode, with two spray swaths in green, and the central collector line along which spray deposition is predicted, similar to the setup of spray drift trials. (For interpretation of the references to colour in this figure legend, the reader is referred to the Web version of this article.)

Table 1
Summary of the spray drift prediction methods A, B, C, and D, with a general description, equations, and references.

Method	Description	Equation	Reference
A	• DAD-drift landscape mode. • Based on rasterized field data, environmental conditions, and application conditions. • Model output raster masked by waterbody shapefile. • Deposition flux summed up for total deposition mass.		
B	• Application area represented by square field. • Area of receiving waterbody defined by length of one side of the square and channel width. • Mean drift fraction by integrating drift curve across waterbody. From the distance from the edge of field to the nearest edge of the waterbody to the distance from the edge of field to the farthest edge of the waterbody.	$m_{drift} = app_{rate}\sqrt{A_{field}}w_{wb}\left[\int_{x_1}^{x_2} d_c(x)dx\right]\frac{1}{x_2 - x_1} = app_{rate}A_{wb}\bar{c}$ (1) Where, app_{rate} (kg m^{-2}) is the application rate, A_{field} (m^2) is the area of the field, w_{wb} (m) is the width of the waterbody, $d_c(x)$ (−) is the drift curve expressing the drift fraction as a function of the edge of field distance x, x_1 (m) is the distance from the edge of field to the nearest edge of the waterbody, x_2 (m) is the distance from the edge of field to the farthest edge of the waterbody, A_{wb} (m^2) is the area of the waterbody, and $\bar{c}$ (−) is the mean drift fraction across the waterbody.	Holvoet et al. (2008)
C	• Application area represented by circular field, with same centroid and area as the actual area. • Area of receiving waterbody defined by projection of circular field onto waterbody. • Drift fraction at shortest distance to waterbody.	$m_{drift} = app_{rate}A_{wb}c_{min}$ (2) Where, app_{rate} (kg m^{-2}) is the application rate, A_{wb} (m^2) is the area of the waterbody, and c_{min} (−) is the drift fraction at the shortest distance between edge of field and waterbody.	Zhang et al. (2018)
D	• Application area represented by circular field, with same centroid and area as the actual area. • Proximity zones around circular field (0–20m, 20–50m, 50–100m, 100–200m, 200–400m). • Drift fraction for each proximity zone by averaging drift curve. • Intersection area between each proximity zone and waterbody. • Area of receiving waterbody as sum of intersection areas. • Mean drift fraction defined by drift fraction of proximity zones, normalized by areas of proximity zones.	$m_{drift} = app_{rate}\left[\sum_{i=0}^{n} A_i\right]\left[\frac{\sum_{i=0}^{n} c_i{}^{*}A_i}{\sum_{i=0}^{n} A_i}\right] = app_{rate}A_{wb}\hat{c}$ (3) Where, app_{rate} (kg m^{-2}) is the application rate, A_i (m^2) is the waterbody area intersecting with the i-th proximity zone, c_i (−) is the drift fraction of the i-th proximity zone, A_{wb} (m^2) is the area of the waterbody, and $\hat{c}$ (−) is the mean drift fraction across the waterbody.	Winchell et al. (2018)

waterbodies as non-target areas (Section 2.4.2), to access method-specific sensitivities towards the landscape organization.

2.3. Landscape-level spray drift drivers

Spray drift at the landscape scale is driven by spatial and temporal variations in environmental and agricultural conditions (Reeg et al., 2017). However, it remains unclear which factors are the main drivers of spray drift at the landscape scale. Therefore, DAD-drift was used in a meta-modeling approach to assess spray drift at the landscape scale.

2.3.1. Model inputs

The model inputs were adapted from the "DG11004" application scenario, the deposition height parameter was set to a value of 0, and the four nozzle types XR, DG, AIXR, and TTI were used. Further, a wide range of environmental conditions was applied to assess spray drift drivers at the landscape scale (Table 2). With four nozzle types, four temperatures, three humidities, four wind speeds, and eight wind directions a total of 1536 different input combinations were used in the simulations.

2.3.2. Meta-model setup

In the meta-modelling approach, spray drift deposition (−) was defined as the dependent variable. Temperature, humidity, wind speed, minimal distance, centroid distance, relative bearing, and parameters describing the DSD, such as 10 % volume diameter (DV0.1), volume median diameter (DV0.5), volume fraction less than 50 µm (V50), volume fraction less than 100 µm (V100), volume fraction less than 150 µm (V150), and volume fraction less than 200 µm (V200), were defined as the predictor variables. The minimal distance describes the distance between two areas (target and non-target) and the centroid distance describes the distance between the centroids of those areas. The relative bearing describes the position of a non-target area relative to the prevailing wind direction, with 0° and 180° describing a non-target area exactly in downwind direction and opposite of the wind direction, respectively. DV0.1, DV0.5, V50, V100, V150, and V200 were

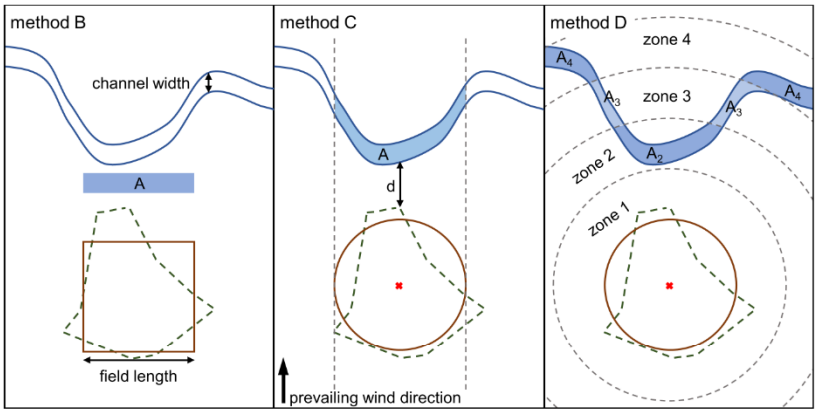


Fig. 2. Schematic representation of spray drift prediction methods B, C, and D. With the actual application area in dashed green, the representation of the application in solid brown, the representation of the waterbody in solid blue. (For interpretation of the references to colour in this figure legend, the reader is referred to the Web version of this article.)

Table 2
Input parameter ranges used during DAD-drift model running.

Parameter	Number of Values	Values
temperature	4	5 °C, 15 °C, 25 °C, 35 °C
humidity	3	35 %, 60 %, 85 %
wind speed	4	0.5 m/s, 2.5 m/s, 4.5 m/s, 6.5 m/s
wind direction	8	0°, 45°, 90°, 135°, 180°, 225°, 270°, 315°

determined based on the previously presented drop size distributions of each nozzle type (Fuchs et al., 2025).

2.3.3. Multiple linear regression analysis

Multiple linear regression (MLR) analysis was used in the meta-modelling approach to determine the drivers of spray drift at the landscape scale. Because the predictor variables in our dataset are fundamentally different in scale, all predictor variables were standardized to have a variance equal to 1, a mean value equal to 0, and a standard deviation equal to 1. Thus, the resulting regression coefficients are also standardized, and regression coefficients for different predictor variables can be directly compared, regardless of the original scale of those predictor variables.

The MLR of in-field deposition contained all data points describing deposition within the intended area of application and included the temperature, humidity, wind speed, DV01, DV05, V50, V100, V150, and V200 as the descriptor variables and the deposition fraction (−) as dependent variable. Excluding combinations of the variables describing the DSD (i.e., DV01, DV05, V50, V100, V150, V200) to avoid colinear descriptor variables, resulted in 56 possible MLR configurations.

The MLR of spray drift deposition within non-target areas contained all data points describing non-target areas, with a drift fraction above 0 and a relative bearing below or equal to 45°, to allow for transformation and avoid skewing the data towards small drift fractions, respectively. The drift fraction (−) was transformed by the natural logarithm, as spray drift decreases exponentially with distance from the edge-of-field. The global MLR included temperature, humidity, wind speed, DV01, DV05, V50, V100, V150, V200, minimal distance, centroid distance and relative bearing as the descriptor variables and the transformed drift fraction (−) as dependent variable. Excluding combinations of the variables describing the DSD (i.e., DV01, DV05, V50, V100, V150, V200) and combinations of minimal and centroid distance to avoid colinear descriptor variables, resulted in 336 possible MLR configurations.

Based on the sensitivity analysis of the DAD-drift model (Fuchs et al., 2025), wind speed, temperature, and humidity were expected to show changes in correlation strength and direction depending on the distance from the application area. Therefore, the meta-modeling of spray drift deposition in non-target areas was split up into three distance classes (i.e., close, medium, far), with one MLR describing each of the respective classes. The close distance class ranged from 0 m to the lower range limit (m), the medium distance class ranged from the lower range limit (m) to the upper range limit (m), and the far distance class contained all distances above the upper range limit (m). The possible values of the lower range limit were defined from 95 m up to 145 m in 5 m steps and the possible values of the upper range limit were defined from 145 m up to 250 m in 5 m steps. To determine appropriate range limits all possible combinations with at least 50 m difference between upper and lower range limits were defined. For each of the combinations the data set was split accordingly to the distance classes and for each class a MLR with centroid distance, wind speed, temperature, humidity, 10 % volume diameter (DV0.1), and relative bearing as descriptor variables was created. The coefficients of determination of the three MLR were then average to describe the performance of the respective lower and upper range limit combination.

2.3.4. Akaike information criterion

For a data set with one dependent variable and N predictor variables, a total number of 2^N MLR models (without interaction) can potentially be defined. The problem of selecting an appropriate model is well known, and in general, for a given level of accuracy, a simpler or a more parsimonious model is preferable (Bozdogan, 1987). The process of selecting the model with the least complexity and the highest information gain has been formalized by the Akaike information criterion (AIC), which was used in this approach and is defined as follows,

$$AIC(k) = -2\log(L(\widehat{\Theta}_k)) + 2k \tag{6}$$

where, $L(\widehat{\Theta}_k)$ is the likelihood function and k is the number of predictor variables (Bozdogan, 1987). For a given set of possible MLR models, the model with the lowest AIC value was selected as the most parsimonious model and considered as the best descriptor for the observed data set.

2.4. Scenarios

The previously described methods were applied to various combinations of application areas and related non-target areas, these combinations will be called application scenarios in the following. These application scenarios were adapted from a land use map (Geobasis, 2023) of the German federal state of North Rhine-Westphalia (NRW).

2.4.1. Spatial spray drift representation

To assess the influence of the spatial spray drift representation by comparing spray drift prediction methods A-D (Section 2.2.2), application scenarios of increasing levels of complexity were defined to assess which parts of the spatial organization are most relevant for those methods. At the first complexity level, application scenario SR-1 contains a rectangular application area and a straight surface waterbody positioned parallel to each other, with the wind blowing directly towards the waterbody (Fig. 3). This represents the simplest possible scenario and is comparable with the current approach for pesticide risk assessment in Europe, where spray drift inputs are determined by the distance between the field edge and the waterbody (FOCUS, 2001). At the second complexity level, application scenario SR-2 contains the same application area and wind direction as scenario SR-1, with the straight surface waterbody rotated by 45° (Fig. 3). At the third complexity level, applications scenario SR-3 contains the same surface waterbody and wind direction as scenario SR-2, with an irregularly shaped application area from the land use map (Fig. 3). At the fourth complexity level, application scenarios SR-4 to SR-13 contain real world combinations of application areas and surface waterbodies from the land use map, representing a range of possible spatial organizations at the landscape scale (Fig. 3). The wind direction of each application scenario was set to one of the eight cardinal wind directions pointing towards the non-target areas.

2.4.2. Landscape-level spray drift drivers

Five application scenarios (LL-1 to LL-5) were defined for the meta-modeling approach (Fig. 4). The scenarios were selected as loose representations of a field as it could typically be found in northern German agricultural areas. For each scenario, a radius of 1 km around the application area centroid was used to determine relevant non-target areas. The non-target areas were subset by land use, with areas defined as mixed usage, forests, agricultural usage (grasslands and agricultural production), and standing waters being selected for the analysis. Only landscape elements without extreme extents (very high width to length ratio) were selected, as those might negatively affect the meta-modelling.

Each of the five scenarios was run at a resolution of 2 × 2 m for the 1536 input combinations defined in Section 2.3.1, with a total of 7680 model runs. The resulting deposition flux of each model run was analyzed for the respective application and non-target areas. The deposition masses within each area were summed up (kg), then normalized by the area (kg m^{-2}), as well as by the application rate (kg m^{-2}) resulting in the drift fraction (−). A total of 1307 different application and non-target areas were analyzed, with 250, 194, 240, 370, and 253 for scenarios LL-1, LL-2, LL-3, LL-4, and LL-5, respectively. The number of application and non-target areas and the number of input combination resulted in a total number of 2007552 unique area-condition combination, available for the meta-modeling approach.

3. Results

3.1. Spatial spray drift representation

The comparison of the DAD-drift model (method A) and the three drift curve based algorithms (methods B-D) showed how these simplified

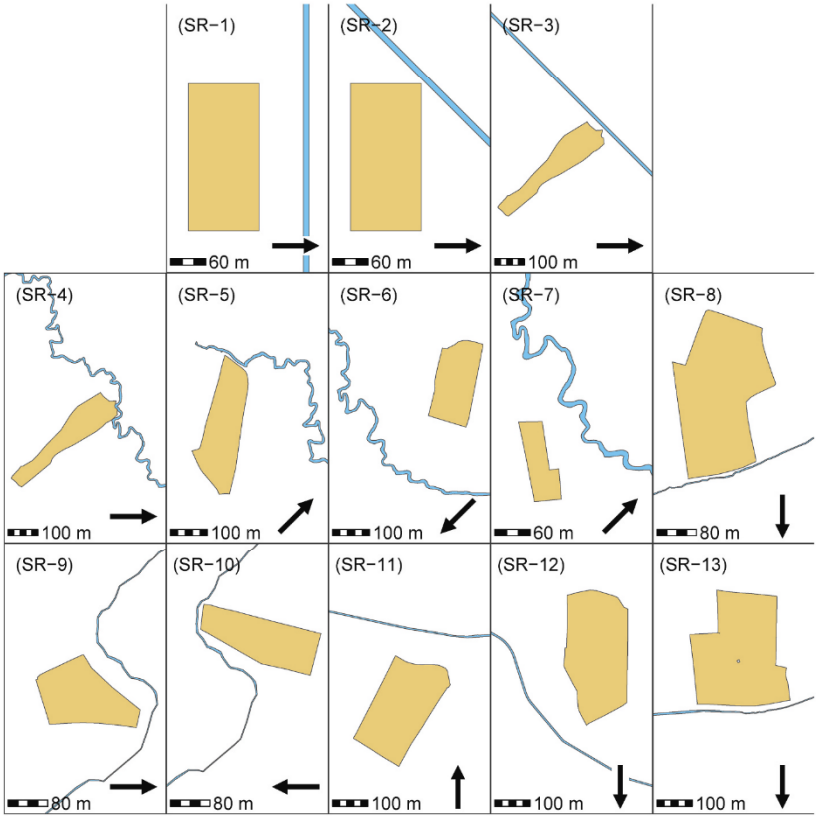


Fig. 3. Application areas (yellow) and receiving surface waterbodies (blue) for the four complexity levels, with arrows indicating the wind direction. Scenarios SR-1, SR-2, SR-3, and SR-4 to SR-13 represent the complexity levels 1, 2, 3, and 4, respectively. Please note the different plot scale for the individual scenarios. (For interpretation of the references to colour in this figure legend, the reader is referred to the Web version of this article.)

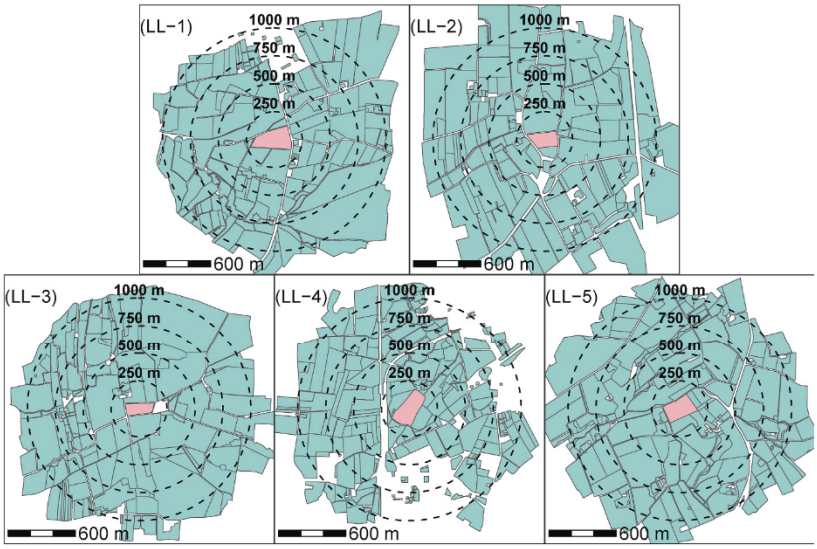


Fig. 4. Application areas in red and their respective non-target areas in green. Non-target areas must be within a distance of 1 km from the centroid of the application area and defined as mixed usage, forest, agricultural usage, or standing waters. The dashed circles indicate distances of 250 m, 500 m, 750 m, and 1000 m from the centroid, and white areas indicate areas excluded from the meta-modeling. (For interpretation of the references to colour in this figure legend, the reader is referred to the Web version of this article.)

spatial representations of application and non-target areas affect the simulated spray drift depositions, resulting in highly variable predictions (Fig. 5, Table S2, Figs. S2–4). At the lowest level of complexity and using the DG nozzle, the spray drift depositions calculated using the four prediction methods range from 1.7 mg for method B to 14.0 mg for method D. At the highest level of complexity, the predictions using the DG nozzle range from 4.5 mg for method D to 13469.8 mg for method C. Overall, the difference between prediction methods increases from less than one order of magnitude for all nozzles at the lowest level of complexity to more than four orders of magnitude for the TTI nozzle at the highest level of complexity (Table S2).

Analysis of the real-world application areas defined at the highest level of complexity (Fig. 3 SR-4 to SR-13) using four spray nozzles and the four prediction methods showed that the predicted spray drift deposition on receiving surface waters decreases with increasing DSD coarseness (Fig. 6). The fine XR nozzle produced the highest drift depositions and the ultra-coarse TTI nozzle produced the lowest drift depositions (Table S2). With the exception of method C for scenario SR-4, where no such decreasing trend was observed. The range of spray drift depositions estimated by the four methods is about one order of magnitude between the lowest median for method B and the highest median for method C for all nozzle trypes. Within the 10 scenarios, the prediction method C showed a high variation as indicated by the large interquantile range and wiskers of the coresponding boxplots in Fig. 6, with the other three methods showing much less variation for the ten

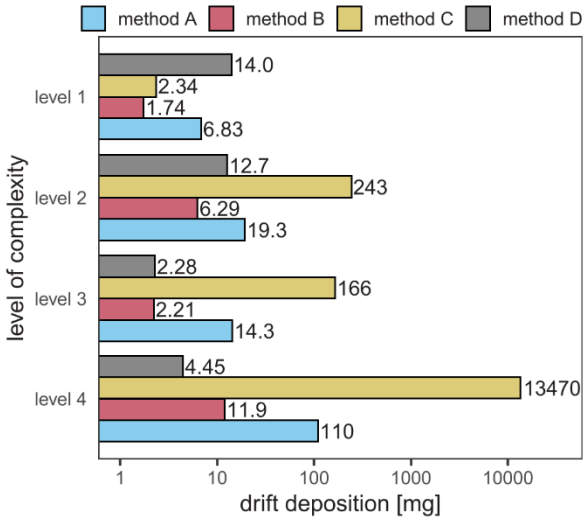


Fig. 5. Spray drift depositions (mg) onto surface waterbodies for the four complexity levels, the four prediction methods, and the DG spray nozzle, with prediction method A in blue, prediction method B in red, prediction method C in yellow, and prediction method D in grey. The complexity levels are described in Fig. 2, with level 1 to 4 corresponding to scenario SR-1, SR 2, SR 3, and SR 4, respectively. (For interpretation of the references to colour in this figure legend, the reader is referred to the Web version of this article.)

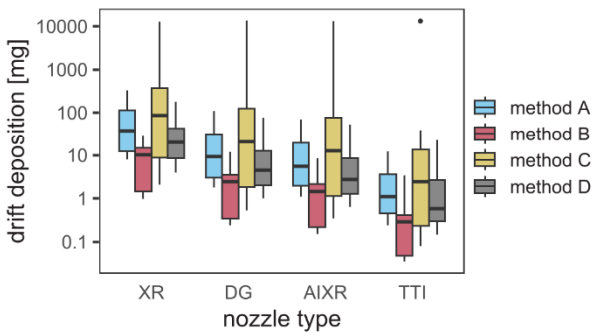


Fig. 6. Boxplots of spray drift deposition (mg) into surface waterbodies, each boxplot represents the ten scenarios of the highest complexity (Fig. 2 SR 4 to SR 13) for a spray nozzle and prediction method combination. With prediction method A in blue, prediction method B in red, prediction method C in yellow, and prediction method D in grey. (For interpretation of the references to colour in this figure legend, the reader is referred to the Web version of this article.)

scenarios.

When comparing the predicted spray drift depositions of the four methods using the DG nozzle for the real-world scenarios (Fig. 3 SR-4 to SR-13), the ranking of method C, A, D, and B (high to low) does not always hold true for the individual scenarios (Fig. 7, Figs. S5-7). While predictions using method C were highest in five scenarios and predictions using method B were lowest in eight scenarios, results were generally more heterogeneous and depend on the specific spatial organization of the landscape. Factors such as distance between application area and surface waterbody, shape of the application area, and flow path of the waterbody affect the prediction methods differently.

3.2. Landscape-level spray drift drivers

3.2.1. In-field deposition

Out of the 56 possible multiple regression models for estimating in-field deposition (Table S3) the most parsimonious (lowest AIC) configuration contained wind speed, temperature, humidity, and volume fraction less than 200 μm (V200) as descriptor variables (Table 3). Higher wind speed, temperature, and V200 result in lower in-field deposition (negative correlation coefficients), whereas an increase in humidity increases the in-field deposition (positive correlation coefficient). This MLR is based on a sample size of 7680 data points, is highly significant ($p < 0.001$), with a model performance of $R^2 = 0.96$, and all descriptor variables are highly significant ($p < 0.001$), see Fig. S8 for model diagnostics. V200 showed the strongest correlation by one order of magnitude, followed by temperature, wind speed and humidity with comparable correlation coefficients.

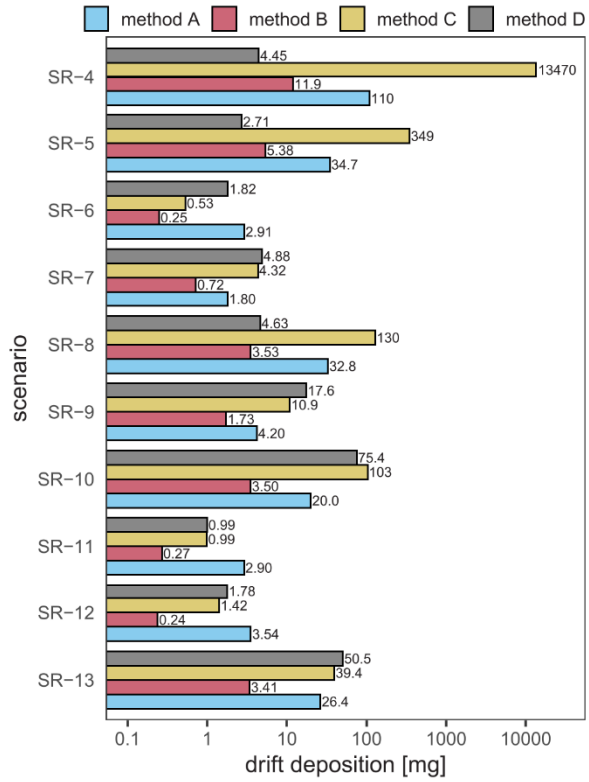


Fig. 7. Spray drift deposition (mg) onto surface waterbodies using the four prediction methods for the ten scenarios of the highest complexity (Fig. 2 SR 4 to SR 13) for the DG spry nozzle, with prediction method A in blue, prediction method B in red, prediction method C in yellow, and prediction method D in grey. (For interpretation of the references to colour in this figure legend, the reader is referred to the Web version of this article.)

Table 3
Results of a multiple linear regression of predicted in-field deposition, based on wind speed, temperature, humidity, and the volume fraction less than 200 μm (V200), with estimated coefficients and their respective confidence intervals. The model is based on a sample size of 7680, is highly significant ($p < 0.001$), with a model performance of $R^2 = 0.964$.

	Estimated Coefficient	t	p
(Intercept)	0.9155 [0.9152, 0.9158]		
wind speed	−0.0042 [-0.0044, −0.0039]	−40.82	<0.001
temperature	−0.0042 [-0.0044, −0.0039]	−41.02	<0.001
humidity	0.0037 [0.0034, 0.0039]	36.19	<0.001
V200	−0.0459 [-0.0462, −0.0456]	−451.14	<0.001
N	7680		
R^2	0.964		
F(4,7675)	52046.53 ($p < 0.001$)		

3.2.2. Non-target area drivers

Of the 336 possible model configurations for predicting spray drift deposition in non-target areas (Table S4), the most parsimonious (lowest AIC) configuration contained centroid distance, wind speed, temperature, humidity, 10 % volume diameter (DV0.1), and relative bearing as descriptor variables (Table 4). Increasing centroid distance, wind speed, humidity, DV0.1, and relative bearing was associated with decreasing deposition in non-target areas (negative correlation coefficients), and higher temperature increased the deposition in non-target areas (positive correlation coefficient). This MLR is based on a sample size of 494592 data points, is highly significant ($p < 0.001$), with a model performance of $R^2 = 0.83$, and all descriptor variables are highly significant ($p < 0.001$), see Fig. S9 for model diagnostics. DV0.1 followed by centroid distance showed the strongest correlation, followed by temperature, humidity, wind speed and relative bearing in order.

The analysis of splitting the data set for spray drift deposition in non-target areas into three distance classes (i.e., close, medium, far), resulted in a lower range limit of 120 m and an upper range limit of 180 m with an average coefficient of determination of 0.89 performing the best (Table S5). The MLR describing the data in each distance class were setup like the MLR describing the complete data set of spray drift deposition in non-target areas (Table 4). The far distance MLR with 486144 data points was based on the largest sample size (Table S8, Fig. S12), compared to 2304 and 6144 data points for the close distance MLR and medium distance MLR (Table S7, Fig. S11), respectively. With a R^2-value of 0.94 the close distance MLR showed the best model performance (Table S6, Fig. S10), the medium distance MLR and the far distance MLR showed model performances of $R^2 = 0.87$ and $R^2 = 0.86$, respectively. While for the far distance MLR all predictor variables were

Table 4
Results of a multiple linear regression of log-transformed spray drift deposition in non-target areas, based on centroid distance, wind speed, temperature, humidity, 10 % volume diameter (DV0.1) of droplets, and relative bearing, with estimated coefficients and their respective confidence intervals. The model is based on a sample size of 494592, is highly significant ($p < 0.001$), with a model performance of $R^2 = 0.832$.

	Estimated Coefficient	t	p
(Intercept)	−11.309 [-11.312, −11.306]		
centroid distance	−0.944 [-0.946, −0.941]	−843.36	<0.001
wind speed	−0.176 [-0.179, −0.173]	−157.29	<0.001
temperature	0.329 [0.326, 0.332]	294.15	<0.001
humidity	−0.271 [-0.274, −0.269]	−242.57	<0.001
DV0.1	−1.395 [-1.398, −1.393]	−1247.22	<0.001
relative bearing	−0.098 [-0.101, −0.095]	−87.82	<0.001
N	494592		
R^2	0.832		
F(6,494585)	407439.22 ($p < 0.001$)		

highly significant ($p < 0.001$), for the close and medium distance MLR all predictor variables, besides relative bearing, were highly significant ($p < 0.001$). All three models were highly significant with p-values below 0.001.

The MLR describing the close, medium, and far distance classes were setup using identical predictor variables (Fig. 8). The correlation strength of the centroid distance was the lowest for the close distance and the highest for the medium distance, for all three distance classes a negative correlation coefficient was observed. DV0.1 showed the strongest correlation for all distance classes, variation between classes was low, and higher DV0.1 resulted in less deposition in non-target areas (negative correlation coefficient). Humidity showed a small positive correlation coefficient for the close and medium distance classes, with a larger negative correlation coefficient for the far distance class. Relative bearing showed a significant negative correlation coefficient for the far distance MLR, an insignificant negative correlation coefficient for the medium distance MLR, and an insignificant positive correlation coefficient for the close distance MLR. Temperature showed a small negative correlation coefficient for the close and medium distance models and a comparably large positive correlation coefficient for the far distance MLR. For the close and medium distance models wind speed showed a relatively large positive correlation coefficient and for the far distance MLR wind speed showed a comparably small negative correlation coefficient.

4. Discussion

4.1. Spatial spray drift representation

The comparison between four methods for spray drift prediction showed that the spatial representation of application and non-target areas has a large impact on predicted spray drift depositions to receiving surface waters. For ten real-world scenarios and four nozzle types, the range between the lowest predictions (method B) and highest predictions (method C) was about one order of magnitude, with 10.65 mg–101.62 mg, 2.57 mg–25.14 mg, 1.56 mg–15.35 mg, and 0.31 mg–2.94 mg for the XR, DG, AIXR, and TTI nozzles, respectively. Differences between spray drift deposition of the four prediction methods

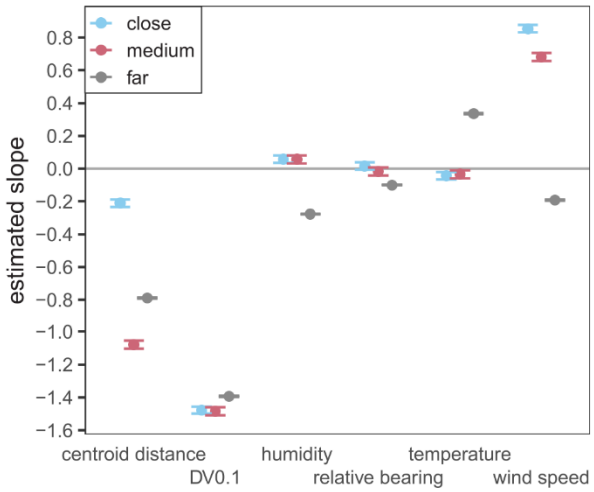


Fig. 8. Estimated coefficients for the predictor parameters centroid distance, 10 % volume diameter (DV0.1), humidity, relative bearing, temperature, and wind speed for the MLRs predicting log-transformed spray drift deposition in non-target areas for close distance (blue), medium distance (red), and far distance (grey), for complete model reports see Tables S6–S8. (For interpretation of the references to colour in this figure legend, the reader is referred to the Web version of this article.)

increased with an increasing level of complexity, being the highest for the most complex real-world scenarios. For the same set of application conditions (e.g., environmental conditions, operational parameters), the differences in predicted spray drift depositions can be directly related to the spatial representations of the respective prediction methods, since all prediction methods are based on the DAD-drift model, either in drift curve mode (methods B, C, D) or in landscape mode (method A).

While the DAD-drift model in landscape mode is spatially fully distributed and able to directly link the spray drift emissions from each unit of application area to each unit of non-target area, the simplified spatial representations of methods B, C, and D are unable to provide this level of detail. The prediction methods are sensitive to factors such as the distance between the application area and the surface waterbody, the shape of the application area, and the flow path of the waterbody. Due to different spatial representations, spray drift predictions of method B, C, and D were differently affected by these factors, resulting in heterogeneous spatial distributions of spray drift depositions.

Method B uses the channel width and an assumed square application area to calculate comparably small receiving surface waterbody areas without considering the flow path of the waterbody. The relevance of the application area shape is limited to determining the distance between the edge-of-field and the nearest and farthest edges of the waterbody. By projecting the circular application area representation onto the receiving surface waterbody, method C does consider the flow path of the waterbody and calculates larger receiving areas than method B. However, the calculation of the drift fraction based on the minimum distance between the application area and the waterbody, makes this method particularly sensitive to the distance between these spatial objects. Method D uses a circular application area representation with proximity zones, resulting in large receiving areas and a high sensitivity to the flow path of the waterbody. The circular representation makes this method highly sensitive to the application area shape, potentially exaggerating the distance between the waterbody and the application area, resulting in underestimated spray drift deposition.

These differences in response to impact factors indicate that the spatial representation of application and non-target areas not only influence the total amount of pesticide deposition but may also influence the spatial distribution of spray drift depositions within the landscape. This could potentially lead to different assessments of the criticality of specific source areas depending on spatial organization of the landscape and the spatial spray drift representation used to predict spray drift. This is of high relevance when predicted spray drift deposition is used as input for subsequent modelling steps, such as pesticide fate modeling (Holvoet et al., 2008; Padovani et al., 2004; Schönenberger et al., 2022; Winchell et al., 2018; Zhang et al., 2018) or ecotoxicological effect modeling (Schad and Schulz, 2011). Prediction methods B, C, and D were adopted from three comparable modeling approaches, all of which used predicted spray drift depositions in combination with the SWAT model to estimate pesticide exposure dynamics and directly relate these modeling results to monitoring data (Holvoet et al., 2008; Winchell et al., 2018; Zhang et al., 2018). For prediction method B it was concluded that the contributions of spray drift losses to the total pesticide losses are of minor importance (Holvoet et al., 2008). The authors of prediction method C summarized that spray drift contributes significantly to the annual in-stream pesticide mass loadings (Zhang et al., 2018). Winchell et al. (2018) concluded that incorporation of spray drift predictions based on increasingly site-specific data combined with the SWAT model accurately predicted observed pesticide concentrations. These findings are consistent with the results presented earlier (Section 3.1), suggesting that the large differences in spray drift predictions resulting from different simplifications of the spatial arrangement of application and non-target areas may also influence the results of higher-level modeling approaches. It remains unclear, however, whether the authors would have reached different conclusions using different spatial representations.

4.2. Landscape-level spray drift drivers

Within the subset of data describing deposition within the application areas used for MLR training (Section 3.2.1, Fig. S8), the deposition fraction (−) ranged from approximately 80 % for the XR nozzle to 97 % for the TTI nozzle. Assuming a closed mass balance, this implies that between 3 % and 20 % of the applied pesticide is leaving the intended area of application as spray drift. The most drift promoting conditions in this meta-modeling approach were the combination of the TeeJet XR11003 nozzle emitting a fine droplet size distribution (TeeJet, 2023) with hot (35 °C) and dry (35 % relative humidity) conditions accelerating droplet evaporation and high wind speed (6.5 m/s) increasing downwind transport of droplets. Due to these extreme conditions, the low in-field depositions predicted by the model are expected. De Nie (2002) reported comparable in-field depositions of 84 % in potatoes, 85 % in maize, 86 % in grains and sugar beets, up 90 % in onions.

Based on a meta-modeling approach (Section 3.2.2), the droplet size distribution (DSD) was found to be the most influential factor for spray drift deposition in non-target areas at the landscape scale, closely followed by the distance between application and non-target areas. Other factors, including wind speed, temperature and humidity were found to influence off-target movement of pesticides with significantly smaller correlation coefficients. The exponential decrease of spray drift with distance is well understood (Felsot et al., 2010), unsprayed buffer zones therefore are considered effective spray mitigation measures (Miller, 2014) and are used as drift reduction measures within the regulatory framework (Adriaanse et al., 2022). The importance of the nozzle type used during application has also been described (Cock et al., 2017; Felsot et al., 2010; Griesang et al., 2017; Lebeau et al., 2011; Nuyttens et al., 2007b; Thompson and Ley, 1983). The results presented here indicate that a reduction of the fraction of small droplets in the DSD by selecting corresponding spray nozzle types is a more effective drift reduction measure than buffer zones when considering spray drift at the landscape scale. The correlation strength of the distance between application and non-target areas and therefore unsprayed buffer strips, might by underestimated in our approach, as DAD-drift represents the landscape as a flat plane with no consideration of topography and pesticide interception by vegetation.

Splitting the data set for spray drift deposition in non-target areas into three distance classes improved the model performance. All MLR showed higher model performance compared to the MLR for the total data set, with R^2-values of 0.94, 0.87, 0.86, and 0.83 for the close distance model, the medium distance model, the far distance model, and the unified model, respectively. The sign of the correlation coefficients of wind speed, temperature, and humidity changed in dependence on distance from the application area. The sign change of the correlation coefficients of temperature and relative humidity can be explained by in-flight droplet mechanics, with high temperature and low relative humidity accelerating droplet evaporation. For high evaporation rates, droplet diameters decrease faster and droplets are transported over greater distances, resulting in lower deposition rates close to the edge-of-field but higher deposition rates at larger distances from the application area. The sign change of the correlation coefficient of wind speed is surprising, while the positive correlation between wind speed and spray drift in the close and medium ranges are expected based on most of the spray drift literature, the negative correlation of wind speed in the MLR for distances greater than 180 m is unexpected. However, this can be explained by higher wind speeds causing stronger atmospheric turbulence and droplet dispersion, resulting in a larger mass of airborne droplets being diluted over an even larger volume of air. Individual non-target areas therefore receive smaller deposition rates, while overall more substance is transported off-target. An unexpected result of the distance classes was the change in correlation strength of the distance between application and non-target areas, which was smallest for the close distance class, even smaller than wind speed, and the largest for the medium distance class. This might be caused by the distance range within the close distance class being limited and therefore no strong linear relationship could be established by the MLR.

There is no clear consensus in the literature on which parameter of the DSD best describes drift behavior of spray nozzles, with some reporting 100 μm as the relevant droplet size (Felsot et al., 2010; Nuyttens et al., 2007a) and others reporting 200 μm as the relevant droplet size (Nuyttens et al., 2007a, 2007b). In the meta-modeling approach, a multitude of parameters (i.e., DV0.1, DV0.5, V50, V100, V150, V200) were provided for model training. For in-field deposition a model containing V200 was selected as most parsimonious, with a model containing V150 following very closely. For the spray drift deposition in non-target areas a model containing DV0.1 was selected as most parsimonious, with a model containing DV0.5 following very closely. This further indicates that no single parameter of the DSD is suitable to describe the drift behavior of spray nozzles in a simple and quick way.

5. Summary & conclusion

Spray drift at the landscape scale is a highly complex process governed by a wide range of environmental and operational parameters, with the spatial organization and characteristics of the landscape playing important roles in its assessment. In this work, a method comparison of different simplified spatial spray drift representations and a meta-modeling approach to identify important spray drift drivers at the landscape scale were performed using the Droplet and Atmospheric Dispersion drift (DAD-drift) model.

The comparison of four spatial spray drift representation methods for ten real-world application scenarios showed median spray drift predictions varied by one order of magnitude between the methods, with up to four orders of magnitude in the worst case. These differences are driven by different sensitivities to influencing factors, such as the distance between application and waterbodies, the shape of the application area, and the flow path of the waterbody. As predicted spray drift deposition might be used in combination with higher-level approaches, such as pesticide fate modeling or ecotoxicological effect modeling, it is advisable to use the DAD-drift model for the prediction, since it is spatially fully distributed and able to directly link spray drift emissions from each unit of application area to each unit of non-target area.

Based on the meta-modeling approach using DAD-drift to predict spray drift deposition at the landscape scale, the droplet size distribution, which is determined by nozzle type, closely followed by the distance between application and non-target area, were found to be the two most influential drivers of spray drift at the landscape scale. This suggests that spray nozzle selection has the potential to be a critical drift reduction measure, with a spray drift mitigation effect comparable to that of unsprayed buffer zones. At close to medium distances up to 180 m, wind speed was found to be the third most influential spray drift driver. In the far field (distances exceeding 180 m) droplet evaporation controlled by temperature and relative humidity was found to be the third most influential driver.

The DAD-drift model is a useful tool to improve the understanding of spray drift exposure at the landscape scale. For future work, the DAD-drift model could be coupled to eco-hydrological models, such as the SWAT + model, for assessing the contribution of spray drift to temporal and spatial exposure dynamics of pesticides in realistic landscapes. In addition, DAD-drift could be used to assess the impact of spray drift on population dynamics and the effectiveness of mitigation measures such as nozzle selection and non-spray buffer zones at the landscape scale.

CRediT authorship contribution statement

Mike Devin Fuchs: Writing – original draft, Visualization, Validation, Software, Methodology, Investigation, Formal analysis, Data curation, Conceptualization. **Sebastian Gebler:** Writing – review & editing, Supervision, Methodology, Conceptualization. **Andreas Lorke:**

Writing – review & editing, Supervision.

Declaration of competing interest

The authors declare the following financial interests/personal relationships which may be considered as potential competing interests: Mike Devin Fuchs reports financial support was provided by BASF SE, Carl-Bosch-Str. 38, 67056 Ludwigshafen, Germany. Sebastian Gebler reports financial support was provided by BASF SE, Carl-Bosch-Str. 38, 67056 Ludwigshafen, Germany. If there are other authors, they declare that they have no known competing financial interests or personal relationships that could have appeared to influence the work reported in this paper.

Appendix A. Supplementary data

Supplementary data to this article can be found online at https://doi.org/10.1016/j.envsoft.2025.106455.

Data availability

Data will be made available on request.

References

Adriaanse, P.I., Buddendorf, W.B., Holterman, H.J., Horst, M.M. ter, 2022. Supporting the development of exposure assessment scenarios for Non-Target Terrestrial Organisms to plant protection products. EFSA Support. Publ. 19. https://doi.org/10.2903/sp.efsa.2022.en-7661.

Adriaanse, P.I., 1996. Fate of Pesticides in Field Ditches: the TOXSWA Simulation Model.

Arnold, J.G., Srinivasan, R., Muttiah, R.S., Williams, J.R., 1998. Large-area hydrologic modeling and assessment: Part I. Model development. J. Am. Water Resour. Assoc. 34, 73–89.

Bozdogan, H., 1987. Model selection and Akaike's Information Criterion (AIC): the general theory and its analytical extensions. Psychometrika 52, 345–370. https://doi.org/10.1007/BF02294361.

Bub, S., Schad, T., Gao, Z., 2020. XDrift—an R package to simulate spatially explicit pesticide spray-drift exposure of non-target-species habitats at landscape scales. SoftwareX 12, 100610. https://doi.org/10.1016/j.softx.2020.100610.

Cock, N. De, Massinon, M., Salah, S.O.T., Lebeau, F., 2017. Investigation on optimal spray properties for ground based agricultural applications using deposition and retention models. Biosyst. Eng. 162, 99–111. https://doi.org/10.1016/j.biosystemseng.2017.08.001.

Felsot, A.S., Unsworth, J.B., Linders, J.B.H.J., Roberts, G., Rautman, D., Harris, C., Carazo, E., 2010. Agrochemical spray drift; assessment and mitigation—a review. J. Environ. Sci. Heal. Part B 46, 1–23. https://doi.org/10.1080/03601234.2010.515161.

FOCUS, 2001. FOCUS surface water scenarios in the EU evaluation process under 91/414/EEC. Report of the FOCUS working group on surface water scenarios. EC Document Reference SANCO/4802/2001-rev. 2, 245.

Fuchs, M.D., 2024. DAD-drift. https://doi.org/10.5281/zenodo.11486371.

Fuchs, M.D., Gebler, S., Lorke, A., 2025. The droplet and atmospheric dispersion drift (DAD-drift) model – a modular approach for estimating spray drift at the landscape scale. Environ. Res. 271, 121104. https://doi.org/10.5281/zenodo.11486371, 10.1016/j.envres.2025.121104Fuchs,M.D.,2024.DAD-drift.

Ganzelmeier, H., Rautmann, D., Spangenberg, R., Streloke, M., Herrmann, D.M., Wenzelburger, D.H.-J., Walter, D.H.-F., 1995. Untersuchungen zur Abtrift von Pflanzenschutzmitteln: Ergebnisse eines bundesweiten Versuchsprogrammes. Blackwell Wissenschafts-Verlag.

Geobasis, N.R.W., 2023. WFS NW ALKIS grundrissdaten vereinfachtes schema [WWW Document]. URL. https://advmis.geodatenzentrum.de/trefferanzeige?docuuid=d840e759-6e8d-4c3b-aa8e-400eba1a5ee8&plugid=/ingrid-group:iplug-csw-dsc&docid=e4Cl9XYBWW0O27vjeYIi. accessed 8.23.23.

Griesang, F., Decaro, R.A., dos Santos, C.A.M., Santos, E.S., de Lima Roque, N.H., da Costa Ferreira, M., 2017. How much do adjuvant and nozzles models reduce the spraying drift? Drift in agricultural spraying. Am. J. Plant Sci. 8, 2785–2794. https://doi.org/10.4236/ajps.2017.811188.

Hilz, E., Vermeer, A.W.P., 2013. Spray drift review: the extent to which a formulation can contribute to spray drift reduction. Crop Prot. 44, 75–83. https://doi.org/10.1016/j.cropro.2012.10.020.

Holterman, H., van de Zande, J., 2008. The Cascade Drift Module : a GIS-based study on regional pesticide deposition. Aspect Appl. Biol. 84, 83–90.

Holterman, H.J., van de Zande, J.C., Huijsmans, J.F.M., Wenneker, M., 2017. An empirical model based on phenological growth stage for predicting pesticide spray drift in pome fruit orchards. Biosyst. Eng. 154, 46–61. https://doi.org/10.1016/j.biosystemseng.2016.08.016.

Holterman, H.J., Van De Zande, J.C., Porskamp, H.A.J., Michielsen, J., 1998. IDEFICS : a Physical Model of Spray Drift from Boom Sprayers in Agriculture. ILASS-Europe, Manchester.

Holvoet, K., Griensven, A. van, Gevaert, V., Seuntjens, P., Vanrolleghem, P.A., 2008. Modifications to the SWAT code for modelling direct pesticide losses. Environ. Model. Software 23, 72–81. https://doi.org/10.1016/j.envsoft.2007.05.002.

Lebeau, F., Verstraete, A., Stainier, C., Destain, M.-F., 2011. RTDrift: a real time model for estimating spray drift from ground applications. Comput. Electron. Agric. 77, 161–174. https://doi.org/10.1016/j.compag.2011.04.009.

Miller, P., 2014. Spray drift. In: Pesticide Application Methods. Wiley, pp. 337–361. https://doi.org/10.1002/9781118351284.ch12.

Mottes, C., Lesueur-Jannoyer, M., Bail, M. Le, Malézieux, E., 2014. Pesticide transfer models in crop and watershed systems. A review. Agron. Sustain. Dev. 34, 229–250. https://doi.org/10.1007/s13593-013-0176-3.

Nie, D.S. De, 2002. Emissie-evaluatie MJP-G 2000; Achtergronden en berekeningen van emissies van gewasbeschermingsmiddelen, vols. 1–169.

Nuyttens, D., Schampheleire, M. De, Baetens, K., Sonck, B., 2007a. The influence of operator-controlled variables on spray drift from field crop sprayers. Trans. ASABE (Am. Soc. Agric. Biol. Eng.) 50, 1129–1140. https://doi.org/10.13031/2013.23622.

Nuyttens, D., Baetens, K., Schampheleire, M. De, Sonck, B., 2007b. Effect of nozzle type, size and pressure on spray droplet characteristics. Biosyst. Eng. 97, 333–345. https://doi.org/10.1016/j.biosystemseng.2007.03.001.

Padovani, L., Capri, E., Trevisan, M., 2004. Landscape-level approach to assess aquatic exposure via spray drift for pesticides: a case study in a mediterranean area. Environ. Sci. Technol. 38, 3239–3246. https://doi.org/10.1021/es049699p.

Rautmann, D., Streloke, M., Winkler, R., 2001. New basic drift values in the Authorization procedure for plant protection products. Mitteilungen aus der Biol. Bundesanstalt für L. 388, 133–141.

Reeg, J., Schad, T., Preuss, T.G., Solga, A., Körner, K., Mihan, C., Jeltsch, F., 2017. Modelling direct and indirect effects of herbicides on non-target grassland communities. Ecol. Model. 348, 44–55. https://doi.org/10.1016/j.ecolmodel.2017.01.010.

Schad, T., Schulz, R., 2011. Xplicit, a novel approach in probabilistic spatiotemporally explicit exposure and risk assessment for plant protection products. Integrated Environ. Assess. Manag. 7, 612–623. https://doi.org/10.1002/ieam.205.

Schönenberger, U.T., Simon, J., Stamm, C., 2022. Are spray drift losses to agricultural roads more important for surface water contamination than direct drift to surface waters? Sci. Total Environ. 809. https://doi.org/10.1016/j.scitotenv.2021.151102.

TeeJet, 2023. TeeJet: broadcast nozzles [WWW Document]. URL. https://www.teejet.com/-/media/dam/agricultural/usa/sales-material/catalog/broadcast_nozzles.pdf. (Accessed 12 December 2023).

Teske, M.E., Bird, S.L., Esterly, D.M., Curbishley, T.B., Ray, S.L., Perry, S.G., 2002. AgDRIFT®: a model for estimating near-field spray drift from aerial applications. Environ. Toxicol. Chem. 21, 659. https://doi.org/10.1897/1551-5028(2002)021<0659:aamfen>2.0.co;2.

Thompson, N., Ley, A.J., 1983. Estimating spray drift using a random-walk model of evaporating drops. J. Agric. Eng. Res. 28, 419–435. https://doi.org/10.1016/0021-8634(83)90134-8.

Vallée, R., Dousset, S., Billet, D., Benoit, M., 2014. Sorption of selected pesticides on soils, sediment and straw from a constructed agricultural drainage ditch or pond. Environ. Sci. Pollut. Res. 21, 4895–4905. https://doi.org/10.1007/s11356-013-1840-5.

Winchell, M.F., Pai, N., Brayden, B.H., Stone, C., Whatling, P., Hanzas, J.P., Stryker, J.J., 2018. Evaluation of watershed-scale simulations of in-stream pesticide concentrations from off-target spray drift. J. Environ. Qual. 47, 79–87. https://doi.org/10.2134/jeq2017.06.0238.

Zhang, X., Luo, Y., Goh, K.S., 2018. Modeling spray drift and runoff-related inputs of pesticides to receiving water. Environ. Pollut. 234, 48–58. https://doi.org/10.1016/j.envpol.2017.11.032.

Appendix III:

Environmental Pollution 397 (2026) 128031

Contents lists available at ScienceDirect

Environmental Pollution

journal homepage: www.elsevier.com/locate/envpol

Evaluating landscape-level pesticide exposure from spray drift: A modeling study in an agriculture-dominated watershed using SWAT+ and DAD-Drift

Mike Devin Fuchs [a,b,*], Sebastian Gebler [b], Andreas Lorke [a]

[a] RPTU Kaiserslautern-Landau, Forststraße 7, 76829, Landau in der Pfalz, Germany
[b] BASF SE, Exposure Modelling, Speyerer Straße 2, 67117, Limburgerhof, Germany

ARTICLE INFO

Keywords:
Spray-drift
Landscape scale
Pesticide exposure
SWAT+
Hydrological variability
Environmental risk assessment

ABSTRACT

Pesticide transport from agricultural fields to surface waters is a major environmental concern, and reliable exposure assessments require models that capture the major transport pathways. While the Soil and Water Assessment Tool (SWAT+) is widely used for landscape-scale pesticide modeling, it lacks a process-based representation of spray drift, which can contribute substantially to surface water contamination. The newly developed Droplet and Atmospheric Dispersion drift (DAD-drift) model provides a mechanistic framework for estimating spray drift deposition under realistic field conditions. In this work, we present the first implementation of DAD-drift into a high-resolution SWAT + model of the upper Funne catchment in North Rhine-Westphalia, Germany. The application of two fungicides and five herbicides within a realistic 5-year crop rotation was simulated to assess the contribution of spray drift to landscape-scale exposure.

The integrated modeling framework showed that spray drift markedly increases predicted pesticide concentrations in surface waters. Its effect was strongest for immobile substances with strong soil adsorption, which otherwise show little transport, while mobile substances were mainly governed by hydrological pathways but still exhibited additional concentration peaks from spray drift. Hydrological processes such as tile drainage, interflow, and surface runoff strongly shaped transport dynamics, controlling both timing and magnitude of pesticide export. Because these processes are sensitive to catchment parameterization, ensemble simulations were essential to capture variability and to robustly quantify the contribution of spray drift across scenarios.

This study demonstrates that spray drift is a critical driver of pesticide exposure at the catchment scale and must be explicitly considered in exposure assessments. The combined SWAT+–DAD-drift framework provides a transferable tool for linking agricultural practices with water quality, and for evaluating the effectiveness of mitigation measures such as no-spray buffer strips or drift-reducing nozzles at landscape scale.

1. Introduction

When pesticides are applied on agricultural crops, a fraction of pesticide mass may be transported from the intended area of application to non-target areas. Off-target transport of pesticides depends on a wide range of factors, including: environmental conditions during and after application; physio-chemical properties of the substance applied; precise timing of application and the methods used for application; spatial variability of soil characteristics and land use; hydraulic connectivity of the landscape (*e.g.*, tile drainage and water allocation); and spatial distribution of mitigation measures (*e.g.*, buffer strips, windbreaks). In the EU, regulatory pesticide exposure assessment addresses this challenge primarily through the FOCUS suite of models, which includes TOXSWA for in-stream fate as well as PELMO, MACRO, and PEARL for soil transport, operating at the field or water body scale under harmonized, conservative scenarios as required under Regulation (EC) No 1107/2009 (Beltman et al., 2006; Dubus et al., 2003; Jarvis, 1994; Leistra et al., 2001). However, these tools abstract away the spatial heterogeneity and hydrological connectivity that govern pesticide dynamics at the catchment scale. Given these limitations of field-scale regulatory approaches and the complexity of off-target transport processes, modeling approaches on the landscape scale have become increasingly relevant for predicting the fate and transport of pesticides in the environment and understanding how mitigation measures can be precisely applied to reduce off-target movement. However, significant uncertainties arise in modeling pesticide dynamics, stemming from variability in input data,

* Corresponding author. RPTU Kaiserslautern-Landau, Fortstr. 7, 76829 Landau, Germany.
E-mail address: md.fuchs@rptu.de (M.D. Fuchs).

https://doi.org/10.1016/j.envpol.2026.128031
Received 3 February 2026; Received in revised form 16 March 2026; Accepted 26 March 2026
Available online 28 March 2026
0269-7491/© 2026 The Authors. Published by Elsevier Ltd. This is an open access article under the CC BY-NC-ND license (http://creativecommons.org/licenses/by-nc-nd/4.0/).

limitations in modelling approaches, assumptions in parameterization, and simplifications in representing complex transport processes.

Much of the recently published literature on pesticide dynamics at the landscape scale utilizes the Soil and Water Assessment Tool (SWAT) (Ippolito and Fait, 2019). SWAT is a spatially distributed, process-based model that represents key hydrological and transport pathways such as surface and subsurface runoff, leaching, and subsurface drainage (Vallée et al., 2014; Zhang et al., 2018). This makes it well suited for assessing pesticide transport across agricultural landscapes. Spray drift, in contrast, has been found to be a potentially significant contributor to off-target transport of pesticides (Mottes et al., 2014; Schönenberger et al., 2022; de Snoo and De Wit, 1998; Zhang et al., 2018), yet it is not represented in SWAT. Therefore, some modeling approaches have incorporated spray drift into SWAT simulations by predicting spray drift deposition onto water surfaces using the AgDRIFT model (Winchell et al., 2018; Zhang et al., 2018), or the German drift database (Holvoet et al., 2008). However, these empirical approaches oversimplify the spatial relation between application and non-target areas, only partly account for wind direction, and consider spray drift deposition only onto stream surfaces. These simplifications were shown to potentially cause large uncertainties in predicted spray drift deposition (Fuchs et al., 2025a), which might affect the subsequent modelling of pesticide dynamics via SWAT.

The recently introduced droplet and atmospheric dispersion drift (DAD-drift) model (Fuchs et al., 2025b) provides a powerful tool for spray drift prediction at the landscape scale. In this study, we coupled DAD-drift with SWAT + to evaluate the role of spray drift in pesticide exposure at landscape scale. The coupled framework was applied to the Funne catchment, a predominantly agricultural lowland basin in North Rhine-Westphalia, Germany. The model setup was based entirely on publicly available data including a digital elevation model, soil and land use maps, stream network, potentially drained areas, crop development database, and weather and streamflow observations.

The objectives of this study are to (1) develop a high-resolution eco-hydrological model of an agriculturally dominated German lowland catchment; (2) present a first implementation of the DAD-drift model into the SWAT + model; (3) show the impact of spray drift deposition on pesticide exposure at the landscape scale through a modelling experiment; (4) assess uncertainties in predicted environmental concentrations resulting from model parameterization.

2. Material & methods

2.1. Study area

Modeling was conducted for the Funne catchment (5440 ha), which is located in the German federal state of North Rhine-Westphalia (NRW), and drains to the Funne river, which is a tributary to the Stever river. The predominant land use in the catchment area is agriculture (>48%), followed by forests (~22%), grasslands (~17%), and urban areas (~10%) (Fig. 1) (Geobasis NRW, 2024a).

In this work, we simulated the sub-catchment upstream of the Selm-Ondrup station, with an area of 3866 ha and a mean elevation of 77 m a.s.l., ranging from a minimum of 52 to a maximum of 110 m a.s.l. The simulated catchment has low hydraulic gradients with an average slope of 6.6‰ within the river network and is dominated by poorly draining soils high in clay content (Geologischer Dienst NRW, 2020) For this reason, large fractions of the catchment are artificially drained by agricultural tile drains (Geobasis NRW, 2024b). Some parts of the stream network have been subject to hydromorphological alteration by being

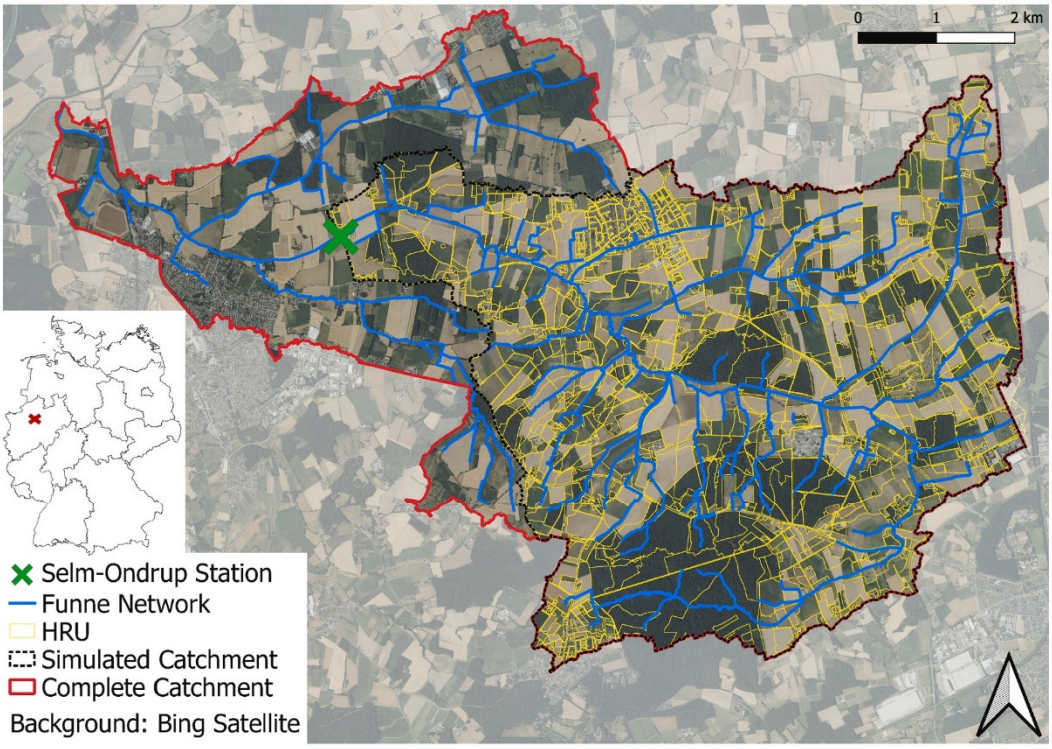


Fig. 1. Study area of the Funne catchment (red line) with stream network (blue lines) and hydraulic response units (HRUs) indicated by yellow lines. The location of the catchment within Germany is marked by the red cross and the location of the gaging station within the catchment is marked by the green cross. Simulations were performed to the sub-catchment upstream of the gauging station (dashed black line). (For interpretation of the references to colour in this figure legend, the reader is referred to the Web version of this article.)

artificially straightened. Irregularities in stream bed elevation create flow limitations during low flow periods, causing some tributaries to become temporarily disconnected from the stream network. Some farmers report regular flooding during heavy rain events (personal communication).

2.2. Modeling framework

The modeling framework presented in this work consists of a wide range of openly available input data, processed datasets, SWAT+, which predicts the eco-hydrology of the Funne catchment as well as pesticide transport, and the DAD-drift model, which predicts spray drift deposition after ground application (Fig. 2). The following sections describe all elements of the modeling framework.

2.2.1. SWAT + model description

The Soil and Water Assessment Tool (SWAT) is a semi-distributed, process-based watershed model developed by the USDA Agricultural Research Service (Arnold et al., 1998). It is based on the combination of the basin-scale surface water model SWRRB (Arnold and Williams, 1987; Williams et al., 1985) with the groundwater flow and height model ROTO (Arnold et al., 1995). The SWAT model has been continuously improved, with the most recent iteration being SWAT+ (Bieger et al., 2017). Much of the original SWAT has been restructured to improve model flexibility and performance in SWAT+.

For this modeling framework, SWAT+ (version 61.0.1) was used. Modifications were made to the source code to enable compilation of the source code without critical errors, enable simulation of pesticide transport without critical model bugs, enable input of pesticide mass to the stream network via the point source interface, which was repurposed to represent spray drift deposition, and to fix inconsistent use of the

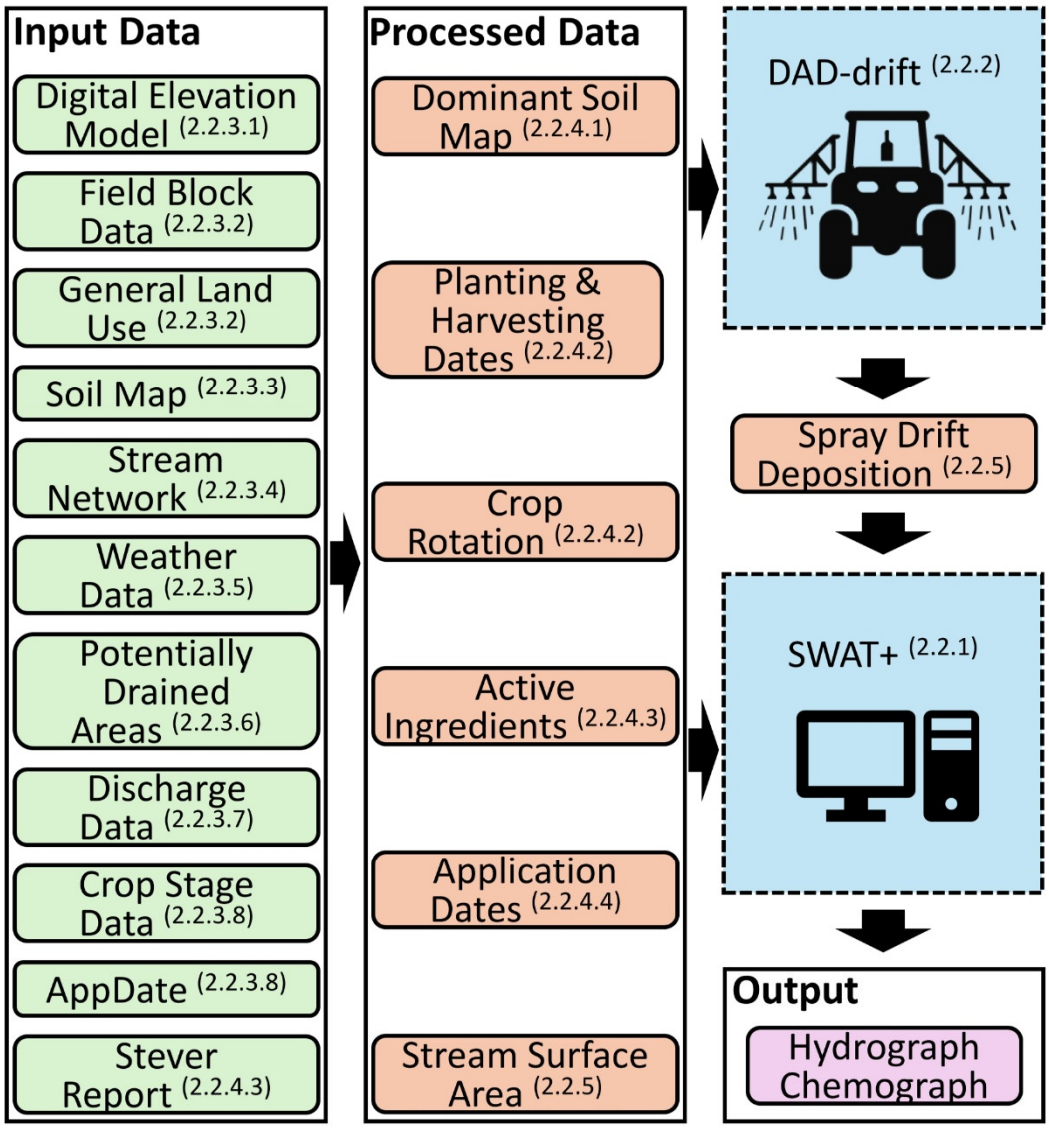


Fig. 2. Schematic representation of the modeling framework. With input data represented by green boxes, processed data represented by salmon boxes, models represented by blue boxes, final modeling results represented by purple boxes. The annotations indicate in which section of this work the respective element is described. (For interpretation of the references to colour in this figure legend, the reader is referred to the Web version of this article.)

channel width as the bottom width of the trapezoidal representation of the channel cross-section, which is critical for small channels such as those found in the Funne catchment. A complete overview of differences between the SWAT + version used in this work and the official SWAT + version 61.0.1 is provided in supplementary material B.

2.2.2. DAD-drift model description

The DAD-drift model is a computationally efficient modeling approach, capable of accounting for the physical basis of spray drift, the relative location of application areas to non-target areas, and local weather conditions at the landscape scale (Fuchs et al., 2025a). The DAD-drift model is a combination of a mechanistic droplet model, a micrometeorological model, and a three-dimensional Gaussian puff model and was developed for ground application of pesticides. The model has been successfully evaluated against two field-scale drift studies for ground application using conventional boom sprayers covering a wide range of drift potentials (Brain et al., 2019; Perine et al., 2021).

2.2.3. Input data

2.2.3.1. Digital elevation model. The digital elevation model (DEM) of the Funne catchment was adopted from the DGM (digital terrain model) dataset obtained from OpenGeoData.NRW (Geobasis NRW, 2020a). The dataset is openly available and consists of 1x1-km tiles with a grid cell resolution of 1 × 1 m.

2.2.3.2. Land use map. The land use map of the Funne catchment was derived from two datasets provided by OpenGeoData.NRW. The first dataset (Geobasis NRW, 2024a) provides information on land use in the catchment in categories including urban areas, roads, forests, grassland, surface waters, and agriculture. However, for the agricultural category, no further information on crops and growing seasons were provided. The second dataset (Geobasis NRW, 2024c) contains field block data with information on crops grown for the years 2019 to 2023, as reported by farmers to the authorities in the process of applying for subsidies. Agricultural areas in the land use map were adopted from the field block data, resulting in detailed crop rotations over five years for each individual field. Gaps caused by deviations in polygon area between the two datasets were filled using nearest neighbor interpolation.

2.2.3.3. Soil map. The soil map of the Funne catchment was derived from the BK50 soil map obtained from OpenGeoData.NRW (Geologischer Dienst NRW, 2020). The BK50 soil map is openly available and with its accompanying ASCII files contains all necessary inputs for the SWAT + model.

2.2.3.4. Stream network. The stream network of the Funne river was adopted from the basis DLM (digital landscape model) dataset obtained from OpenGeoData.NRW (Geobasis NRW, 2020b). It is openly available and contains streams within the German federal state of North Rhine-Westphalia (NRW) within the "gew01_l" layer.

2.2.3.5. Weather data. The weather data was obtained from the Climate Data Center (CDC) of the German weather service (DWD). Daily precipitation data were derived from the four HYRAS grid cells (Deutscher Wetterdienst, 2024a) overlapping with the catchment. Temperature and relative humidity data were adopted from daily observations of station number 6337 (Deutscher Wetterdienst, 2024b). Solar radiation data was derived from daily observations of station number 5480, gaps in the record were filled with daily observations of station number 7374 (Deutscher Wetterdienst, 2024b). Wind speed and direction were adapted from hourly observations of station number 5480. Gaps in the record were filled with hourly observations from station number 13901 after bias correction based on the mean wind speeds of both stations between 2009 and 2023 (Deutscher Wetterdienst, 2024c).

2.2.3.6. Potentially tile-drained areas. Potentially tile-drained areas of the Funne catchments were derived from the water balance model mGROWA obtained from OpenGeoData.NRW (Geobasis NRW, 2024b). The potentially drained areas were predicted based on the DEM, land use, soil map, and more (Tetzlaff, 2021), maintaining a resolution of 100 × 100 m. Agricultural areas that intersect with potentially drained areas were defined as being drained within the SWAT + model. About 46.6% of the simulated catchment (3866 ha) and 96.7% of the agriculturally used area within the simulated catchment were defined as potentially drained.

2.2.3.7. Discharge data. Discharge observations from the Funne river were retrieved from the ELWAS-Web portal (Land NRW, 2020). The dataset retrieved for this work describes the daily mean river discharge in m^3/s at the Selm-Ondrup station (ID:2788630000200), which is the pour point for the simulated catchment. Peaks in stream discharge did not occur simultaneously with heavy rainfall events, likely attributable to differences in recording conventions between the two independent data sources (Deutscher Wetterdienst, 2024a; Land NRW, 2020). The discharge data were therefore shifted by one day to ensure proper temporal alignment between precipitation forced discharge response. Without this correction a meaningful model calibration with satisfactory Nash-Sutcliff efficiency (NSE) (Moriasi et al., 2007) was not possible.

2.2.3.8. Crop development database. Two crop development databases were used in this modeling approach. The CropLife Europe Crop Development Database (C2D2) is an open-source, pan European, harmonized crop development database that uses efficacy trial data generated for regulatory submissions when registering plant protection products under Regulation (EU)1107/2009 (Hughes et al., 2023). The C2D2 database was used to derive sowing dates and application time windows based on observations reported for Germany. Harvest dates were adopted from the AppDate tool (Klein, 2019), as harvest dates were not reported in the C2D2 database.

2.2.4. SWAT + model setup

Two distinct SWAT + model setups were created (base and drift). In the base setup, pesticide transport to the stream network via interflow, surface runoff, leaching, and tile drainage was predicted. In the drift setup, pesticide transport via spray drift was added to the model via DAD-drift.

2.2.4.1. Dominant soil. In SWAT+, hydraulic response units (HRU) are defined as unique combinations of land use, soil type, and slope. To reduce the total number of HRUs and the runtime of the SWAT + model for the Funne catchment, the dominant soil was defined as the one with the largest coverage in each polygon in the land use map. This ensures only one HRU is generated per polygon, while maintaining most of the resolution of the soil map.

2.2.4.2. Crop rotations. Based on the field block data (Geobasis NRW, 2024c), a 5-year crop rotation from 2019 to 2023 was created for each field in the Funne catchment. For the years 2010 to 2018, crops were randomly assigned to each field with an equal distribution to the field block data, assuming no change in crop use has occurred. To reduce model complexity, crops were grouped into six groups consisting of winter wheat, spring cereals, maize, winter rye, legumes, and grassland. For each crop, the associated sowing date was derived from the C2D2 database (Hughes et al., 2023). Harvest dates were adopted from the AppDate tool (Klein, 2019) and are triggered by total degree days (heat units) as calculated in SWAT+. Fields were assumed to be plowed after each harvest and cultivated prior to sowing. For more realistic runoff conditions during the winter period, red clover was used in the model as

a generic cover crop on fields which would otherwise be bare. Changes in runoff conditions were represented by changing the runoff curve number, used by SWAT + for runoff calculation, upon sowing or harvesting.

2.2.4.3. Active ingredients. The Funne catchment is part of the Stever catchment which drains into the Haltern reservoir used as a public drinking water supply. To ensure water quality and lower costs for drinking water production, a cooperation between farmers, the chamber of agriculture of North Rhine-Westphalia, and water management (*i.e.*, Gelsenwasser AG) was established more than 30 years ago. This cooperation publishes an annual report on the results of ongoing consulting and monitoring in the Stever catchment. Based on the reports for the years 2019, 2020, and 2021, the most relevant pesticidal active ingredients applied in the Funne catchment were selected (Lammers, 2021, 2020, 2019). To ensure two applications (herbicide & fungicide) per crop (winter wheat, winter rye, spring wheat, maize), two additional fungicides were selected. Physiochemical properties of the active ingredients (Table S1) were obtained from publicly available registration dossiers and the PubChem database (Kim et al., 2023). All active ingredients were anonymized by rounding and modifying their physiochemical properties to the extent necessary and are referred to as F1 and F2 for the two fungicides and H1 to H5 for the five herbicides.

2.2.4.4. Application timing. The pesticide database of the Federal Office of Consumer Protection and Food Safety (BVL, 2024) was searched for products containing the selected active ingredients. The spray solution concentration, application rate, crop, and the lower and upper growth stage limits for application were determined for each product. For each crop-active ingredient combination, all products were analyzed for solution concentration, application rate, and the lower and upper growth stage limits. Application windows were derived by cross-referencing the growth stage limits with the C2D2 database (Hughes et al., 2023). Application dates for each crop, year, and active ingredient combination (Table S2) were determined using a simple forward-oriented pesticide application timer similar to Bach et al. (2017). Application date selection rules include i) less than 5 mm precipitation on the day before and after application and ii) no precipitation on the day of application, with the first day in the application window fitting these criteria being selected as the application date.

2.2.4.5. Drift prediction. Pesticides, application dates, and application rates were taken from the base setup. Spray drift prediction was performed by running DAD-drift (Fuchs, 2026) using the standard TeeJet XR11003 nozzle scenario previously parameterized (Fuchs et al., 2025b). For each simulated drift event the parameters were adapted with substance-specific properties, date-specific weather conditions, and application-specific parameters (i.e., boom height, canopy height, and leaf area index (LAI)), distinguishing between bare soil conditions for herbicide applications and established crop canopy conditions for fungicide applications (Table S3). Without spray reduction nozzle and buffer strips this represents the worst-case application scenario in the catchment. The land use map was modified to represent the stream channel surface area as estimated by the SWAT + model and was then used to determine spray drift deposition for each HRU and channel for each of the simulated drift events. Drift deposition onto the channel network was transferred to the SWAT + model by defining pesticide input via point sources for each channel segment if the received pesticide drift mass exceeded 10^{-9} kg (*i.e.*, 1 μg). Drift deposition in the landscape was transferred to the SWAT + model, using the input logic for application events, if HRUs receive a rate greater than 10^{-9} kg/ha.

2.2.5. Predicted environmental concentrations

We assessed the contribution of spray drift by comparing daily time series of predicted environmental concentrations (PEC) at the outlet of the simulated catchment. Additionally, the maximum predicted environmental concentration (PEC_{max}) and the 90th percentile predicted environmental concentration (PEC_{90}) were calculated for each of the active ingredients based on all daily PEC values for 2019 to 2023.

2.3. Sensitivity analysis, hydrological Parametrization and ensemble setup

A one-at-a-time sensitivity analysis was performed on 158 parameters in the SWAT + model as a screening step to identify parameters irrelevant to discharge, in order to reduce the computational cost of the global sensitivity analysis (GSA). Forty-three parameters were found to be relevant for discharge (Table S4) and were used in a GSA following the Sobol' approach (Sobol', 1990), a variance decomposition method that allows to characterize the contribution of each input factor individually and the contribution of interactive effects between input factors. Sensitivity indices were calculated based on simulated and observed discharge between 2018 and 2021.

In total, 15,000 model runs were performed to parameterize the model hydrology. The parameter space of 19 model parameters was sampled using Latin Hypercube Sampling (LHS) (McKay et al., 1979) (see Table S5 for the parameter names, the related input file, the upper and lower limit, and the type of change made to the parameter value).

The years 2014, 2016, 2017, 2018, and 2021 were defined as the parameterization period, and consequently the years 2013, 2015, 2019, and 2020 were defined as the validation period. This split was chosen to ensure that mean climatic conditions during parameterization and validation were representative of the overall simulation period, minimizing climatic bias in parameter estimation (Tables S6–7). Performance for both periods was evaluated by comparing simulated and observed discharge at the Selm-Ondrup station. The metrics used were the NSE, the percent bias (PBIAS), and the Kling-Gupta efficiency (KGE) (Gupta et al., 2009; Moriasi et al., 2007).

An ensemble of 20 simulation runs with different parameterizations was selected to represent the hydrology of the Funne catchment using the SWAT + model. Parameter sets were chosen based on model performance, with the top ten runs according to NSE and the top ten runs according to KGE being selected. NSE tends to emphasize peak flows and is more sensitive to high-flow events and KGE incorporates correlation, bias, and variability, offering a more holistic assessment of model performance across all flow conditions. By combining both metrics, the ensemble balances the evaluation across different aspects of the hydrograph and better represents the hydrological behaviour in the catchment.

3. Results

3.1. Global sensitivity analysis and hydrological parameterization

First-order sensitivity reflects the influence of an individual parameter on the model output when varied alone. Among all parameters, tile drainage depth showed the highest first-order sensitivity. Channel slope and side slope, snowfall temperature and minimum water content as well as soil bulk density and available water content also showed increased first-order sensitivity (Fig. S1, Table S8). The remaining parameters showed comparable values for first-order sensitivity. Total sensitivity captures both the individual effects of a parameter and its interactions with other input parameters. Tile drainage depth, soil bulk density, and channel slope showed the highest total sensitivity. Overall, parameters related to tile drainage, soil properties, channel routing, and snow formation showed high total sensitivity indices (Fig. S1, Table S8), while those related to aquifer routing showed lower total sensitivity overall.

The hydrological parameterization of the SWAT + model resulted in an ensemble of 20 realizations (Table S9) with KGE values ranging from 0.77 up to 0.86 for the parameterization period (2014, 2016, 2017,

2018, 2021) (Table S10). NSE values and PBIAS values ranged from 0.71 to 0.79 and from −3.2 to 8.7, respectively. For the validation period (2013, 2015, 2019, 2020), KGE values ranged from 0.77 to 0.86, NSE values ranged from 0.51 to 0.8, and PBIAS values ranged from 6.4 to 25.6 (Table S10).

During winter periods, the model described the discharge dynamics of the Funne river very well, reproducing both the timing and amplitude of discharge peaks (Fig. S2). During the summer months, the modeled discharge dynamics were acceptable although low flow periods are generally overestimated (*e.g.*, 2018, 2019) (Fig. S2). The timing and amplitude of discharge peaks were generally well represented by the model, with some minor exceptions of underestimation (*e.g.*, summer 2014, summer 2016) or prediction of additional flow peaks (*e.g.*, summer 2015, summer 2018, summer 2019) (Fig. S2).

3.2. Predicted environmental concentrations

The fungicide F1 is strongly sorbing and has short half-lives in soil, foliage and water (Table S1). It was applied to maize at the end of June during low discharge conditions (Table S2). In the base setup, most of the mass was sorbed to the soil profile and only 1.5 g of the applied mass of 453.9 kg were transported out of the catchment (Table S14). This resulted in median PEC_{90} and PEC_{max} values of 0.00 ng/L and 0.49 ng/L, respectively (Fig. 4, Table S11, Table S12). In the drift setup, a significant fraction of the applied F1 was transported to the stream network via spray drift (Fig. S3), resulting in short-duration concentration peaks occurring immediately after application (Fig. 3), resulting in 44.6 g of F1 (0.012% of the applied mass) being transported out of the catchment (Table S14). Consequently, the median PEC_{max} increased significantly to 656.6 ng/L while the median PEC_{90} values stayed at 0.00 ng/L (Fig. 4, Table S11, Table S12).

The fungicide F2 was applied on winter wheat and winter rye at the beginning of April and on spring cereals in the middle of May (Table S2). During the application windows, discharge was generally decreasing with the exception of two discharge peaks during 2022 and 2023. F2 is a strongly sorbing fungicide with low solubility and a long water half-life (Table S1). Due to strong soil adsorption only 0.007% of the applied mass was transported out of the catchment with transport to the stream network dominated by surface runoff (Table S14, Fig. S3), resulting in in median PEC_{90} and PEC_{max} values of 0.16 ng/L and 51.72 ng/L, respectively (Fig. 4, Table S11, Table S12). In the drift setup, F2 concentration peaks after application to winter wheat are visible (Fig. 3) and mass export from the catchment is increased to 0.157% of the applied mass (Table S14). Median PEC_{90} and PEC_{max} values are increased to 21.51 ng/L and 4.48 µg/L, respectively (Fig. 4, Table S11, Table S12). This increase in F2 export from the catchment is mainly caused by transport to the stream network via spray drift, with a notable increase in transport via surface runoff in the drift setup compared to the base setup (Fig. S3).

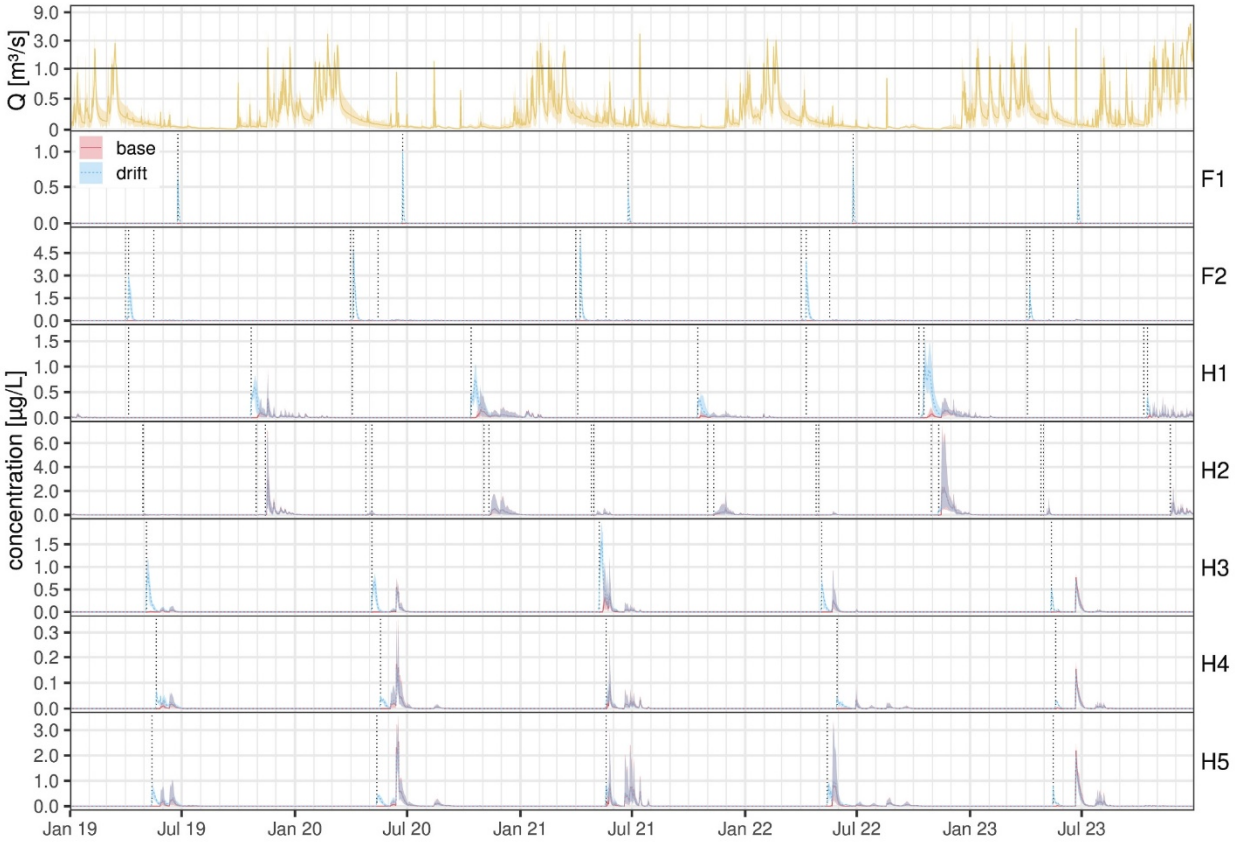


Fig. 3. Daily discharge at the gauging station in yellow in the upper panel, with linear scaling up to 1 m^3/s and logarithmic scaling above 1 m^3/s. Daily predicted environmental concentration [µg/L] at the outlet (gauging station) of the simulated catchment for the seven active ingredients (fungicides F1 and F2, herbicides H1 to H5) in the following panels. With the blue solid line and blue ribbon representing the data of the base setup and the red dashed line and red ribbon representing the data of the drift setup. The lines represent the daily mean concentration or discharge of the 20 ensemble runs representing different parameterizations and the ribbons represent the daily minimum to maximum range for concentration or discharge of said ensemble. (For interpretation of the references to colour in this figure legend, the reader is referred to the Web version of this article.)

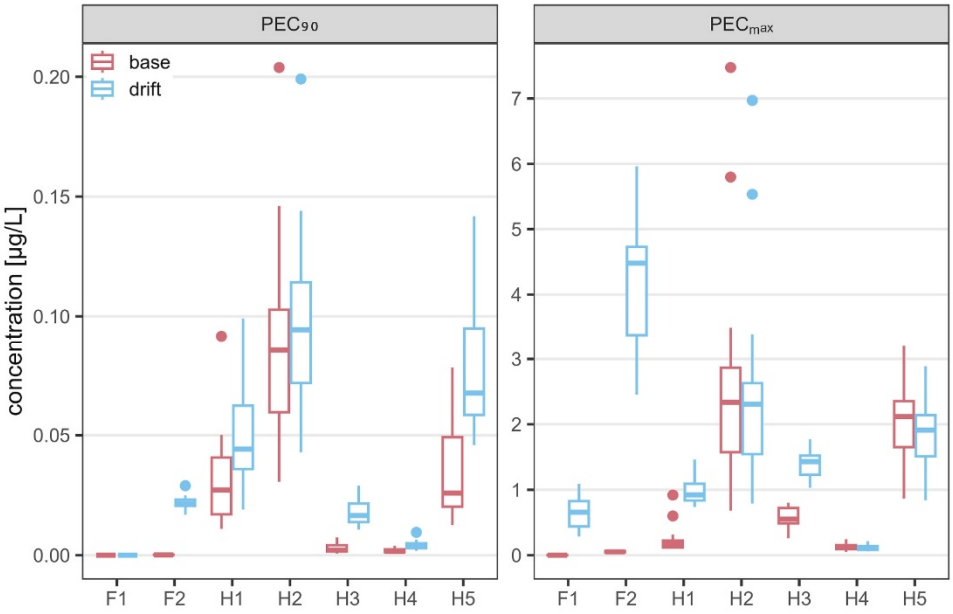


Fig. 4. Comparison of PEC90 (left) and PECmax (right) values at the outlet (gauging station) of the simulated catchment for the base and drift setup across seven active ingredients (fungicides F1 and F2, herbicides H1 to H5) over the period 2019 to 2023. With the base setup in red and the drift setup in blue. Each boxplot represents 20 PEC90 or PECmax values derived from daily predicted environmental concentrations, based on an ensemble of 20 hydrological parameter sets. The box denotes the interquartile range (Q1-Q3), with the median (Q2) indicated by a horizontal line, whiskers extend to 1.5 times the interquartile range, and individual point represent outliers. (For interpretation of the references to colour in this figure legend, the reader is referred to the Web version of this article.)

The physio-chemical properties of herbicide H1 are of intermediate magnitude, indicating moderate sorption, solubility, and persistence compared to the other active ingredients (Table S1). H1 was applied on winter wheat and winter rye in mid-October, shortly before discharge was increased by heavy rain events, and on spring cereals at the beginning of April during a period of generally decreasing discharge (Table S2). In the base setup, the H1 concentration was increasing about two weeks after application, with export from the catchment lasting until mid-February (Figure F3). H1 was transported to the stream network via interflow, surface runoff and tile drainage (Fig. S3), which resulted in 0.167% of the total applied mass reaching the catchment outlet (Table S14). In the drift setup, pronounced concentration peaks immediately after application were observed for H1, with the pesticide dynamics of the remaining year being similar to the base setup (Fig. 3) and total mass transport via spray drift being comparable to that via tile drainage (Fig. S3). While the addition of spray drift increased median PEC_{90} and PEC_{max} values from 27.17 ng/L to 44.22 ng/L and 168.92 ng/L to 922.91 ng/L, respectively (Fig. 4, Table S11, Table S12), the total H1 export from the catchment was increased to 0.204% of the total applied mass (Table S14).

The herbicide H2 was applied on winter rye, winter wheat, maize, and spring cereals at the end of October, mid-November, end of April, and end of April (Table S2), respectively. The low soil adsorption coefficient of H2 is noteworthy (Table S1), indicating it has a high potential for transport to surface water. The herbicide H2 was transported to the stream network via tile drainage and interflow. In the base setup, transport out of the catchment occurred with a time delay after application on winter rye and winter wheat, with sharp concentration peaks in 2019 and 2022 and elevated concentrations lasting for about 1.5 months coinciding with increased discharge dynamics caused by heavy rain events. After application on maize and spring cereals, small concentration peaks were observed during generally low discharge conditions (Fig. 3). In the drift setup, total mass transport to the stream network via spray drift was insignificant compared to that of tile drainage and interflow (Fig. S3) and concentration dynamics at the catchment outlet were equal to the base setup, with the exception of 2022 when a small concentration peak immediately after application to winter wheat was visible (Fig. 3). This resulted in the median PEC_{90} and PEC_{max} values staying nearly unchanged between the base and drift setups (Fig. 4, Table S11, Table S12). Similarly, transport to the catchment outlet was only increased from 2.307% to 2.337% by the drift setup (Table S14). Most of the export from the catchment happened during 2019 and 2023, when about 4.8% of the applied mass was exported in each year (Table S13).

The herbicide H3 is highly water soluble and was applied to maize during generally low discharge conditions at the beginning of May (Table S1, Table S2). Following application, transport of H3 to the catchment outlet was delayed from two weeks in 2021 up to five weeks in 2023 (Fig. 3). About 0.090% of the applied H3 mass was exported from the catchment (Table S14) with median PEC_{90} and PEC_{max} values of 2.13 ng/L and 550.44 ng/L, respectively (Fig. 4, Table S11, Table S12). The addition of spray drift resulted in additional concentration peaks immediately after application, with the amplitude of those peaks being comparable to the base setup in 2020, 2022, and 2023 and significantly higher in 2019 and 2021 (Fig. 3). In the base setup, H3 transport to the stream network was dominated by surface runoff with some interflow; however, in the drift setup, spray drift was the second most relevant transport pathway after surface runoff (Fig. S3). This increased transport to the stream network resulted in increased H3 mass transport to the catchment outlet (0.143% of the applied mass) (Table S14) and significantly increased median PEC_{90} and PEC_{max} values of 16.57 ng/L and 1.429 µg/L, respectively (Fig. 4, Table S11, Table S12).

The herbicide H4 is highly water soluble and was applied to maize at the end of May during low flow conditions (Table S1, Table S2). Transport generally occurred with a delay of one to four weeks in the base setup, with sharp concentration peaks during 2020, 2021, and 2023 (Fig. 3). The exception was 2021, when transport to the catchment outlet happened immediately after application. The herbicide H4 entered the stream network via surface runoff, interflow and tile

drainage, in descending order of relevance (Fig. S3). In the drift setup, concentration dynamics were similar to the base setup with additional concentration peaks at the outlet observable for 2019, 2020, 2022, and 2023 (Fig. 3). However, total mass transport of H4 to the stream network via spray drift was smaller than that of surface runoff, interflow and tile drainage (Fig. S3). This resulted in similar export from the catchment of 0.424% and 0.477% (Table S14) and similar median PEC_{max} values of 123.41 ng/L and 110.46 ng/L for the base setup and drift setup, respectively (Fig. 4, Table S11). Only the median PEC_{90} values were significantly elevated from 1.63 ng/L to 3.55 ng/L by the addition of spray drift (Fig. 4, Table S12).

The herbicide H5 was applied to maize in mid-May during low flow conditions (Table S2). The physico-chemical properties of H5 are intermediate in terms of sorption and solubility relative to the other active ingredients. However, it is characterized by a very long water half-life (Table S1). In the base setup, transport of H5 to the outlet occurred with a delay ranging from days after application in 2021 up to about five weeks after application in 2023 (Fig. 3). The addition of spray drift resulted in additional concentration peaks immediately after application with a lower amplitude than the other concentration peaks already present in the base setup (Fig. 3). In the base setup, H5 transport to the stream network occurred mainly via surface runoff, interflow, and tile drainage. In the drift setup, total mass transport via spray drift was comparatively minor (Fig. S3). This resulted in similar median PEC_{max} values of 2.117 μg/L and 1.911 μg/L and similar transport of H5 to the catchment outlet of 0.548% and 0.625% for the base setup and drift setup, respectively (Fig. 4, Table S11, Table S14). Only the median PEC_{90} values were significantly elevated from 25.91 ng/L to 67.53 ng/L by the addition of spray drift (Fig. 4, Table S12).

4. Discussion

4.1. Global sensitivity analysis and hydrological parameterization

The global sensitivity analysis (GSA) following Sobol' (1990) provides valuable insight into the model's response to parameter variation. Differences between first-order and total sensitivity indices clearly demonstrate the non-linear and interactive nature of the SWAT + model for the Funne catchment, a feature typical for process-based hydrological models due to complex linkages among sub-modules (Gupta et al., 2009; Moriasi et al., 2007). Consequently, parameters cannot be calibrated independently but must be optimized simultaneously to ensure physically consistent system behavior. This structural complexity often produces multiple parameter sets that reproduce hydrological observations with comparable goodness of fit, yet represent distinct internal processes, and thus, different hydrological realities. This condition, known as equifinality (Beven, 2006), underscores the importance of viewing calibrated model results as one possible realization among many plausible system representations.

Parameters related to tile drainage (*e.g.*, tile drainage depth, drainage coefficient), soil properties (*e.g.*, bulk density, available water content), channel routing (*e.g.*, channel slope, Manning's roughness coefficient, median particle size of suspended and benthic sediment, channel erodibility factor, channel side slope), and snow formation (*e.g.*, snowfall temperature, minimum snow water content, snowmelt factor) showed the highest total sensitivity indices. Input parameters related to the simulation of groundwater dynamics overall showed relatively low total sensitivity indices. This contrasts with previous studies, where groundwater parameters are often described as sensitive and included in model parameterization (Fohrer et al., 2014; Holvoet et al., 2005; Rathjens et al., 2023; Wagner et al., 2022).

During low-flow conditions the hydrology of catchments is generally driven by groundwater dynamics. However, the simplified groundwater equations of the SWAT model have been identified as an oversimplification of the physically based rise and fall of groundwater near streams (Bailey et al., 2020a, 2020b). In addition, groundwater parameters have been identified as the primary cause of poor model performance during low-discharge periods in lowland catchments (Pfannerstill et al., 2014). These findings, combined with the aforementioned insensitivity of groundwater parameters, indicates that the SWAT + model of the Funne catchment would greatly benefit from improved groundwater representation. The newly developed physically based, spatially distributed groundwater flow module (Bailey et al., 2020b) could be the next step for this modeling approach if pesticide transport via the groundwater is implemented in a future update.

Parameterization of the SWAT + model of the Funne catchment was successful, as NSE and PBIAS performance were "very good" during the parameterization period and NSE performance was "good" to "very good" during the validation period according to the classification proposed by Moriasi et al. (2007). Merely PBIAS performance during the validation period was subpar with three parameter sets performing "unsatisfactory". Since great care was taken when splitting the simulation period into parameterization and validation periods based on climatic conditions, significant bias in conditions between the two periods can be rejected as the cause of the PBIAS performance during validation. The occurrence of prolonged periods of low discharge in the years 2013, 2019, and 2020, which were generally overpredicted by SWAT+, combined with the aforementioned limitations in groundwater representation, can explain the diminished PBIAS in the validation period.

4.2. Predicted environmental concentrations

The comparison between the base setup and the drift setup clearly indicates that spray drift deposition is of high importance for understanding and estimating pesticide exposure at the landscape scale. For all simulated active ingredients, additional concentration peaks at the catchment outlet were observed immediately after application, caused by spray drift deposition into surface waters. Furthermore, for all substances, the PEC_{max} and PEC_{90} values increased by between 10% and several orders of magnitude when spray drift deposition was implemented in the SWAT + model of the Funne catchment. The impact of spray drift on exposure dynamics strongly depends on the physiochemical properties of the individual substances. For the two modeled fungicides, export from the catchment in the base setup was very low (0.0–0.007% of the applied mass) due to their high soil adsorption coefficients (F1, F2), low water solubility (F2), and short half-lives in relevant environmental matrices (F1). Consequently, transport via spray drift had a pronounced influence on pesticide dynamics for these compounds. A substantial proportion of herbicide mass is already mobilized through existing transport pathways, such as interflow (H1–H5), surface runoff (H1, H3, H4, H5), and tile drainage (H1, H2, H4, H5), in the base setup. The inclusion of spray drift as an additional transport pathway in the drift setup therefore did not result in a significant increase in total herbicide export from the catchment.

This modeling approach uses an ensemble of 20 realizations with different hydrological parameterizations of the SWAT + model of the upper Funne catchment. The performance metrics (NSE, KGE, PBIAS) indicate that all 20 parameter sets are similarly capable of reproducing the observed discharge dynamics. Nevertheless, small differences in hydrological behavior among these parameterizations resulted in substantial variations in predicted pesticide concentrations. Ensemble variability differed systematically between the base and drift setups because spray drift deposition is identical across all 20 ensemble members. As a result, absolute concentration levels increase while ensemble variability remains driven by hydrological parameterization, reducing the relative spread among realizations. However, this effect is substance-dependent, as for mobile substances (H2), where transport to the stream network is dominated by hydrological pathways, ensemble variability remains largely unaffected by the addition of spray drift. For immobile substances with high soil adsorption (F1, F2), where spray drift is the dominant transport pathway, the shared drift signal governs predicted concentrations and relative ensemble variability is strongly

reduced. These findings reflect the tight coupling between pesticide transport pathways and catchment hydrology: where transport is dominated by surface runoff, interflow, and tile drainage, structural and parametric differences between hydrological realizations translate directly into divergent predictions of pesticide fate, whereas where spray drift dominates, this hydrological uncertainty becomes less influential. Similar patterns have been reported in previous studies, which found that uncertainty in hydrological calibration is a dominant driver of variability in simulated pesticide concentrations (Beven, 2006; Fohrer et al., 2014; Holvoet et al., 2005). Our findings therefore show that uncertainty in hydrological parameterization directly propagates into predicted environmental concentrations and that ensemble-based modeling provides an inherent framework for assessing this uncertainty at the landscape scale, where the variability among ensemble members serves as a direct indicator of model reliability and predictive strength.

4.3. Study limitations

The presented modelling approach has some potential for refinement. The implemented pesticide application timer similar to Bach et al. (2017) does not account for wind speed, which might lead to unfavorable wind conditions during application resulting in elevated spray drift. In a given application window, ideal wind and precipitation conditions occurring simultaneously is unlikely, hence a potential conflict between spray drift mitigation and mitigation of precipitation related transport processes (*e.g.*, washoff, surface runoff) might arise. The previously described DAD-drift limitations of a flat representation of the landscape, the simplified two-phase representation of the spray mixture without adjuvants and the missing representation of plant canopy interception (Fuchs et al., 2025a, 2025b) also apply to this modelling approach. As a result, simulated spray drift may be transported farther as it is not intercepted by the canopy of bushes or trees forming natural spray drift barriers, which are known to reduce spray drift (Felsot et al., 2010). Some of the relevant processes related to pesticide transport require improvement in SWAT+. Washoff from the foliage to the soil is triggered by a simple threshold of 2.54 mm precipitation, leading to near complete washoff when precipitation exceeds this threshold multiple times. This simplification does not reflect the actual behavior of pesticide washoff, which has been shown to follow first-order kinetics, meaning that the removal rate decreases proportionally with the remaining mass, so that a certain fraction of the substance always remains on the foliage after rainfall (Dang et al., 2016; Potter et al., 2011).

When simulating pesticide transport through the stream network in SWAT+, several structural and numerical limitations need to be considered. The daily simulation time step results in a temporal resolution that is lower than the expected water residence times in stream segments. As a consequence, concentration peaks caused by spray drift deposition into the streams are artificially diluted over more than two weeks (Fig. 3), potentially underestimating the true magnitude and duration of short-term concentration spikes. Moreover, the current implementation of benthic–water exchange processes in SWAT + can introduce numerical artefacts and unrealistic retention behavior. Processes such as sorption to sediments, subsequent deposition and resuspension, and diffusive exchange between the water column and the benthic layer are implemented in a way that strongly affects model stability and can distort downstream transport dynamics, particularly when sediment dynamics are not calibrated. To avoid introducing additional numerical uncertainty and unrealistic transport delays, these processes were deactivated (see Supplementary B).

5. Summary & conclusion

The Soil and Water Assessment Tool (SWAT) is a common model for predicting off-target movement of pesticides after application to agricultural crops. It simulates some of the most relevant transport pathways, such as surface and subsurface runoff, leaching and subsurface drainage, in a spatially distributed manner, but lacks any representation of pesticide transport via spray drift. In this work, we present the implementation of the newly developed Droplet and Atmospheric Dispersion drift (DAD-drift) model into a high-resolution SWAT + model of the upper Funne catchment in North Rhine-Westphalia, Germany.

The implementation was tested for a set of substances and the results showed that spray drift deposition is of high relevance for pesticide exposure at the landscape scale. The impact of spray drift on simulated pesticide concentrations was higher for immobile substances (high soil adsorption coefficients) and lower for substances already transported to the stream network via surface runoff, interflow, and tile drainage. In the spray drift setup of our model, increased pesticide export from the catchment, increased PEC_{max} and PEC_{90} values, as well as additional concentration peaks at the outflow could be observed. Simulating the pesticide dynamics for the ensemble of 20 hydrological parameterizations, it is clear that the catchment hydrology introduces uncertainties in predicted pesticide exposure, as most transport pathways are directly driven by catchment hydrology.

A global sensitivity analysis showed that the SWAT + model of the upper Funne catchment is generally of non-linear nature. The simulated discharge showed high sensitivity to input parameters related to tile drainage, soil properties, channel routing, and snow formation. The hydrology of the model was successfully parameterized using Latin Hypercube Sampling for 19 input parameters. Overall, model performance was very good during the parameterization period and remained satisfactory to very good during validation. Streamflow dynamics were represented very well and acceptable during winter periods and summer periods, respectively; however, during low discharge conditions streamflow was systematically overpredicted.

The modeling approach presented in this work can be used to explore the effectiveness of different best management practices (BMP), such as drift reduction nozzles and no-spray buffer strips for their potential to reduce exposure at the landscape scale. Furthermore, an analysis of critical source areas as well as a sensitivity analysis of the application timing and distribution in the catchment can be performed. The SWAT + simulated in-stream concentrations can be linked with ecotoxicological modeling approaches to identify vulnerable surface waterbodies.

CRediT authorship contribution statement

Mike Devin Fuchs: Writing – original draft, Visualization, Validation, Software, Methodology, Investigation, Formal analysis, Data curation, Conceptualization. **Sebastian Gebler:** Writing – review & editing, Supervision, Methodology, Conceptualization. **Andreas Lorke:** Writing – review & editing, Supervision.

Declaration of competing interest

The authors declare the following financial interests/personal relationships which may be considered as potential competing interests: Mike Devin Fuchs reports financial support was provided by BASF SE, Carl-Bosch-Str. 38, 67056 Ludwigshafen, Germany. Sebastian Gebler reports financial support was provided by BASF SE, Carl-Bosch-Str. 38, 67056 Ludwigshafen, Germany. If there are other authors, they declare that they have no known competing financial interests or personal relationships that could have appeared to influence the work reported in this paper.

Appendix A. Supplementary data

Supplementary data to this article can be found online at https://doi.org/10.1016/j.envpol.2026.128031.

Data availability

Data will be made available on request.

References

Arnold, J.G., Srinivasan, R., Muttiah, R.S., Williams, J.R., 1998. Large area hydrologic modeling and assessment part I: model development. JAWRA J. Am. Water Resour. Assoc. 34, 73–89. https://doi.org/10.1111/j.1752-1688.1998.tb05961.x.

Arnold, J.G., Williams, J.R., Maidment, D.R., 1995. Continuous-time water and sediment-routing model for large basins. J. Hydraul. Eng. 121, 171–183. https://doi.org/10.1061/(ASCE)0733-9429(1995)121:2(171.

Arnold, J.G., Williams, J.R., 1987. Validation of SWRRB - simulator for water resources in rural basins. J. Water Resour. Plann. Manag. 113, 243–256. https://doi.org/10.1061/(ASCE)0733-9496(1987)113:2(243.

Bach, M., Guerniche, D., Thomas, K., Trapp, M., Kubiak, R., Hommen, U., Klein, M., Reichenberger, S., Pires, J., Preuß, T., 2017. Bewertung des Eintrags von Pflanzenschutzmitteln in Oberflächengewässer – Runoff, Erosion und Drainage. Umweltbundesamt. Dessau-Roßlau, Germany.

Bailey, R.T., Park, S., Bieger, K., Arnold, J.G., Allen, P.M., 2020a. Enhancing SWAT+ simulation of groundwater flow and groundwater-surface water interactions using MODFLOW routines. Environ. Model. Software 126, 104660. https://doi.org/10.1016/j.envsoft.2020.104660.

Bailey, R.T., Bieger, K., Arnold, J.G., Bosch, D.D., 2020b. A new physically-based spatially-distributed groundwater flow module for SWAT+. Hydrology 7, 1–23. https://doi.org/10.3390/hydrology7040075.

Beltman, W.H.J., Ter Horst, M.M.S., Adriaanse, P.I., De Jong, A., 2006. Manual of FOCUS_TOXSWA version 2.2. 1. Alterra, Wageningen UR, Wageningen, Netherlands.

Beven, K., 2006. A manifesto for the equifinality thesis. J. Hydrol. 320, 18–36. https://doi.org/10.1016/j.jhydrol.2005.07.007.

Bieger, K., Arnold, J.G., Rathjens, H., White, M.J., Bosch, D.D., Allen, P.M., Volk, M., Srinivasan, R., 2017. Introduction to SWAT+, A completely restructured version of the soil and water assessment tool. J. Am. Water Resour. Assoc. 53, 115–130. https://doi.org/10.1111/1752-1688.12482.

Brain, R., Goodwin, G., Abi-Akar, F., Lee, B., Rodgers, C., Flatt, B., Lynn, A., Kruger, G., Perkins, D., 2019. Winds of change, developing a non-target plant bioassay employing field-based pesticide drift exposure: a case study with atrazine. Sci. Total Environ. 678, 239–252. https://doi.org/10.1016/j.scitotenv.2019.04.411.

BVL, 2024. Verzeichnis zugelassener pflanzenschutzmittel [WWW Document]. Bundesamt für Verbraucherschutz und Leb. URL. https://psm-zulassung.bvl.bund.de/psm/jsp/, 11.15.24.

Dang, A., Silburn, M., Craig, I., Shaw, M., Foley, J., 2016. Washoff of residual photosystem II herbicides from sugar cane trash under a rainfall simulator. J. Agric. Food Chem. 64, 3967–3974. https://doi.org/10.1021/acs.jafc.5b04717.

Deutscher Wetterdienst, 2024a. Raster data set of daily sums of precipitation in mm for Germany - hyras-de-pre. Version v5.0 [WWW Document]. URL. https://opendata.dwd.de/climate_environment/CDC/grids_germany/daily/hyras_de/precipitation/.

Deutscher Wetterdienst, 2024b. Daily station observations (temperature, pressure, precipitation, sunshine duration, etc.) for Germany. Version v24.3 [WWW Document]. URL. https://opendata.dwd.de/climate_environment/CDC/observations_germany/climate/daily/kl/, 12.1.24).

Deutscher Wetterdienst, 2024c. Hourly mean value from station observations of wind speed and wind direction for Germany. Version v24.03 [WWW Document]. URL. https://opendata.dwd.de/climate_environment/CDC/observations_germany/climate/hourly/wind/, 12.1.24.

Dubus, I.G., Brown, C.D., Beulke, S., 2003. Sensitivity analyses for four pesticide leaching models. Pest Manag. Sci. 59, 962–982. https://doi.org/10.1002/ps.723.

Felsot, A.S., Unsworth, J.B., Linders, J.B.H.J., Roberts, G., Rautman, D., Harris, C., Carazo, E., 2010. Agrochemical spray drift; assessment and mitigation—A review. J. Environ. Sci. Heal. Part B 46, 1–23. https://doi.org/10.1080/03601234.2010.515161.

Fohrer, N., Dietrich, A., Kolychalow, O., Ulrich, U., 2014. Assessment of the environmental fate of the herbicides flufenacet and metazachlor with the SWAT model. J. Environ. Qual. 43, 75–85. https://doi.org/10.2134/jeq2011.0382.

Fuchs, M.D., 2026. DAD-drift, v1.0. https://doi.org/10.5281/zenodo.18174928.

Fuchs, M.D., Gebler, S., Lorke, A., 2025a. Landscape-level assessment of spray drift – a virtual experiment using the droplet and atmospheric dispersion drift (DAD-drift) model. Environ. Model. Software 189, 106455. https://doi.org/10.1016/j.envsoft.2025.106455.

Fuchs, M.D., Gebler, S., Lorke, A., 2025b. The droplet and atmospheric dispersion drift (DAD-drift) model – a modular approach for estimating spray drift at the landscape scale. Environ. Res. 271, 121104. https://doi.org/10.1016/j.envres.2025.121104.

Geobasis NRW, 2024a. WFS NW ALKIS grundrissdaten vereinfachtes schema [WWW Document]. URL. https://advmis.geodatenzentrum.de/trefferanzeige?docuid=d840e759-6e8d-4c3b-aa8e-400eba1a5ee8#metadata_info, 7.9.24.

Geobasis NRW, 2024b. Potentiell drainierte flächen in NRW (mGROWA) als TIFF [WWW Document]. URL. https://www.opengeodata.nrw.de/produkte/umwelt_klima/wasser/grundwasser/mgrowa/potentiell-drainierte-flaechen_EPSG25832_TIFF.zip.

Geobasis NRW, 2024c. Beantragte und als förderfähig festgestellte Teilschläge in NRW als Shape [WWW Document]. URL. https://www.opengeodata.nrw.de/produkte/umwelt_klima/bodennutzung/landwirtschaft/LWK-TSCHLAG_EPSG25832_Shape.zip, 7.1.24.

Geobasis NRW, 2020a. Digitales Geländemodell NW Gitterweite 1m [WWW Document]. URL. https://www.opengeodata.nrw.de/produkte/geobasis/hm/dgm1_tiff/dgm1_tiff/, 8.21.20.

Geobasis NRW, 2020b. Digitales Basis-Landschaftsmodell NW [WWW Document]. URL. https://www.opengeodata.nrw.de/produkte/geobasis/lm/akt/basis-dlm/, 8.21.20.

Geologischer Dienst NRW, 2020. IS BK 50 Bodenkarte von NRW 1 : 50. 000 - Atom-Feed [WWW Document]. URL. https://www.opengeodata.nrw.de/produkte/geologie/boden/BK/ISBK50/ISBK50bis20161231_EPSG25832_Shape.zip, 8.21.20.

Gupta, H.V., Kling, H., Yilmaz, K.K., Martinez, G.F., 2009. Decomposition of the mean squared error and NSE performance criteria: implications for improving hydrological modelling. J. Hydrol. 377, 80–91. https://doi.org/10.1016/j.jhydrol.2009.08.003.

Holvoet, K., Griensven, A. van, Gevaert, V., Seuntjens, P., Vanrolleghem, P.A., 2008. Modifications to the SWAT code for modelling direct pesticide losses. Environ. Model. Software 23, 72–81. https://doi.org/10.1016/j.envsoft.2007.05.002.

Holvoet, K., Griensven, A. van, Seuntjens, P., Vanrolleghem, P.A., 2005. Sensitivity analysis for hydrology and pesticide supply towards the river in SWAT. Phys. Chem. Earth 30, 518–526. https://doi.org/10.1016/j.pce.2005.07.006.

Hughes, G.O., Eatherall, A., Bird, M., Blake, J., Branford, P.R., Gebler, S., Lozano, A., Massey, P.A., Reinken, G., Terry, A.S., Whitworth, E.H., 2023. C2D2: an open-source, pan-European, harmonised crop development database for use in regulatory pesticide exposure modelling and risk assessment. https://doi.org/10.5281/zenodo.8393135.

Ippolito, A., Fait, G., 2019. Pesticides in surface waters: from edge-of-field to global modelling. Curr. Opin. Environ. Sustain. 36, 78–84. https://doi.org/10.1016/j.cosust.2018.10.023.

Jarvis, N.J., 1994. The MACRO model (version 3.1), Technical description and sample simulations. Reports and Dissertations. Department of Soil Science, Swedish University of Agricultural Sciences, Uppsala, Sweden.

Kim, S., Chen, J., Cheng, T., Gindulyte, A., He, J., He, S., Li, Q., Shoemaker, B.A., Thiessen, P.A., Yu, B., Zaslavsky, L., Zhang, J., Bolton, E.E., 2023. PubChem 2023 update. Nucleic Acids Res. 51, D1373–D1380. https://doi.org/10.1093/nar/gkac956.

Klein, M., 2019. AppDate 3.05. Estimation of consistent application dates dependent on BBCH crop development stages for FOCUS models. In: Fraunhofer IME. Schmallenberg, Germany.

Lammers, M., 2021. Kooperation Landwirtschaft und Wasserwirtschaft im Einzugsgebiet der Stevertalsperre. In: Ein Bericht Über Die Ergebnisse Der Beratung in 2021. Landwirtschaftskammer Nordrhein-Westfalen, Coesfeld, Germany.

Lammers, M., 2020. Kooperation Landwirtschaft und Wasserwirtschaft im Einzugsgebiet der Stevertalsperre. In: Ein Bericht Über Die Ergebnisse Der Beratung in 2020. Landwirtschaftskammer Nordrhein-Westfalen, Coesfeld, Germany.

Lammers, M., 2019. Kooperation Landwirtschaft Und Wasserwirtschaft Im Einzugsgebiet Der Stevertalsperre: Ein Bericht Über Die Ergebnisse Der Beratung in 2019. Landwirtschaftskammer Nordrhein-Westfalen, Coesfeld, Germany.

Land NRW, 2020. Elektronisches Wasserwirtschaftliches Verbundsystem (ELWAS) für die Wasserwirtschaftsverwaltung in NRW [WWW Document]. URL. https://www.elwasweb.nrw.de/elwas-web/index.

Leistra, M., Van der Linden, A.M.A., Boesten, J.J.T.I., Tiktak, A., Van den Berg, F., 2001. PEARL model for pesticide behaviour and emissions in soil-plant systems: description of the processes in FOCUS PEARL v 1.1, 1. Alterra, Green World Research, Wageningen, p. 115.

McKay, M.D., Beckman, R.J., Conover, W.J., 1979. A comparison of three methods for selecting values of input variables in the analysis of output from a computer code. Technometrics 21, 239. https://doi.org/10.2307/1268522.

Moriasi, D.N., Arnold, J.G., Liew, M.W. Van, Bingner, R.L., v, R.D., Veith, T.L., 2007. Model evaluation guidelines for systematic quantification of accuracy in watershed simulations. Trans. ASABE (Am. Soc. Agric. Biol. Eng.) 50, 885–900. https://doi.org/10.13031/2013.23153.

Mottes, C., Lesueur-Jannoyer, M., Bail, M. Le, Malézieux, E., 2014. Pesticide transfer models in crop and watershed systems: a review. Agron. Sustain. Dev. 34, 229–250. https://doi.org/10.1007/s13593-013-0176-3.

Perine, J., Anderson, J.C., Kruger, G.R., Abi-Akar, F., Overmyer, J., 2021. Effect of nozzle selection on deposition of thiamethoxam in actara® spray drift and implications for off-field risk assessment. Sci. Total Environ. 772, 144808. https://doi.org/10.1016/j.scitotenv.2020.144808.

Pfannerstill, M., Guse, B., Fohrer, N., 2014. A multi-storage groundwater concept for the SWAT model to emphasize nonlinear groundwater dynamics in lowland catchments. Hydrol. Process. 28, 5599–5612. https://doi.org/10.1002/hyp.10062.

Potter, T.L., Truman, C.C., Webster, T.M., Bosch, D.D., Strickland, T.C., 2011. Tillage, cover-crop residue management, and irrigation incorporation impact on fomesafen runoff. J. Agric. Food Chem. 59, 7910–7915. https://doi.org/10.1021/jf201731u.

Rathjens, H., Kiesel, J., Winchell, M., Arnold, J., Sur, R., 2023. Technical note: extending the SWAT model to transport chemicals through tile and groundwater flow. Hydrol. Earth Syst. Sci. 27, 159–167. https://doi.org/10.5194/hess-27-159-2023.

Schönenberger, U.T., Simon, J., Stamm, C., 2022. Are spray drift losses to agricultural roads more important for surface water contamination than direct drift to surface waters? Sci. Total Environ. 809. https://doi.org/10.1016/j.scitotenv.2021.151102.

de Snoo, G.R., De Wit, P.J., 1998. Buffer zones for reducing pesticide drift to ditches and risks to aquatic organisms. Ecotoxicol. Environ. Saf. 41, 112–118. https://doi.org/10.1006/eesa.1998.1678.

Sobol', I.M., 1990. On Sensitivity Estimation for Nonlinear Mathematical Models, Matematicheskoe Modelirovanie. Russian Academy of Sciences, Branch of Mathematical Sciences.

Tetzlaff, B., 2021. Kooperationsprojekt GROWA + NRW 2021 Teil IIb: Ausweisung potenziell dränierter Flächen unter landwirtschaftlicher Nutzung in Nordrhein-

Westfalen. In: Landesamt Für Natur, Umwelt Und Verbraucherschutz Nordrhein-Westfalen (LANUV). Recklinghausen, Germany.

Vallée, R., Dousset, S., Billet, D., Benoit, M., 2014. Sorption of selected pesticides on soils, sediment and straw from a constructed agricultural drainage ditch or pond. Environ. Sci. Pollut. Res. 21, 4895–4905. https://doi.org/10.1007/s11356-013-1840-5.

Wagner, P.D., Bieger, K., Arnold, J.G., Fohrer, N., 2022. Representation of hydrological processes in a rural lowland catchment in Northern Germany using SWAT and SWAT +. Hydrol. Process. 36, 1–14. https://doi.org/10.1002/hyp.14589.

Williams, J.R., Nicks, A.D., Arnold, J.G., 1985. Simulator for water resources in rural basins. J. Hydraul. Eng. 111, 970–986. https://doi.org/10.1061/(ASCE)0733-9429(1985)111:6(970.

Winchell, M.F., Pai, N., Brayden, B.H., Stone, C., Whatling, P., Hanzas, J.P., Stryker, J.J., 2018. Evaluation of watershed-scale simulations of In-Stream pesticide concentrations from off-target spray drift. J. Environ. Qual. 47, 79–87. https://doi.org/10.2134/jeq2017.06.0238.

Zhang, X., Luo, Y., Goh, K.S., 2018. Modeling spray drift and runoff-related inputs of pesticides to receiving water. Environ. Pollut. 234, 48–58. https://doi.org/10.1016/j.envpol.2017.11.032.

Appendix IV:

The droplet and atmospheric dispersion drift (DAD-drift) model – A modular approach for estimating spray drift on the landscape scale

Mike Devin Fuchs[1,2,], Sebastian Gebler[1], Andreas Lorke[2].*

[1]BASF SE, Global Environmental Fate Modelling, Limburgerhof, Germany.

[2]Institute for Environmental Sciences, University of Kaiserslautern-Landau, Landau in der Pfalz, Germany

*Corresponding author.

Tel.: +49 152 21942146

E-mail: mike-devin.fuchs@basf.com (M. D. Fuchs)

Supplementary Material

Table S 1: Parameters of the drop size distribution for different nozzles as reported in the literature, the nozzles used for model evaluation are highlighted in bold, with DV0.1 as the 10% volume diameter, DV0.5 as the volume median diameter, DV0.9 as the 90% volume diameter, V100 as the volume fraction less than 100 µm and V150 as the volume fraction less than 150 µm.

Nozzle Type	DV0.1 [µm]	DV0.5 [µm]	DV0.9 [µm]	V100 [%]	V150 [%]	Pressure [kPa]	Source
XR11003	**85**	**213**	**-**	**-**	**32**	**300**	**(Ferguson et al., 2016)**
XR11003	61	175	387	24.32	-	300	(Gil et al., 2014)
DG11004	**162**	**342**	**545**	**3.3**	**-**	**200**	**(Porskamp et al., 2002)**
DG11004	168	322	507	1.9	-	300	(Van de Zande et al., 2014)
AIXR11002	**178**	**386**	**604**	**2.01**	**-**	**207**	**(Alves et al., 2020)**
AIXR11002	215	502	905	2.78	-	300	(Gil et al., 2014)
AIXR11002	193	392	-	-	5	300	(Ferguson et al., 2016)
AIXR11002	224	416	613	-	-	207	(Ferguson et al., 2020)
TTI11004	**455**	**879**	**1296**	**-**	**-**	**207**	**(Ferguson et al., 2020)**
TTI11004	323	645	1024	-	-	100	(Van de Zande et al., 2012)

Table S 2: Parametrization performance for the vertical and horizontal wind standard deviation.

parameter value [m]	sigma_horizontal		sigma_vertical	
	R^2 [-]	RSR [-]	R^2 [-]	RSR [-]
0.01	0.472	0.721	0.833	0.405
0.013	0.574	0.647	0.844	0.392
0.016	0.625	0.607	0.853	0.380
0.02	0.662	0.577	0.863	0.367
0.025	0.688	0.554	0.873	0.353
0.032	0.709	0.535	0.884	0.337
0.04	0.722	0.523	0.892	0.326
0.05	0.733	0.513	0.898	0.317
0.063	0.743	0.503	0.905	0.307
0.079	0.751	0.495	0.913	0.292
0.1	0.760	0.486	0.919	0.282
0.13	0.771	0.475	0.922	0.278
0.16	0.781	0.464	0.924	0.273
0.2	0.795	0.449	0.929	0.264
0.25	0.813	0.429	0.928	0.266
0.32	0.837	0.401	0.926	0.271
0.4	0.860	0.372	0.919	0.283
0.5	0.882	0.341	0.907	0.302
0.63	0.902	0.310	0.889	0.330
0.79	0.919	0.282	0.863	0.367
1	0.929	0.264	0.834	0.404

parameter value [m]	sigma_horizontal		sigma_vertical	
	R^2 [-]	RSR [-]	R^2 [-]	RSR [-]
1.3	0.926	0.269	0.787	0.458
1.6	0.906	0.304	0.756	0.490
2	0.857	0.375	0.689	0.553
2.5	0.773	0.473	0.610	0.620
3.2	0.639	0.596	0.553	0.663
4	0.487	0.710	0.484	0.712
5	0.310	0.824	0.372	0.786
6.3	0.101	0.941	0.457	0.731
7.9	-0.130	1.054	0.483	0.713
10	-0.396	1.172	0.558	0.659

45 *Table S 3: Analysis of the parameter space around the two optimised values for vertical and horizontal wind standard deviation.*

Change [%]		R^2 [-]	RSR [-]
sigma_vertical	sigma_horizontal		
10	5	0.9310	0.2605
10	10	0.9308	0.2609
5	10	0.9306	0.2613
5	5	0.9304	0.2617
10	0	0.9303	0.2618
0	10	0.9300	0.2624
0	5	0.9297	0.2629
5	0	0.9296	0.2632
-5	10	0.9292	0.2639
10	-5	0.9290	0.2642
0	0	0.9289	0.2644
-5	5	0.9288	0.2645
-10	10	0.9286	0.2649
-10	5	0.9282	0.2657
5	-5	0.9282	0.2656
-5	0	0.9279	0.2662
0	-5	0.9275	0.2670
-10	0	0.9273	0.2674
10	-10	0.9271	0.2677
-5	-5	0.9265	0.2689
5	-10	0.9263	0.2692
-10	-5	0.9258	0.2702
0	-10	0.9255	0.2706
-5	-10	0.9245	0.2726
-10	-10	0.9237	0.2739

Table S 4: Parameter description with units.

Parameter Name	Unit	Description
Application Parameters		
tractor_speed	(m s^{-1})	Driving speed of the tractor
boom_width	(m)	Width of the spray boom
boom_height	(m)	Height of the spray boom above ground
nozzle_angle	(°)	Deviation of nozzle angle from vertically downward spraying
application_pres	(kPa)	Spray pressure used during application
app_rate_mha	(m^3 ha^{-1})	Application rate in meters cubes per hectare
app_rate_kgha	(kg ha^{-1})	Application rate in kilograms per hectare
swath_number	(-)	Number of spray swaths
field_length	(m)	Length of the field (spray swath)
Formulation Parameters		
AI_density	(kg m^{-3})	Density of the active ingredient
AI_molar_mass	(kg mol^{-1})	Molar mass of the active ingredient
AI_vapor_pressure	(Pa)	Vapor pressure of the active ingredient
sol_concentration	(kg m^{-3})	Concentration of the spray solution
Environmental Conditions		
temperature	(°C)	Ambient temperature
humidity	(-)	Relative humidity
wind_speed	(m s^{-1})	Wind speed
wind_height	(m)	Height at which the wind speed was measured
wind_direction	(°)	Wind direction relative to the spray path
ambient_pressure	(kPa)	Ambient pressure
Calibration Parameters		
sigma_horizontal	(m s^{-1})	Standard deviation of the horizontal wind velocity
sigma_vertical	(m s^{-1})	Standard deviation of the vertical wind velocity
roughness_height	(m)	Surface roughness height
canopy_height	(m)	Canopy height
LAI	(m^2 m^{-2})	Leaf area index
deposition_height	(m)	Height at which the deposition is calculated

Table S 5: Parameter changes during sensitivity analysis.

Parameter Name	Type of Change	Value
Application Parameters		
boom_width	percent change	-25%, 0%, +25%
boom_height	percent change	-25%, 0%, +25%
nozzle_angle	absolute value	0°, 22.5°, 45°
application_pres	percent change	-25%, 0%, +25%
app_rate_kgha	percent change	-25%, 0%, +25%

swath_number	absolute value	1, 2, 3
field_length	percent change	-25%, 0%, +25%
Formulation Parameters		
AI_density	percent change	-25%, 0%, +25%
AI_molar_mass	percent change	-25%, 0%, +25%
AI_vapor_pressure	percent change	-25%, 0%, +25%
sol_concentration	percent change	-25%, 0%, +25%
Environmental Conditions		
temperature	percent change	-25%, 0%, +25%
humidity	percent change	-25%, 0%, +25%
wind_speed	percent change	-25%, 0%, +25%
wind_height	percent change	-25%, 0%, +25%
wind_direction	percent change	-25%, 0%, +25%
ambient_pressure	percent change	-25%, 0%, +25%
Calibration Parameters		
sigma_horizontal	percent change	-25%, 0%, +25%
sigma_vertical	percent change	-25%, 0%, +25%
roughness_height	percent change	-25%, 0%, +25%
canopy_height	percent change	-25%, 0%, +25%
LAI	percent change	-25%, 0%, +25%

Table S 6: Drift reduction potential of the DG11004 nozzle and the AIXR11002 nozzle compared to the XR11003 standard nozzle.

Distance [m]	**Predicted drift fraction of XR11003 nozzle [-]**	**Predicted drift fraction of DG11004 nozzle [-]**	**Predicted drift fraction of AIXR11002 nozzle [-]**	**Drift reduction of DG11004 nozzle [%]**	**Drift reduction of AIXR11002 nozzle [%]**
3.8	4.87E-2	1.55E-2	8.92E-3	68.3	81.7
7.6	2.42E-2	6.93E-3	3.89E-3	71.4	84.0
15.2	9.86E-3	2.58E-3	1.39E-3	73.9	85.9
22.9	5.17E-3	1.30E-3	6.75E-4	74.9	86.9
30.5	3.01E-3	7.43E-4	3.74E-4	75.3	87.6
45.7	1.19E-3	2.95E-4	1.44E-4	75.2	87.9
61.0	5.43E-4	1.41E-4	7.28E-5	74.1	86.6
76.2	3.07E-4	8.16E-5	4.80E-5	73.4	84.4
99.1	1.97E-4	4.97E-5	3.44E-5	74.8	82.6
121.9	1.58E-4	3.77E-5	2.81E-5	76.1	82.2
mean				73.7	85.0

55

Table S 7: Parameter sensitivity in RSR, for the seven application scenarios.

parameter	XR 11003	DG 11004	AIXR 11002	TTI 11004 trial 1	TTI 11004 trial 2	TTI 11004 trial 3	TTI 11004 trial 4
Application Parameters							
boom_width	0.061	0.053	0.055	0.060	0.054	0.059	0.053
boom_height	0.165	0.152	0.144	0.127	0.142	0.131	0.151
nozzle_angle	0.042	0.031	0.029	0.038	0.047	0.040	0.048
application_pres	0.011	0.013	0.014	0.015	0.022	0.016	0.022
app_rate_kgha	0.017	0.008	0.007	0.000	0.001	0.000	0.001
swath_number	0.111	0.096	0.101	0.107	0.098	0.107	0.095
field_length	0.064	0.056	0.058	0.059	0.058	0.059	0.056
Formulation Parameters							
AI_density	0.016	0.012	0.015	0.010	0.009	0.010	0.010
AI_molar_mass	0.004	0.003	0.003	0.003	0.002	0.002	0.002
AI_vapor_pressure	0.000	0.000	0.000	0.000	0.000	0.000	0.000
sol_concentration	0.044	0.035	0.037	0.028	0.028	0.029	0.028
Environmental Conditions							
temperature	0.109	0.092	0.090	0.068	0.068	0.069	0.062
humidity	0.131	0.123	0.123	0.039	0.033	0.027	0.026
wind_speed	0.116	0.102	0.100	0.038	0.060	0.037	0.067
wind_height	0.010	0.009	0.009	0.009	0.007	0.009	0.007
wind_direction	0.011	0.016	0.006	0.014	0.026	0.041	0.024
ambient_pressure	0.035	0.022	0.023	0.028	0.034	0.031	0.036
Calibration Parameters							
roughness_height	0.011	0.011	0.011	0.011	0.009	0.010	0.010
sigma_horizontal	0.091	0.078	0.077	0.041	0.043	0.039	0.045
roughness_height	0.011	0.011	0.011	0.011	0.009	0.010	0.010
canopy_height	0.002	0.002	0.002	0.002	0.002	0.002	0.002
LAI	0.000	0.000	0.000	0.000	0.000	0.000	0.000

60

6

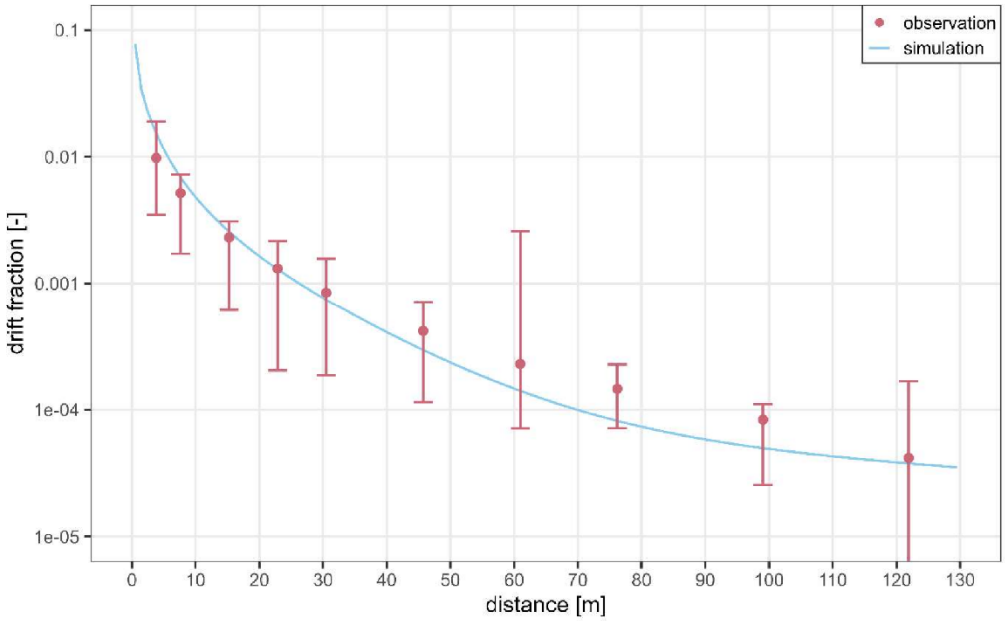


Figure S 1: Model evaluation for the "DG11004" scenario (R^2 = 0.956, RSR = 0.200), with simulated drift fractions in blue, observed drift fractions in red, error bars indicate lowest and highest drift fractions measured, and points indicate mean drift fractions.

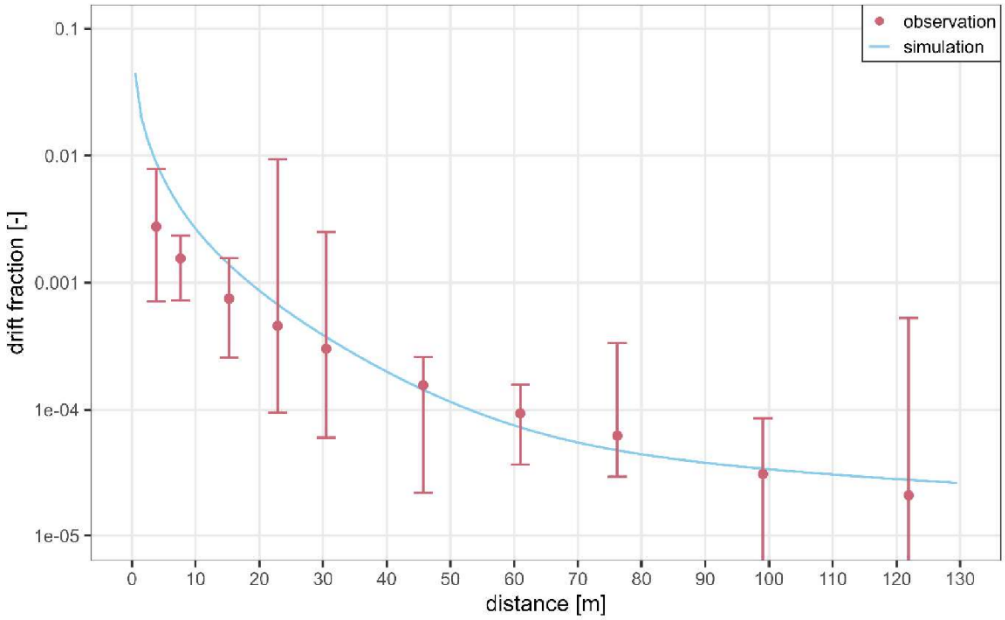


Figure S 2: Model evaluation for the "AIXR11002" scenario (R^2 = 0.874, RSR = 0.336), with simulated drift fractions in blue, observed drift fractions in red, error bars indicate lowest and highest drift fractions measured, and points indicate mean drift fractions.

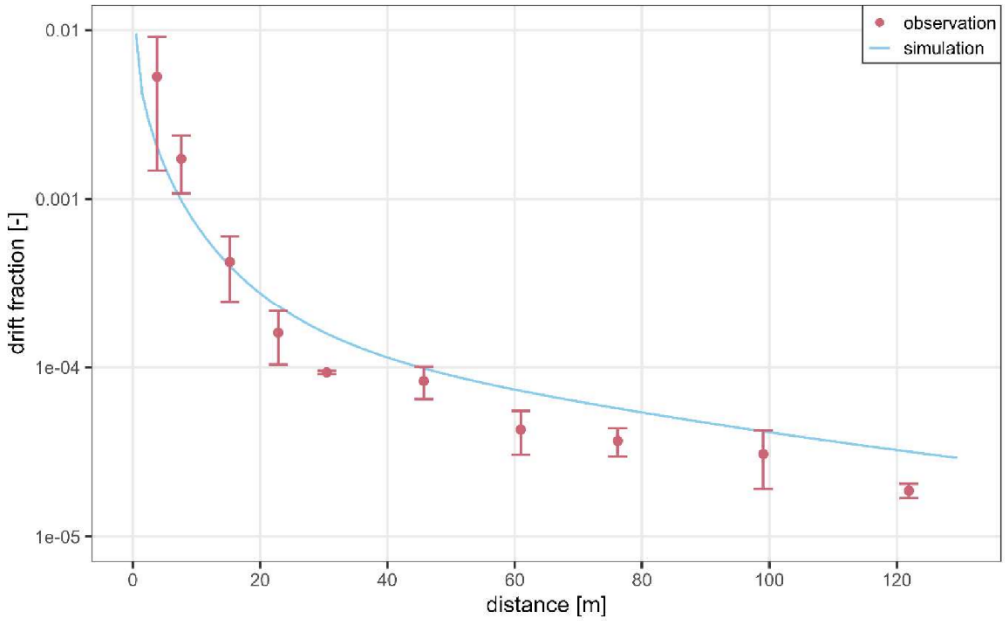


Figure S 3: Model evaluation for the "TTI11004 trial 1" scenario (R^2 = 0.918, RSR = 0.271), with simulated drift fractions in blue, observed drift fractions in red, error bars indicate the standard deviation of measured drift fractions, and points indicate mean drift fractions.

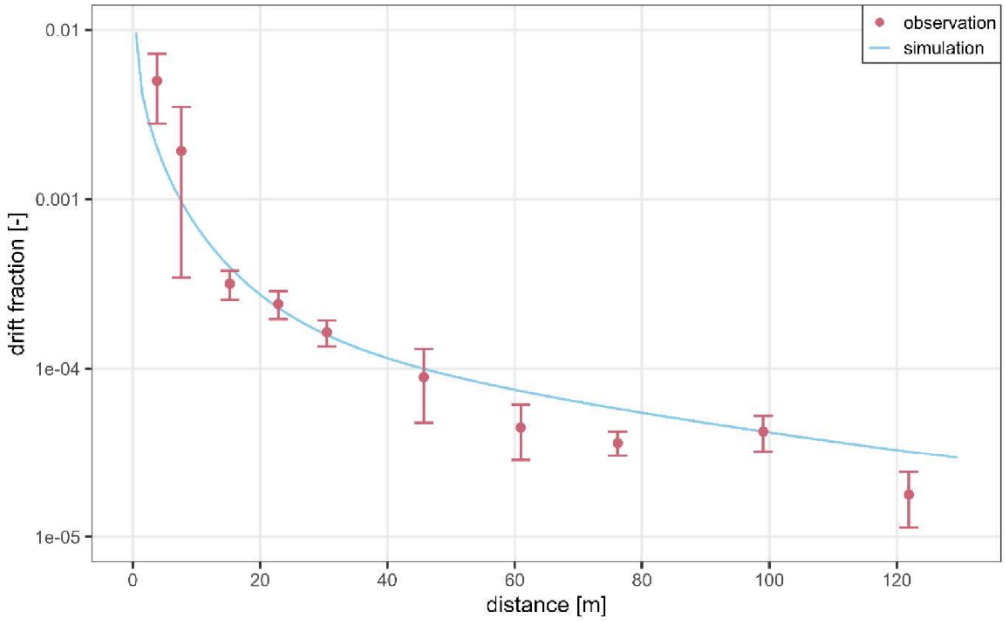


Figure S 4: Model evaluation for the "TTI11004 trial 3" scenario (R^2 = 0.927, RSR = 0.257), with simulated drift fractions in blue, observed drift fractions in red, error bars indicate the standard deviation of measured drift fractions, and points indicate mean drift fractions.

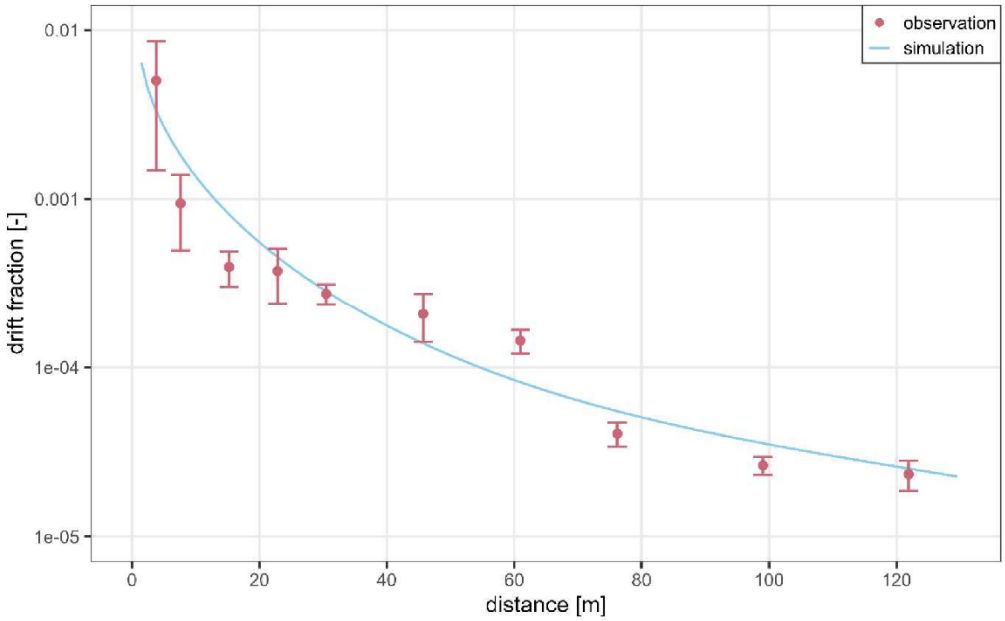


Figure S 5: Model evaluation for the "TTI11004 trial 4" scenario (R^2 = 0.927, RSR = 0.256), with simulated drift fractions in blue, observed drift fractions in red, error bars indicate the standard deviation of measured drift fractions, and points indicate mean drift fractions.

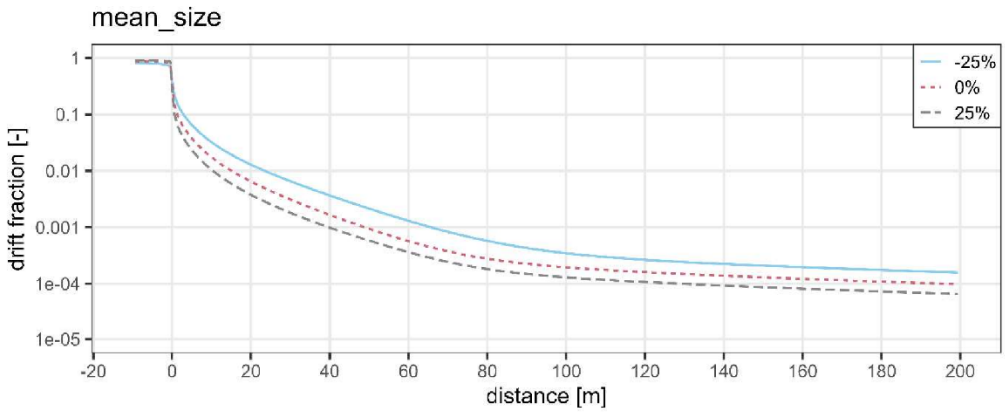
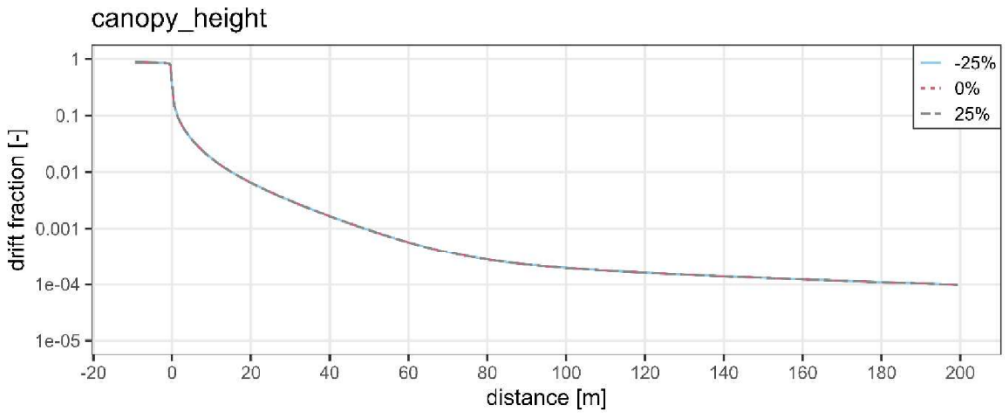


Figure S 6: Drift curves for parameter changes of "mena_size" during sensitivity analysis, using the "XR11003" scenario.



95 *Figure S 7: Drift curves for parameter changes of "boom_height" during sensitivity analysis, using the "XR11003" scenario.*

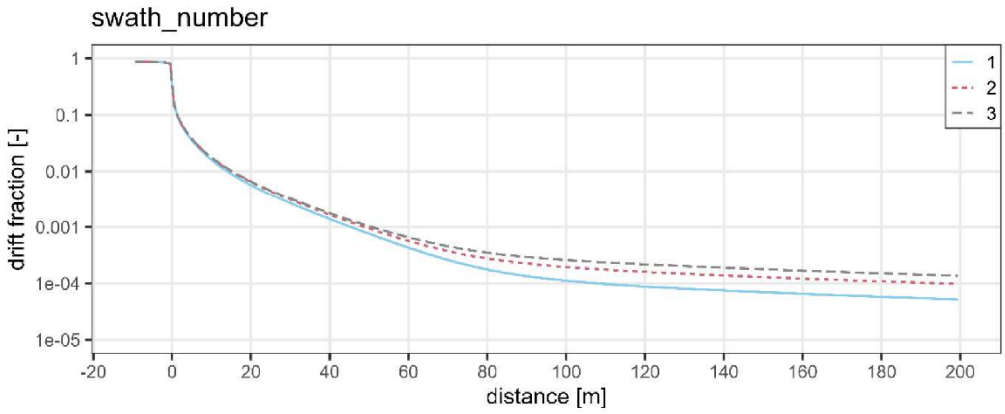


Figure S 8: Drift curves for parameter changes of "swath_number" during sensitivity analysis, using the "XR11003" scenario.

96

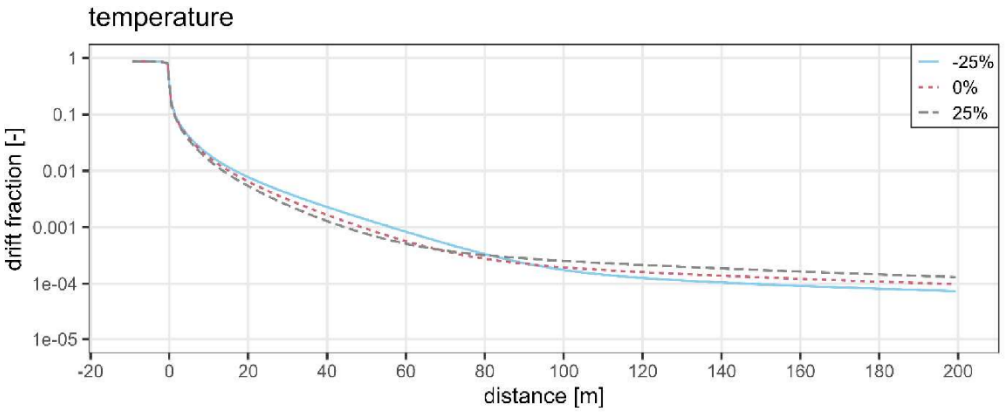


Figure S 9: Drift curves for parameter changes of "temperature" during sensitivity analysis, using the "XR11003" scenario.

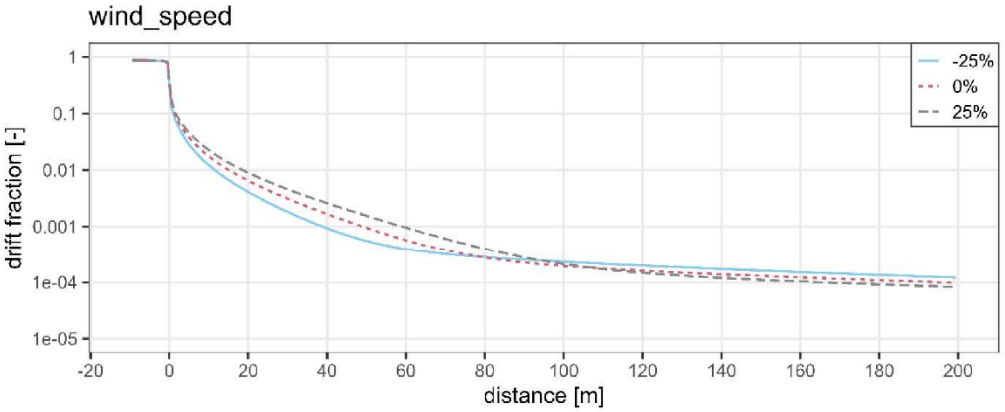


Figure S 10: Drift curves for parameter changes of "wind_speed" during sensitivity analysis, using the "XR11003" scenario.

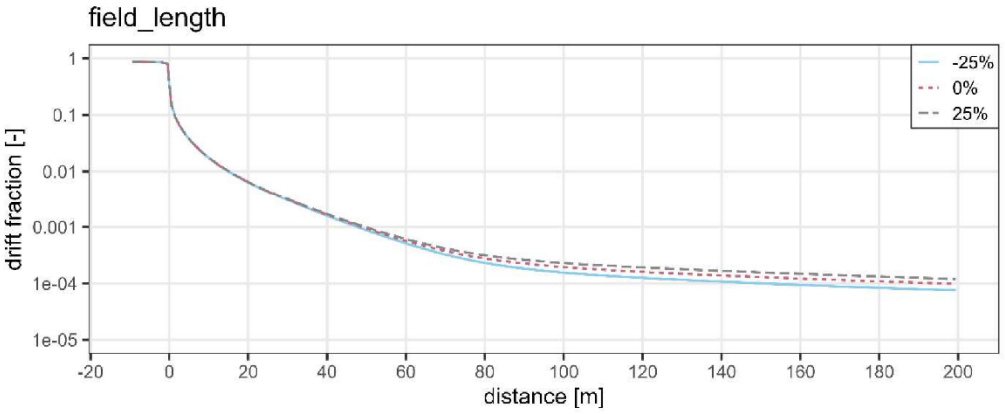


Figure S 11: Drift curves for parameter changes of "field_length" during sensitivity analysis, using the "XR11003" scenario.

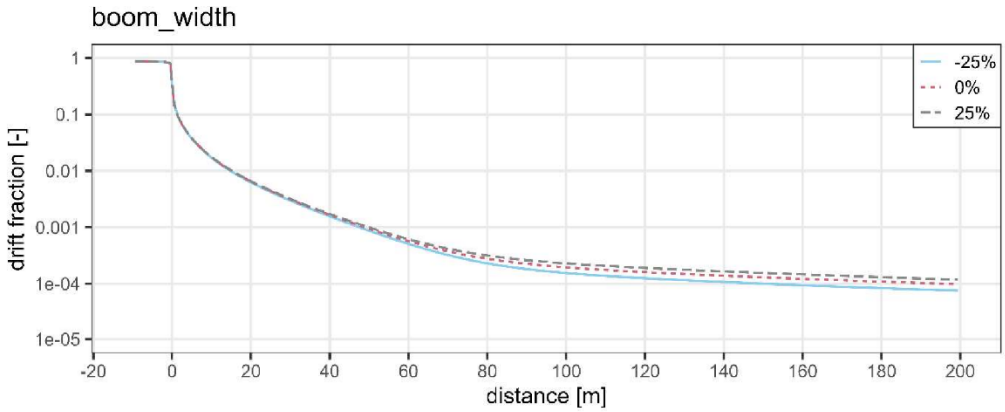


Figure S 12: Drift curves for parameter changes of "boom_width" during sensitivity analysis, using the "XR11003" scenario.

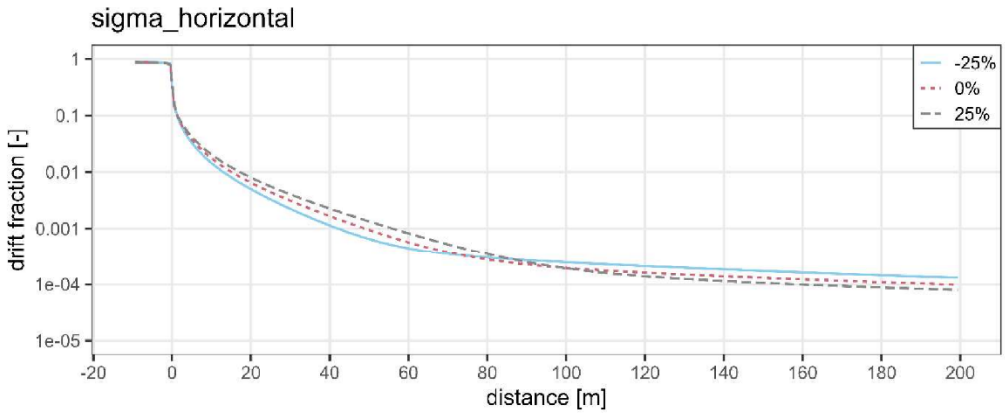


Figure S 13: Drift curves for parameter changes of "sigma_horizontal" during sensitivity analysis, using the "XR11003" scenario.

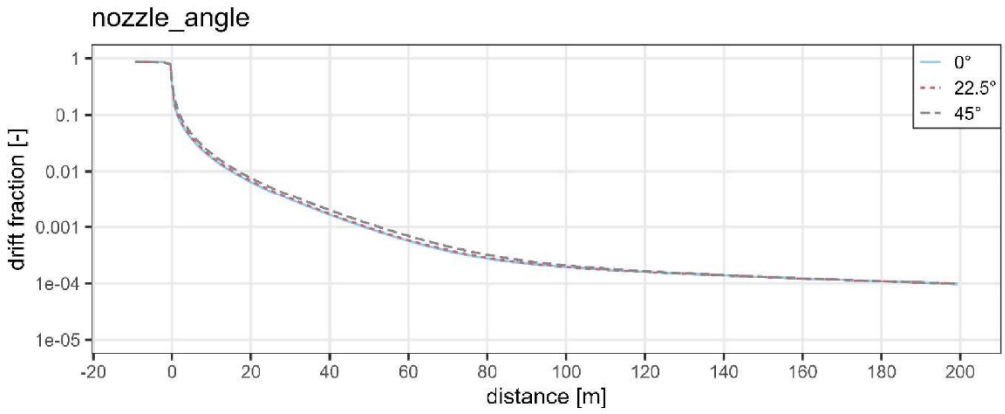


Figure S 14: Drift curves for parameter changes of "nozzle_angle" during sensitivity analysis, using the "XR11003" scenario.

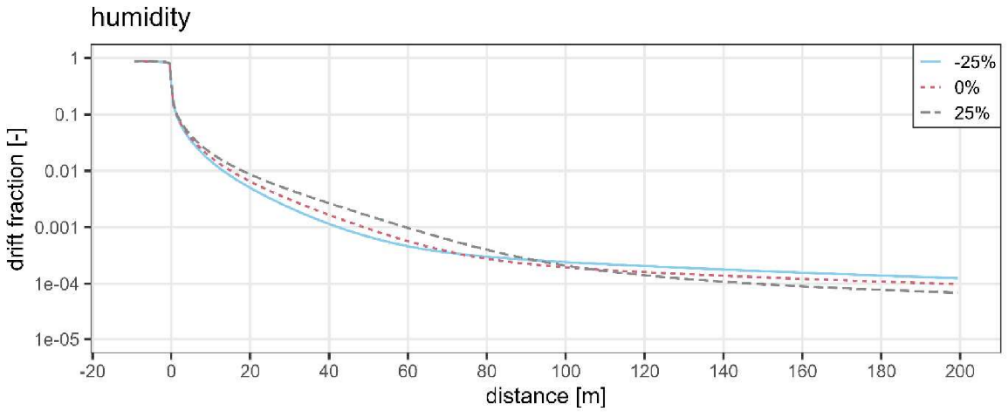


Figure S 15: Drift curves for parameter changes of "humidity" during sensitivity analysis, using the "XR11003" scenario.

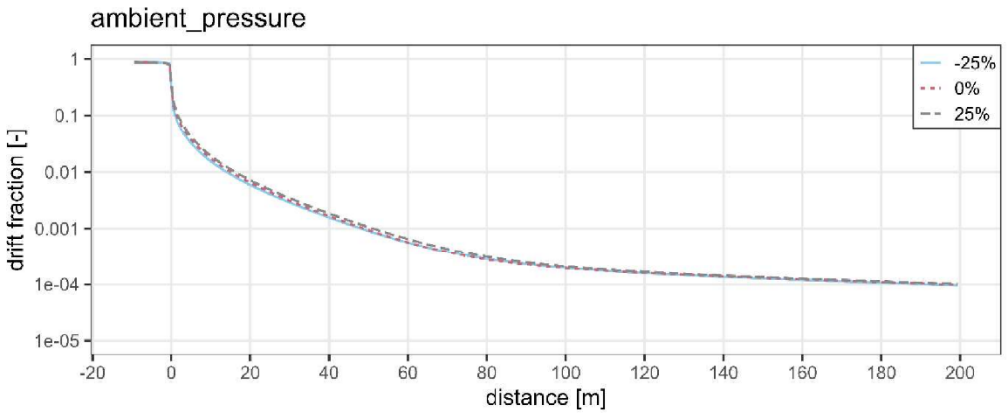


Figure S 16: Drift curves for parameter changes of "ambient_pressure" during sensitivity analysis, using the "XR11003" scenario.

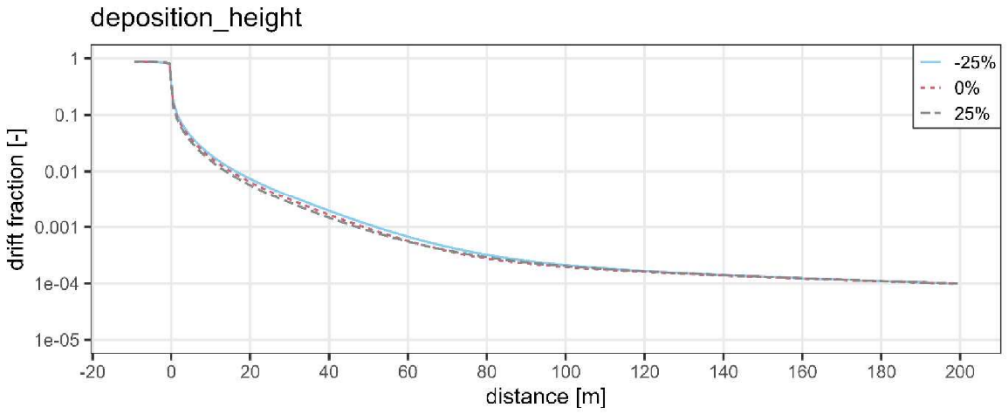


Figure S 17: Drift curves for parameter changes of "deposition_height" during sensitivity analysis, using the "XR11003" scenario.

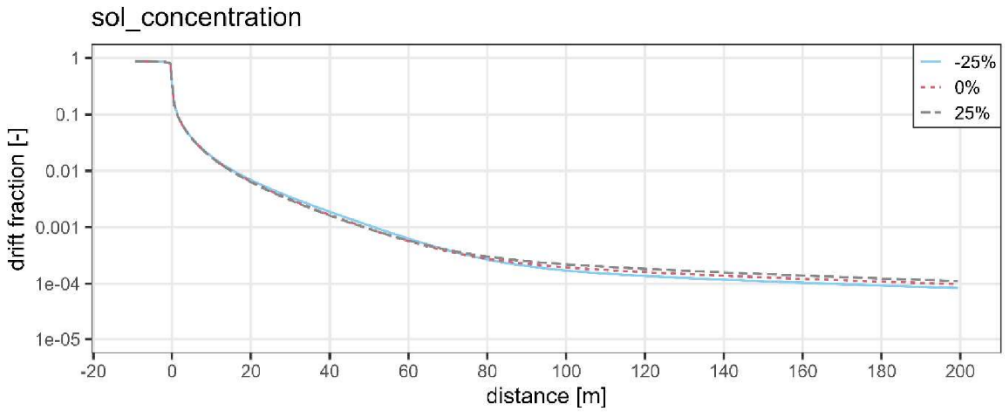
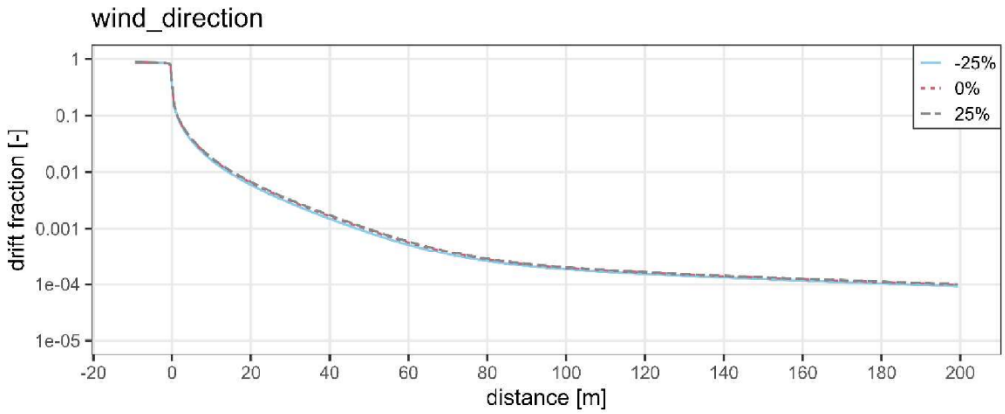
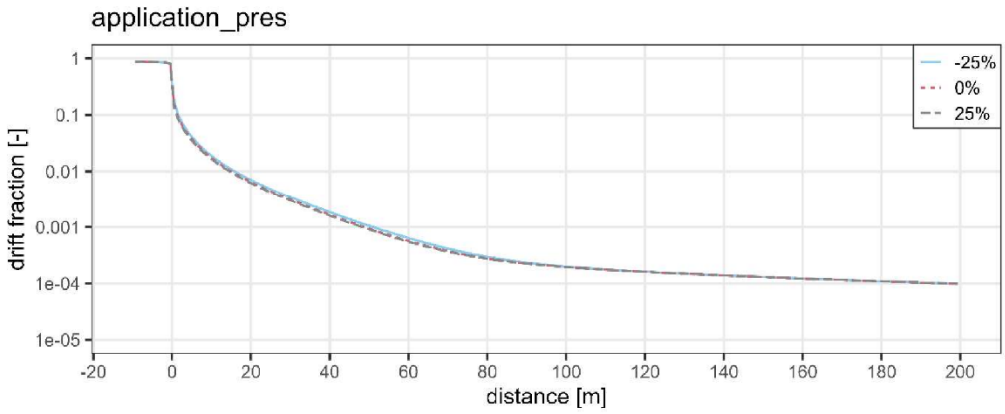


Figure S 18: Drift curves for parameter changes of "sol_concentration" during sensitivity analysis, using the "XR11003" scenario.



130

Figure S 19: Drift curves for parameter changes of "wind_direction" during sensitivity analysis, using the "XR11003" scenario.



135 *Figure S 20: Drift curves for parameter changes of "application_pres" during sensitivity analysis, using the "XR11003" scenario.*

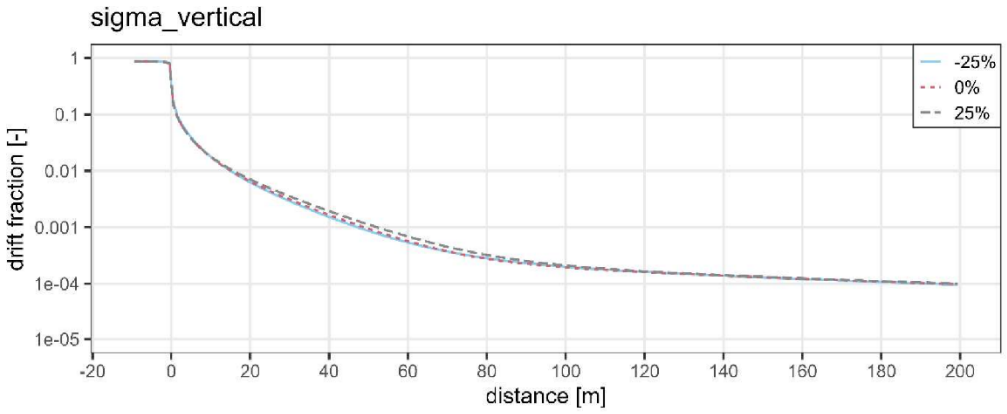
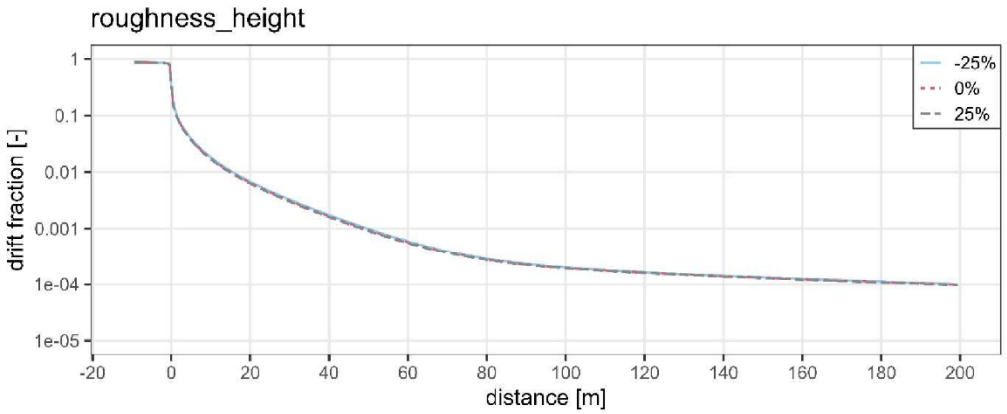


Figure S 21: Drift curves for parameter changes of "sigma_vertical" during sensitivity analysis, using the "XR11003" scenario.



140 *Figure S 22: Drift curves for parameter changes of "roughness_height" during sensitivity analysis, using the "XR11003" scenario.*

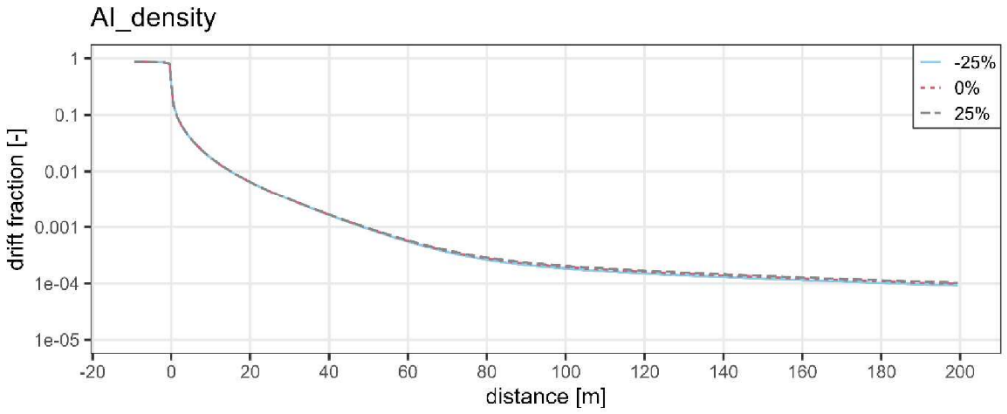
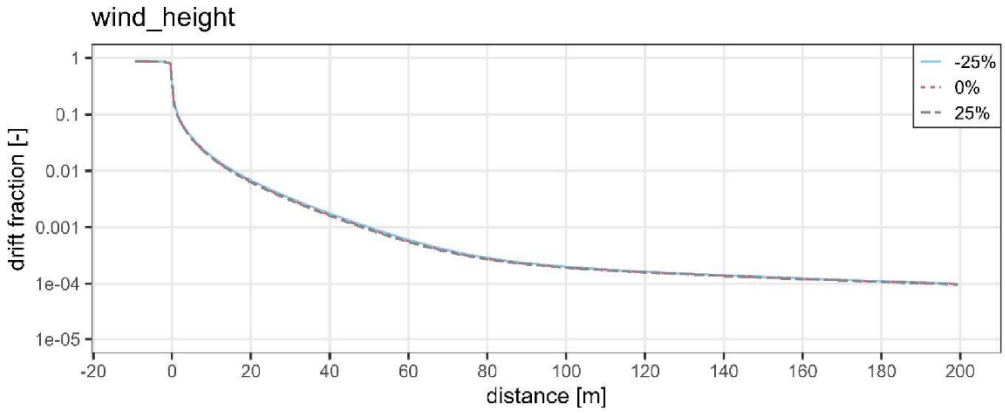
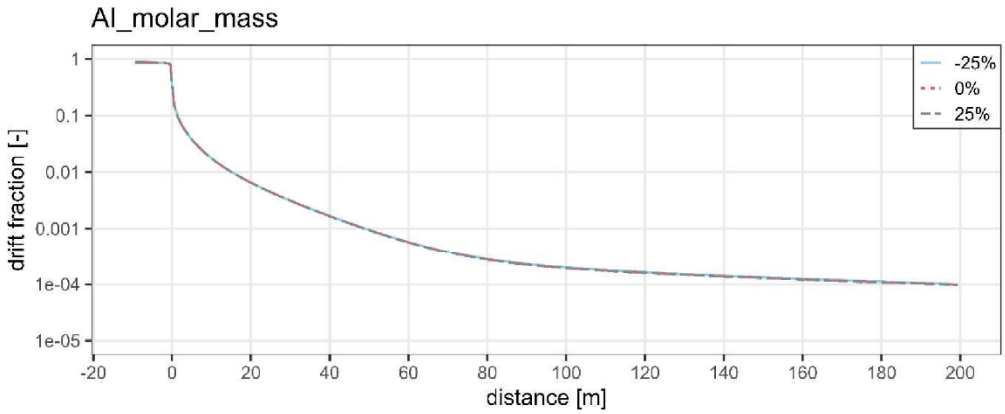


Figure S 23: Drift curves for parameter changes of "AI_density" during sensitivity analysis, using the "XR11003" scenario.



145

Figure S 24: Drift curves for parameter changes of "wind_height" during sensitivity analysis, using the "XR11003" scenario.



150 *Figure S 25: Drift curves for parameter changes of "Al_molar_mass" during sensitivity analysis, using the "XR11003" scenario.*

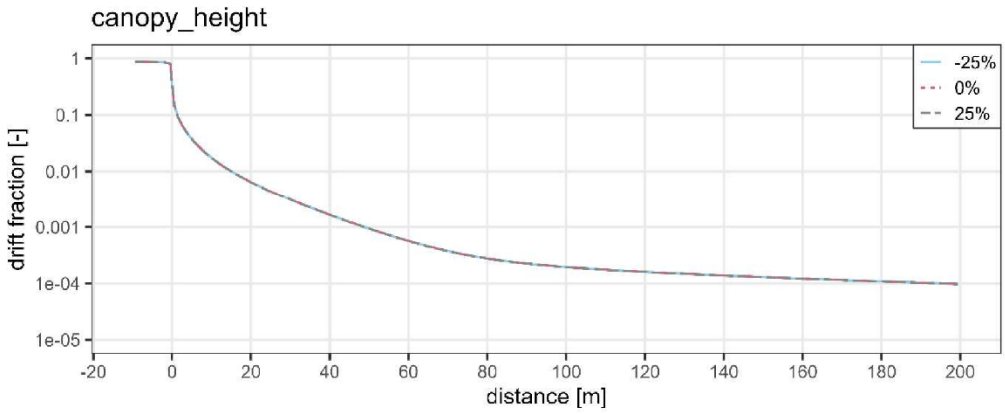
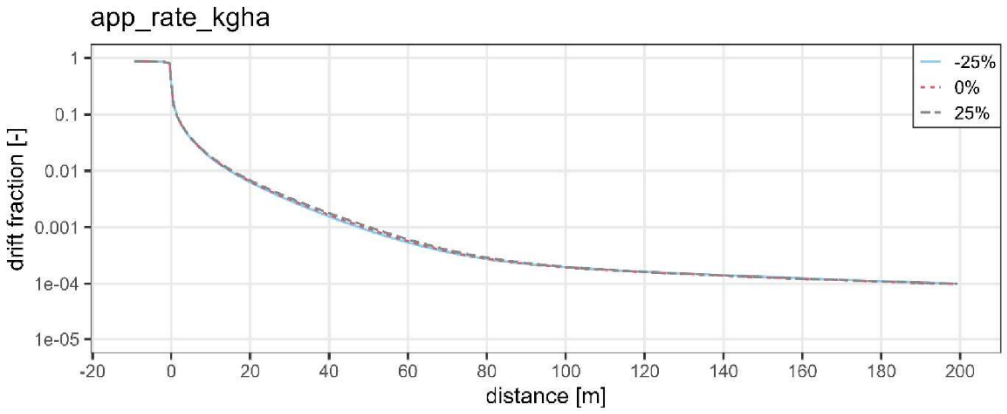


Figure S 26: Drift curves for parameter changes of "canopy_height" during sensitivity analysis, using the "XR11003" scenario.



155 *Figure S 27: Drift curves for parameter changes of "app_rate_kgha" during sensitivity analysis, using the "XR11003" scenario.*

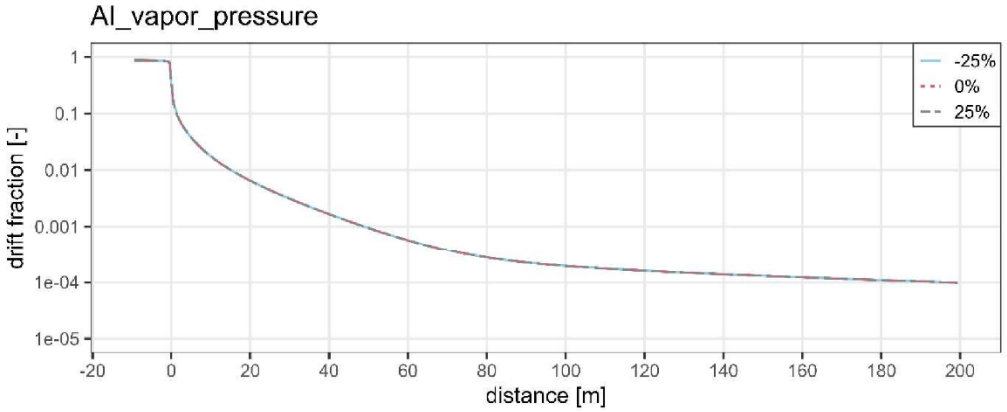
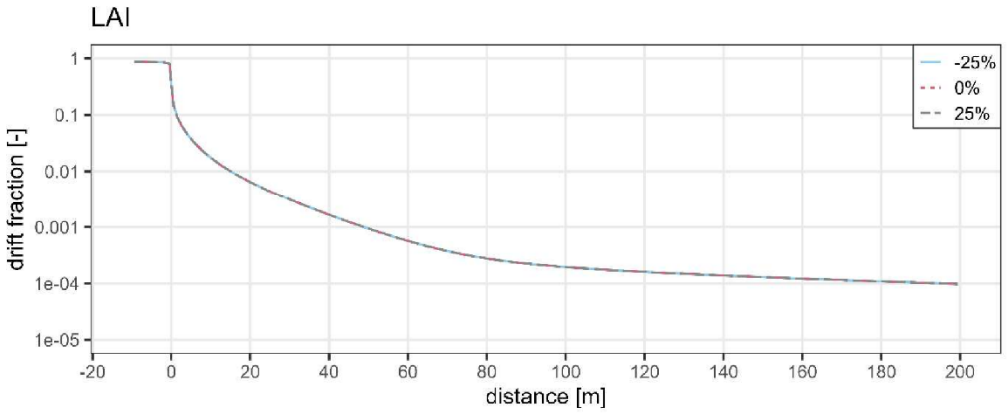


Figure S 28: Drift curves for parameter changes of "AI_vapor_pressure" during sensitivity analysis, using the "XR11003" scenario.



160 *Figure S 29: Drift curves for parameter changes of "LAI" during sensitivity analysis, using the "XR11003" scenario.*

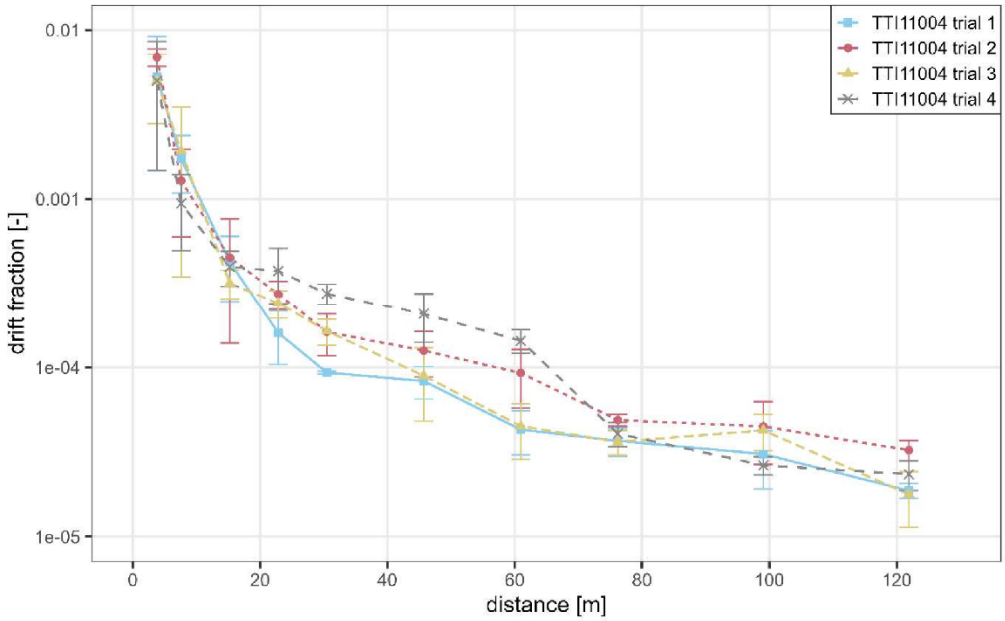
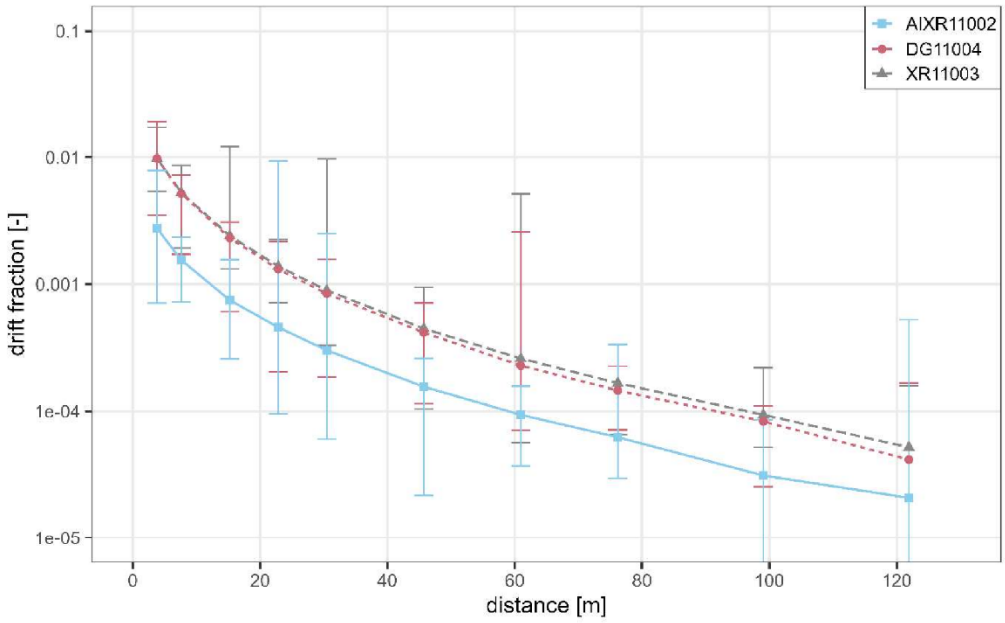


Figure S 30: Deposition curves reported by Study 1, error bars indicate standard deviation of measurements.



165 *Figure S 31: Deposition curves reported by Study 2, error bars indicate lowest and highest drift fraction measured.*

References

Alves, G. S., Vieira, B. C., Butts, T. R., Silva, S. M., Da Cunha, J. P. A. R., & Kruger, G. R. (2020). Drift potential from glyphosate and 2,4-d applications as influenced by nozzle type, adjuvant, and airspeed. *Applied Engineering in Agriculture*, *36*(5), 687–696. https://doi.org/10.13031/AEA.13604

Ferguson, J. C., Chechetto, R. G., O'Donnell, C. C., Dorr, G. J., Moore, J. H., Baker, G. J., Powis, K. J., & Hewitt, A. J. (2016). Determining the drift potential of Venturi nozzles compared with standard nozzles across three insecticide spray solutions in a wind tunnel. *Pest Management Science*, *72*(8), 1460–1466. https://doi.org/10.1002/ps.4214

Ferguson, J. C., Hewitt, A. J., O'Donnell, C. C., & Kruger, G. R. (2020). Comparison of water-sensitive paper, Kromekote and Mylar collectors for droplet deposition with a visible fluorescent dye solution. *Journal of Plant Protection Research*, *60*(1), 98–105. https://doi.org/10.24425/jppr.2020.132210

Gil, E., Balsari, P., Gallart, M., Llorens, J., Marucco, P., Andersen, P. G., Fàbregas, X., & Llop, J. (2014). Determination of drift potential of different flat fan nozzles on a boom sprayer using a test bench. *Crop Protection*, *56*, 58–68. https://doi.org/10.1016/j.cropro.2013.10.018

Porskamp, H. A. J., Van de Zande, J. C., & Porskamp, J. (2002). *Druppelgroottemetingen Teejet, Hardi en Lechler spuitdoppen ter verkrijging van de status driftarm volgens het Lozingenbesluit* (Nota / IMAG : V 2002-60). IMAG. https://edepot.wur.nl/36856

Van de Zande, J. C., Groot, T. T., & Holterman, H. J. (2012). *Drift bij hoge rijsnelheid*. 68.

Van de Zande, J. C., Michielsen, J. G. P., Stallinga, H., & Velde, P. van. (2014). Spray drift of reducing nozzle types spraying a bare soil surface with a boom sprayer. *International Advances in Pesticide Application, Oxford, UK*, *122*, 245–254. http://edepot.wur.nl/352735

Appendix V:

Landscape-level assessment of spray drift – A virtual experiment using the Droplet and Atmospheric Dispersion drift (DAD-drift) model

Supplementary

Table S 1: DAD-drift model inputs, for the original "DG11004" application scenario (Fuchs et al., 2024)*, the drift curve mode, the landscape-level mode, and the meta-modelling approach. With -99 indicating the default no data value of DAD-drift and bolt entries indicating changes compared to the original DG11004 application scenario.*

Parameter Name	Unit	DG11004 Scenario	Drift Curve Mode Adaption	Landscape-Level Mode Adaption	Meta-Modeling Adaption
Application Parameters					
tractor_speed	(m s^{-1})	3.1	3.1	3.1	3.1
boom_width	(m)	30.5	30.5	30.5	30.5
boom_height	(m)	0.600	0.600	0.600	0.600
nozzle_angle	(°)	0	0	0	0
application_pres	(kPa)	165.5	**per nozzle**	**per nozzle**	**per nozzle**
app_rate_mha	(m^3 ha^{-1})	0.0935	0.0935	0.0935	0.0935
app_rate_kgha	(kg ha^{-1})	0.096	0.096	0.096	0.096
swath_number	(-)	2	2	**-99**	**-99**
field_length	(m)	183	183	**-99**	**-99**
Formulation Parameters					
AI_density	(kg m^{-3})	1570	1570	1570	1570
AI_molar_mass	(kg mol^{-1})	0.292	0.292	0.292	0.292
AI_vapor_pressure	(Pa)	6.6E-9	6.6E-9	6.6E-9	6.6E-9
sol_concentration	(kg m^{-3})	1.03	1.03	1.03	1.03
Environmental Conditions					
temperature	(°C)	23.6	23.6	23.6	**(5, 15, 25, 35)**
humidity	(-)	0.62	0.62	0.62	**(0.35, 0.60, 0.85)**
wind_speed	(m s^{-1})	4.3	4.3	4.3	**(0.5, 2.5, 4.5, 6.5)**
wind_height	(m)	2	2	2	2
wind_direction	(°)	65.3	**90.0**	**per scenario**	**(0, 45, 90, 135, 180, 225, 270, 315)**
ambient_pressure	(kPa)	100.0	100.0	100.0	100.0
Calibration Parameters					
sigma_horizontal	(m s^{-1})	1.05	1.05	1.05	1.05
sigma_vertical	(m s^{-1})	0.22	0.22	0.22	0.22
roughness_height	(m)	0.05	0.05	0.05	0.05
canopy_height	(m)	0.025	0.025	0.025	0.025
LAI	(m^2 m^{-2})	0.5	0.5	0.5	0.5
deposition_height	(m)	0.145	**0.0**	**0.0**	**0.0**

Table S 2: Spray drift deposition (mg) and (µg/m²) onto surface waterbodies for the four prediction methods, the 13 scenarios, and the four spray nozzle types.

scenario	method	spray drift deposition (mg)				spray drift deposition (µg/m²)			
		XR	DG	AIXR	TTI	XR	DG	AIXR	TTI
SR-1	A	28.634	6.832	4.301	0.962	2.291	0.547	0.344	0.077
SR-2	A	80.134	19.299	11.901	2.405	6.207	1.495	0.922	0.186
SR-3	A	62.078	14.333	8.816	1.804	4.037	0.932	0.573	0.117
SR-4	A	330.946	109.879	69.128	12.328	25.271	8.390	5.279	0.941
SR-5	A	128.950	34.708	21.428	4.099	10.821	2.912	1.798	0.344
SR-6	A	11.678	2.913	1.881	0.439	0.866	0.216	0.139	0.033
SR-7	A	8.029	1.804	1.112	0.239	0.617	0.139	0.085	0.018
SR-8	A	116.179	32.807	20.258	3.771	44.445	12.551	7.750	1.443
SR-9	A	18.993	4.203	2.560	0.520	6.962	1.541	0.938	0.190
SR-10	A	77.374	20.017	12.287	2.339	18.766	4.855	2.980	0.567
SR-11	A	11.793	2.903	1.860	0.429	2.128	0.524	0.336	0.077
SR-12	A	14.306	3.538	2.273	0.526	2.448	0.605	0.389	0.090
SR-13	A	109.455	26.426	16.227	3.214	24.253	5.856	3.596	0.712
SR-1	B	7.969	1.742	1.052	0.219	4.601	1.005	0.607	0.126
SR-2	B	26.031	6.290	3.841	0.746	15.029	3.632	2.217	0.431
SR-3	B	9.398	2.213	1.353	0.268	5.466	1.287	0.787	0.156
SR-4	B	29.601	11.947	8.440	3.451	23.211	9.368	6.618	2.706
SR-5	B	21.138	5.384	3.300	0.630	16.184	4.122	2.526	0.483
SR-6	B	0.989	0.249	0.161	0.037	0.874	0.220	0.142	0.033
SR-7	B	3.347	0.721	0.436	0.089	6.009	1.294	0.782	0.161
SR-8	B	13.308	3.532	2.170	0.408	25.065	6.653	4.088	0.768
SR-9	B	7.985	1.731	1.043	0.205	23.682	5.135	3.092	0.608
SR-10	B	13.827	3.502	2.141	0.407	41.329	10.468	6.400	1.215
SR-11	B	1.088	0.270	0.172	0.039	1.121	0.278	0.177	0.040
SR-12	B	0.968	0.238	0.152	0.035	0.898	0.221	0.141	0.032
SR-13	B	14.905	3.412	2.075	0.410	12.401	2.839	1.727	0.341
SR-1	C	10.935	2.344	1.410	0.290	5.579	1.196	0.720	0.148
SR-2	C	872.105	243.366	149.725	27.705	314.628	87.799	54.016	9.995
SR-3	C	627.335	165.950	101.752	19.139	228.656	60.487	37.087	6.976
SR-4	C	12733.977	13469.748	13340.391	13134.017	4587.881	4852.969	4806.363	4732.010
SR-5	C	1130.980	348.815	216.180	38.793	514.897	158.804	98.420	17.661
SR-6	C	2.090	0.533	0.344	0.080	1.108	0.282	0.182	0.042
SR-7	C	20.686	4.317	2.587	0.509	24.923	5.202	3.117	0.614
SR-8	C	387.910	129.563	80.862	14.164	693.641	231.678	144.593	25.327
SR-9	C	46.903	10.887	6.621	1.283	82.714	19.200	11.677	2.263
SR-10	C	338.524	103.416	64.052	11.528	492.227	150.371	93.134	16.762
SR-11	C	4.468	0.988	0.598	0.125	4.139	0.915	0.554	0.116
SR-12	C	6.451	1.417	0.857	0.179	4.384	0.963	0.582	0.121

scenario	method	spray drift deposition (mg)				spray drift deposition (µg/m²)			
		XR	DG	AIXR	TTI	XR	DG	AIXR	TTI
SR-13	C	156.331	39.386	24.086	4.588	162.583	40.961	25.050	4.772
SR-1	D	62.921	14.048	8.541	1.716	6.584	1.470	0.894	0.180
SR-2	D	56.760	12.668	7.706	1.554	5.947	1.327	0.807	0.163
SR-3	D	9.037	2.277	1.460	0.337	0.997	0.251	0.161	0.037
SR-4	D	19.358	4.454	2.765	0.601	1.958	0.451	0.280	0.061
SR-5	D	11.230	2.707	1.706	0.381	1.552	0.374	0.236	0.053
SR-6	D	7.267	1.820	1.170	0.271	0.841	0.211	0.135	0.031
SR-7	D	21.643	4.882	3.000	0.631	2.716	0.613	0.377	0.079
SR-8	D	20.711	4.625	2.807	0.559	9.086	2.029	1.232	0.245
SR-9	D	53.120	17.557	11.924	4.273	18.393	6.079	4.129	1.480
SR-10	D	178.843	75.370	53.627	22.445	66.109	27.860	19.823	8.297
SR-11	D	3.945	0.994	0.637	0.147	1.002	0.253	0.162	0.037
SR-12	D	7.593	1.783	1.115	0.246	1.679	0.394	0.246	0.054
SR-13	D	129.990	50.496	35.423	14.177	32.450	12.605	8.843	3.539

Table S 3: All possible model configurations for in-field deposition, based on the predictor variables temperature, humidity, wind speed, DV0.1, DV0.5, V50, V100, V150, and V200 without colinear combinations of the drop size spectrum parameters DV0.1, DV0.5, V50, V100, V150, and V200. Model configurations are ranked by the AIC from most parsimonious to least parsimonious, with R^2 indicating model performance. Each row represents one model configuration, with a value of 1 or 0 indicating that the predictor variable was used or not used, respectively.

temperature	humidity	wind speed	DV0.1	DV0.5	V50	V100	V150	V200	R^2	AIC
1	1	1	0	0	0	0	0	1	0.964	-50695
1	1	1	0	0	0	0	1	0	0.962	-50261
1	0	1	0	0	0	0	0	1	0.958	-49487
1	1	0	0	0	0	0	0	1	0.957	-49188
0	1	1	0	0	0	0	0	1	0.957	-49175
1	0	1	0	0	0	0	1	0	0.956	-49115
1	1	0	0	0	0	0	1	0	0.955	-48830
0	1	1	0	0	0	0	1	0	0.955	-48817
1	0	0	0	0	0	0	0	1	0.951	-48182
0	0	1	0	0	0	0	0	1	0.951	-48171
1	1	1	0	0	0	1	0	0	0.950	-48056
0	1	0	0	0	0	0	0	1	0.949	-47919
1	0	0	0	0	0	0	1	0	0.949	-47867
0	0	1	0	0	0	0	1	0	0.949	-47856
0	1	0	0	0	0	0	1	0	0.947	-47614
1	1	1	0	0	1	0	0	0	0.947	-47599
1	0	1	0	0	0	1	0	0	0.944	-47180
0	0	0	0	0	0	0	0	1	0.943	-47058
1	1	0	0	0	0	1	0	0	0.942	-46958
0	1	1	0	0	0	1	0	0	0.942	-46948

temperature	humidity	wind speed	DV0.1	DV0.5	V50	V100	V150	V200	R^2	AIC
0	0	0	0	0	0	0	1	0	0.941	-46785
1	0	1	0	0	1	0	0	0	0.941	-46772
1	1	0	0	0	1	0	0	0	0.939	-46561
0	1	1	0	0	1	0	0	0	0.939	-46551
1	0	0	0	0	0	1	0	0	0.936	-46194
0	0	1	0	0	0	1	0	0	0.936	-46185
0	1	0	0	0	0	1	0	0	0.934	-45989
1	0	0	0	0	1	0	0	0	0.933	-45833
0	0	1	0	0	1	0	0	0	0.933	-45825
0	1	0	0	0	1	0	0	0	0.931	-45638
0	0	0	0	0	0	1	0	0	0.928	-45312
0	0	0	0	0	1	0	0	0	0.925	-44990
1	1	1	0	1	0	0	0	0	0.598	-32074
1	1	1	1	0	0	0	0	0	0.598	-32065
1	0	1	0	1	0	0	0	0	0.592	-31961
1	0	1	1	0	0	0	0	0	0.592	-31952
1	1	0	0	1	0	0	0	0	0.591	-31930
0	1	1	0	1	0	0	0	0	0.590	-31928
1	1	0	1	0	0	0	0	0	0.590	-31921
0	1	1	1	0	0	0	0	0	0.590	-31920
1	0	0	0	1	0	0	0	0	0.585	-31819
0	0	1	0	1	0	0	0	0	0.584	-31818
1	0	0	1	0	0	0	0	0	0.584	-31810
0	0	1	1	0	0	0	0	0	0.584	-31809
0	1	0	0	1	0	0	0	0	0.583	-31787
0	1	0	1	0	0	0	0	0	0.582	-31778
0	0	0	0	1	0	0	0	0	0.577	-31678
0	0	0	1	0	0	0	0	0	0.576	-31670
1	1	1	0	0	0	0	0	0	0.022	-25239
1	0	1	0	0	0	0	0	0	0.016	-25194
1	1	0	0	0	0	0	0	0	0.014	-25181
0	1	1	0	0	0	0	0	0	0.014	-25180
1	0	0	0	0	0	0	0	0	0.008	-25136
0	0	1	0	0	0	0	0	0	0.008	-25135
0	1	0	0	0	0	0	0	0	0.006	-25122
0	0	0	0	0	0	0	0	0	0.000	-25078

20

Table S 4: All possible model configurations for the non-target areas, based on the predictor variables temperature, humidity, wind speed, DV0.1, DV0.5, V50, V100, V150, V200, minimal distance, centroid distance, and relative bearing without colinear combinations of the drop size spectrum parameters DV0.1, DV0.5, V50, V100, V150, and V200 or colinear combinations of minimal distance and centroid distance. Model configurations are ranked by the AIC from most parsimonious to least parsimonious, with R^2 indicating model performance. Each row represents one model configuration, with a value of 1 or 0 indicating that the predictor variable was used or not used, respectively.

temperature	humidity	wind speed	DV0.1	DV0.5	V50	V100	V150	V200	minimal dist.	centroid dist.	relative bearing	R^2	AIC
1	1	1	1	0	0	0	0	0	0	1	1	0.832	1166456
1	1	1	0	1	0	0	0	0	0	1	1	0.831	1167790
1	1	1	1	0	0	0	0	0	0	1	0	0.829	1174107
1	1	1	0	1	0	0	0	0	0	1	0	0.829	1175421
1	1	0	1	0	0	0	0	0	0	1	1	0.823	1190596
1	1	0	0	1	0	0	0	0	0	1	1	0.823	1191867
1	1	0	1	0	0	0	0	0	0	1	0	0.821	1197885
1	1	1	1	0	0	0	0	0	1	0	1	0.820	1198480
1	1	0	0	1	0	0	0	0	0	1	0	0.820	1199137
1	1	1	0	1	0	0	0	0	1	0	1	0.820	1199730
1	1	1	1	0	0	0	0	0	1	0	0	0.818	1205655
1	1	1	0	1	0	0	0	0	1	0	0	0.817	1206887
1	1	0	1	0	0	0	0	0	1	0	1	0.812	1221141
1	0	1	1	0	0	0	0	0	0	1	1	0.812	1222049
1	1	0	0	1	0	0	0	0	1	0	1	0.812	1222335
1	0	1	0	1	0	0	0	0	0	1	1	0.811	1223241
1	1	0	1	0	0	0	0	0	1	0	0	0.809	1227996
1	0	1	1	0	0	0	0	0	0	1	0	0.809	1228892
1	1	0	0	1	0	0	0	0	1	0	0	0.809	1229174
1	0	1	0	1	0	0	0	0	0	1	0	0.809	1230068
1	0	0	1	0	0	0	0	0	0	1	1	0.803	1243678
1	0	0	0	1	0	0	0	0	0	1	1	0.803	1244819
0	1	1	1	0	0	0	0	0	0	1	1	0.802	1246193
0	1	1	0	1	0	0	0	0	0	1	1	0.802	1247329
1	0	0	1	0	0	0	0	0	0	1	0	0.801	1250230
1	0	1	1	0	0	0	0	0	1	0	1	0.800	1250765
1	0	0	0	1	0	0	0	0	0	1	0	0.800	1251356
1	0	1	0	1	0	0	0	0	1	0	1	0.800	1251890
0	1	1	1	0	0	0	0	0	0	1	0	0.800	1252712
0	1	1	0	1	0	0	0	0	0	1	0	0.799	1253833
1	0	1	1	0	0	0	0	0	1	0	0	0.798	1257225
1	0	1	0	1	0	0	0	0	1	0	0	0.797	1258335
0	1	0	1	0	0	0	0	0	0	1	1	0.794	1266813
0	1	0	0	1	0	0	0	0	0	1	1	0.793	1267902
1	0	0	1	0	0	0	0	0	1	0	1	0.792	1271199
1	0	0	0	1	0	0	0	0	1	0	1	0.792	1272278
0	1	0	1	0	0	0	0	0	0	1	0	0.791	1273067
0	1	1	1	0	0	0	0	0	1	0	1	0.791	1273578
0	1	0	0	1	0	0	0	0	0	1	0	0.791	1274143

temperature	humidity	wind speed	DV0.1	DV0.5	V50	V100	V150	V200	minimal dist.	centroid dist.	relative bearing	R^2	AIC
0	1	1	0	1	0	0	0	0	1	0	1	0.791	1274653
1	0	0	1	0	0	0	0	0	1	0	0	0.789	1277398
1	0	0	0	1	0	0	0	0	1	0	0	0.789	1278464
0	1	1	1	0	0	0	0	0	1	0	0	0.788	1279748
0	1	1	0	1	0	0	0	0	1	0	0	0.788	1280810
1	1	1	0	0	0	0	0	1	0	1	1	0.787	1283565
1	1	1	0	0	0	0	0	1	0	1	0	0.784	1289612
0	1	0	1	0	0	0	0	0	1	0	1	0.783	1293109
0	0	1	1	0	0	0	0	0	0	1	1	0.782	1293894
0	1	0	0	1	0	0	0	0	1	0	1	0.782	1294141
0	0	1	0	1	0	0	0	0	0	1	1	0.782	1294925
0	1	0	1	0	0	0	0	0	1	0	0	0.780	1299041
0	0	1	1	0	0	0	0	0	0	1	0	0.780	1299817
0	1	0	0	1	0	0	0	0	1	0	0	0.780	1300062
0	0	1	0	1	0	0	0	0	0	1	0	0.779	1300836
1	1	0	0	0	0	0	0	1	0	1	1	0.778	1302712
1	1	0	0	0	0	0	0	1	0	1	0	0.776	1308531
1	1	1	0	0	0	0	0	1	1	0	1	0.776	1309007
0	0	0	1	0	0	0	0	0	0	1	1	0.774	1312653
0	0	0	0	1	0	0	0	0	0	1	1	0.773	1313646
1	1	1	0	0	0	0	0	1	1	0	0	0.773	1314753
0	0	0	1	0	0	0	0	0	0	1	0	0.771	1318357
0	0	1	1	0	0	0	0	0	1	0	1	0.771	1318824
0	0	0	0	1	0	0	0	0	0	1	0	0.771	1319338
0	0	1	0	1	0	0	0	0	1	0	1	0.771	1319804
0	0	1	1	0	0	0	0	0	1	0	0	0.768	1324457
0	0	1	0	1	0	0	0	0	1	0	0	0.768	1325427
1	1	0	0	0	0	0	0	1	1	0	1	0.767	1327212
1	0	1	0	0	0	0	0	1	0	1	1	0.767	1327945
1	1	0	0	0	0	0	0	1	1	0	0	0.764	1332751
1	0	1	0	0	0	0	0	1	0	1	0	0.764	1333477
0	0	0	1	0	0	0	0	0	1	0	1	0.763	1336677
0	0	0	0	1	0	0	0	0	1	0	1	0.762	1337623
0	0	0	1	0	0	0	0	0	1	0	0	0.760	1342112
0	0	0	0	1	0	0	0	0	1	0	0	0.760	1343047
1	0	0	0	0	0	0	0	1	0	1	1	0.758	1345478
0	1	1	0	0	0	0	0	1	0	1	1	0.757	1347527
1	0	0	0	0	0	0	0	1	0	1	0	0.756	1350817
1	0	1	0	0	0	0	0	1	1	0	1	0.755	1351255
0	1	1	0	0	0	0	0	1	0	1	0	0.755	1352844
1	0	1	0	0	0	0	0	1	1	0	0	0.753	1356533
0	1	0	0	0	0	0	0	1	0	1	1	0.749	1364390
1	0	0	0	0	0	0	0	1	1	0	1	0.747	1367994
0	1	0	0	0	0	0	0	1	0	1	0	0.746	1369530
0	1	1	0	0	0	0	0	1	1	0	1	0.746	1369952

temperature	humidity	wind speed	DV0.1	DV0.5	V50	V100	V150	V200	minimal dist.	centroid dist.	relative bearing	R^2	AIC
1	0	0	0	0	0	0	0	1	1	0	0	0.744	1373097
1	1	1	0	0	0	0	1	0	0	1	1	0.744	1374351
0	1	1	0	0	0	0	0	1	1	0	0	0.743	1375035
1	1	1	0	0	0	0	1	0	0	1	0	0.741	1379389
0	1	0	0	0	0	0	0	1	1	0	1	0.738	1386079
0	0	1	0	0	0	0	0	1	0	1	1	0.737	1386731
1	1	0	0	0	0	0	1	0	0	1	1	0.735	1390338
0	1	0	0	0	0	0	0	1	1	0	0	0.735	1391000
0	0	1	0	0	0	0	0	1	0	1	0	0.735	1391645
1	1	0	0	0	0	0	1	0	0	1	0	0.733	1395217
1	1	1	0	0	0	0	1	0	1	0	1	0.733	1395617
1	1	1	0	0	0	0	1	0	1	0	0	0.730	1400444
0	0	0	0	0	0	0	0	1	0	1	1	0.729	1402329
0	0	0	0	0	0	0	0	1	0	1	0	0.726	1407091
0	0	1	0	0	0	0	0	1	1	0	1	0.726	1407482
1	1	0	0	0	0	0	1	0	1	0	1	0.724	1410942
1	0	1	0	0	0	0	1	0	0	1	1	0.724	1411561
0	0	1	0	0	0	0	0	1	1	0	0	0.723	1412195
1	1	0	0	0	0	0	1	0	1	0	0	0.722	1415622
1	0	1	0	0	0	0	1	0	0	1	0	0.721	1416236
0	0	0	0	0	0	0	0	1	1	0	1	0.718	1422449
1	0	0	0	0	0	0	1	0	0	1	1	0.715	1426407
0	0	0	0	0	0	0	0	1	1	0	0	0.715	1427022
0	1	1	0	0	0	0	1	0	0	1	1	0.714	1428147
1	0	0	0	0	0	0	1	0	0	1	0	0.713	1430944
1	0	1	0	0	0	0	1	0	1	0	1	0.713	1431317
0	1	1	0	0	0	0	1	0	0	1	0	0.712	1432668
1	1	1	0	0	0	1	0	0	0	1	1	0.710	1435154
1	0	1	0	0	0	0	1	0	1	0	0	0.710	1435809
1	1	1	0	0	0	1	0	0	0	1	0	0.708	1439612
0	1	0	0	0	0	0	1	0	0	1	1	0.706	1442510
1	0	0	0	0	0	0	1	0	1	0	1	0.704	1445589
1	1	1	0	0	1	0	0	0	0	1	1	0.704	1445734
0	1	0	0	0	0	0	1	0	0	1	0	0.703	1446903
0	1	1	0	0	0	0	1	0	1	0	1	0.703	1447264
1	1	0	0	0	0	1	0	0	0	1	1	0.702	1449318
1	0	0	0	0	0	0	1	0	1	0	0	0.701	1449954
1	1	1	0	0	1	0	0	0	0	1	0	0.701	1450097
0	1	1	0	0	0	0	1	0	1	0	0	0.700	1451614
1	1	0	0	0	0	1	0	0	0	1	0	0.699	1453650
1	1	1	0	0	0	1	0	0	1	0	1	0.699	1454007
1	1	1	0	0	0	1	0	0	1	0	0	0.696	1458298
1	1	0	0	0	1	0	0	0	0	1	1	0.696	1459602
0	1	0	0	0	0	0	1	0	1	0	1	0.695	1461090
0	0	1	0	0	0	0	1	0	0	1	1	0.694	1461649

temperature	humidity	wind speed	DV0.1	DV0.5	V50	V100	V150	V200	minimal dist.	centroid dist.	relative bearing	R^2	AIC
1	1	0	0	0	1	0	0	0	0	1	0	0.693	1463845
1	1	1	0	0	1	0	0	0	1	0	1	0.693	1464194
0	1	0	0	0	0	0	1	0	1	0	0	0.692	1465320
0	0	1	0	0	0	0	1	0	0	1	0	0.692	1465875
1	1	0	0	0	0	1	0	0	1	0	1	0.691	1467648
1	0	1	0	0	0	1	0	0	0	1	1	0.690	1468200
1	1	1	0	0	1	0	0	0	1	0	0	0.690	1468399
1	1	0	0	0	0	1	0	0	1	0	0	0.688	1471823
1	0	1	0	0	0	1	0	0	0	1	0	0.688	1472371
0	0	0	0	0	0	0	1	0	0	1	1	0.686	1475084
1	1	0	0	0	1	0	0	0	1	0	1	0.684	1477561
1	0	1	0	0	1	0	0	0	0	1	1	0.684	1478103
0	0	0	0	0	0	0	1	0	0	1	0	0.683	1479197
0	0	1	0	0	0	0	1	0	1	0	1	0.683	1479536
1	0	0	0	0	0	1	0	0	0	1	1	0.682	1481460
1	1	0	0	0	1	0	0	0	1	0	0	0.682	1481654
1	0	1	0	0	1	0	0	0	0	1	0	0.681	1482191
0	1	1	0	0	0	1	0	0	0	1	1	0.681	1483018
0	0	1	0	0	0	0	1	0	1	0	0	0.680	1483612
1	0	0	0	0	0	1	0	0	0	1	0	0.679	1485521
1	0	1	0	0	0	1	0	0	1	0	1	0.679	1485855
0	1	1	0	0	0	1	0	0	0	1	0	0.678	1487066
1	0	1	0	0	0	1	0	0	1	0	0	0.676	1489880
1	0	0	0	0	1	0	0	0	0	1	1	0.676	1491103
0	0	0	0	0	0	0	1	0	1	0	1	0.675	1492499
0	1	1	0	0	1	0	0	0	0	1	1	0.675	1492631
1	0	0	0	0	1	0	0	0	0	1	0	0.673	1495086
1	0	1	0	0	1	0	0	0	1	0	1	0.673	1495414
0	1	0	0	0	0	1	0	0	0	1	1	0.672	1495892
0	0	0	0	0	0	0	1	0	1	0	0	0.672	1496471
0	1	1	0	0	1	0	0	0	0	1	0	0.672	1496601
1	0	0	0	0	0	1	0	0	1	0	1	0.671	1498657
1	0	1	0	0	1	0	0	0	1	0	0	0.670	1499362
0	1	0	0	0	0	1	0	0	0	1	0	0.670	1499836
0	1	1	0	0	0	1	0	0	1	0	1	0.670	1500161
1	0	0	0	0	0	1	0	0	1	0	0	0.668	1502579
0	1	1	0	0	0	1	0	0	1	0	0	0.667	1504072
0	1	0	0	0	1	0	0	0	0	1	1	0.666	1505260
1	0	0	0	0	1	0	0	0	1	0	1	0.664	1507973
0	1	0	0	0	1	0	0	0	0	1	0	0.664	1509131
0	1	1	0	0	1	0	0	0	1	0	1	0.663	1509450
1	0	0	0	0	1	0	0	0	1	0	0	0.662	1511823
0	1	0	0	0	0	1	0	0	1	0	1	0.661	1512602
0	0	1	0	0	0	1	0	0	0	1	1	0.661	1513106
0	1	1	0	0	1	0	0	0	1	0	0	0.661	1513288

temperature	humidity	wind speed	DV0.1	DV0.5	V50	V100	V150	V200	minimal dist.	centroid dist.	relative bearing	R^2	AIC
0	1	0	0	0	0	1	0	0	1	0	0	0.659	1516416
0	0	1	0	0	0	1	0	0	0	1	0	0.658	1516916
0	1	0	0	0	1	0	0	0	1	0	1	0.655	1521662
0	0	1	0	0	1	0	0	0	0	1	1	0.655	1522157
0	0	0	0	0	0	1	0	0	0	1	1	0.652	1525230
0	1	0	0	0	1	0	0	0	1	0	0	0.652	1525407
0	0	1	0	0	1	0	0	0	0	1	0	0.652	1525898
0	0	0	0	0	0	1	0	0	0	1	0	0.650	1528948
0	0	1	0	0	0	1	0	0	1	0	1	0.650	1529254
0	0	1	0	0	0	1	0	0	1	0	0	0.647	1532942
0	0	0	0	0	1	0	0	0	0	1	1	0.646	1534063
0	0	0	0	0	1	0	0	0	0	1	0	0.644	1537715
0	0	1	0	0	1	0	0	0	1	0	1	0.643	1538017
0	0	0	0	0	0	1	0	0	1	0	1	0.641	1540992
0	0	1	0	0	1	0	0	0	1	0	0	0.641	1541640
0	0	0	0	0	0	1	0	0	1	0	0	0.639	1544594
0	0	0	0	0	1	0	0	0	1	0	1	0.635	1549551
0	0	0	0	0	1	0	0	0	1	0	0	0.632	1553091
1	1	1	1	0	0	0	0	0	0	0	1	0.590	1607243
1	1	1	0	1	0	0	0	0	0	0	1	0.589	1607790
1	1	1	1	0	0	0	0	0	0	0	0	0.587	1610394
1	1	1	0	1	0	0	0	0	0	0	0	0.587	1610938
1	1	0	1	0	0	0	0	0	0	0	1	0.581	1617286
1	1	0	0	1	0	0	0	0	0	0	1	0.581	1617822
1	1	0	1	0	0	0	0	0	0	0	0	0.579	1620374
1	1	0	0	1	0	0	0	0	0	0	0	0.578	1620907
1	0	1	1	0	0	0	0	0	0	0	1	0.570	1630804
1	0	1	0	1	0	0	0	0	0	0	1	0.569	1631326
1	0	1	1	0	0	0	0	0	0	0	0	0.567	1633809
1	0	1	0	1	0	0	0	0	0	0	0	0.567	1634328
1	0	0	1	0	0	0	0	0	0	0	1	0.561	1640384
1	0	0	0	1	0	0	0	0	0	0	1	0.561	1640896
0	1	1	1	0	0	0	0	0	0	0	1	0.560	1641515
0	1	1	0	1	0	0	0	0	0	0	1	0.560	1642026
1	0	0	1	0	0	0	0	0	0	0	0	0.559	1643332
1	0	0	0	1	0	0	0	0	0	0	0	0.558	1643841
0	1	1	1	0	0	0	0	0	0	0	0	0.558	1644456
0	1	1	0	1	0	0	0	0	0	0	0	0.557	1644964
0	1	0	1	0	0	0	0	0	0	0	1	0.552	1650892
0	1	0	0	1	0	0	0	0	0	0	1	0.551	1651393
0	1	0	1	0	0	0	0	0	0	0	0	0.549	1653778
0	1	0	0	1	0	0	0	0	0	0	0	0.549	1654276
1	1	1	0	0	0	0	0	1	0	0	1	0.545	1658670
1	1	1	0	0	0	0	0	1	0	0	0	0.542	1661511
0	0	1	1	0	0	0	0	0	0	0	1	0.540	1663533

temperature	humidity	wind speed	DV0.1	DV0.5	V50	V100	V150	V200	minimal dist.	centroid dist.	relative bearing	R^2	AIC
0	0	1	0	1	0	0	0	0	0	0	1	0.540	1664022
0	0	1	1	0	0	0	0	0	0	0	0	0.538	1666346
0	0	1	0	1	0	0	0	0	0	0	0	0.537	1666832
1	1	0	0	0	0	0	0	1	0	0	1	0.536	1667730
1	1	0	0	0	0	0	0	1	0	0	0	0.534	1670520
0	0	0	1	0	0	0	0	0	0	0	1	0.532	1672505
0	0	0	0	1	0	0	0	0	0	0	1	0.531	1672985
0	0	0	1	0	0	0	0	0	0	0	0	0.529	1675268
0	0	0	0	1	0	0	0	0	0	0	0	0.529	1675745
1	0	1	0	0	0	0	0	1	0	0	1	0.525	1679954
1	0	1	0	0	0	0	0	1	0	0	0	0.522	1682675
1	0	0	0	0	0	0	0	1	0	0	1	0.516	1688636
0	1	1	0	0	0	0	0	1	0	0	1	0.515	1689661
1	0	0	0	0	0	0	0	1	0	0	0	0.514	1691310
0	1	1	0	0	0	0	0	1	0	0	0	0.513	1692330
0	1	0	0	0	0	0	0	1	0	0	1	0.507	1698176
0	1	0	0	0	0	0	0	1	0	0	0	0.504	1700799
1	1	1	0	0	0	0	1	0	0	0	1	0.502	1703275
1	1	1	0	0	0	0	1	0	0	0	0	0.499	1705871
0	0	1	0	0	0	0	0	1	0	0	1	0.495	1709678
1	1	0	0	0	0	0	1	0	0	0	1	0.493	1711560
0	0	1	0	0	0	0	0	1	0	0	0	0.493	1712241
1	1	0	0	0	0	0	1	0	0	0	0	0.491	1714113
0	0	0	0	0	0	0	0	1	0	0	1	0.487	1717857
0	0	0	0	0	0	0	0	1	0	0	0	0.484	1720378
1	0	1	0	0	0	0	1	0	0	0	1	0.482	1722759
1	0	1	0	0	0	0	1	0	0	0	0	0.479	1725255
1	0	0	0	0	0	0	1	0	0	0	1	0.473	1730726
0	1	1	0	0	0	0	1	0	0	0	1	0.472	1731669
1	0	0	0	0	0	0	1	0	0	0	0	0.471	1733183
0	1	1	0	0	0	0	1	0	0	0	0	0.470	1734120
1	1	1	0	0	0	1	0	0	0	0	1	0.468	1735475
1	1	1	0	0	0	1	0	0	0	0	0	0.466	1737908
0	1	0	0	0	0	0	1	0	0	0	1	0.464	1739495
1	1	1	0	0	1	0	0	0	0	0	1	0.462	1741267
0	1	0	0	0	0	0	1	0	0	0	0	0.461	1741908
1	1	0	0	0	0	1	0	0	0	0	1	0.460	1743242
1	1	1	0	0	1	0	0	0	0	0	0	0.459	1743672
1	1	0	0	0	0	1	0	0	0	0	0	0.457	1745637
1	1	0	0	0	1	0	0	0	0	0	1	0.454	1748944
0	0	1	0	0	0	0	1	0	0	0	1	0.452	1750085
1	1	0	0	0	1	0	0	0	0	0	0	0.451	1751312
0	0	1	0	0	0	0	1	0	0	0	0	0.450	1752447
1	0	1	0	0	0	1	0	0	0	0	1	0.448	1753753
1	0	1	0	0	0	1	0	0	0	0	0	0.446	1756098

temperature	humidity	wind speed	DV0.1	DV0.5	V50	V100	V150	V200	minimal dist.	centroid dist.	relative bearing	R^2	AIC
0	0	0	0	0	0	0	1	0	0	0	1	0.444	1757627
1	0	1	0	0	1	0	0	0	0	0	1	0.442	1759336
0	0	0	0	0	0	0	1	0	0	0	0	0.441	1759954
1	0	0	0	0	0	1	0	0	0	0	1	0.440	1761240
1	0	1	0	0	1	0	0	0	0	0	0	0.439	1761655
0	1	1	0	0	0	1	0	0	0	0	1	0.439	1762126
1	0	0	0	0	0	1	0	0	0	0	0	0.437	1763549
0	1	1	0	0	0	1	0	0	0	0	0	0.436	1764431
1	0	0	0	0	1	0	0	0	0	0	1	0.434	1766740
0	1	1	0	0	1	0	0	0	0	0	1	0.433	1767616
1	0	0	0	0	1	0	0	0	0	0	0	0.431	1769024
0	1	0	0	0	0	1	0	0	0	0	1	0.430	1769488
0	1	1	0	0	1	0	0	0	0	0	0	0.430	1769896
0	1	0	0	0	0	1	0	0	0	0	0	0.428	1771760
0	1	0	0	0	1	0	0	0	0	0	1	0.424	1774898
0	1	0	0	0	1	0	0	0	0	0	0	0.422	1777145
0	0	1	0	0	0	1	0	0	0	0	1	0.419	1779462
0	0	1	0	0	0	1	0	0	0	0	0	0.416	1781688
0	0	1	0	0	1	0	0	0	0	0	1	0.413	1784764
0	0	0	0	0	0	1	0	0	0	0	1	0.410	1786572
0	0	1	0	0	1	0	0	0	0	0	0	0.410	1786966
0	0	0	0	0	0	1	0	0	0	0	0	0.408	1788766
0	0	0	0	0	1	0	0	0	0	0	1	0.404	1791799
0	0	0	0	0	1	0	0	0	0	0	0	0.402	1793970
1	1	1	0	0	0	0	0	0	0	1	1	0.302	1869737
1	1	1	0	0	0	0	0	0	0	1	0	0.300	1871592
1	1	0	0	0	0	0	0	0	0	1	1	0.294	1875668
1	1	0	0	0	0	0	0	0	0	1	0	0.291	1877501
1	1	1	0	0	0	0	0	0	1	0	1	0.291	1877654
1	1	1	0	0	0	0	0	0	1	0	0	0.289	1879480
1	1	0	0	0	0	0	0	0	1	0	1	0.283	1883491
1	0	1	0	0	0	0	0	0	0	1	1	0.282	1883730
1	1	0	0	0	0	0	0	0	1	0	0	0.280	1885296
1	0	1	0	0	0	0	0	0	0	1	0	0.280	1885533
1	0	0	0	0	0	0	0	0	0	1	1	0.274	1889496
0	1	1	0	0	0	0	0	0	0	1	1	0.273	1890180
1	0	0	0	0	0	0	0	0	0	1	0	0.271	1891279
1	0	1	0	0	0	0	0	0	1	0	1	0.271	1891428
0	1	1	0	0	0	0	0	0	0	1	0	0.270	1891960
1	0	1	0	0	0	0	0	0	1	0	0	0.269	1893204
0	1	0	0	0	0	0	0	0	0	1	1	0.265	1895872
1	0	0	0	0	0	0	0	0	1	0	1	0.263	1897106
0	1	0	0	0	0	0	0	0	0	1	0	0.262	1897632
0	1	1	0	0	0	0	0	0	1	0	1	0.262	1897780
1	0	0	0	0	0	0	0	0	1	0	0	0.260	1898861

temperature	humidity	wind speed	DV0.1	DV0.5	V50	V100	V150	V200	minimal dist.	centroid dist.	relative bearing	R^2	AIC
0	1	1	0	0	0	0	0	0	1	0	0	0.259	1899533
0	1	0	0	0	0	0	0	0	1	0	1	0.253	1903385
0	0	1	0	0	0	0	0	0	0	1	1	0.253	1903614
0	1	0	0	0	0	0	0	0	1	0	0	0.251	1905119
0	0	1	0	0	0	0	0	0	0	1	0	0.250	1905347
0	0	0	0	0	0	0	0	0	0	1	1	0.245	1909155
0	0	0	0	0	0	0	0	0	0	1	0	0.242	1910868
0	0	1	0	0	0	0	0	0	1	0	1	0.242	1911011
0	0	1	0	0	0	0	0	0	1	0	0	0.239	1912718
0	0	0	0	0	0	0	0	0	1	0	1	0.233	1916470
0	0	0	0	0	0	0	0	0	1	0	0	0.231	1918158
1	1	1	0	0	0	0	0	0	0	0	1	0.060	2017039
1	1	1	0	0	0	0	0	0	0	0	0	0.058	2018416
1	1	0	0	0	0	0	0	0	0	0	1	0.052	2021448
1	1	0	0	0	0	0	0	0	0	0	0	0.049	2022814
1	0	1	0	0	0	0	0	0	0	0	1	0.040	2027465
1	0	1	0	0	0	0	0	0	0	0	0	0.038	2028814
1	0	0	0	0	0	0	0	0	0	0	1	0.032	2031783
0	1	1	0	0	0	0	0	0	0	0	1	0.031	2032297
1	0	0	0	0	0	0	0	0	0	0	0	0.029	2033120
0	1	1	0	0	0	0	0	0	0	0	0	0.028	2033632
0	1	0	0	0	0	0	0	0	0	0	1	0.023	2036573
0	1	0	0	0	0	0	0	0	0	0	0	0.020	2037897
0	0	1	0	0	0	0	0	0	0	0	1	0.011	2042409
0	0	1	0	0	0	0	0	0	0	0	0	0.008	2043717
0	0	0	0	0	0	0	0	0	0	0	1	0.003	2046599
0	0	0	0	0	0	0	0	0	0	0	0	0.000	2047896

30 *Table S 5: Analysis of the lower and upper threshold distance, MLR model performance (R^2) of the close, medium, and far distance models and the respective mean R^2 for the different combinations of lower and upper threshold values.*

lower threshold (m)	upper threshold (m)	MLR performance (R^2)			
		close	medium	far	mean
95	145	0.945	0.851	0.855	0.884
95	150	0.945	0.838	0.855	0.879
95	155	0.945	0.844	0.856	0.882
95	160	0.945	0.833	0.857	0.878
95	165	0.945	0.833	0.858	0.879
95	170	0.945	0.833	0.858	0.879
95	175	0.945	0.837	0.858	0.880
95	180	0.945	0.834	0.858	0.879
95	185	0.945	0.831	0.859	0.879
95	190	0.945	0.663	0.867	0.825

lower threshold (m)	upper threshold (m)	MLR performance (R^2)			
		close	medium	far	mean
95	195	0.945	0.676	0.868	0.830
95	200	0.945	0.680	0.872	0.833
95	205	0.945	0.688	0.874	0.836
95	210	0.945	0.704	0.876	0.842
95	215	0.945	0.709	0.876	0.843
95	220	0.945	0.691	0.880	0.839
95	225	0.945	0.699	0.881	0.842
95	230	0.945	0.704	0.881	0.844
95	235	0.945	0.711	0.883	0.846
95	240	0.945	0.711	0.886	0.848
95	245	0.945	0.722	0.887	0.851
95	250	0.945	0.735	0.887	0.856
100	150	0.945	0.834	0.855	0.878
100	155	0.945	0.839	0.856	0.880
100	160	0.945	0.837	0.857	0.880
100	165	0.945	0.834	0.858	0.879
100	170	0.945	0.834	0.858	0.879
100	175	0.945	0.840	0.858	0.881
100	180	0.945	0.842	0.858	0.882
100	185	0.945	0.835	0.859	0.880
100	190	0.945	0.650	0.867	0.821
100	195	0.945	0.663	0.868	0.825
100	200	0.945	0.669	0.872	0.829
100	205	0.945	0.677	0.874	0.832
100	210	0.945	0.694	0.876	0.838
100	215	0.945	0.700	0.876	0.840
100	220	0.945	0.682	0.880	0.836
100	225	0.945	0.689	0.881	0.839
100	230	0.945	0.696	0.881	0.841
100	235	0.945	0.703	0.883	0.844
100	240	0.945	0.703	0.886	0.845
100	245	0.945	0.714	0.887	0.849
100	250	0.945	0.728	0.887	0.853
105	155	0.945	0.839	0.856	0.880
105	160	0.945	0.837	0.857	0.880
105	165	0.945	0.834	0.858	0.879
105	170	0.945	0.834	0.858	0.879
105	175	0.945	0.840	0.858	0.881
105	180	0.945	0.842	0.858	0.882
105	185	0.945	0.835	0.859	0.880
105	190	0.945	0.650	0.867	0.821
105	195	0.945	0.663	0.868	0.825
105	200	0.945	0.669	0.872	0.829
105	205	0.945	0.677	0.874	0.832
105	210	0.945	0.694	0.876	0.838

lower threshold (m)	upper threshold (m)	MLR performance (R^2)			
		close	medium	far	mean
105	215	0.945	0.700	0.876	0.840
105	220	0.945	0.682	0.880	0.836
105	225	0.945	0.689	0.881	0.839
105	230	0.945	0.696	0.881	0.841
105	235	0.945	0.703	0.883	0.844
105	240	0.945	0.703	0.886	0.845
105	245	0.945	0.714	0.887	0.849
105	250	0.945	0.728	0.887	0.853
110	160	0.945	0.837	0.857	0.880
110	165	0.945	0.834	0.858	0.879
110	170	0.945	0.834	0.858	0.879
110	175	0.945	0.840	0.858	0.881
110	180	0.945	0.842	0.858	0.882
110	185	0.945	0.835	0.859	0.880
110	190	0.945	0.650	0.867	0.821
110	195	0.945	0.663	0.868	0.825
110	200	0.945	0.669	0.872	0.829
110	205	0.945	0.677	0.874	0.832
110	210	0.945	0.694	0.876	0.838
110	215	0.945	0.700	0.876	0.840
110	220	0.945	0.682	0.880	0.836
110	225	0.945	0.689	0.881	0.839
110	230	0.945	0.696	0.881	0.841
110	235	0.945	0.703	0.883	0.844
110	240	0.945	0.703	0.886	0.845
110	245	0.945	0.714	0.887	0.849
110	250	0.945	0.728	0.887	0.853
115	165	0.945	0.834	0.858	0.879
115	170	0.945	0.834	0.858	0.879
115	175	0.945	0.840	0.858	0.881
115	180	0.945	0.842	0.858	0.882
115	185	0.945	0.835	0.859	0.880
115	190	0.945	0.650	0.867	0.821
115	195	0.945	0.663	0.868	0.825
115	200	0.945	0.669	0.872	0.829
115	205	0.945	0.677	0.874	0.832
115	210	0.945	0.694	0.876	0.838
115	215	0.945	0.700	0.876	0.840
115	220	0.945	0.682	0.880	0.836
115	225	0.945	0.689	0.881	0.839
115	230	0.945	0.696	0.881	0.841
115	235	0.945	0.703	0.883	0.844
115	240	0.945	0.703	0.886	0.845
115	245	0.945	0.714	0.887	0.849
115	250	0.945	0.728	0.887	0.853

lower threshold (m)	upper threshold (m)	MLR performance (R^2)			
		close	medium	far	mean
120	170	0.944	0.863	0.858	0.888
120	175	0.944	0.869	0.858	0.890
120	180	0.944	0.873	0.858	0.892
120	185	0.944	0.850	0.859	0.884
120	190	0.944	0.634	0.867	0.815
120	195	0.944	0.649	0.868	0.820
120	200	0.944	0.654	0.872	0.824
120	205	0.944	0.664	0.874	0.828
120	210	0.944	0.682	0.876	0.834
120	215	0.944	0.689	0.876	0.836
120	220	0.944	0.669	0.880	0.831
120	225	0.944	0.677	0.881	0.834
120	230	0.944	0.684	0.881	0.837
120	235	0.944	0.693	0.883	0.840
120	240	0.944	0.693	0.886	0.841
120	245	0.944	0.705	0.887	0.845
120	250	0.944	0.720	0.887	0.850
125	175	0.900	0.859	0.858	0.872
125	180	0.900	0.863	0.858	0.874
125	185	0.900	0.840	0.859	0.866
125	190	0.900	0.618	0.867	0.795
125	195	0.900	0.634	0.868	0.801
125	200	0.900	0.643	0.872	0.805
125	205	0.900	0.653	0.874	0.809
125	210	0.900	0.672	0.876	0.816
125	215	0.900	0.678	0.876	0.818
125	220	0.900	0.661	0.880	0.814
125	225	0.900	0.669	0.881	0.817
125	230	0.900	0.676	0.881	0.819
125	235	0.900	0.684	0.883	0.822
125	240	0.900	0.685	0.886	0.824
125	245	0.900	0.697	0.887	0.828
125	250	0.900	0.712	0.887	0.833
130	180	0.900	0.863	0.858	0.874
130	185	0.900	0.840	0.859	0.866
130	190	0.900	0.618	0.867	0.795
130	195	0.900	0.634	0.868	0.801
130	200	0.900	0.643	0.872	0.805
130	205	0.900	0.653	0.874	0.809
130	210	0.900	0.672	0.876	0.816
130	215	0.900	0.678	0.876	0.818
130	220	0.900	0.661	0.880	0.814
130	225	0.900	0.669	0.881	0.817
130	230	0.900	0.676	0.881	0.819
130	235	0.900	0.684	0.883	0.822

lower threshold (m)	upper threshold (m)	MLR performance (R^2)			
		close	medium	far	mean
130	240	0.900	0.685	0.886	0.824
130	245	0.900	0.697	0.887	0.828
130	250	0.900	0.712	0.887	0.833
135	185	0.898	0.823	0.859	0.860
135	190	0.898	0.581	0.867	0.782
135	195	0.898	0.601	0.868	0.789
135	200	0.898	0.619	0.872	0.797
135	205	0.898	0.627	0.874	0.800
135	210	0.898	0.648	0.876	0.807
135	215	0.898	0.654	0.876	0.809
135	220	0.898	0.643	0.880	0.807
135	225	0.898	0.651	0.881	0.810
135	230	0.898	0.655	0.881	0.811
135	235	0.898	0.662	0.883	0.814
135	240	0.898	0.667	0.886	0.817
135	245	0.898	0.678	0.887	0.821
135	250	0.898	0.694	0.887	0.826
140	190	0.889	0.556	0.867	0.771
140	195	0.889	0.578	0.868	0.778
140	200	0.889	0.604	0.872	0.788
140	205	0.889	0.610	0.874	0.791
140	210	0.889	0.632	0.876	0.799
140	215	0.889	0.636	0.876	0.800
140	220	0.889	0.631	0.880	0.800
140	225	0.889	0.639	0.881	0.803
140	230	0.889	0.641	0.881	0.804
140	235	0.889	0.647	0.883	0.806
140	240	0.889	0.654	0.886	0.810
140	245	0.889	0.665	0.887	0.814
140	250	0.889	0.681	0.887	0.819
145	195	0.864	0.543	0.868	0.758
145	200	0.864	0.582	0.872	0.773
145	205	0.864	0.582	0.874	0.774
145	210	0.864	0.607	0.876	0.782
145	215	0.864	0.610	0.876	0.783
145	220	0.864	0.613	0.880	0.786
145	225	0.864	0.620	0.881	0.789
145	230	0.864	0.620	0.881	0.788
145	235	0.864	0.625	0.883	0.791
145	240	0.864	0.634	0.886	0.795
145	245	0.864	0.646	0.887	0.799
145	250	0.864	0.663	0.887	0.805

Table S 6: MLR predicting of log-transformed spray drift deposition on non-target areas for the close distance (0-120m), based on centroid distance, wind speed, temperature, humidity, 10% volume diameter (DV0.1), and relative bearing with estimated slopes and their respective confidence intervals in unscaled (Est.) and scaled (Est. (scaled)) form. The model is based on a sample size of 2304, is highly significant ($p < 0.001$), and a model performance of $R^2 = 0.944$.

	Est.	t	p
(Intercept)	-5.849 [-5.871, -5.826]		
centroid distance	-0.210 [-0.232, -0.187]	-24	<0.001
wind speed	0.854 [0.831, 0.876]	97.75	<0.001
temperature	-0.043 [-0.065, -0.020]	-4.91	<0.001
humidity	0.057 [0.035, 0.080]	6.58	<0.001
DV0.1	-1.477 [-1.500, -1.455]	-169.13	<0.001
relative bearing	0.016 [-0.007, 0.038]	1.81	0.071
N	2304		
R^2	0.944		
F(6,2297)	6467.6 ($p < 0.001$)		

Table S 7: MLR predicting of log-transformed spray drift deposition on non-target areas for the medium distance (120-180m), based on centroid distance, wind speed, temperature, humidity, 10% volume diameter (DV0.1), and relative bearing with estimated slopes and their respective confidence intervals in unscaled (Est.) and scaled (Est. (scaled)) form. The model is based on a sample size of 6144, is highly significant ($p < 0.001$), and a model performance of $R^2 = 0.873$.

	Est.	t	p
(Intercept)	-6.779 [-6.804, -6.755]		
centroid distance	-1.079 [-1.104, -1.055]	-113.23	<0.001
wind speed	0.681 [0.657, 0.706]	71.48	<0.001
temperature	-0.033 [-0.058, -0.009]	-3.5	<0.001
humidity	0.058 [0.033, 0.082]	6.08	<0.001
DV0.1	-1.484 [-1.509, -1.460]	-155.72	<0.001
relative bearing	-0.017 [-0.041, 0.008]	-1.77	0.077
N	6144		
R^2	0.873		
F(6,6137)	7038.52 ($p < 0.001$)		

Table S 8: MLR predicting of log-transformed spray drift deposition on non-target areas for the far distance (> 180m), based on centroid distance, wind speed, temperature, humidity, 10% volume diameter (DV0.1), and relative bearing with estimated slopes and their respective confidence intervals in unscaled (Est.) and scaled (Est. (scaled)) form. The model is based on a sample size of 486144, is highly significant (p < 0.001), and a model performance of R^2 = 0.858.

	Est.	t	p
(Intercept)	-11.392 [-11.395, -11.390]		
centroid distance	-0.789 [-0.792, -0.787]	-808.24	<0.001
wind speed	-0.192 [-0.194, -0.189]	-196.33	<0.001
temperature	0.335 [0.333, 0.338]	343.56	<0.001
humidity	-0.277 [-0.280, -0.275]	-283.82	<0.001
DV0.1	-1.394 [-1.396, -1.391]	-1427.63	<0.001
relative bearing	-0.100 [-0.102, -0.097]	-102.21	<0.001
N	486144		
R^2	0.858		
F(6,486137)	489824.72 (p < 0.001)		

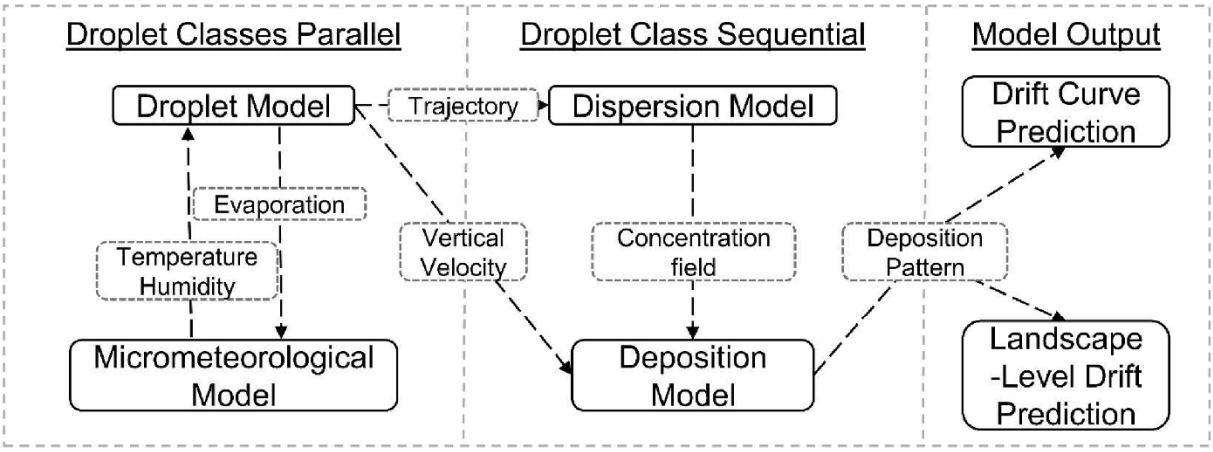


Figure S 1: Schematic representation of the DAD-drift model. With solid boxes representing sub-models, and dashed boxes and arrows representing intermediate results being forwarded between sub-models. The sub-models in the left column are executed first and in parallel for all droplet classes, the sub-models in the middle column are executed second and sequentially for all droplet classes, finally the model outputs are calculated in the right column.

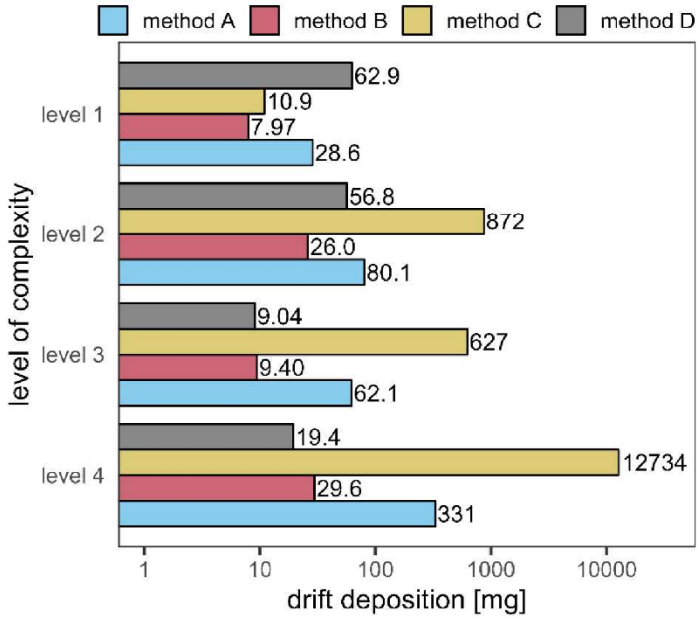


Figure S 2: Spray drift depositions (mg) onto surface waterbodies for the four complexity levels, the four prediction methods, and the XR spray nozzle, with prediction method A in blue, prediction method B in red, prediction method C in yellow, and prediction method D in grey. The complexity levels are described in Figure 1, with level 1 equal to scenario (a), level 2 equal to scenario (b), level 4 equal to scenario (c), and level 4 equal to scenario (d).

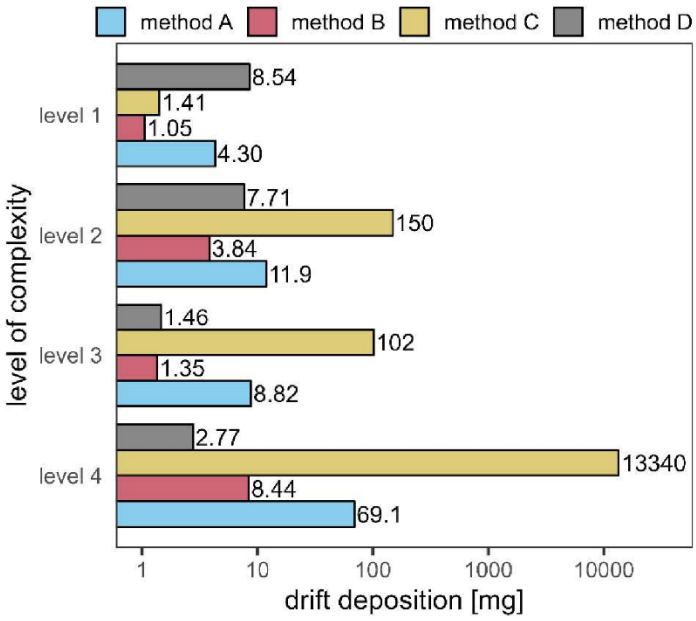


Figure S 3: Spray drift depositions (mg) onto surface waterbodies for the four complexity levels, the four prediction methods, and the AIXR spray nozzle, with prediction method A in blue, prediction method B in red, prediction method C in yellow, and prediction method D in grey. The complexity levels are described in Figure 1, with level 1 equal to scenario (a), level 2 equal to scenario (b), level 4 equal to scenario (c), and level 4 equal to scenario (d).

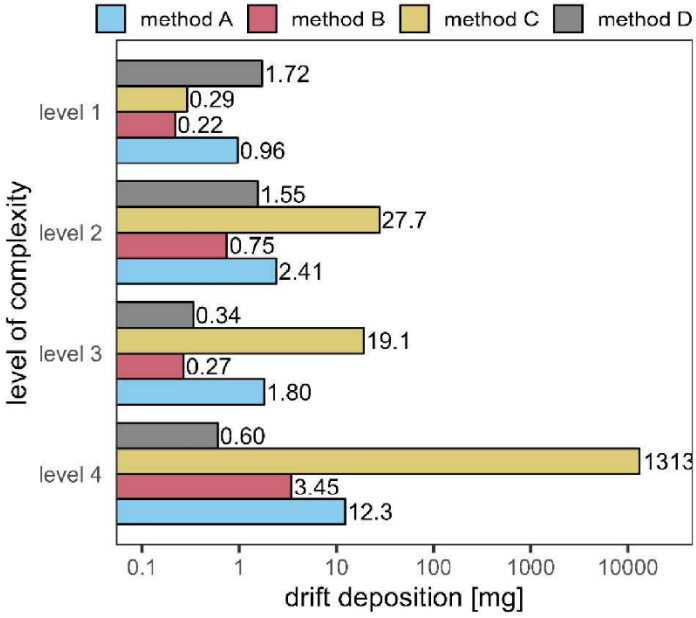


Figure S 4: Spray drift depositions (mg) onto surface waterbodies for the four complexity levels, the four prediction methods, and the TTI spray nozzle, with prediction method A in blue, prediction method B in red, prediction method C in yellow, and prediction method D in grey. The complexity levels are described in Figure 1, with level 1 equal to scenario (a), level 2 equal to scenario (b), level 4 equal to scenario (c), and level 4 equal to scenario (d).

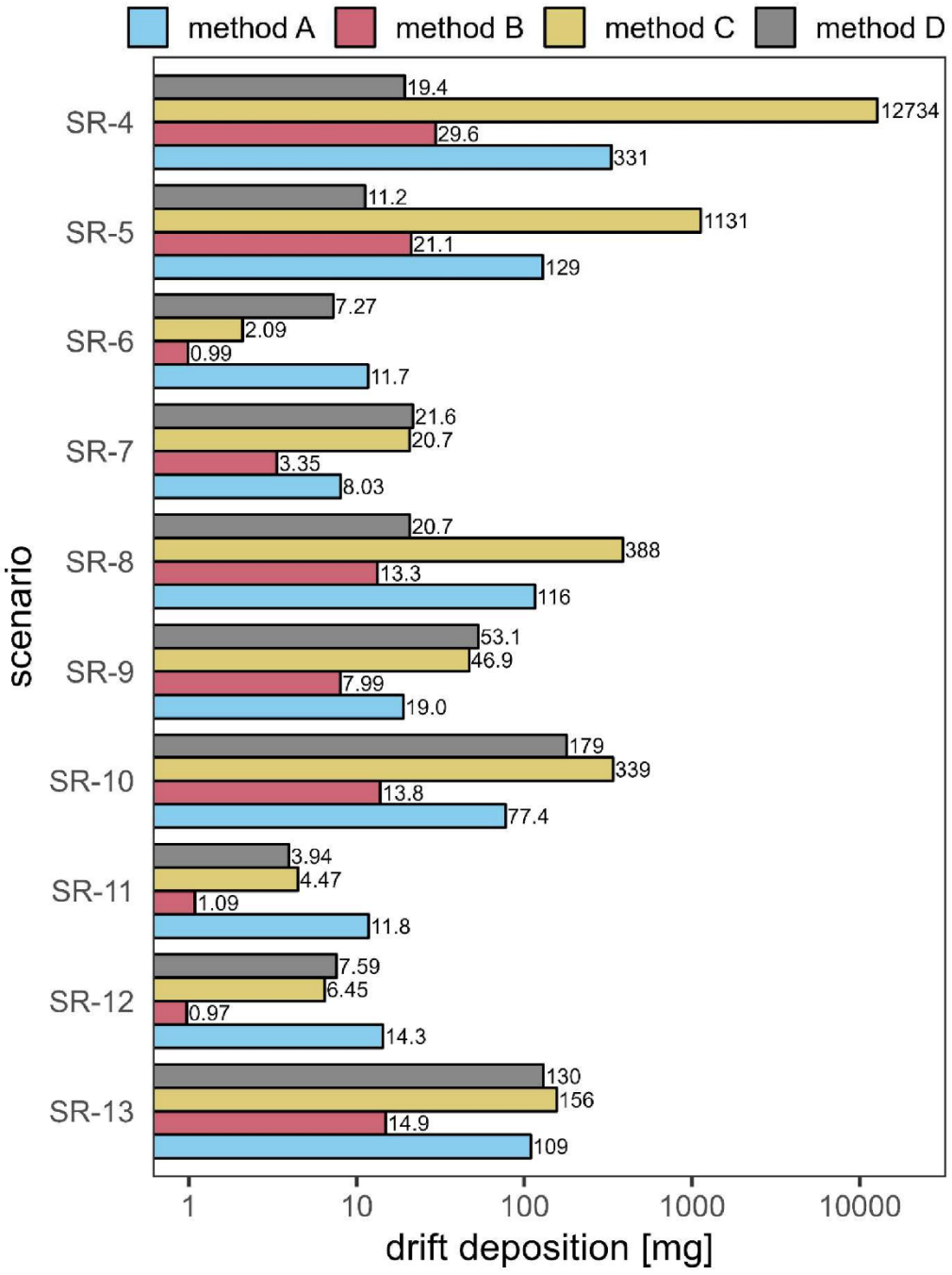


Figure S 5: Spray drift deposition (mg) onto surface waterbodies using the four prediction methods for the 10 scenarios (Figure 1) for the XR spry nozzle, with prediction method A in blue, prediction method B in red, prediction method C in yellow, and prediction method D in grey.

100

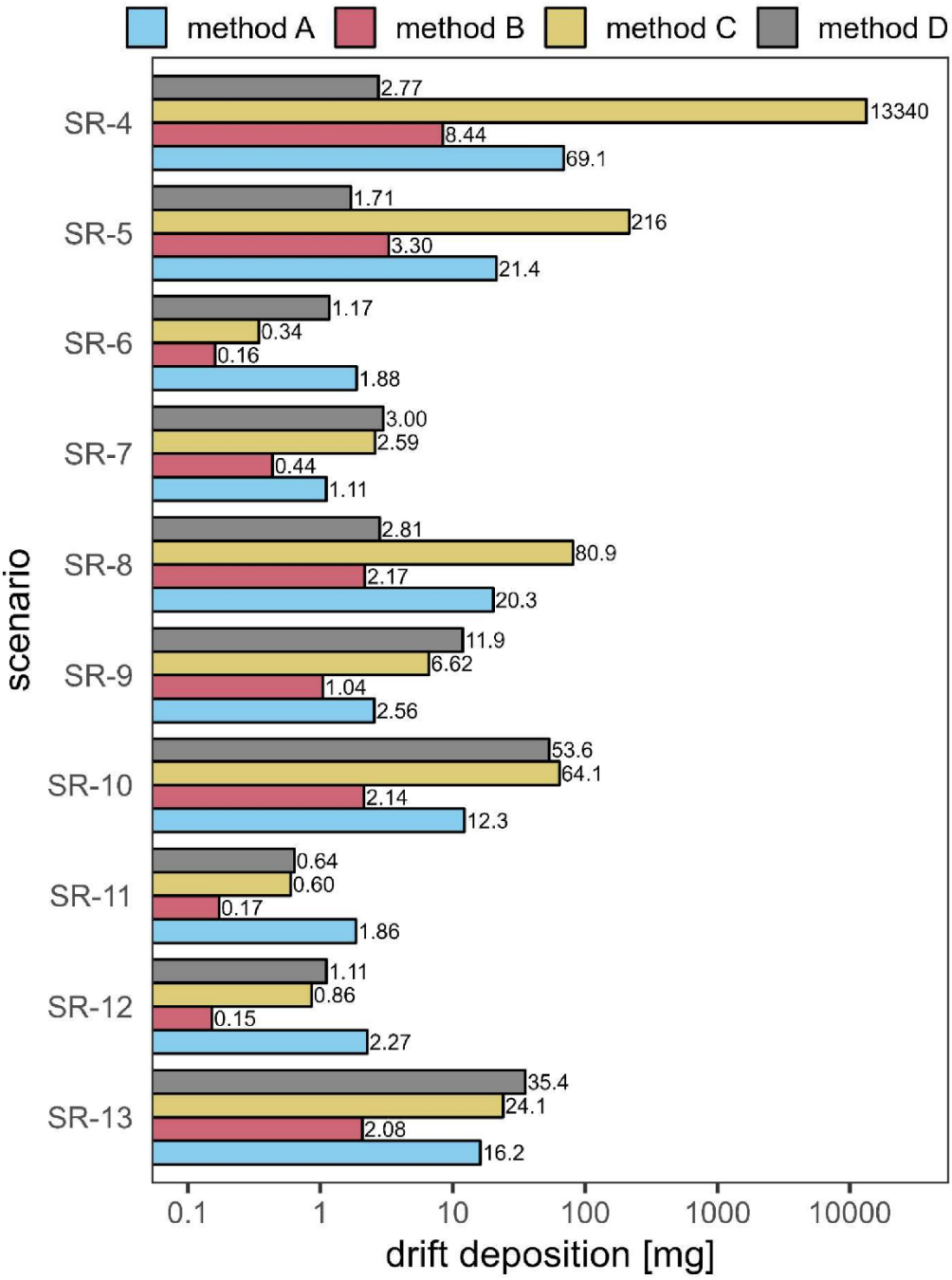


Figure S 6: Spray drift deposition (mg) onto surface waterbodies using the four prediction methods for the 10 scenarios (Figure 1) for the AIXR spry nozzle, with prediction method A in blue, prediction method B in red, prediction method C in yellow, and prediction method D in grey.

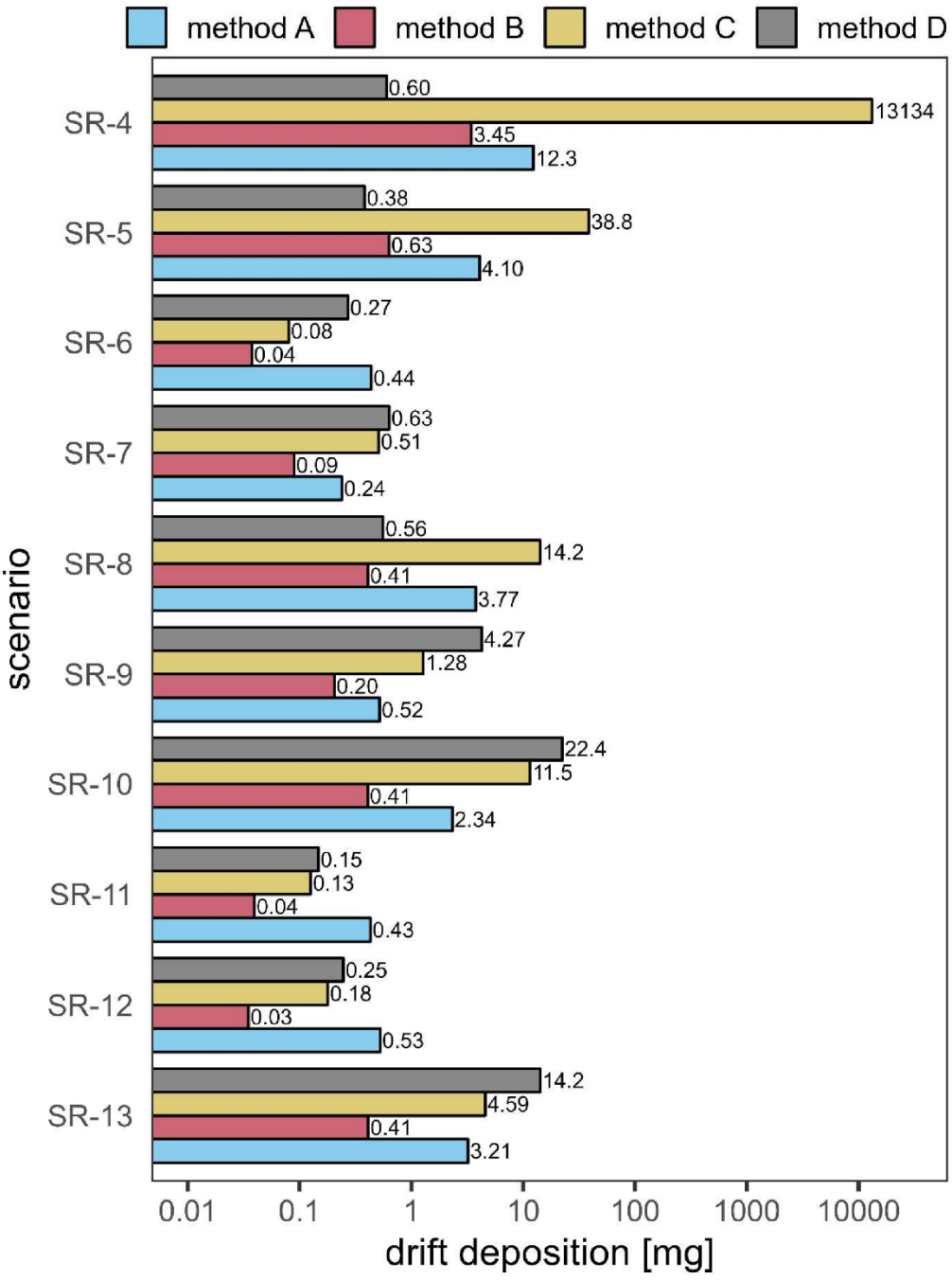


Figure S 7: Spray drift deposition (mg) onto surface waterbodies using the four prediction methods for the 10 scenarios (Figure 1) for the TTI spry nozzle, with prediction method A in blue, prediction method B in red, prediction method C in yellow, and prediction method D in grey.

110

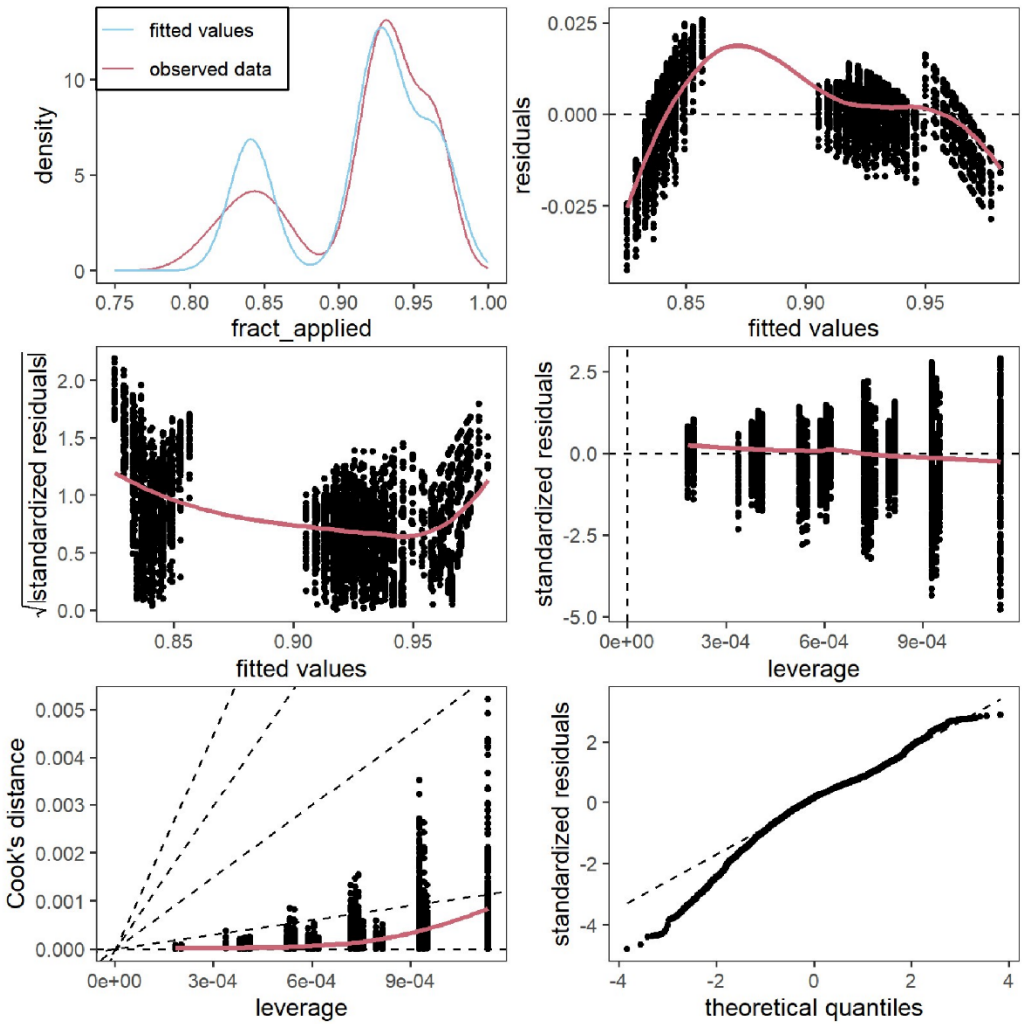


Figure S 8: Model diagnostics for the MLR predicting in-field deposition; top left: posterior prediction check, lines of observed and fitted values should overlap; top right: check for linearity, a linear relationship between predictors and outcome is indicated by a flat horizontal line; middle left: check for homogeneity of variance of the residuals, a constant variance of the residuals (homoscedasticity) is indicated by a horizontal line with equally spread points; middle right: check for influential observations, an influential data point is indicated by a high leverage value, a high standardized residual, and large distance to other data points; bottom left: check for influential observations, relating leverage to Cook's distance with points along the dashed lines having similar influence on the model; bottom right: check for normality of residuals, normal distribution of residuals is indicated by the point following a straight line.

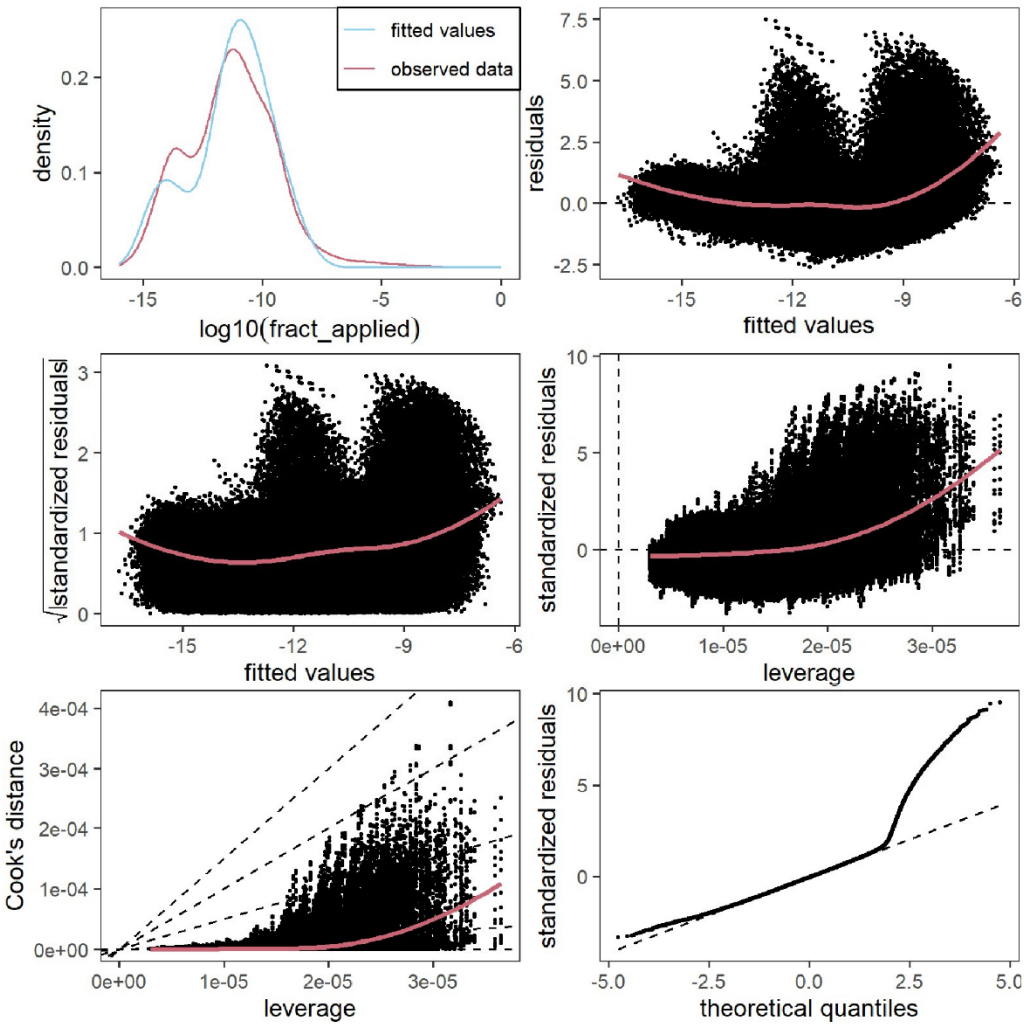


Figure S 9: Model diagnostics for the MLR predicting natural logarithm scaled spray drift depositions on non-target areas; top left: posterior prediction check, lines of observed and fitted values should overlap; top right: check for linearity, a linear relationship between predictors and outcome is indicated by a flat horizontal line; middle left: check for homogeneity of variance of the residuals, a constant variance of the residuals (homoscedasticity) is indicated by a horizontal line with equally spread points; middle right: check for influential observations, an influential data point is indicated by a high leverage value, a high standardized residual, and large distance to other data points; bottom left: check for influential observations, relating leverage to Cook's distance with points along the dashed lines having similar influence on the model; bottom right: check for normality of residuals, normal distribution of residuals is indicated by the point following a straight line.

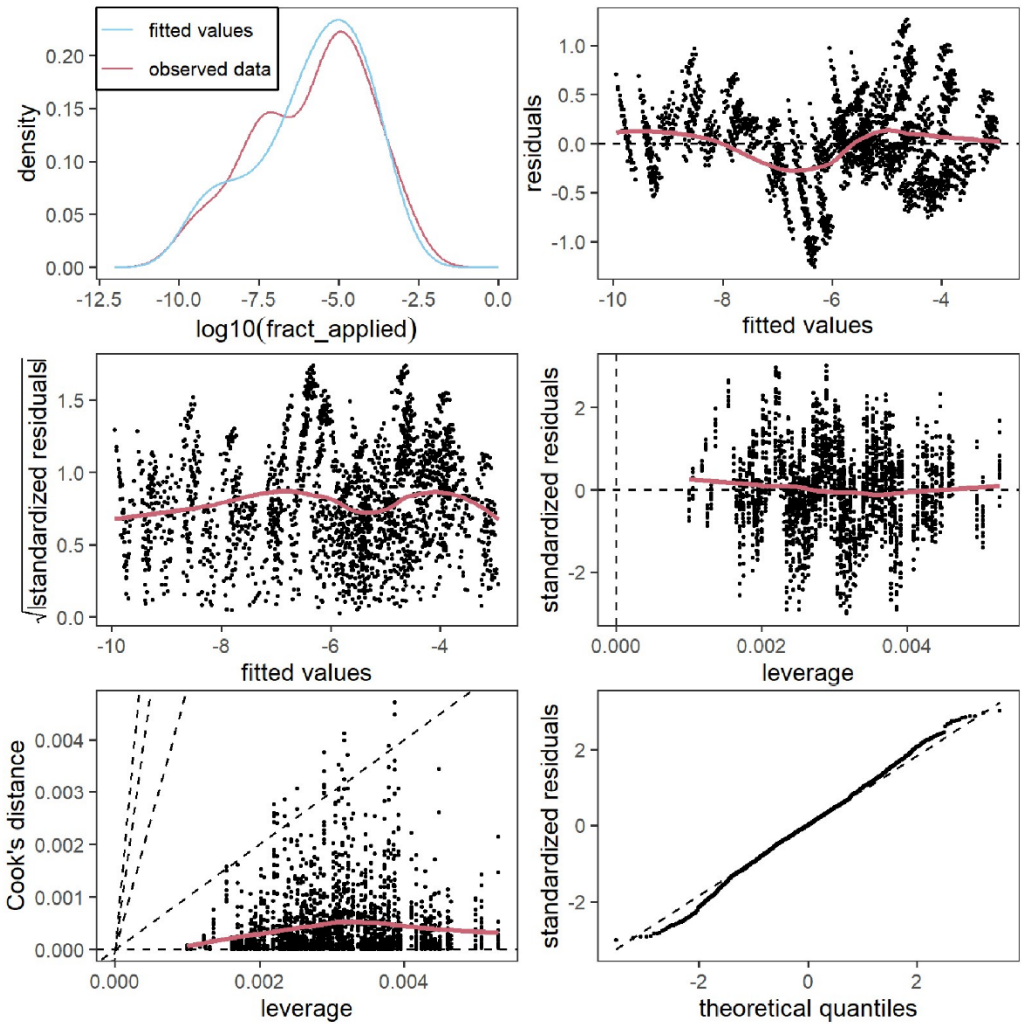


Figure S 10: Model diagnostics for the MLR predicting natural logarithm scaled spray drift depositions on non-target areas for the close distance (0-120m); top left: posterior prediction check, lines of observed and fitted values should overlap; top right: check for linearity, a linear relationship between predictors and outcome is indicated by a flat horizontal line; middle left: check for homogeneity of variance of the residuals, a constant variance of the residuals (homoscedasticity) is indicated by a horizontal line with equally spread points; middle right: check for influential observations, an influential data point is indicated by a high leverage value, a high standardized residual, and large distance to other data points; bottom left: check for influential observations, relating leverage to Cook's distance with points along the dashed lines having similar influence on the model; bottom right: check for normality of residuals, normal distribution of residuals is indicated by the point following a straight line.

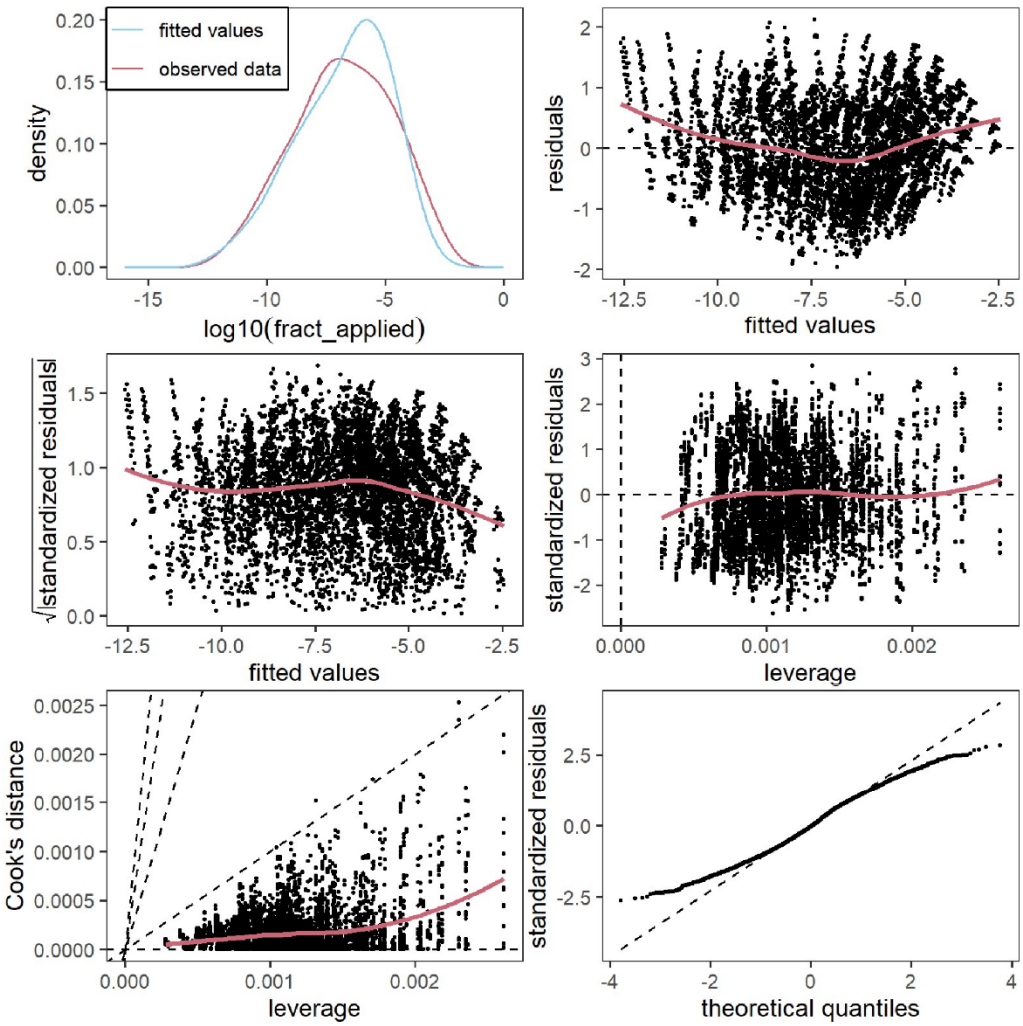
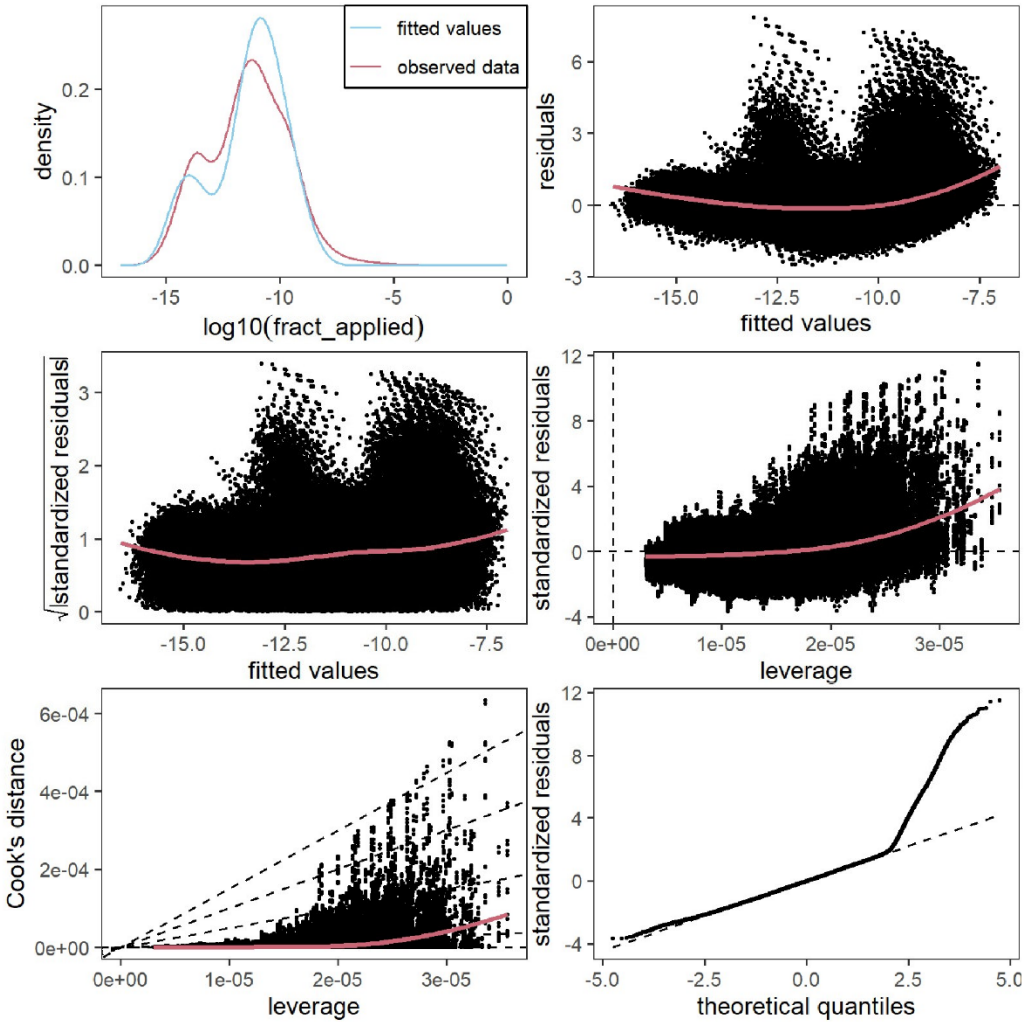


Figure S 11: Model diagnostics for the MLR predicting natural logarithm scaled spray drift depositions on non-target areas for the medium distance (120-180m); top left: posterior prediction check, lines of observed and fitted values should overlap; top right: check for linearity, a linear relationship between predictors and outcome is indicated by a flat horizontal line; middle left: check for homogeneity of variance of the residuals, a constant variance of the residuals (homoscedasticity) is indicated by a horizontal line with equally spread points; middle right: check for influential observations, an influential data point is indicated by a high leverage value, a high standardized residual, and large distance to other data points; bottom left: check for influential observations, relating leverage to Cook's distance with points along the dashed lines having similar influence on the model; bottom right: check for normality of residuals, normal distribution of residuals is indicated by the point following a straight line.



155 *Figure S 12: Model diagnostics for the MLR predicting natural logarithm scaled spray drift depositions on non-target areas for the far distance (> 180m); top left: posterior prediction check, lines of observed and fitted values should overlap; top right: check for linearity, a linear relationship between predictors and outcome is indicated by a flat horizontal line; middle left: check for homogeneity of variance of the residuals, a constant variance of the residuals (homoscedasticity) is indicated by a horizontal line with equally spread points; middle right: check for influential*
160 *observations, an influential data point is indicated by a high leverage value, a high standardized residual, and large distance to other data points; bottom left: check for influential observations, relating leverage to Cook's distance with points along the dashed lines having similar influence on the model; bottom right: check for normality of residuals, normal distribution of residuals is indicated by the point following a straight line.*

References

165 Fuchs, M., Gebler, S., Lorke, A., 2024. The droplet and atmospheric dispersion drift (DAD-drift) model – A modular approach for estimating spray drift at the landscape scale [Manuscript submitted for publication]. Inst. Environ. Sci. Univ. Kaiserslautern-Landau.

Appendix VI:

Evaluating Landscape-Level Pesticide Exposure from Spray Drift:

A Modeling Study in an Agriculture-Dominated Watershed Using SWAT+ and DAD-Drift

Mike Devin Fuchs [a,b,*], *Sebastian Gebler* [a], *Andreas Lorke* [b].

[a] BASF SE, Exposure Modelling, Speyerer Straße 2, 67117 Limburgerhof, Germany.

[b] Institute for Environmental Sciences, University of Kaiserslautern-Landau, Forststraße 7, 76829 Landau in der Pfalz, Germany

*Corresponding author.

E-mail: m.d.fuchs@protonmail.com (M. D. Fuchs)

Supplementary Material A

Tables

Table S 1: Pesticide.pes input file containing the physio-chemical properties of the defined active ingredients.

	F1	F2	H1	H2	H3	H4	H5
Soil Adsorption Coefficient [(mg/kg)/(mg/L)]	2000	10000	500	10	200	75	150
Washoff Fraction [-]	0.3	0.1	0.2	0.2	0.4	0.5	0.1
Foliage Halflife [days]	1	18	10	5	5	8	10
Soil Halflife [days]	3	35	20	10	10	15	20
Solubility [mg/L]	275	2	45	40	1600	3500	10
Water Halflife [days]	1	1000	50	50	30	35	1000
Aquatic Volatilization Coefficient [m/day)	0	0	0	0	0	0	0
Molar Weight [g/mol]	350	375	350	450	280	450	210
Resuspension Velocity [m/day]	0	0	0	0	0	0	0
Setteling Velocity [m/day]	0	0	0	0	0	0	0
Depth of the active benthic layer [m/day]	0.3	0.3	0.3	0.3	0.3	0.3	0.3
Burial Velocity [m/day]	0	0	0	0	0	0	0
Benthic Halflife [days]	1000	25	100	50	1000	30	60
Plant Uptake [-/day]	0	0	0	0	0	0	0

30

Table S 2: Application dates as predicted by the pesticide application timer for each year-AI-crop combination, with application rates.

Year	DOY	Plant	AI	Application Rate [g/ha]	Application Date
2010	128	corn	H3	850	08.05.2010
2011	125	corn	H3	850	05.05.2011
2012	128	corn	H3	850	07.05.2012
2013	125	corn	H3	850	05.05.2013
2014	135	corn	H3	850	15.05.2014
2015	127	corn	H3	850	07.05.2015
2016	125	corn	H3	850	04.05.2016
2017	125	corn	H3	850	05.05.2017
2018	125	corn	H3	850	05.05.2018
2019	125	corn	H3	850	05.05.2019
2020	126	corn	H3	850	05.05.2020
2021	129	corn	H3	850	09.05.2021
2022	125	corn	H3	850	05.05.2022
2023	133	corn	H3	850	13.05.2023
2010	134	corn	H5	499.5	14.05.2010
2011	138	corn	H5	499.5	18.05.2011
2012	134	corn	H5	499.5	13.05.2012
2013	147	corn	H5	499.5	27.05.2013
2014	135	corn	H5	499.5	15.05.2014
2015	134	corn	H5	499.5	14.05.2015
2016	134	corn	H5	499.5	13.05.2016
2017	135	corn	H5	499.5	15.05.2017
2018	135	corn	H5	499.5	15.05.2018
2019	134	corn	H5	499.5	14.05.2019
2020	134	corn	H5	499.5	13.05.2020
2021	140	corn	H5	499.5	20.05.2021
2022	134	corn	H5	499.5	14.05.2022
2023	136	corn	H5	499.5	16.05.2023
2010	117	corn	H2	50	27.04.2010
2011	116	corn	H2	50	26.04.2011
2012	119	corn	H2	50	28.04.2012
2013	117	corn	H2	50	27.04.2013
2014	121	corn	H2	50	01.05.2014
2015	121	corn	H2	50	01.05.2015
2016	122	corn	H2	50	01.05.2016
2017	116	corn	H2	50	26.04.2017
2018	117	corn	H2	50	27.04.2018
2019	119	corn	H2	50	29.04.2019
2020	116	corn	H2	50	25.04.2020
2021	116	corn	H2	50	26.04.2021

Year	DOY	Plant	AI	Application Rate [g/ha]	Application Date
2022	116	corn	H2	50	26.04.2022
2023	116	corn	H2	50	26.04.2023
2010	140	corn	H4	45	20.05.2010
2011	140	corn	H4	45	20.05.2011
2012	140	corn	H4	45	19.05.2012
2013	147	corn	H4	45	27.05.2013
2014	140	corn	H4	45	20.05.2014
2015	141	corn	H4	45	21.05.2015
2016	140	corn	H4	45	19.05.2016
2017	141	corn	H4	45	21.05.2017
2018	140	corn	H4	45	20.05.2018
2019	141	corn	H4	45	21.05.2019
2020	140	corn	H4	45	19.05.2020
2021	140	corn	H4	45	20.05.2021
2022	150	corn	H4	45	30.05.2022
2023	140	corn	H4	45	20.05.2023
2010	176	corn	F1	125	25.06.2010
2011	178	corn	F1	125	27.06.2011
2012	178	corn	F1	125	26.06.2012
2013	181	corn	F1	125	30.06.2013
2014	176	corn	F1	125	25.06.2014
2015	176	corn	F1	125	25.06.2015
2016	186	corn	F1	125	04.07.2016
2017	176	corn	F1	125	25.06.2017
2018	176	corn	F1	125	25.06.2018
2019	176	corn	F1	125	25.06.2019
2020	176	corn	F1	125	24.06.2020
2021	176	corn	F1	125	25.06.2021
2022	176	corn	F1	125	25.06.2022
2023	176	corn	F1	125	25.06.2023
2010	286	wwht	H1	240	13.10.2010
2011	287	wwht	H1	240	14.10.2011
2012	292	wwht	H1	240	18.10.2012
2013	286	wwht	H1	240	13.10.2013
2014	287	wwht	H1	240	14.10.2014
2015	291	wwht	H1	240	18.10.2015
2016	286	wwht	H1	240	12.10.2016
2017	286	wwht	H1	240	13.10.2017
2018	286	wwht	H1	240	13.10.2018
2019	295	wwht	H1	240	22.10.2019
2020	287	wwht	H1	240	13.10.2020
2021	289	wwht	H1	240	16.10.2021
2022	291	wwht	H1	240	18.10.2022
2023	289	wwht	H1	240	16.10.2023

Year	DOY	Plant	AI	Application Rate [g/ha]	Application Date
2010	319	wwht	H2	50	15.11.2010
2011	315	wwht	H2	50	11.11.2011
2012	316	wwht	H2	50	11.11.2012
2013	315	wwht	H2	50	11.11.2013
2014	316	wwht	H2	50	12.11.2014
2015	315	wwht	H2	50	11.11.2015
2016	317	wwht	H2	50	12.11.2016
2017	318	wwht	H2	50	14.11.2017
2018	318	wwht	H2	50	14.11.2018
2019	318	wwht	H2	50	14.11.2019
2020	316	wwht	H2	50	11.11.2020
2021	315	wwht	H2	50	11.11.2021
2022	315	wwht	H2	50	11.11.2022
2023	326	wwht	H2	50	22.11.2023
2010	96	wwht	F2	200	06.04.2010
2011	96	wwht	F2	200	06.04.2011
2012	96	wwht	F2	200	05.04.2012
2013	97	wwht	F2	200	07.04.2013
2014	99	wwht	F2	200	09.04.2014
2015	97	wwht	F2	200	07.04.2015
2016	100	wwht	F2	200	09.04.2016
2017	96	wwht	F2	200	06.04.2017
2018	96	wwht	F2	200	06.04.2018
2019	96	wwht	F2	200	06.04.2019
2020	96	wwht	F2	200	05.04.2020
2021	98	wwht	F2	200	08.04.2021
2022	100	wwht	F2	200	10.04.2022
2023	98	wwht	F2	200	08.04.2023
2010	95	agrl	H1	240	05.04.2010
2011	95	agrl	H1	240	05.04.2011
2012	96	agrl	H1	240	05.04.2012
2013	94	agrl	H1	240	04.04.2013
2014	95	agrl	H1	240	05.04.2014
2015	94	agrl	H1	240	04.04.2015
2016	95	agrl	H1	240	04.04.2016
2017	94	agrl	H1	240	04.04.2017
2018	96	agrl	H1	240	06.04.2018
2019	96	agrl	H1	240	06.04.2019
2020	94	agrl	H1	240	03.04.2020
2021	94	agrl	H1	240	04.04.2021
2022	100	agrl	H1	240	10.04.2022
2023	94	agrl	H1	240	04.04.2023
2010	120	agrl	H2	50	30.04.2010
2011	120	agrl	H2	50	30.04.2011

Year	DOY	Plant	AI	Application Rate [g/ha]	Application Date
2012	120	agrl	H2	50	29.04.2012
2013	120	agrl	H2	50	30.04.2013
2014	121	agrl	H2	50	01.05.2014
2015	121	agrl	H2	50	01.05.2015
2016	122	agrl	H2	50	01.05.2016
2017	120	agrl	H2	50	30.04.2017
2018	121	agrl	H2	50	01.05.2018
2019	120	agrl	H2	50	30.04.2019
2020	126	agrl	H2	50	05.05.2020
2021	120	agrl	H2	50	30.04.2021
2022	120	agrl	H2	50	30.04.2022
2023	120	agrl	H2	50	30.04.2023
2010	136	agrl	F2	200	16.05.2010
2011	138	agrl	F2	200	18.05.2011
2012	138	agrl	F2	200	17.05.2012
2013	147	agrl	F2	200	27.05.2013
2014	136	agrl	F2	200	16.05.2014
2015	137	agrl	F2	200	17.05.2015
2016	137	agrl	F2	200	16.05.2016
2017	137	agrl	F2	200	17.05.2017
2018	137	agrl	F2	200	17.05.2018
2019	137	agrl	F2	200	17.05.2019
2020	136	agrl	F2	200	15.05.2020
2021	140	agrl	F2	200	20.05.2021
2022	138	agrl	F2	200	18.05.2022
2023	136	agrl	F2	200	16.05.2023
2010	283	rye	H1	240	10.10.2010
2011	287	rye	H1	240	14.10.2011
2012	283	rye	H1	240	09.10.2012
2013	286	rye	H1	240	13.10.2013
2014	283	rye	H1	240	10.10.2014
2015	283	rye	H1	240	10.10.2015
2016	283	rye	H1	240	09.10.2016
2017	285	rye	H1	240	12.10.2017
2018	283	rye	H1	240	10.10.2018
2019	295	rye	H1	240	22.10.2019
2020	287	rye	H1	240	13.10.2020
2021	289	rye	H1	240	16.10.2021
2022	283	rye	H1	240	10.10.2022
2023	283	rye	H1	240	10.10.2023
2010	305	rye	H2	50	01.11.2010
2011	303	rye	H2	50	30.10.2011
2012	305	rye	H2	50	31.10.2012
2013	303	rye	H2	50	30.10.2013

Year	DOY	Plant	AI	Application Rate [g/ha]	Application Date
2014	304	rye	H2	50	31.10.2014
2015	303	rye	H2	50	30.10.2015
2016	303	rye	H2	50	29.10.2016
2017	305	rye	H2	50	01.11.2017
2018	307	rye	H2	50	03.11.2018
2019	303	rye	H2	50	30.10.2019
2020	308	rye	H2	50	03.11.2020
2021	305	rye	H2	50	01.11.2021
2022	303	rye	H2	50	30.10.2022
2023	326	rye	H2	50	22.11.2023
2010	92	rye	F2	200	02.04.2010
2011	91	rye	F2	200	01.04.2011
2012	91	rye	F2	200	31.03.2012
2013	91	rye	F2	200	01.04.2013
2014	91	rye	F2	200	01.04.2014
2015	93	rye	F2	200	03.04.2015
2016	91	rye	F2	200	31.03.2016
2017	92	rye	F2	200	02.04.2017
2018	96	rye	F2	200	06.04.2018
2019	91	rye	F2	200	01.04.2019
2020	91	rye	F2	200	31.03.2020
2021	91	rye	F2	200	01.04.2021
2022	92	rye	F2	200	02.04.2022
2023	93	rye	F2	200	03.04.2023

35

Table S 3: DAD-drift model inputs adapted from the TeeJet XR11003 nozzle scenario previously parameterized (Fuchs et al., 2024).

Parameter Name	F1	F2	H1	H2	H3	H4	H5
Application Parameters							
tractor_speed				2.6			
boom_width				30.5			
boom_height	1.6	1.6	0.6	0.6	0.6	0.6	0.6
nozzle_angle				0			
application_pres				275.8			
app_rate_mha				-99			
app_rate_kgha	0.125	0.200	0.240	0.050	0.850	0.045	0.4995
swath_number				-99			
field_length				-99			
Formulation Parameters							
AI_density	1300	1300	1300	1700	1200	1400	1100
AI_molar_mass	350	375	350	450	280	450	210
AI_vapor_pressure	1e-7	1e-8	1e-6	1e-7	1e-3	1e-10	1e-4
sol_concentration	125	150	400	500	280	30	250
Environmental Conditions							
temperature	Based on weather conditions during application						
humidity	Based on weather conditions during application						
wind_speed	Based on weather conditions during application						
wind_height	10						
wind_direction	Based on weather conditions during application						
ambient_pressure	100.0						
Calibration Parameters							
sigma_horizontal				1.05			
sigma_vertical				0.22			
roughness_height				0.05			
canopy_height	1.0	1.0	0.025	0.025	0.025	0.025	0.025
LAI	2.5	2.5	0.5	0.5	0.5	0.5	0.5
Controle Parameters							
mode				0			
depostion_height				0			
max_dist				1000			

40

Table S 4: Inputs of the global sensitivity analysis (GSA) after Sobol, with the parameter name, the associated input file, the lower and upper limits, and the type of change.

Parameter Name	Input File	Lower Limit	Upper Limit	Unit	Type of Change	Description
alb	soils.sol	-50	50	-	percent change	moist soil albedo of the top layer
alpha_bf	aquifer.aqu	0	1	1/days	absolute value	baseflow alpha factor
awc	soils.sol	-50	50	mm/mm	percent change	soil available water content
bd	soils.sol	-50	50	g/cm³	percent change	soil bulk density
bio_mix	hydrology.hyd	0	1	-	absolute value	biological mixing efficiency
can_max	hydrology.hyd	0	100	mm	absolute value	maximum canopy storage
clay_soil	soils.sol	-50	50	%	percent change	soil clay content
cn	cntable.lum	-50	0	-	percent change	condition II Curve Number
cn3_swf	hydrology.hyd	0	0.99	-	absolute value	soil water adjustment factor for CN3
d50	hyd-sed-lte.cha	-50	50	mm	percent change	median particle size of suspended and benthic sediment
dep_bot	aquifer.aqu	0	10	m	absolute value	depth from mid-slope surface to bottom of aquifer
dep_wt	aquifer.aqu	0	10	m	absolute value	depth from mid-slope surface to initial water table
dp	hyd-sed-lte.cha	-50	50	m	percent change	channel depth
dp_tile	tiledrain.str	500	1500	mm	absolute value	tile drainage depth
drain	tiledrain.str	1	51	mm/day	absolute value	drainage coefficient
epco	hydrology.hyd	0.01	1	-	absolute value	plant uptake compensation factor
erod_fact	hyd-sed-lte.cha	0.001	0.1	-	absolute value	channel erodibility factor
esco	hydrology.hyd	0.01	1	-	absolute value	soil evaporation compensation factor
fall_tmp	snow.sno	-5	5	°C	absolute value	snowfall temperature
flo_min	aquifer.aqu	0	10	m	absolute value	threshold depth from surface to water table for groundwater flow to occur
frac_dc_imp	urban.urb	-99	5	-	percent change	fraction of directly connected impervious area in urban land type
gw_flo	aquifer.aqu	0	2	mm	absolute value	initial groundwater flow
lag	tiledrain.str	0	100	hours	absolute value	drain tile lag time
lat_len	topography.hyd	-75	75	m	percent change	average slope length for lateral subsurface flow
lat_ttime	hydrology.hyd	0	180	days	absolute value	lateral flow travel time
latq_co	hydrology.hyd	0.05	1	-	absolute value	lateral flow coefficient
len	hyd-sed-lte.cha	-50	50	km	percent change	channel length
mann	hyd-sed-lte.cha	0.001	0.1	-	absolute value	manning's roughness coefficient

Parameter Name	Input File	Lower Limit	Upper Limit	Unit	Type of Change	Description
melt_max	snow.sno	0	10	mm(H2O)/dayºC	absolute value	melt factor for snow on 21.07.
melt_min	snow.sno	0	10	mm(H2O)/dayºC	absolute value	melt factor for snow on 21.12.
melt_tmp	snow.sno	-5	5	°C	absolute value	snow melt base temperature
ovn	ovn_table.lum	-50	50	-	percent change	overland flow Manning's n value
perco	hydrology.hyd	0	1	-	absolute value	percolation coefficient
rchg_dp	aquifer.aqu	0	1	-	absolute value	percolation coefficient from shallow to deep aquifer
revap_min	aquifer.aqu	0	10	m	absolute value	threshold depth from surface to water table for revap to occur
side_slp	hyd-sed-lte.cha	-50	50	m/m	percent change	channel side slope
slp	hyd-sed-lte.cha	-50	50	m/m	percent change	channel slope
slp_topo	topography.hyd	-75	75	m/m	percent change	average slope steepness
snow_h2o	snow.sno	0	500	mm	absolute value	minimum snow water content
soil_k	soils.sol	-50	50	mm/hr	percent change	soil saturated hydraulic conductivity
surq_lag	parameters.bsn	1	24	-	absolute value	surface runoff lag coefficient
sw_init	parameters.bsn	0	1	-	absolute value	initial soil water content
wd	hyd-sed-lte.cha	-50	50	m	percent change	channel width

Table S 5: List of parameters used for model parameterization, with parameter name, related input file, lower and upper limits, and type of change applied.

Parameter Name	Input File	Lower Limit	Upper Limit	Units	Type of Change	Description
alpha_bf	aquifer.aqu	0	1	1/days	absolute value	baseflow alpha factor
awc	soils.sol	-10	10	mm/mm	percent change	soil available water content
bd	soils.sol	-10	10	g/cm³	percent change	soil bulk density
can_max	hydrology.hyd	0	5	mm	absolute value	maximum canopy storage
d50	hyd-sed-lte.cha	-50	50	mm	percent change	median particle size of suspended and benthic sediment
dep_bot	aquifer.aqu	0	10	m	absolute value	depth from mid-slope surface to bottom of aquifer
dp_tile	tiledrain.str	600	1200	mm	absolute value	tile drainage depth
epco	hydrology.hyd	0.01	0.75	-	absolute value	plant uptake compensation factor
esco	hydrology.hyd	0.01	0.5	-	absolute value	soil evaporation compensation factor
fall_tmp	snow.sno	1	4	°C	absolute value	snowfall temperature
flo_min	aquifer.aqu	0	10	m	absolute value	threshold depth from surface to water table for groundwater flow to occur
lag	tiledrain.str	25	75	hours	absolute value	drain tile lag time
lat_len	topography.hyd	-50	50	m	percent change	average slope length for lateral subsurface flow
mann	hyd-sed-lte.cha	0.001	0.1	-	absolute value	manning's roughness coefficient
melt_tmp	snow.sno	0	5	°C	absolute value	snow melt base temperature
perco	hydrology.hyd	0	1	-	absolute value	percolation coefficient
snow_h2o	snow.sno	0	200	mm	absolute value	minimum snow water content
soil_k	soils.sol	-10	10	mm/hr	percent change	soil saturated hydraulic conductivity
surq_lag	parameters.bsn	1	24	-	absolute value	surface runoff lag coefficient

Table S 6: Summary of the weather conditions such as solar radiation, temperature, precipitation, and humidity for the Funne catchment, for the total period, the validation period, and the parameterization period.

Period	Years	Solar Radiation [MJ/m²/d]	Temperature [°C]	Humidity [%]	Precipitation [mm]			
total	2013 - 2021	10.6	10.9	78.9%	690.1	690.5	697.2	687.7
validation	2013, 2015, 2019, 2020	10.4	10.9	78.0%	690.4	691.0	700.2	688.2
parametrization	2014, 2016, 2017, 2018, 2021	10.7	10.9	79.5%	689.8	690.2	694.9	687.2

Table S 7: Annual weather conditions such as solar radiation, temperature, precipitation, and humidity for the Funne catchment from 2013 until 2023.

Year	Solar Radiation [MJ/m²/d]	Temperature [°C]	Humidity [%]	Precipitation [mm]			
2013	9.7	9.7	80.4%	657.5	649.5	664.0	640.9
2014	9.9	11.5	81.1%	777.9	779.6	786.9	778.7
2015	10.0	11.0	80.3%	786.0	784.0	816.1	789.5
2016	10.7	10.7	80.9%	680.9	672.4	688.2	657.9
2017	10.4	10.8	80.4%	775.1	786.4	779.5	793.5
2018	11.9	11.5	73.4%	502.3	512.5	511.9	511.0
2019	10.8	11.2	75.3%	670.5	667.8	677.6	683.8
2020	11.2	11.5	76.1%	647.6	662.7	643.0	638.8
2021	10.4	10.2	81.8%	712.7	700.0	707.9	695.1

Table S 8: Parameter sensitivities resulting from the global sensitivity analysis (GSA) after Sobol, for each model parameter and the two performance metrics Nash-Sutcliff efficiency (NSE) and the Kling-Gupta efficiency (KGE).

Parameter	Metric	Sensitivity	Original	Bias	Standard Error	Lower Confidence Interval	Higher Confidence Interval
alb	NSE	Si	2.27E-02	-2.22E-03	3.01E-02	-3.41E-02	8.40E-02
alpha_bf	NSE	Si	2.19E-02	-2.14E-03	3.01E-02	-3.51E-02	8.31E-02
awc	NSE	Si	6.59E-02	-4.58E-03	3.09E-02	9.98E-03	1.31E-01
bd	NSE	Si	5.65E-02	-2.08E-04	3.14E-02	-4.77E-03	1.18E-01
bio_mix	NSE	Si	2.27E-02	-2.21E-03	3.02E-02	-3.43E-02	8.41E-02
can_max	NSE	Si	3.42E-02	1.44E-04	2.82E-02	-2.12E-02	8.94E-02
clay_soil	NSE	Si	3.69E-02	-3.04E-03	3.10E-02	-2.08E-02	1.01E-01
cn	NSE	Si	3.69E-02	-1.84E-03	3.10E-02	-2.21E-02	9.95E-02
cn3_swf	NSE	Si	3.46E-02	-1.88E-03	3.19E-02	-2.62E-02	9.91E-02
d50	NSE	Si	5.48E-02	-2.25E-03	3.06E-02	-2.95E-03	1.17E-01
dep_bot	NSE	Si	3.64E-02	-2.24E-03	3.02E-02	-2.04E-02	9.78E-02
dep_wt	NSE	Si	2.21E-02	-2.62E-03	2.99E-02	-3.38E-02	8.33E-02
dp	NSE	Si	3.70E-02	-3.12E-03	2.99E-02	-1.85E-02	9.88E-02
dp_tile	NSE	Si	2.22E-01	-3.58E-03	3.57E-02	1.55E-01	2.95E-01
drain	NSE	Si	4.45E-02	-1.26E-03	3.00E-02	-1.31E-02	1.05E-01
epco	NSE	Si	4.55E-02	-1.96E-03	3.17E-02	-1.48E-02	1.10E-01
erod_fact	NSE	Si	2.63E-02	-2.49E-03	3.30E-02	-3.59E-02	9.35E-02
esco	NSE	Si	3.58E-02	-2.49E-03	2.96E-02	-1.97E-02	9.63E-02
fall_tmp	NSE	Si	8.89E-02	-1.52E-04	2.84E-02	3.33E-02	1.45E-01
flo_min	NSE	Si	3.82E-02	-2.50E-03	3.21E-02	-2.22E-02	1.04E-01
frac_dc_imp	NSE	Si	2.63E-02	-2.51E-03	3.06E-02	-3.11E-02	8.87E-02
gw_flo	NSE	Si	2.25E-02	-2.20E-03	3.02E-02	-3.44E-02	8.39E-02
lag	NSE	Si	3.87E-02	-1.01E-03	3.02E-02	-1.95E-02	9.89E-02
lat_len	NSE	Si	2.93E-02	-2.66E-03	3.02E-02	-2.74E-02	9.12E-02
lat_ttime	NSE	Si	2.72E-02	-2.04E-03	3.04E-02	-3.03E-02	8.88E-02
latq_co	NSE	Si	2.22E-02	-1.69E-03	2.98E-02	-3.46E-02	8.24E-02
len	NSE	Si	2.89E-02	-2.31E-03	3.02E-02	-2.79E-02	9.03E-02
mann	NSE	Si	5.25E-02	-6.85E-04	2.66E-02	1.17E-03	1.05E-01
melt_max	NSE	Si	2.09E-02	-1.70E-04	2.82E-02	-3.43E-02	7.64E-02
melt_min	NSE	Si	3.37E-02	-1.91E-03	2.91E-02	-2.15E-02	9.27E-02
melt_tmp	NSE	Si	2.94E-02	-1.84E-03	3.05E-02	-2.85E-02	9.09E-02
ovn	NSE	Si	2.34E-02	-2.05E-03	3.02E-02	-3.37E-02	8.45E-02
perco	NSE	Si	4.36E-02	-4.26E-04	3.23E-02	-1.93E-02	1.07E-01
rchg_dp	NSE	Si	2.35E-02	-1.26E-03	3.19E-02	-3.77E-02	8.73E-02
revap_min	NSE	Si	2.00E-02	-1.66E-03	3.05E-02	-3.80E-02	8.14E-02
side_slp	NSE	Si	6.47E-02	-1.85E-03	3.01E-02	7.54E-03	1.25E-01
slp	NSE	Si	6.07E-02	-3.17E-03	3.01E-02	4.83E-03	1.23E-01
slp_topo	NSE	Si	2.74E-02	-2.91E-03	3.09E-02	-3.03E-02	9.09E-02
snow_h2o	NSE	Si	6.20E-02	-3.01E-03	2.77E-02	1.08E-02	1.19E-01
soil_k	NSE	Si	2.66E-02	-2.17E-03	3.00E-02	-3.01E-02	8.76E-02
surq_lag	NSE	Si	1.92E-02	-2.17E-03	3.00E-02	-3.74E-02	8.02E-02

Parameter	Metric	Sensitivity	Original	Bias	Standard Error	Lower Confidence Interval	Higher Confidence Interval
sw_init	NSE	Si	2.53E-02	-2.47E-03	3.01E-02	-3.12E-02	8.67E-02
wd	NSE	Si	3.37E-02	-2.94E-03	3.11E-02	-2.42E-02	9.76E-02
alb	NSE	Ti	1.23E-05	8.97E-08	5.99E-06	5.07E-07	2.40E-05
alpha_bf	NSE	Ti	1.86E-03	-2.90E-05	3.07E-04	1.28E-03	2.49E-03
awc	NSE	Ti	9.11E-02	-4.03E-04	6.03E-03	7.97E-02	1.03E-01
bd	NSE	Ti	1.78E-01	4.42E-04	1.36E-02	1.51E-01	2.04E-01
bio_mix	NSE	Ti	3.53E-05	3.34E-07	6.91E-06	2.15E-05	4.86E-05
can_max	NSE	Ti	2.95E-02	2.92E-04	2.93E-03	2.35E-02	3.49E-02
clay_soil	NSE	Ti	1.72E-02	-2.32E-04	2.42E-03	1.27E-02	2.22E-02
cn	NSE	Ti	3.28E-02	3.19E-04	3.06E-03	2.65E-02	3.85E-02
cn3_swf	NSE	Ti	5.96E-02	8.17E-04	5.80E-03	4.74E-02	7.02E-02
d50	NSE	Ti	5.78E-02	-1.82E-05	5.31E-03	4.75E-02	6.83E-02
dep_bot	NSE	Ti	2.03E-02	-1.18E-04	3.78E-03	1.30E-02	2.78E-02
dep_wt	NSE	Ti	3.31E-03	-3.74E-06	1.02E-03	1.32E-03	5.32E-03
dp	NSE	Ti	1.32E-02	-1.76E-04	1.71E-03	1.00E-02	1.67E-02
dp_tile	NSE	Ti	2.89E-01	-1.42E-03	1.84E-02	2.54E-01	3.26E-01
drain	NSE	Ti	2.15E-02	1.11E-05	2.50E-03	1.66E-02	2.64E-02
epco	NSE	Ti	3.44E-02	1.79E-04	3.15E-03	2.80E-02	4.04E-02
erod_fact	NSE	Ti	5.27E-02	-2.31E-05	5.85E-03	4.12E-02	6.41E-02
esco	NSE	Ti	1.60E-02	-7.84E-05	1.64E-03	1.29E-02	1.93E-02
fall_tmp	NSE	Ti	8.79E-02	4.41E-04	6.62E-03	7.44E-02	1.00E-01
flo_min	NSE	Ti	3.22E-02	5.76E-04	5.23E-03	2.13E-02	4.18E-02
frac_dc_imp	NSE	Ti	8.40E-03	-1.10E-05	6.90E-04	7.05E-03	9.76E-03
gw_flo	NSE	Ti	7.79E-06	-2.69E-07	2.77E-06	2.62E-06	1.35E-05
lag	NSE	Ti	2.84E-02	-1.23E-05	2.41E-03	2.37E-02	3.31E-02
lat_len	NSE	Ti	7.73E-03	1.28E-04	1.32E-03	5.02E-03	1.02E-02
lat_ttime	NSE	Ti	6.95E-03	1.35E-04	1.56E-03	3.77E-03	9.87E-03
latq_co	NSE	Ti	8.26E-03	2.05E-04	1.06E-03	5.98E-03	1.01E-02
len	NSE	Ti	3.26E-02	5.77E-04	2.98E-03	2.62E-02	3.79E-02
mann	NSE	Ti	7.58E-02	9.43E-04	7.45E-03	6.02E-02	8.95E-02
melt_max	NSE	Ti	4.54E-02	6.92E-04	5.04E-03	3.48E-02	5.46E-02
melt_min	NSE	Ti	1.52E-02	3.93E-04	2.83E-03	9.22E-03	2.03E-02
melt_tmp	NSE	Ti	1.96E-02	3.62E-04	2.41E-03	1.45E-02	2.39E-02
ovn	NSE	Ti	2.48E-04	-5.69E-06	3.84E-05	1.78E-04	3.29E-04
perco	NSE	Ti	6.10E-02	6.44E-04	6.21E-03	4.82E-02	7.26E-02
rchg_dp	NSE	Ti	2.18E-02	-8.00E-05	2.99E-03	1.60E-02	2.77E-02
revap_min	NSE	Ti	1.68E-03	-2.99E-05	4.90E-04	7.51E-04	2.67E-03
side_slp	NSE	Ti	3.61E-02	2.00E-04	4.49E-03	2.71E-02	4.47E-02
slp	NSE	Ti	1.13E-01	1.90E-04	8.97E-03	9.48E-02	1.30E-01
slp_topo	NSE	Ti	4.62E-03	1.93E-04	8.84E-04	2.70E-03	6.16E-03
snow_h2o	NSE	Ti	5.78E-02	1.78E-04	5.69E-03	4.65E-02	6.88E-02
soil_k	NSE	Ti	4.72E-03	7.66E-05	6.07E-04	3.45E-03	5.83E-03
surq_lag	NSE	Ti	3.70E-03	2.20E-05	5.63E-04	2.58E-03	4.78E-03

Parameter	Metric	Sensitivity	Original	Bias	Standard Error	Lower Confidence Interval	Higher Confidence Interval
sw_init	NSE	Ti	1.26E-03	2.76E-05	3.26E-04	5.88E-04	1.87E-03
wd	NSE	Ti	1.47E-02	9.18E-05	1.60E-03	1.15E-02	1.78E-02
alb	KGE	Si	2.13E-02	1.26E-03	3.15E-02	-4.17E-02	8.19E-02
alpha_bf	KGE	Si	1.87E-02	1.12E-03	3.19E-02	-4.48E-02	8.01E-02
awc	KGE	Si	8.94E-02	1.19E-03	2.88E-02	3.17E-02	1.45E-01
bd	KGE	Si	1.07E-01	2.59E-03	3.56E-02	3.43E-02	1.74E-01
bio_mix	KGE	Si	2.14E-02	1.26E-03	3.16E-02	-4.17E-02	8.20E-02
can_max	KGE	Si	3.52E-02	1.64E-03	3.16E-02	-2.83E-02	9.55E-02
clay_soil	KGE	Si	3.79E-02	8.63E-04	3.21E-02	-2.58E-02	1.00E-01
cn	KGE	Si	2.33E-02	3.64E-04	3.19E-02	-3.96E-02	8.55E-02
cn3_swf	KGE	Si	2.96E-02	7.64E-04	3.37E-02	-3.72E-02	9.48E-02
d50	KGE	Si	3.93E-02	7.63E-04	3.24E-02	-2.49E-02	1.02E-01
dep_bot	KGE	Si	4.24E-02	2.40E-03	3.26E-02	-2.39E-02	1.04E-01
dep_wt	KGE	Si	2.04E-02	7.17E-04	3.10E-02	-4.11E-02	8.04E-02
dp	KGE	Si	2.70E-02	1.59E-03	3.14E-02	-3.62E-02	8.69E-02
dp_tile	KGE	Si	3.42E-01	-6.34E-03	3.12E-02	2.87E-01	4.10E-01
drain	KGE	Si	2.67E-02	-5.06E-04	3.17E-02	-3.49E-02	8.93E-02
epco	KGE	Si	5.93E-02	1.17E-03	3.23E-02	-5.13E-03	1.21E-01
erod_fact	KGE	Si	1.65E-02	2.71E-04	3.14E-02	-4.54E-02	7.79E-02
esco	KGE	Si	3.68E-02	1.07E-03	3.09E-02	-2.48E-02	9.62E-02
fall_tmp	KGE	Si	6.54E-02	2.69E-03	2.87E-02	6.48E-03	1.19E-01
flo_min	KGE	Si	5.04E-02	-1.20E-03	3.17E-02	-1.05E-02	1.14E-01
frac_dc_imp	KGE	Si	2.45E-02	1.11E-03	3.11E-02	-3.77E-02	8.44E-02
gw_flo	KGE	Si	2.14E-02	1.29E-03	3.15E-02	-4.17E-02	8.18E-02
lag	KGE	Si	3.75E-02	6.76E-04	3.19E-02	-2.57E-02	9.93E-02
lat_len	KGE	Si	2.21E-02	1.80E-03	3.19E-02	-4.23E-02	8.29E-02
lat_ttime	KGE	Si	2.57E-02	1.31E-03	3.26E-02	-3.94E-02	8.82E-02
latq_co	KGE	Si	1.60E-02	1.66E-03	3.29E-02	-5.02E-02	7.89E-02
len	KGE	Si	2.23E-02	5.53E-04	3.11E-02	-3.93E-02	8.27E-02
mann	KGE	Si	2.09E-02	3.71E-04	3.17E-02	-4.16E-02	8.26E-02
melt_max	KGE	Si	1.50E-02	1.96E-03	3.11E-02	-4.79E-02	7.40E-02
melt_min	KGE	Si	2.82E-02	1.24E-03	3.20E-02	-3.58E-02	8.97E-02
melt_tmp	KGE	Si	2.10E-02	5.05E-04	3.20E-02	-4.23E-02	8.33E-02
ovn	KGE	Si	2.11E-02	1.27E-03	3.15E-02	-4.19E-02	8.16E-02
perco	KGE	Si	6.49E-02	1.01E-03	3.33E-02	-1.48E-03	1.29E-01
rchg_dp	KGE	Si	2.71E-02	3.07E-03	3.39E-02	-4.25E-02	9.05E-02
revap_min	KGE	Si	1.84E-02	1.45E-03	3.18E-02	-4.53E-02	7.93E-02
side_slp	KGE	Si	4.29E-02	1.51E-03	3.16E-02	-2.05E-02	1.03E-01
slp	KGE	Si	2.77E-02	2.19E-03	3.09E-02	-3.51E-02	8.61E-02
slp_topo	KGE	Si	2.30E-02	8.86E-04	3.19E-02	-4.04E-02	8.46E-02
snow_h2o	KGE	Si	5.00E-02	-3.23E-05	3.21E-02	-1.28E-02	1.13E-01
soil_k	KGE	Si	2.73E-02	1.48E-03	3.16E-02	-3.61E-02	8.79E-02
surq_lag	KGE	Si	2.19E-02	9.87E-04	3.18E-02	-4.14E-02	8.32E-02

Parameter	Metric	Sensitivity	Original	Bias	Standard Error	Lower Confidence Interval	Higher Confidence Interval
sw_init	KGE	Si	2.22E-02	1.24E-03	3.15E-02	-4.08E-02	8.28E-02
wd	KGE	Si	2.25E-02	1.72E-03	3.17E-02	-4.13E-02	8.30E-02
alb	KGE	Ti	2.35E-06	-7.58E-08	1.19E-06	9.68E-08	4.76E-06
alpha_bf	KGE	Ti	2.84E-03	-8.35E-06	7.21E-04	1.43E-03	4.26E-03
awc	KGE	Ti	1.25E-01	1.01E-03	8.14E-03	1.08E-01	1.40E-01
bd	KGE	Ti	1.72E-01	2.80E-03	1.19E-02	1.46E-01	1.93E-01
bio_mix	KGE	Ti	1.41E-05	-4.80E-08	2.14E-06	9.93E-06	1.83E-05
can_max	KGE	Ti	1.76E-02	2.46E-04	1.27E-03	1.49E-02	1.98E-02
clay_soil	KGE	Ti	1.46E-02	3.32E-04	1.90E-03	1.05E-02	1.80E-02
cn	KGE	Ti	1.26E-02	2.23E-04	1.69E-03	9.07E-03	1.57E-02
cn3_swf	KGE	Ti	2.69E-02	2.37E-04	2.98E-03	2.08E-02	3.25E-02
d50	KGE	Ti	1.92E-02	2.87E-04	1.85E-03	1.53E-02	2.26E-02
dep_bot	KGE	Ti	5.11E-02	-5.09E-04	5.76E-03	4.03E-02	6.29E-02
dep_wt	KGE	Ti	5.63E-03	2.41E-04	1.26E-03	2.91E-03	7.86E-03
dp	KGE	Ti	3.64E-03	1.32E-04	5.54E-04	2.42E-03	4.59E-03
dp_tile	KGE	Ti	3.49E-01	2.41E-04	1.75E-02	3.15E-01	3.84E-01
drain	KGE	Ti	1.33E-02	2.25E-04	2.19E-03	8.73E-03	1.73E-02
epco	KGE	Ti	4.63E-02	4.52E-04	3.90E-03	3.83E-02	5.35E-02
erod_fact	KGE	Ti	2.21E-02	4.83E-04	2.24E-03	1.72E-02	2.60E-02
esco	KGE	Ti	1.24E-02	-1.97E-05	1.11E-03	1.03E-02	1.46E-02
fall_tmp	KGE	Ti	7.81E-02	4.43E-04	7.10E-03	6.38E-02	9.16E-02
flo_min	KGE	Ti	8.34E-02	-3.25E-04	9.85E-03	6.45E-02	1.03E-01
frac_dc_imp	KGE	Ti	3.38E-03	5.72E-05	2.80E-04	2.77E-03	3.87E-03
gw_flo	KGE	Ti	7.18E-06	4.37E-07	4.33E-06	-1.75E-06	1.52E-05
lag	KGE	Ti	1.84E-02	1.68E-04	1.74E-03	1.49E-02	2.17E-02
lat_len	KGE	Ti	7.50E-03	-2.06E-05	9.03E-04	5.75E-03	9.29E-03
lat_ttime	KGE	Ti	5.76E-03	7.25E-05	8.80E-04	3.96E-03	7.41E-03
latq_co	KGE	Ti	7.90E-03	-2.71E-05	6.95E-04	6.57E-03	9.29E-03
len	KGE	Ti	8.88E-03	-1.47E-05	8.54E-04	7.23E-03	1.06E-02
mann	KGE	Ti	2.26E-02	1.52E-04	2.25E-03	1.80E-02	2.68E-02
melt_max	KGE	Ti	1.99E-02	9.69E-05	2.32E-03	1.53E-02	2.44E-02
melt_min	KGE	Ti	9.55E-03	9.16E-05	1.74E-03	6.05E-03	1.29E-02
melt_tmp	KGE	Ti	9.14E-03	1.63E-04	1.21E-03	6.61E-03	1.13E-02
ovn	KGE	Ti	8.82E-05	1.42E-06	1.45E-05	5.84E-05	1.15E-04
perco	KGE	Ti	7.10E-02	1.04E-03	7.82E-03	5.47E-02	8.53E-02
rchg_dp	KGE	Ti	4.15E-02	-4.61E-04	4.92E-03	3.23E-02	5.16E-02
revap_min	KGE	Ti	3.32E-03	-1.16E-06	3.97E-04	2.55E-03	4.10E-03
side_slp	KGE	Ti	1.39E-02	2.79E-04	1.50E-03	1.07E-02	1.65E-02
slp	KGE	Ti	4.53E-02	9.64E-04	3.38E-03	3.77E-02	5.09E-02
slp_topo	KGE	Ti	4.65E-03	7.01E-05	5.91E-04	3.43E-03	5.74E-03
snow_h2o	KGE	Ti	3.76E-02	5.19E-04	4.95E-03	2.74E-02	4.68E-02
soil_k	KGE	Ti	2.85E-03	2.94E-05	2.82E-04	2.27E-03	3.37E-03
surq_lag	KGE	Ti	1.30E-03	1.80E-05	1.98E-04	8.90E-04	1.67E-03

Parameter	Metric	Sensitivity	Original	Bias	Standard Error	Lower Confidence Interval	Higher Confidence Interval
sw_init	KGE	Ti	3.36E-04	1.10E-06	3.86E-05	2.60E-04	4.11E-04
wd	KGE	Ti	5.01E-03	1.31E-05	5.47E-04	3.92E-03	6.07E-03

Table S 9: Parameter values of the 20 ensembles.

Parameter Name	Run 1	Run 2	Run 3	Run 4	Run 5	Run 6	Run 7	Run 8	Run 9	Run 10
alpha_bf	0.94	0.25	0.17	0.04	0.31	0.85	0.59	0.37	0.10	0.19
awc	-4.62	2.81	-7.89	6.99	0.13	-8.01	-4.52	9.63	4.73	5.37
bd	7.37	7.23	7.65	2.21	9.40	8.81	7.65	3.56	6.42	1.77
can_max	0.14	0.44	0.21	0.24	0.26	0.58	0.78	0.92	0.02	0.03
d50	16.66	-12.61	-15.54	-24.16	36.98	40.69	-29.72	5.02	25.34	-25.04
dep_bot	9.66	3.85	2.56	8.19	1.35	3.36	9.29	6.45	3.39	5.25
dp_tile	973.90	791.58	693.00	783.21	730.82	796.22	1131.42	611.74	843.89	916.38
epco	0.64	0.35	0.06	0.16	0.74	0.09	0.05	0.17	0.20	0.35
esco	0.04	0.06	0.24	0.04	0.01	0.13	0.07	0.04	0.05	0.08
fall_tmp	1.61	2.00	2.39	2.38	2.38	1.61	2.05	1.74	2.75	2.41
flo_min	0.81	4.19	8.47	3.18	8.36	3.68	0.31	9.21	6.99	8.16
lag	61.11	51.33	31.19	34.41	51.46	60.19	48.45	32.48	51.96	30.07
lat_len	33.27	-33.98	-39.09	-35.59	-39.25	-44.27	13.88	-30.72	-47.39	-47.42
mann	0.03	0.08	0.06	0.01	0.01	0.06	0.07	0.05	0.05	0.03
melt_tmp	2.04	1.85	1.95	2.81	1.96	2.40	2.19	2.12	1.20	2.05
perco	0.08	0.01	0.64	0.65	0.15	0.01	0.80	0.66	0.49	0.39
snow_h2o	38.37	32.75	0.08	2.82	46.38	27.82	9.48	23.15	9.51	20.34
soil_k	8.00	7.00	-2.11	6.44	5.50	-2.96	-1.61	-3.44	2.33	5.98
surq_lag	5.03	15.76	18.34	13.51	5.61	20.88	13.45	17.54	16.56	14.96
Parameter Name	**Run 11**	**Run 12**	**Run 13**	**Run 14**	**Run 15**	**Run 16**	**Run 17**	**Run 18**	**Run 19**	**Run 20**
alpha_bf	0.59	0.52	0.82	0.35	0.89	0.33	0.59	0.13	0.43	0.37
awc	-8.30	-1.04	6.10	-9.50	-3.15	-9.52	9.83	8.52	0.48	-4.58
bd	6.95	6.18	6.11	9.35	5.05	8.71	6.67	1.11	-0.61	2.50
can_max	0.95	0.59	3.03	2.42	4.78	0.47	0.67	0.46	2.89	0.71
d50	-44.65	29.44	-17.66	37.37	9.67	6.91	-24.09	-21.41	-38.60	8.48
dep_bot	6.42	7.19	8.41	4.64	0.03	2.37	8.71	1.59	4.16	7.50
dp_tile	987.13	916.74	1032.73	864.67	863.33	850.61	798.87	802.49	746.51	702.28
epco	0.55	0.34	0.06	0.26	0.02	0.30	0.37	0.04	0.19	0.28
esco	0.05	0.01	0.07	0.01	0.38	0.04	0.11	0.17	0.06	0.11
fall_tmp	2.40	1.52	1.54	2.14	1.47	1.70	2.33	2.90	3.44	2.65
flo_min	7.22	7.44	5.45	3.29	6.97	5.75	9.09	1.11	2.40	5.76
lag	31.12	30.12	27.87	30.32	25.21	52.75	33.42	38.79	29.55	30.81
lat_len	33.24	-2.82	36.53	1.39	43.40	47.62	27.85	-2.59	7.34	29.96
mann	0.09	0.07	0.04	0.06	0.01	0.03	0.05	0.07	0.09	0.04
melt_tmp	2.95	2.98	2.13	1.07	1.55	0.79	1.57	1.66	2.20	2.06
perco	0.28	0.60	0.11	0.38	0.55	0.10	0.18	0.23	0.03	0.10
snow_h2o	3.80	11.30	19.96	27.17	45.74	34.52	30.06	15.47	24.77	1.69
soil_k	-3.46	8.77	-8.78	-5.75	2.16	6.13	-5.44	-9.60	-8.10	3.58
surq_lag	21.11	16.22	7.34	3.00	22.66	12.69	12.10	9.10	12.75	9.63

Table S 10: Model performance of the 20 ensemble runs when compared to the observed flow rates at the Selm-Ondrup station, for the parameterization period and the validation period, reported as Nash-Sutcliff efficiency (NSE), the percent bias (PBIAS), and the Kling-Gupta efficiency (KGE).

run number	parameterization period			validation period		
	NSE	KGE	PBIAS	NSE	KGE	PBIAS
1	0.79	0.83	0.1	0.79	0.84	12.6
2	0.78	0.82	2.1	0.80	0.82	15.1
3	0.78	0.83	3.5	0.66	0.69	25.6
4	0.78	0.82	0.2	0.78	0.83	11.7
5	0.78	0.77	8.7	0.79	0.74	21.5
6	0.78	0.82	7	0.72	0.70	27.2
7	0.78	0.81	6	0.66	0.71	23.8
8	0.78	0.82	5.3	0.78	0.78	18.9
9	0.78	0.77	4.2	0.78	0.78	18.2
10	0.78	0.81	0.6	0.79	0.82	13.4
11	0.73	0.86	1.3	0.71	0.78	14.9
12	0.77	0.85	7.3	0.76	0.76	20.4
13	0.71	0.85	5.3	0.51	0.61	23.8
14	0.75	0.84	1.9	0.74	0.80	15.1
15	0.72	0.84	-0.2	0.58	0.64	25.8
16	0.76	0.84	5.9	0.73	0.75	20.6
17	0.73	0.84	-5	0.76	0.86	6.4
18	0.76	0.84	-0.5	0.67	0.74	19
19	0.71	0.84	-1.7	0.73	0.83	9.5
20	0.74	0.84	-3.2	0.75	0.84	10.3

Table S 11: Summary of 100 annual PECmax values (20 ensemble and 5 years) of the seven active ingredients for the base and the drift setup.

AI	Setup	Minimum PECmax [ng/L]	Lower Quantile PECmax [ng/L]	Median PECmax [ng/L]	Mean PECmax [ng/L]	Upper Quantile PECmax [ng/L]	Maximum PECmax [ng/L]
F1	base	0.09	0.30	0.49	0.83	1.22	2.35
F1	drift	287.11	439.80	656.63	654.86	827.44	1088.66
F2	base	29.86	43.46	51.72	52.56	62.29	70.01
F2	drift	2453.66	3376.31	4478.86	4260.12	4729.47	5960.78
H1	base	99.55	118.35	168.92	225.62	224.56	919.94
H1	drift	737.83	837.26	922.91	970.70	1091.01	1461.39
H2	base	681.37	1573.34	2337.63	2544.02	2863.54	7474.03
H2	drift	789.36	1544.51	2306.93	2464.31	2628.49	6970.87
H3	base	258.96	487.21	550.44	579.76	722.15	804.38
H3	drift	1031.88	1229.19	1428.76	1390.45	1521.39	1769.80
H4	base	50.07	93.42	123.41	131.47	154.91	245.32
H4	drift	60.28	82.86	110.46	119.05	137.71	215.49
H5	base	864.08	1651.14	2116.67	2004.53	2352.43	3197.69
H5	drift	838.54	1509.60	1910.60	1849.09	2139.46	2886.83

70

Table S 12: Summary of 100 annual PEC90 values (20 ensemble and 5 years) of the seven active ingredients for the base and the drift setup.

AI	Setup	Minimum PECmax [ng/L]	Lower Quantile PECmax [ng/L]	Median PECmax [ng/L]	Mean PECmax [ng/L]	Upper Quantile PECmax [ng/L]	Maximum PECmax [ng/L]
F1	base	0.00	0.00	0.00	0.00	0.00	0.00
F1	drift	0.00	0.00	0.00	0.00	0.00	0.00
F2	base	0.08	0.11	0.16	0.16	0.19	0.27
F2	drift	16.89	20.57	21.51	21.79	23.15	28.96
H1	base	10.99	17.05	27.17	31.64	40.71	91.64
H1	drift	19.09	35.86	44.22	50.25	62.30	99.04
H2	base	30.58	59.57	85.44	85.86	102.74	203.87
H2	drift	42.87	71.78	94.33	96.30	114.14	199.08
H3	base	0.66	1.55	2.13	2.84	4.15	7.43
H3	drift	10.72	13.82	16.57	17.98	21.55	28.98
H4	base	0.63	1.22	1.63	1.89	2.41	3.99
H4	drift	1.87	2.94	3.55	4.11	4.97	9.54
H5	base	12.51	20.24	25.91	34.21	49.15	78.16
H5	drift	45.94	58.46	67.53	78.02	94.86	141.76

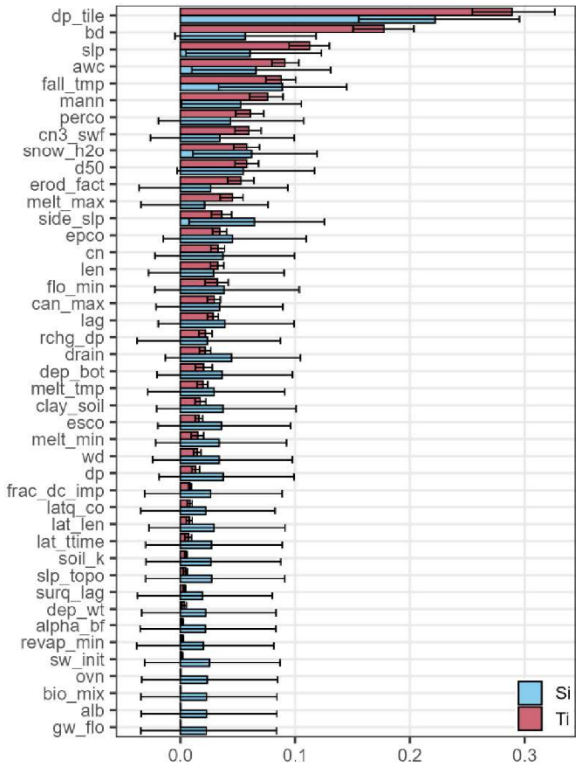
Table S 13: Total annual AI mass applied on HRUs in the catchment, for the base and drift setup, with the deposition onto the stream for the drift setup.

AI	Year	Applied Mass [kg]		Deposition on Stream [g]	Exported Mass [g]		Exported Mass [%]	
		base	drift		base	drift	base	drift
F1	2019	87.9	72.9	101.7	0.0	5.6	0.000	0.008
F1	2020	91.2	76.0	118.2	0.0	10.3	0.000	0.013
F1	2021	91.0	77.2	91.1	1.5	13.8	0.002	0.018
F1	2022	104.4	88.3	108.5	0.0	6.9	0.000	0.008
F1	2023	79.5	68.0	62.5	0.0	8.1	0.000	0.012
F2	2019	195.3	166.8	198.8	0.0	208.6	0.000	0.125
F2	2020	217.1	182.0	267.2	6.4	291.2	0.003	0.160
F2	2021	211.3	178.7	281.1	16.1	333.2	0.008	0.186
F2	2022	202.6	172.5	264.7	0.9	280.2	0.000	0.162
F2	2023	187.7	162.6	167.7	48.6	244.0	0.026	0.150
H1	2019	115.4	103.2	35.2	216.6	242.3	0.188	0.235
H1	2020	125.5	112.2	30.4	74.7	100.6	0.060	0.090
H1	2021	112.7	101.2	22.2	126.4	135.1	0.112	0.134
H1	2022	109.2	97.8	26.8	63.2	82.6	0.058	0.084
H1	2023	128.7	115.4	23.4	505.1	521.6	0.392	0.452
H2	2019	40.5	36.6	14.3	1947.9	1787.2	4.810	4.881
H2	2020	37.3	33.8	9.1	114.0	115.2	0.306	0.341
H2	2021	39.5	35.9	8.0	182.2	171.8	0.461	0.478
H2	2022	34.8	31.5	9.5	249.6	241.8	0.718	0.768
H2	2023	39.6	35.7	10.9	1928.9	1738.6	4.868	4.874
H3	2019	152.9	135.9	59.6	4.7	66.1	0.003	0.049
H3	2020	123.9	109.9	47.2	71.1	105.5	0.057	0.096
H3	2021	131.2	114.3	99.6	137.9	251.6	0.105	0.220
H3	2022	152.1	135.6	31.5	19.7	53.6	0.013	0.040
H3	2023	121.2	107.4	48.5	379.5	385.5	0.313	0.359
H4	2019	6.2	5.5	2.8	1.8	6.7	0.028	0.122
H4	2020	8.7	7.6	2.6	25.1	25.2	0.287	0.331
H4	2021	6.2	5.4	2.0	46.5	44.7	0.751	0.824
H4	2022	10.0	8.8	1.8	1.6	3.5	0.016	0.040
H4	2023	5.5	5.0	2.0	80.8	74.2	1.457	1.476
H5	2019	89.5	79.1	32.5	25.3	75.2	0.028	0.095
H5	2020	85.1	75.5	24.8	349.5	353.3	0.411	0.468
H5	2021	100.0	88.5	29.9	788.8	782.0	0.789	0.884
H5	2022	110.3	97.4	42.4	83.1	153.1	0.075	0.157
H5	2023	67.1	59.0	43.3	1232.3	1135.4	1.836	1.924

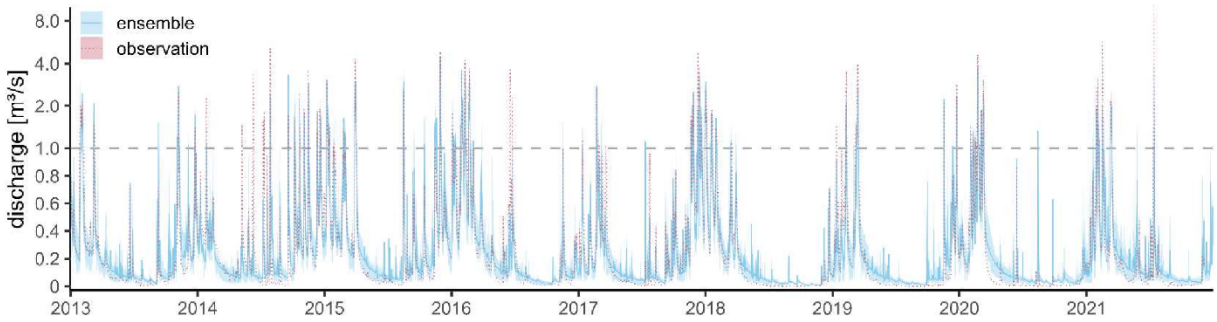
Table S 14: Total AI mass applied on HRUs in the catchment, for the base and drift setup, with the deposition onto the stream for the drift setup.

AI	Applied Mass [kg]		Deposition on Stream [g]	Exported Mass [g]		Exported Mass [%]	
	base	drift		base	drift	base	drift
F1	453.9	382.5	481.9	1.5	44.6	0.000	0.012
F2	1014.0	862.5	1179.4	72.0	1357.2	0.007	0.157
H1	591.5	529.8	138.1	986.0	1082.2	0.167	0.204
H2	191.7	173.5	51.8	4422.6	4054.5	2.307	2.337
H3	681.4	603.2	286.5	613.0	862.4	0.090	0.143
H4	36.7	32.4	11.3	155.7	154.3	0.424	0.477
H5	452.1	399.6	173.0	2479.0	2499.0	0.548	0.625

Plots



90 *Figure S 1: Sensitivity indices for the tested model parameters based on the NSE between simulated and observed flow rate between 2018 and 2021, with red indicating total sensitivity and blue indicating first-order sensitivity.*



95 *Figure S 2: Discharge of the Funne river at the Selm-Ondrup gauge between 2013 and 2021, with the red dashed line indicating flow observations, the blue solid line indicating the mean flow rate of the ensemble, the blue area indicating the range between minimum and maximum flow rate of the ensemble, and the dashed grey line indicating where the y-axis changes from linear scaling below 1 to logarithmic scaling above 1.*

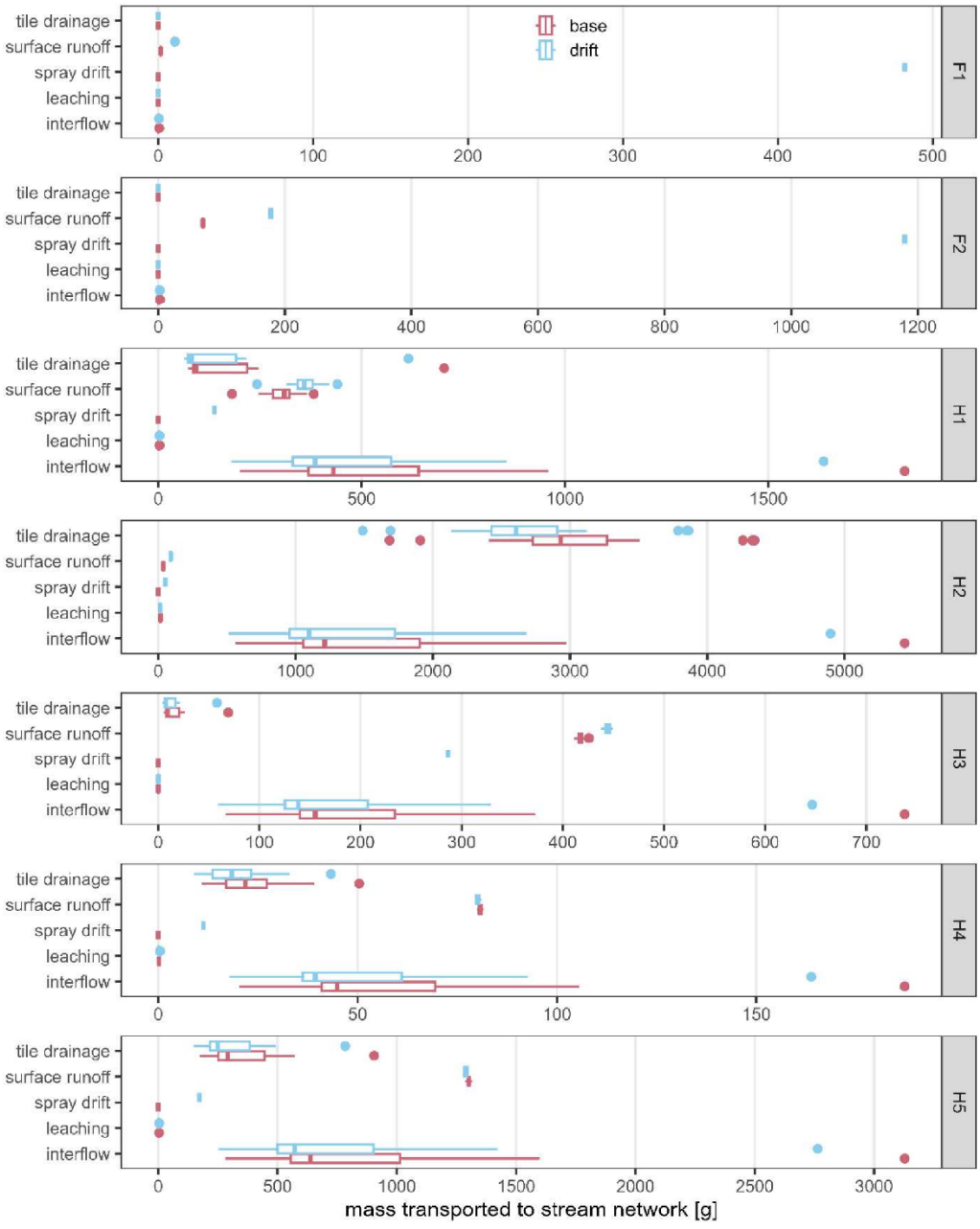


Figure S 3: Comparison between the base and drift model setup. Comparing the total amount of pesticide transported via the different transport pathways, each boxplot represents 20 data points one for each realization of the ensemble.

References

Brain, R., Goodwin, G., Abi-Akar, F., Lee, B., Rodgers, C., Flatt, B., Lynn, A., Kruger, G., & Perkins, D. (2019). Winds of change, developing a non-target plant bioassay employing field-based pesticide drift exposure: A case study with atrazine. *Science of The Total Environment*, *678*, 239–252. https://doi.org/10.1016/j.scitotenv.2019.04.411

Kim, S., Chen, J., Cheng, T., Gindulyte, A., He, J., He, S., Li, Q., Shoemaker, B. A., Thiessen, P. A., Yu, B., Zaslavsky, L., Zhang, J., & Bolton, E. E. (2023). PubChem 2023 update. *Nucleic Acids Research*, *51*(D1), D1373–D1380. https://doi.org/10.1093/nar/gkac956

Perine, J., Anderson, J. C., Kruger, G. R., Abi-Akar, F., & Overmyer, J. (2021). Effect of nozzle selection on deposition of thiamethoxam in Actara® spray drift and implications for off-field risk assessment. *Science of The Total Environment*, *772*, 144808. https://doi.org/10.1016/j.scitotenv.2020.144808

Zhang, L. (2001). A size-segregated particle dry deposition scheme for an atmospheric aerosol module. *Atmospheric Environment*, *35*(3), 549–560. https://doi.org/10.1016/S1352-2310(00)00326-5

Appendix VII:

Evaluating Landscape-Level Pesticide Exposure from Spray Drift:

A Modeling Study in an Agriculture-Dominated Watershed Using SWAT+ and DAD-Drift

Mike Devin Fuchs [a,b,*], *Sebastian Gebler* [a], *Andreas Lorke* [b].

[a] BASF SE, Exposure Modelling, Speyerer Straße 2, 67117 Limburgerhof, Germany.

[b] Institute for Environmental Sciences, University of Kaiserslautern-Landau, Forststraße 7, 76829 Landau in der Pfalz, Germany

*Corresponding author.

E-mail: m.d.fuchs@protonmail.com (M. D. Fuchs)

Supplementary Material B

GIT diff file:

```
"aqu_1d_control.f90"
@@ -9,8 +9,8 @@
      use pesticide_data_module
      use aqu_pesticide_module
      use salt_module
-     use salt_aquifer
-     use cs_aquifer
+     use salt_aquifer_module
+     use cs_aquifer_module
      use ch_pesticide_module

      implicit none
"aqu_cs_output.f90"
@@ -4,7 +4,7 @@
      use basin_module
      use aquifer_module
      use hydrograph_module, only : ob, sp_ob1
-     use cs_aquifer
+     use cs_aquifer_module
      use constituent_mass_module

      implicit none
"aqu_initial.f90"
@@ -5,9 +5,9 @@
      use constituent_mass_module
      use aqu_pesticide_module
      use salt_module !rtb salt
-     use salt_aquifer !rtb salt
+     use salt_aquifer_module !rtb salt
      use cs_module !rtb cs
-     use cs_aquifer !rtb cs
+     use cs_aquifer_module !rtb cs

      implicit none

@@ -122,7 +122,9 @@
        allocate (aqupst_a(iaq)%pest(cs_db%num_pests))
        allocate (cs_aqu(iaq)%path(cs_db%num_paths))
        allocate (cs_aqu(iaq)%hmet(cs_db%num_metals))
-       allocate (cs_aqu(iaq)%salt(cs_db%num_salts))
+       cs_aqu(iaq)%pest = 0.
+                    cs_aqu(iaq)%path = 0.
+                    cs_aqu(iaq)%hmet = 0.
      end if
      !salts !rtb salt
      if (cs_db%num_salts > 0) then
aqu_salt_output.f90"
@@ -4,7 +4,7 @@
      use basin_module
      use aquifer_module
      use hydrograph_module, only : ob, sp_ob1
-     use salt_aquifer
+     use salt_aquifer_module
      use constituent_mass_module

      implicit none
"carbon_module.f90"
@@ -14,16 +14,16 @@
      real :: part_DOC_para = 4000.    !            |organic carbon partition coefficient 1000 to 1200 ! 500-2000 !replacing
KOC=Liquid-solid partition coefficient for Microbial Biomass (10^3 m3 Mg-1)
```

```
        real :: hlife_doc_para = 50.          !days     |DOC half life in groundwater, calculating DOC decay in groundwater ! 0-100
90      !Allocation of CO2 and Carbon transformation
-       real :: ABCO2_para_sur = 0.6    !       |Allocation from Microbial Biomass C pool to CO2; 0.6 (surface Litter),
0.85 - 0.68 × (CLAY+SILT) (all other layers) (Parton et al., 1993, 1994)
-       real :: ABCO2_para_sub = 0.     !       |Calculated -Allocation from Microbial Biomass C pool to CO2; 0.6 (surface
Litter), 0.85 - 0.68 × (CLAY+SILT) (all other layers) (Parton et al., 1993, 1994)
95  +       real :: ABCO2_para_sur = 0.6    !       |Allocation from Microbial Biomass C pool to CO2; 0.6 (surface Litter),
0.85 - 0.68 x (CLAY+SILT) (all other layers) (Parton et al., 1993, 1994)
+       real :: ABCO2_para_sub = 0.     !       |Calculated -Allocation from Microbial Biomass C pool to CO2; 0.6 (surface
Litter), 0.85 - 0.68 x (CLAY+SILT) (all other layers) (Parton et al., 1993, 1994)
        real :: ABP_para_sur = 0.0      !       |Allocation from Biomass to passive Humus; 0 (surface Litter), 0.003 + 0.032
100 x SOL_CLAY (all other layers) (Parton et al., 1993, 1994)
        real :: ABP_para_sub = 0.0      !       |Calculated - Allocation from Biomass to passive Humus; 0 (surface Litter), 0.003
+ 0.032 x SOL_CLAY (all other layers) (Parton et al., 1993, 1994)
        real :: ALMCO2_para_sur         = 0.6   !       |Allocation from metabolic Litter to CO2; 0.6 (surface Litter), 0.55 (all
other layers) (Parton et al., 1993, 1994)
105     real :: ALMCO2_para_sub         = 0.55  !       |Allocation from metabolic Litter to CO2; 0.6 (surface Litter), 0.55 (all
other layers) (Parton et al., 1993, 1994)
        real :: ALSLNCO2_para_sur = 0.6!        |Allocation from non-lignin of structural Litter to CO2; 0.6 (surface Litter), 0.55
(all other layers) (Parton et al., 1993, 1994)
        real :: ALSLNCO2_para_sub =0.55 !               |Allocation from non-lignin of structural Litter to CO2; 0.6 (surface
110 Litter), 0.55 (all other layers) (Parton et al., 1993, 1994)
-       real :: ASP_para_sur = 0.0              !       |Allocation from slow Humus to passive; 0 (surface Litter), 0.003 + 0.00009
× CLAF (all other layers) (Parton et al., 1993, 1994)
-       real :: ASP_para_sub = 0.0              !       |Calculated - Allocation from slow Humus to passive; 0 (surface Litter), 0.003
+ 0.00009 × CLAF (all other layers) (Parton et al., 1993, 1994)
115 +       real :: ASP_para_sur = 0.0              !       |Allocation from slow Humus to passive; 0 (surface Litter), 0.003 + 0.00009
x CLAF (all other layers) (Parton et al., 1993, 1994)
+       real :: ASP_para_sub = 0.0              !       |Calculated - Allocation from slow Humus to passive; 0 (surface Litter), 0.003
+ 0.00009 x CLAF (all other layers) (Parton et al., 1993, 1994)
        real :: ALSLCO2_para = 0.3              !       |Allocation from lignin of structural Litter to CO2; 0.3 (Parton et al., 1993,
120 1994)
        real :: APCO2_para = 0.55               !       |Allocation from passive Humus to CO2; 0.55 (Parton et al., 1993, 1994)
        real :: ASCO2_para = 0.55               !       |Allocation from slow Humus to CO2; 0.55 (Parton et al., 1993, 1994)
@@ -39,9 +39,9 @@
        real :: LSR_para_sur = 0.0107   !       |Rate of potential transformation of structural Litter under optimal conditions
125 (surface = 0.0107 d-1; all other layers = 0.0132 d-1) (Parton et al., 1994)
        real :: LSR_para_sub = 0.0132   !       |Rate of potential transformation of structural Litter under optimal conditions
(surface = 0.0107 d-1; all other layers = 0.0132 d-1) (Parton et al., 1994)
        !Soil texture controls of microbial activity
-       real :: XBM_para_sur = 1.0              !       |Control on transformation of microbial Biomass by soil texture and structure.
130 Its values: surface Litter layer = 1; all other layers = 1 – 0.75 × (SILT + CLAY) (Parton et al., 1993, 1994)
-       real :: XBM_para_sub = 0.0              !       |Calculated - Control on transformation of microbial Biomass by soil texture
and structure. Its values: surface Litter layer = 1; all other layers = 1 – 0.75 × (SILT + CLAY) (Parton et al., 1993, 1994)
-       real :: XLSLF_para = 0.0                !       |Calculated - Control on potential transformation of structural Litter by lignin
fraction of structural Litter [XLSLF = exp(-3 × LSLF) (Parton et al., 1993, 1994)]
135 +       real :: XBM_para_sur = 1.0              !       |Control on transformation of microbial Biomass by soil texture and structure.
Its values: surface Litter layer = 1; all other layers = 1  0.75 x (SILT + CLAY) (Parton et al., 1993, 1994)
+       real :: XBM_para_sub = 0.0              !       |Calculated - Control on transformation of microbial Biomass by soil texture
and structure. Its values: surface Litter layer = 1; all other layers = 1  0.75 x (SILT + CLAY) (Parton et al., 1993, 1994)
+       real :: XLSLF_para = 0.0                !       |Calculated - Control on potential transformation of structural Litter by lignin
140 fraction of structural Litter [XLSLF = exp(-3 x LSLF) (Parton et al., 1993, 1994)]
        !Oxygen factor control parameters
        real :: OX_aa_para = 10.0               !       !Coefficient in calculating oxygen factor
        real :: OX_bb_para = 0.035              !       |Coefficient in calculating oxygen factor
@@ -512,4 +512,4 @@
145     hru2%emit_c = hru1%emit_c / const
      end function carbon_plant_gl_div

-   end module carbon_module
+    end module carbon_module
```

```
"cbn_zhang2.f90"
@@ -19,7 +19,7 @@
       !!============================================
       !! local variables
       !rnmn
-      !abco2   : allocation from biomass to co2; 0.6 (surface litter), 0.85–0.68*(claf + silf) (all other layers) (parton et al., 1993, 1994)
+      !abco2   : allocation from biomass to co2; 0.6 (surface litter), 0.850.68*(claf + silf) (all other layers) (parton et al., 1993, 1994)
       !abl     : carbon allocation from biomass to leaching; abl = (1-exp(-f/(0.01* sw+ 0.1*(kdbm)*db)) (williams, 1995)
       !abp     : allocation from biomass to passive humus; 0 (surface litter), 0.003 + 0.032*claf (all other layers) (parton et al., 1993, 1994)
       !almco2  : allocation from metabolic litter to co2; 0.6 (surface litter), 0.55 (all other layers) (parton et al., 1993, 1994)
@@ -42,7 +42,7 @@
       !cpn3     : potential n deficit resulting from the transformation of microbial biomass; calc as (pn5+pn6)-bmntp if bmntp < (pn5+pn6), otherwise = 0 (kg n ha-1 day-1)
       !cpn4    : potential n deficit resulting from the transformation of slow humus; calc as (pn7+pn8)-hsntp if hsntp < (pn7+pn8), otherwise = 0 (kg n ha-1 day-1)
       !cpn5    : potential n deficit resulting from the transformation of passive humus; calc as pn9-hpntp if hpntp < pn9, otherwise = 0 (kg n ha-1 day-1)
-      !cs      : combined factor controlling biological processes [cs = sqrt(cdg×sut)* 0.8*ox*x1), cs < 10; cs = 10, cs>=10 (williams, 1995)]
+      !cs       : combined factor controlling biological processes [cs = sqrt(cdg * sut)* 0.8*ox*x1), cs < 10; cs = 10, cs>=10 (williams, 1995)]
       !dbp     : soil bulk density of plow layer (mg m-3) (not used)
       !hsctp   : potential transformation of c in slow humus (kg ha-1 day-1)
       !hsntp   : potential transformation of n in slow humus (kg ha-1 day-1)
@@ -52,7 +52,7 @@
       !hsr     : rate of transformation of slow humus under optimal conditions (all layers
                != 0.0005 day-1) (parton et al., 1993, 1994; vitousek et al., 1993)
-      !koc     : liquid–solid partition coefficient for microbial biomass (10^3 m^3 mg-1)
+      !koc     : liquid solid partition coefficient for microbial biomass (10^3 m^3 mg-1)
       !lmf     : fraction of the litter that is metabolic
       !lmnf    : fraction of metabolic litter that is n (kg kg-1)
       !lmr     : rate of transformation of metabolic litter under optimal conditions (surface =
@@ -897,4 +897,4 @@
     end do     !soil layer loop

     return
-  end subroutine cbn_zhang2
+  end subroutine cbn_zhang2
"ch_rtmusk.f90"
@@ -218,14 +218,14 @@

       !! compute water balance - precip, evap and seep
       !! km * m * 1000 m/km * ha/10000 m2 = ha
-      ch_wat_d(ich)%area_ha = sd_ch(ich)%chl * sd_ch(ich)%chw / 10.
+      ch_wat_d(jrch)%area_ha = sd_ch(jrch)%chl * (sd_ch(jrch)%chw + 2. * sd_ch(jrch)%chd * sd_ch(jrch)%chss) / 10.
       !! m3 = 10. * mm * ha
-      ch_wat_d(ich)%precip = 10. * wst(iwst)%weat%precip * ch_wat_d(ich)%area_ha
-      ch_wat_d(ich)%evap = 10. * bsn_prm%evrch * wst(iwst)%weat%pet * ch_wat_d(ich)%area_ha
-      ch_wat_d(ich)%seep = 10. * sd_ch(ich)%chk * ch_wat_d(ich)%area_ha      !k units to mm/d
+      ch_wat_d(jrch)%precip = 10. * wst(iwst)%weat%precip * ch_wat_d(jrch)%area_ha
+      ch_wat_d(jrch)%evap = 10. * bsn_prm%evrch * wst(iwst)%weat%pet * ch_wat_d(jrch)%area_ha
+      ch_wat_d(jrch)%seep = 10. * sd_ch(jrch)%chk * ch_wat_d(jrch)%area_ha      !k units to mm/d

       !! add precip
-      ht2%flo = ht2%flo + ch_wat_d(ich)%precip
+      ht2%flo = ht2%flo + ch_wat_d(jrch)%precip
```

```
      !! calculate transmission losses
      if (ht2%flo > 1.e-6) then
@@ -249,7 +249,7 @@
        if (dep_flo <= sd_ch(jrch)%chd) then
          topw = ch_rcurv(jrch)%out2%surf_area
        else
-         topw = 1000. * sd_ch(jrch)%chl * sd_ch(jrch)%chw
+         topw = 1000. * sd_ch(jrch)%chl * (sd_ch(jrch)%chw + 2. * sd_ch(jrch)%chd * sd_ch(jrch)%chss)
        end if
        iwst = ob(icmd)%wst
        !! mm/day * m2 / (1000. * sd_ch(jrch)%msk%nsteps)
"ch_rtpest.f90"
@@ -104,6 +104,11 @@
      real :: pest_init       !mg          |amount of pesticide before decay
      real :: pest_end        !mg          |amount of pesticide after decay
      real :: rto_out         !none        |ratio of outflow to sum of outflow and storage
+             real :: rto_end
+             real :: pest_in_end
+             real :: pest_stor_end
+             real :: c_in
+    real :: c_stor

      !! zero outputs
      chpst_d(jrch) = chpstz
@@ -146,6 +151,7 @@

        !! calculate fraction of soluble and sorbed pesticide
        frsol = 1. / (1. + kd * sedcon)
+       frsol = max(min(frsol,1.),0.)
        frsrb = 1. - frsol

        !! ASSUME DENSITY=2.6E6; KD2=KD1
@@ -160,7 +166,7 @@
        !! calculate amount of pesticide that undergoes chemical or biological degradation on day in reach
        pest_init = chpstmass
        if (pest_init > 1.e-12) then
-         pest_end = chpstmass * (pestcp(jpst)%decay_a * tday)
+         pest_end = chpstmass * Exp(-.693 / pestdb(jpst)%aq_hlife * tday)
          chpstmass = pest_end
          chpst%pest(ipest)%react = pest_init - pest_end
          !! add decay to daughter pesticides
@@ -204,7 +210,8 @@
        chpstmass = chpstmass + chpst%pest(ipest)%resus

        !! calculate diffusion of pesticide between reach and sediment
-       chpst%pest(ipest)%difus = sd_ch(jrch)%aq_mix(ipest) * (fd2 * sedpstmass - frsol * chpstmass) * tday / depth
+                 chpst%pest(ipest)%difus = 0.
+       !chpst%pest(ipest)%difus = sd_ch(jrch)%aq_mix(ipest) * (fd2 * sedpstmass - frsol * chpstmass) * tday / depth
        if (chpst%pest(ipest)%difus > 0.) then
          if (chpst%pest(ipest)%difus > sedpstmass) then
            chpst%pest(ipest)%difus = sedpstmass
@@ -271,12 +278,41 @@
      end if
      ch_benthic(jrch)%pest(ipest) = sedpstmass

-     !! calculate outflow and storage in water column
-     rto_out = ht2%flo / (1.e-6 + ht2%flo + ch_stor(jrch)%flo)
-     rto_out = Min (1., rto_out)
-     hcs2%pest(ipest) = rto_out * chpstmass
-     ch_water(jrch)%pest(ipest) = (1. - rto_out) * chpstmass
+     !! check incomming and stored concentration
```

```
+       c_in = pstin / wtrin
+       c_stor = ch_water(jrch)%pest(ipest) / ch_stor(jrch)%flo

+       if (c_in >= c_stor) then
+         !! calculate outflow and storage in water column
+         rto_out = ht2%flo / (1.e-6 + ht2%flo + ch_stor(jrch)%flo)
+         rto_out = Min (1., rto_out)
+         hcs2%pest(ipest) = rto_out * chpstmass
+         ch_water(jrch)%pest(ipest) = (1. - rto_out) * chpstmass
+       else
+         !! calculate ratio of initial pesticide available at end of timestep
+                       rto_end = chpstmass / (pstin + ch_water(jrch)%pest(ipest))
+                       rto_end = max(0.,min(1.,rto_end))
+
+                       !! calculate pesticide incomming and stored at the end of the timestep
+                       pest_in_end = pstin * rto_end
+                       pest_stor_end = ch_water(jrch)%pest(ipest) * rto_end
+
+                       !! calculate outflow and storage in water column
+                       rto_out = ht2%flo / ch_stor(jrch)%flo
+
+                       if(rto_out <= 1.)then
+                         hcs2%pest(ipest) = rto_out * pest_stor_end
+                         ch_water(jrch)%pest(ipest) = pest_in_end + pest_stor_end * (1. - rto_out)
+                       else
+                         rto_out = (wtrin - ht2%flo) / ht1%flo
+                         rto_out = max(0.,min(1.,rto_out))
+
+                         hcs2%pest(ipest) = pest_stor_end + (1. - rto_out) * pest_in_end
+                         ch_water(jrch)%pest(ipest) = pest_in_end * rto_out
+                       end if
+       end if
+

     end do

     return
"command.f90"
@@ -327,6 +327,7 @@

           if(cs_db%num_salts > 0) call recall_salt(irec) !rtb salt
           if(cs_db%num_cs > 0) call recall_cs(irec) !rtb cs
+          if(cs_db%num_pests > 0) call recall_pest(irec) !rtb cs

       !case ("exco")   ! export coefficient hyds are set at start

"constit_db_read.f90"
@@ -35,33 +35,33 @@
       if (eof < 0) exit
       read (106,*,iostat=eof) cs_db%num_pests
       if (eof < 0) exit
-      allocate (cs_db%pests(0:cs_db%num_pests))
-      allocate (cs_db%pest_num(0:cs_db%num_pests))
+      allocate (cs_db%pests(1:cs_db%num_pests))
+      allocate (cs_db%pest_num(1:cs_db%num_pests))
       read (106,*,iostat=eof) (cs_db%pests(i), i = 1, cs_db%num_pests)
       if (eof < 0) exit
       read (106,*,iostat=eof) cs_db%num_paths
       if (eof < 0) exit
       allocate (cs_db%paths(cs_db%num_paths))
-      allocate (cs_db%path_num(0:cs_db%num_paths))
```

```
+       allocate (cs_db%path_num(1:cs_db%num_paths))
        read (106,*,iostat=eof) (cs_db%paths(i), i = 1, cs_db%num_paths)
        if (eof < 0) exit
        read (106,*,iostat=eof) cs_db%num_metals
        if (eof < 0) exit
        allocate (cs_db%metals(cs_db%num_metals))
-       allocate (cs_db%metals_num(0:cs_db%num_metals))
+       allocate (cs_db%metals_num(1:cs_db%num_metals))
        read (106,*,iostat=eof) (cs_db%metals(i), i = 1, cs_db%num_metals)
        if (eof < 0) exit
        !salt ions
        read (106,*,iostat=eof) cs_db%num_salts
        if (eof < 0) exit
        allocate (cs_db%salts(cs_db%num_salts))
-       allocate (cs_db%salts_num(0:cs_db%num_salts))
+       allocate (cs_db%salts_num(1:cs_db%num_salts))
        read (106,*,iostat=eof) (cs_db%salts(i), i = 1, cs_db%num_salts)
        !other constituents
        read (106,*,iostat=eof) cs_db%num_cs
        if (eof < 0) exit
        allocate (cs_db%cs(cs_db%num_cs))
-       allocate (cs_db%cs_num (0:cs_db%num_cs))
+       allocate (cs_db%cs_num (1:cs_db%num_cs))
        read (106,*,iostat=eof) (cs_db%cs(i), i = 1, cs_db%num_cs)
        exit
      end do
"constituent_mass_module.f90"
@@ -235,7 +235,7 @@
       character (len=16) :: name
       integer :: num = 0                !number of elements
       integer :: typ                    !recall type - 1=day, 2=mon, 3=year
-      character(len=13) :: filename     !filename
+      character(len=20) :: filename     !filename
       !hyd_output units are in cms and mg/L
       type (constituent_mass), dimension (:,:), allocatable :: hd_pest
     end type recall_pesticide_inputs
"cs_aquifer_module.f90"
rename from "cs_aquifer.f90"
rename to "cs_aquifer_module.f90"
@@ -1,5 +1,5 @@
     !module for constituent mass balance in aquifers (rtb cs)
-    module cs_aquifer
+    module cs_aquifer_module

     implicit none

"cs_balance.f90"
@@ -13,7 +13,7 @@
     use time_module
     use constituent_mass_module
     use cs_module
-    use cs_aquifer
+    use cs_aquifer_module
     use res_cs_module, only : wetcs_d,rescs_d
     use ch_cs_module, only: chcs_d
     use gwflow_module, only : gw_solute_flag,gwsol_ss,ncell,ncell,gw_state,gwsol_state
"cs_divert.f90"
@@ -12,7 +12,7 @@
     use hru_module, only : hru
     use basin_module, only : bsn_cc
     use cs_module !rtb cs
```

```
-     use cs_aquifer !rtb cs
+     use cs_aquifer_module !rtb cs
      use ch_cs_module !rtb cs
      use res_cs_module !rtb cs
      use constituent_mass_module
"cs_irrig.f90"
@@ -11,7 +11,7 @@
      use hydrograph_module, only : irrig,res,sp_ob1,ob
      use hru_module, only : hru
      use cs_module !rtb cs
-     use cs_aquifer !rtb cs
+     use cs_aquifer_module !rtb cs
      use ch_cs_module !rtb cs
      use res_cs_module !rtb cs
      use basin_module, only : bsn_cc
"cs_rctn_aqu.f90"
@@ -9,7 +9,7 @@
      use cs_data_module
      use organic_mineral_mass_module
      use cs_module
-     use cs_aquifer
+     use cs_aquifer_module

      implicit none

"cs_sorb_aqu.f90"
@@ -7,7 +7,7 @@
      use aquifer_module
      use organic_mineral_mass_module
      use constituent_mass_module
-     use cs_aquifer
+     use cs_aquifer_module
      use cs_data_module

      implicit none
dr_path_read.f90"
rename from " dr_read_path.f90"
rename to "dr_path_read.f90"
"header_const.f90"
@@ -7,7 +7,7 @@
     use ch_cs_module
     use res_cs_module
     use cs_module
-    use cs_aquifer
+    use cs_aquifer_module

     implicit none

"header_salt.f90"
@@ -7,7 +7,7 @@
     use ch_salt_module
     use res_salt_module
     use salt_module
-    use salt_aquifer
+    use salt_aquifer_module

     implicit none

"hyd_connect.f90"
@@ -162,6 +162,7 @@
       call recall_read
```

```
455           call recall_read_salt !rtb salt
              call recall_read_cs !rtb cs
+             call recall_read_pest
            end if

460         !read connect file for export coefficients
"ls_read_lsparms_cal.f90"
rename from " ls_read_parms_cal.f90"
rename to " ls_read_lsparms_cal.f90"
"mgt_operatn.f90"
465 @@ -42,7 +42,7 @@
              mgt = sched(isched)%mgt_ops(hru(j)%cur_op)

-             do while(mgt%mon == time%mo .and. mgt%day == time%day_mo)
+             do while(mgt%mon == time%mo .and. mgt%day == time%day_mo .and. mgt%year == time%yrc)
470           call mgt_sched (isched)
              if (sched(isched)%num_ops == 1) exit
              if (yr_skip(j) == 1) exit
"pest_decay.f90"
@@ -35,6 +35,7 @@
475         real :: pest_end          !kg/ha    |amount of pesticide present at end of day
            real :: pst_decay         !kg/ha    |amount of pesticide decay in soil layer during day
            real :: pst_decay_s       !kg/ha    |amount of pesticide decay in soil profile during day
+           real :: pst_decay_f       !kg/ha    |amount of pesticide decay in foliage during day
            real :: metab_decay       !kg/ha    |amount of metabolite decay in soil layer during day
480
           j = ihru
@@ -69,24 +70,27 @@
              hpestb_d(j)%pest(k)%decay_s = pst_decay_s

485          !! calculate degradation on plant foliage
-                !! adjust foliar pesticide for wash off
+                pst_decay_f = 0.
+                    !! adjust foliar pesticide for wash off
             do ipl = 1, pcom(j)%npl
490           pest_init = cs_pl(j)%pl_on(ipl)%pest(k)
              if (pest_init > 1.e-12) then
               pest_end = pest_init * pestcp(ipest_db)%decay_f
              cs_pl(j)%pl_on(ipl)%pest(k) = pest_end
-             hpestb_d(j)%pest(k)%decay_f = pest_init - pest_end
495          pst_decay = (pest_init - pest_end)
+            pst_decay_f = pst_decay_f + pst_decay
             !! add decay to daughter pesticides
             do imeta = 1, pestcp(ipest_db)%num_metab
              ipseq = pestcp(ipest_db)%daughter(imeta)%num
500          ipdb = cs_db%pest_num(ipseq)
             mol_wt_rto = pestdb(ipdb)%mol_wt / pestdb(ipest_db)%mol_wt
-            hpestb_d(j)%pest(ipseq)%metab_f = hpestb_d(j)%pest(ipseq)%metab_f + (pest_init - pest_end) *     &
-                          pestcp(ipest_db)%daughter(imeta)%soil_fr * mol_wt_rto
-            cs_pl(j)%pl_on(ipl)%pest(ipseq) = cs_pl(j)%pl_on(ipl)%pest(ipseq) + hpestb_d(j)%pest(ipseq)%metab_f
505          metab_decay = pst_decay * pestcp(ipest_db)%daughter(imeta)%foliar_fr * mol_wt_rto
+            hpestb_d(j)%pest(ipseq)%metab_f = hpestb_d(j)%pest(ipseq)%metab_f + metab_decay
+            cs_pl(j)%pl_on(ipl)%pest(ipseq) = cs_pl(j)%pl_on(ipl)%pest(ipseq) + metab_decay
            end do
           end if
510       end do
+         hpestb_d(j)%pest(k)%decay_f = pst_decay_f
          end if
        end do

515 "pest_lch.f90"
```

```
@@ -54,6 +54,7 @@
          hpestb_d(j)%pest(k)%perc = 0.
          hpestb_d(j)%pest(k)%surq = 0.
          hpestb_d(j)%pest(k)%latq = 0.
+                    hpestb_d(j)%pest(k)%tileq = 0.
        end do

        do ly = 1, soil(j)%nly
"pest_pl_up.f90"
@@ -32,7 +32,7 @@
          if (cs_pl(j)%pl_on(ipl)%pest(k) >= 0.0001) then
            if (ipest_db > 0) then
              do ly = 1, soil(j)%nly
-               pest_up = pestdb(ipest_db)%pl_uptake * pcom(j)%plcur(ipl)%uptake(ly) / soil(j)%phys(k)%st   &
+               pest_up = pestdb(ipest_db)%pl_uptake * pcom(j)%plcur(ipl)%uptake(ly) / soil(j)%phys(ly)%st   &
                                                     * cs_soil(j)%ly(ly)%pest(k)
                if (pest_up > cs_soil(j)%ly(ly)%pest(k)) pest_up = cs_soil(j)%ly(ly)%pest(k)
                cs_soil(j)%ly(ly)%pest(k) = cs_soil(j)%ly(ly)%pest(k) - pest_up
"pest_soil_tot.f90"
@@ -22,9 +22,11 @@
      if (cs_db%num_pests == 0) return

      do k = 1, cs_db%num_pests
+       hpestb_d(j)%pest(k)%plant = 0.
+                    hpestb_d(j)%pest(k)%in_plant = 0.
        do ipl = 1, pcom(j)%npl
-         hpestb_d(j)%pest(k)%plant = cs_pl(j)%pl_on(ipl)%pest(k)
-         hpestb_d(j)%pest(k)%in_plant = cs_pl(j)%pl_in(ipl)%pest(k)
+         hpestb_d(j)%pest(k)%plant = hpestb_d(j)%pest(k)%plant + cs_pl(j)%pl_on(ipl)%pest(k)
+         hpestb_d(j)%pest(k)%in_plant = hpestb_d(j)%pest(k)%in_plant + cs_pl(j)%pl_in(ipl)%pest(k)
        end do
        hpestb_d(j)%pest(k)%soil = 0.
        do ly = 1, soil(j)%nly
"pest_washp.f90"
@@ -26,6 +26,7 @@
      do k = 1, cs_db%num_pests
        ipest_db = cs_db%pest_num(k)
              !! adjust foliar pesticide for wash off
+       hpestb_d(j)%pest(k)%wash = 0.
        do ipl = 1, pcom(j)%npl
          if (cs_pl(j)%pl_on(ipl)%pest(k) >= 0.0001) then
            if (ipest_db > 0) then
@@ -33,7 +34,7 @@
              if (pest_soil > cs_pl(j)%pl_on(ipl)%pest(k)) pest_soil = cs_pl(j)%pl_on(ipl)%pest(k)
              cs_soil(j)%ly(1)%pest(k) = cs_soil(j)%ly(1)%pest(k) + pest_soil
              cs_pl(j)%pl_on(ipl)%pest(k) = cs_pl(j)%pl_on(ipl)%pest(k) - pest_soil
-             hpestb_d(j)%pest(k)%wash = pest_soil
+             hpestb_d(j)%pest(k)%wash = hpestb_d(j)%pest(k)%wash + pest_soil
            end if
          end if
        end do
"pl_grow.f90"
@@ -23,7 +23,7 @@

        !! check for start and end of dormancy of temp-based growth plant
        idp = pcom(j)%plcur(ipl)%idplt
-       if (pldb(idp)%trig == "temp_gro") then
+       if (pldb(idp)%trig == "temp_gro" .and. pcom(j)%plcur(ipl)%gro == "y") then
          call pl_dormant
        end if
```

```
"pl_waterup.f90"
@@ -122,14 +122,7 @@
            sum = epmax(ipl) * (1. - Exp(-uptake%water_dis * gx / pcom(j)%plg(ipl)%root_dep)) / uptake%water_norm
          end if

-       pcom(j)%plcur(ipl)%epco = 0.9
-       !! let second layer compensate - 10 mm layer causes problems wehn root depth is shallow
-       if (k == 2) then
-         wuse = sum      !epco is always 1.0 for second layer
-       else
-         wuse = sum - sump * (1. - pcom(j)%plcur(ipl)%epco)
-       end if
-
+       wuse = sum - sump * (1. - pcom(j)%plcur(ipl)%epco)
        ! adjust for impervious area
        ulu = hru(j)%luse%urb_lu
        !wuse = wuse * urbdb(ulu)%fcimp
"read_mgtops.f90"
@@ -23,7 +23,7 @@
      read (107,*)   sched(isched)%mgt_ops(iop)%op,             & !! operation character
                     sched(isched)%mgt_ops(iop)%mon,            &
                     sched(isched)%mgt_ops(iop)%day,            &
-                    sched(isched)%mgt_ops(iop)%husc,           &
+                    sched(isched)%mgt_ops(iop)%year,           &
                     sched(isched)%mgt_ops(iop)%op_char,        & !! operation type character
                     sched(isched)%mgt_ops(iop)%op_plant,       & !! plant character
                     sched(isched)%mgt_ops(iop)%op3             !! override
@@ -31,7 +31,7 @@
        day = sched(isched)%mgt_ops(iop)%day
        mon = sched(isched)%mgt_ops(iop)%mon
        sched(isched)%mgt_ops(iop)%jday = Jdt(ndays,day,mon)
-       sched(isched)%mgt_ops(iop)%year = iyear
+       sched(isched)%mgt_ops(iop)%husc = 0
        if (sched(isched)%mgt_ops(iop)%op == "skip") iyear = iyear + 1

     select case(sched(isched)%mgt_ops(iop)%op)
"recall_pest.f90"
@@ -0,0 +1,81 @@
+    !rtb cs
+    !include constituent mass from point sources
+    subroutine recall_pest(irec)
+
+
+    use basin_module
+    use hydrograph_module
+    use time_module
+    use constituent_mass_module
+    use ch_cs_module
+
+    implicit none
+
+    !incoming variables
+    integer :: irec
+
+    !local variables
+    integer :: ipest                                        !         |constituent counter
+    integer :: ichan       !         |id of source channel
+    real :: pest_conc      !g/m3     |concentration of constituent in source channel
+    real :: div_mass       !kg       |mass of constituent in diversion water
+
+
```

```
+    !depending on the point source type, add/remove constituent mass to object
+    obcs(icmd)%hd(1)%pest = 0.
+    if (cs_db%num_pests > 0) then
+      select case (rec_pest(irec)%typ)
+        case (1)    !daily
+          if (time%yrc >= recall(irec)%start_yr .and. time%yrc <= recall(irec)%end_yr) then
+            do ipest=1,cs_db%num_pests
+              if(recall(irec)%hd(time%day,time%yrs)%flo < 0) then
+                !diversion: remove mass from channel directly
+                ichan = ob(icmd)%obtypno_out(1) !channel from which water is diverted
+                if(ch_stor(ichan)%flo > 10.) then !only proceed if channel has water
+                  pest_conc = (ch_water(ichan)%pest(ipest)*1000.) / ch_stor(ichan)%flo !g/m3 in channel water
+                  div_mass = (pest_conc * recall(irec)%hd(time%day,time%yrs)%flo) / 1000. !kg/day
+                  if((div_mass*(-1)) > ch_water(ichan)%pest(ipest)) then
+                    div_mass = ch_water(ichan)%pest(ipest) * (-1) !only take what is there
+                  endif
+                  ch_water(ichan)%pest(ipest) = ch_water(ichan)%pest(ipest) + div_mass
+                endif
+              else
+                !source: add mass
+                obcs(icmd)%hd(1)%pest(ipest) = rec_pest(irec)%hd_pest(time%day,time%yrs)%pest(ipest)
+                                                endif
+            enddo
+            recoutcsb_d(irec)%pest = obcs(icmd)%hd(1)%pest
+          else
+            obcs(icmd)%hd(1) = hin_csz
+          endif
+        case (2)    !monthly
+          if (time%yrc >= recall(irec)%start_yr .and. time%yrc <= recall(irec)%end_yr) then
+            do ipest=1,cs_db%num_pests
+              obcs(icmd)%hd(1)%pest(ipest) = rec_pest(irec)%hd_pest(time%mo,time%yrs)%pest(ipest)
+            enddo
+              recoutcsb_d(irec)%pest = rec_pest(irec)%hd_pest(time%mo,time%yrs)%pest
+          else
+            obcs(icmd)%hd(1) = hin_csz
+          endif
+        case (3)    !annual
+          if (time%yrc >= rec_cs(irec)%start_yr .or. time%yrc <= rec_cs(irec)%end_yr) then
+            do ipest=1,cs_db%num_pests
+              obcs(icmd)%hd(1)%pest(ipest) = rec_pest(irec)%hd_pest(1,time%yrs)%pest(ipest)
+            enddo
+              recoutcsb_d(irec)%pest = rec_pest(irec)%hd_pest(1,time%yrs)%pest
+          else
+            obcs(icmd)%hd(1) = hin_csz
+          endif
+        case (4)    !average annual
+          if (time%yrc >= recall(irec)%start_yr .and. time%yrc <= recall(irec)%end_yr) then
+            do ipest=1,cs_db%num_pests
+              obcs(icmd)%hd(1)%pest(ipest) = rec_pest(irec)%hd_pest(1,1)%pest(ipest)
+            enddo
+              recoutcsb_d(irec)%pest = rec_pest(irec)%hd_pest(1,1)%pest
+          endif
+        end select
+      endif
+
+
+      return
+      end subroutine recall_pest
"recall_read.f90"
@@ -26,7 +26,6 @@
      integer :: iyrs              !         |
```

```
      integer :: iyr_prev          !none      |previous year
      integer :: istep             !          |
-     integer :: ipestcom_db       !none      !pointer to pestcom_db - fix*** ??
      integer :: ipc               !none      |counter
      integer :: ii                !none      |counter
      integer :: i                 !          |
@@ -233,84 +232,5 @@
      enddo
      endif

-     !read all rec_pest files
-     inquire (file="pest.com", exist=i_exist)
-     if (i_exist ) then
-     do
-       open (107,file="pest.com")
-       read (107,*,iostat=eof) titldum
-       if (eof < 0) exit
-       read (107,*,iostat=eof) header
-       if (eof < 0) exit
-       imax = 0
-         do while (eof == 0)
-           read (107,*,iostat=eof) i
-           if (eof < 0) exit
-           imax = Max(imax,i)
-         end do
-
-     allocate (rec_pest(0:imax))
-     rewind (107)
-     read (107,*,iostat=eof) titldum
-     if (eof < 0) exit
-     read (107,*,iostat=eof) header
-     if (eof < 0) exit
-
-     do ipc = 1, db_mx%pestcom
-       read (107,*,iostat=eof) ipestcom_db   !pointer to pestcom_db - fix***
-       if (eof < 0) exit
-
-        do ii = 1, imax
-          read (107,*,iostat=eof) i
-          if (eof < 0) exit
-          backspace (107)
-          read (107,*,iostat = eof) k, rec_pest(i)%name, rec_pest(i)%typ, rec_pest(i)%filename
-          if (eof < 0) exit
-          open (108,file = rec_pest(i)%filename)
-          read (108,*,iostat=eof) titldum
-          if (eof < 0) exit
-          read (108,*,iostat=eof) nbyr
-          if (eof < 0) exit
-          read (108,*,iostat=eof) header
-          if (eof < 0) exit

-       select case (rec_pest(i)%typ)
-         case (1) !! daily
-          allocate (rec_pest(i)%hd_pest(366,nbyr))

-         case (2) !! monthly
-          allocate (rec_pest(i)%hd_pest(12,nbyr))

-         case (3) !! annual
-          allocate (rec_pest(i)%hd_pest(1,nbyr))
-       end select
```

```
-
-      ! read and store entire year
-      do
-        read (108,*,iostat=eof) iyr, istep
-        if (eof < 0) exit
-        if (iyr == time%yrc) exit
-      end do
-
-      backspace (108)
-      iyr_prev = iyr
-      iyrs = 1
-
-      do
-        read (108,*,iostat=eof) iyr, istep, recall(i)%hd(istep,iyrs)
-        if (eof < 0) exit
-        !call hyd_convert_mass (recall(i)%hd(istep,iyrs))
-        if (iyr /= iyr_prev) then
-          iyr_prev = iyr
-          iyrs = iyrs + 1
-        endif
-      end do
-      close (108)
-        end do
-      end do
-      close (107)
-    end do
-    end if
-
      return
      end subroutine recall_read
"recall_read_cs.f90"
@@ -40,7 +40,7 @@

      !read all recall files
      inquire (file="cs_recall.rec", exist=i_exist)
-    if (i_exist .or. in_rec%recall_rec /= "null") then
+    if (i_exist) then
      do
       open (107,file="cs_recall.rec")
       read (107,*,iostat=eof) titldum
"recall_read_pest.f90"
@@ 0,0 +1,150 @@
+    !read point source data for constituents !rtb cs
+    subroutine recall_read_pest
+
+    use hydrograph_module
+    use input_file_module
+    use organic_mineral_mass_module
+    use constituent_mass_module
+    use maximum_data_module
+    use time_module
+    use exco_module
+
+    implicit none
+
+    character (len=80) :: titldum   !          |title of file
+    character (len=80) :: header    !          |header of file
+    character(len=16) :: ob_name
+    character(len=8) :: ob_typ
+    character(len=16) :: pest_name
+           character(len=16) :: pest_cur
```

```
+           real :: pest_mass
+     integer :: imax               !none       |end of loop
+     integer :: iyr               !          |
+     integer :: jday               !          |
+     integer :: mo                 !          |
+     integer :: day_mo               !          |
+     integer :: eof                !          |end of file
+     logical :: i_exist            !none       |check to determine if file exists
+     integer :: nbyr               !none       !number of years the land use occurred
+     integer :: k                 !          |
+     integer :: iyrs               !          |
+     integer :: iyr_prev             !none       |previous year
+     integer :: iyr_beg            !          |
+           integer :: istep              !          |
+     integer :: ipc                !none       |counter
+     integer :: ii                 !none       |counter
+     integer :: i                  !          |
+     integer :: iexco_om
+     integer :: ifirst             !          |
+     integer :: iexo_allo = 0
+     integer :: ics,jj,kk,pr,pc,ipest
+
+     eof = 0
+     imax = 0
+
+           !read all rec_pest files
+           inquire (file="pest_recall.rec", exist=i_exist)
+           if (i_exist ) then
+     do
+           open (107,file="pest_recall.rec")
+           read (107,*,iostat=eof) titldum
+           if (eof < 0) exit
+           read (107,*,iostat=eof) header
+           if (eof < 0) exit
+           imax = 0
+           do while (eof == 0)
+           read (107,*,iostat=eof) i
+           if (eof < 0) exit
+           imax = Max(imax,i)
+     end do
+     end do
+
+           if (imax > 0) then
+           allocate (rec_pest(0:imax))
+           !point sources originating from outside the watershed
+      if (.not. allocated(recoutcsb_d)) allocate (recoutcsb_d(imax))
+      if (.not. allocated(recoutcsb_m)) allocate (recoutcsb_m(imax))
+      if (.not. allocated(recoutcsb_y)) allocate (recoutcsb_y(imax))
+      if (.not. allocated(recoutcsb_a)) allocate (recoutcsb_a(imax))
+      do ii=1,imax
+        allocate (recoutcsb_d(ii)%pest(cs_db%num_pests))
+        allocate (recoutcsb_m(ii)%pest(cs_db%num_pests))
+        allocate (recoutcsb_y(ii)%pest(cs_db%num_pests))
+        allocate (recoutcsb_a(ii)%pest(cs_db%num_pests))
+        do ipest=1,cs_db%num_pests
+          recoutcsb_d(ii)%pest(ipest) = 0.
+          recoutcsb_m(ii)%pest(ipest) = 0.
+          recoutcsb_y(ii)%pest(ipest) = 0.
+          recoutcsb_a(ii)%pest(ipest) = 0.
+        enddo
+      enddo
```

```
+
+       rewind (107)
+       read (107,*,iostat=eof) titldum
+       read (107,*,iostat=eof) header
+       do ii = 1, imax
+           read (107,*,iostat = eof) k, rec_pest(ii)%name, rec_pest(ii)%typ, rec_pest(ii)%filename
+           open (108,file = rec_pest(ii)%filename)
+           read (108,*,iostat=eof) titldum
+           read (108,*,iostat=eof) nbyr
+           read (108,*,iostat=eof) header
+
+       select case (rec_pest(ii)%typ)
+           case (1) !! daily
+           allocate (rec_pest(ii)%hd_pest(366,nbyr))
+           do pr = 1, 366
+             do pc = 1, nbyr
+               allocate (rec_pest(ii)%hd_pest(pr,pc)%pest(cs_db%num_pests))
+               rec_pest(ii)%hd_pest(pr,pc)%pest = 0.
+             end do
+           end do
+
+           case (2) !! monthly
+           allocate (rec_pest(ii)%hd_pest(12,nbyr))
+           do pr = 1, 12
+             do pc = 1, nbyr
+               allocate (rec_pest(ii)%hd_pest(pr,pc)%pest(cs_db%num_pests))
+               rec_pest(ii)%hd_pest(pr,pc)%pest = 0.
+             end do
+           end do
+
+           case (3) !! annual
+           allocate (rec_pest(ii)%hd_pest(1,nbyr))
+           do pr = 1, 1
+             do pc = 1, nbyr
+               allocate (rec_pest(ii)%hd_pest(pr,pc)%pest(cs_db%num_pests))
+               rec_pest(ii)%hd_pest(pr,pc)%pest = 0.
+             end do
+           end do
+       end select
+
+       read (108,*,iostat=eof) jday, mo, day_mo, iyr, ob_typ, ob_name, pest_name, pest_mass
+       iyr_beg = iyr
+       backspace (108)
+
+       iyrs = 1
+       pest_cur = "xyz"
+       do
+         if (eof < 0) exit
+           read (108,*,iostat=eof) jday, mo, day_mo, iyr, ob_typ, ob_name, pest_name, pest_mass
+           if(trim(pest_name) /= trim(pest_cur)) then
+             do kk = 1, cs_db%num_pests
+               if (trim(cs_db%pests(kk)) == trim(pest_name)) then
+                 ipest = cs_db%pest_num(kk)
+                 pest_cur = cs_db%pests(kk)
+               end if
+             end do
+           end if
+
+           iyrs = iyr - iyr_beg + 1
+           rec_pest(k)%hd_pest(jday,iyrs)%pest(ipest) = pest_mass
+       end do
```

```
+
+             close (108)
+             end do
+             close (107)
+             end if
+             end if
+
+     return
+     end subroutine recall_read_pest
"recall_read_salt.f90"
@@ -39,7 +39,7 @@

      !read all recall files
      inquire (file="salt_recall.rec", exist=i_exist)
-     if (i_exist .or. "salt_recall.rec" /= "null") then
+     if (i_exist) then
      do
        open (107,file="salt_recall.rec")
        read (107,*,iostat=eof) titldum
"res_rel_conds.f90"
rename from "res_rel_ctbl.f90"
rename to "res_rel_conds.f90"
"salt_aquifer_module.f90"
rename from "salt_aquifer.f90"
rename to "salt_aquifer_module.f90"
@@ -1,4 +1,4 @@
-     module salt_aquifer
+     module salt_aquifer_module

      implicit none

"salt_balance.f90"
@@ -12,7 +12,7 @@
      use soil_module
      use time_module
      use salt_module
-     use salt_aquifer
+     use salt_aquifer_module
      use constituent_mass_module
      use res_salt_module, only : wetsalt_d,ressalt_d
      use ch_salt_module, only : chsalt_d
"salt_chem_aqu.f90"
@@ -27,7 +27,7 @@
      use salt_data_module
      use hydrograph_module, only : ob,icmd
      use salt_module
-     use salt_aquifer
+     use salt_aquifer_module

      implicit none

"salt_irrig.f90"
@@ -11,7 +11,7 @@
      use hydrograph_module, only : irrig,res,sp_ob1,ob
      use hru_module, only : hru
      use salt_module !rtb salt
-     use salt_aquifer !rtb salt
+     use salt_aquifer_module !rtb salt
      use ch_salt_module !rtb salt
      use res_salt_module !rtb salt
      use basin_module, only : bsn_cc
```

```
"sd_channel_control.f90"
@@ -225,7 +225,7 @@
            if(bsn_cc%gwflow.eq.1) then
              flood_freq(ich) = 1 !flag to indicate the water is in the floodplain
              call gwflow_fpln(ich)
-                                                    endif
+           endif

            sd_ch(ich)%overbank = "ob"
            rcharea = sd_ch_vel(ich)%area
@@ -406,7 +406,7 @@
          !! Peters latest channel erosion model
          !!vel = 1.37 * (sd_ch(ich)%chs ** 0.31) * (12. * sd_ch(ich)%chw) ** 0.32      !annual ave for SWIFT
          !! mean daily to peak ratio developed from GARDAY - THE STUDY OF MOST PROBABLE MEAN DAILY BANKFULL
RUNOFF VOLUMES
-         !! IN SMALL WATERSHEDS DOMINATED BY CONVECTIVE/FRONTAL CHANNEL FORMING EVENTS AND THE CO-
INCIDENT INNER BERM CHANNELS – PART I.
+          !! IN SMALL WATERSHEDS DOMINATED BY CONVECTIVE/FRONTAL CHANNEL FORMING EVENTS AND THE
CO-INCIDENT INNER BERM CHANNELS PART I.
          !! Another eq from Peter - Qmax=Qmean*(1+2.66*Drainage Area^-.3)
          pk_rto = 0.2 + 0.5 / 250. * ob(icmd)%area_ha
          pk_rto = amin1 (1., pk_rto)
@@ -490,7 +490,7 @@
        end if

        !! compute sediment leaving the channel - washload only
-               sedout = ht1%sed - dep + hc_sed + ebank_t     !  + ebtm_t
+       sedout = ht1%sed - dep + hc_sed + ebank_t     !  + ebtm_t

        !! set values for outflow hydrograph
        !! calculate flow velocity and travel time  ht2 = ht1   !***jga
@@ -543,10 +543,10 @@
          ht2%solp = ht2%solp + ebank_t * sd_ch(ich)%p_bio

          !! route constituents
-         call ch_rtpest
+          !call ch_rtpest
          !! call mike winchell's new routine for pesticide routing
          ! call ch_rtpest2
-         call ch_rtpath
+          !call ch_rtpath
        end if

        end if    ! peakrate > 0
@@ -554,7 +554,7 @@
        flo_ls = ht2%flo
        !! compute water balance - precip, evap and seep
        !! km * m * 1000 m/km * ha/10000 m2 = ha
-       ch_wat_d(ich)%area_ha = sd_ch(ich)%chl * sd_ch(ich)%chw / 10.
+       ch_wat_d(ich)%area_ha = sd_ch(ich)%chl * (sd_ch(ich)%chw + 2. * sd_ch(ich)%chd * sd_ch(ich)%chss) / 10.
        !! m3 = 10. * mm * ha
        ch_wat_d(ich)%precip = 10. * wst(iwst)%weat%precip * ch_wat_d(ich)%area_ha
        ch_wat_d(ich)%evap = 10. * bsn_prm%evrch * wst(iwst)%weat%pet * ch_wat_d(ich)%area_ha
@@ -654,6 +654,12 @@
          hcs3 = hcs2 + ch_water(ich) !incoming + storage
        endif

+       !! route constituents
+        call ch_rtpest
+       !! call mike winchell's new routine for pesticide routing
+       ! call ch_rtpest2
```

```
+       call ch_rtpath
+
        !rtb hydrograph separation
        if (rttime > det) then      ! ht1 = incoming + storage
          !! travel time > timestep -- then all incoming is stored and frac of stored is routed
@@ -837,4 +843,4 @@

        return

-     end subroutine sd_channel_control
+     end subroutine sd_channel_control
"sd_hydsed_init.f90"
@@ -127,14 +127,8 @@
        d = 0.
        chside = sd_ch(i)%chss
        fps = 4.
-       b = sd_ch(i)%chw - 2. * sd_ch(i)%chd * chside
-
-       !! check IF bottom width (b) is < 0
-       if (b <= 0.) then
-          b = .5 * sd_ch(i)%chw
-          b = Max(0., b)
-          chside = (sd_ch(i)%chw - b) / (2. * sd_ch(i)%chd)
-       end if
+       b = sd_ch(i)%chw
+
        sd_ch_vel(i)%wid_btm = b
        sd_ch_vel(i)%dep_bf = sd_ch(i)%chd  !delete sd_ch_vel when finished
        !! compute travel time coefficients - delete when finished with flood plain
"sd_rating_curve.f90"
@@ -23,13 +23,7 @@
      real :: vel                !             |
      real :: frac_abov

-     b = sd_ch(i)%chw - 2. * sd_ch(i)%chd * sd_ch(i)%chss
-     !! check if bottom width (b) is < 0
-     if (b <= 0.) then
-       b = .5 * sd_ch(i)%chw
-       b = Max(0., b)
-       sd_ch(i)%chss = (sd_ch(i)%chw - b) / (2. * sd_ch(i)%chd)
-     end if
+     b = sd_ch(i)%chw

      !! compute rating curve at 0.1 and 1.0 times bankfull depth
      do i_dep = 1, 2
@@ -76,7 +70,7 @@
        ch_rcurv(i)%elev(ifp_dep)%dep = (1. + frac_abov) * sd_ch(i)%chd
        ch_rcurv(i)%elev(ifp_dep)%wet_perim = p
        ch_rcurv(i)%elev(ifp_dep)%xsec_area = a
-       ch_rcurv(i)%elev(ifp_dep)%top_wid = sd_ch(i)%chw + 2. * dep / sd_ch(i)%fps
+       ch_rcurv(i)%elev(ifp_dep)%top_wid = ch_rcurv(i)%elev(2)%top_wid + 2. * dep / sd_ch(i)%fps
        ch_rcurv(i)%elev(ifp_dep)%surf_area = ch_rcurv(i)%elev(ifp_dep)%top_wid * sd_ch(i)%chl
        ch_rcurv(i)%elev(ifp_dep)%vol_ch = vol_bf
        ch_rcurv(i)%elev(ifp_dep)%vol_fp = ch_rcurv(i)%elev(ifp_dep)%top_wid * dep * sd_ch(i)%chl * 1000.
```